Mines and Minerals Division

Ontario Geological Survey
Miscellaneous Paper 131

Exploration Technology Development Program of the Board of Industrial Leadership and Development

Summary of Research 1985–1986

edited by V.G. Milne and R.B. Barlow

Program funded by the Board of Industrial Leadership and Development

1986

Ministry of
Northern Development
and Mines
Ontario

©1986 Government of Ontario
Printed in Ontario, Canada

ISSN 0704–2752 (series)
ISSN 0826–791X (subseries)

Publications of the Ontario Geological Survey, Ministry of Northern Development and Mines, are available from the following sources. Orders for publications should be accompanied by cheque or money order payable to the *Treasurer of Ontario*.

Reports, maps and price lists (personal shopping or mail order):

Public Information Centre, Ministry of Natural Resources
Room 1640, Whitney Block, Queen's Park
Toronto, Ontario M7A 1W3

Reports and accompanying maps only (personal shopping):

Main Floor, 880 Bay Street
Toronto, Ontario

Reports and accompanying maps (mail order or telephone orders):

Publications Services Section, Ministry of Government Services
5th Floor, 880 Bay Street
Toronto, Ontario M7A 1N8
Telephone (local calls) 965–6015
Toll–free long distance 1–800–268–7540
Toll–free from Area Code 807 0–ZENITH–67200

A project funded by the Board of Industrial Leadership and Development.

Every possible effort is made to ensure the accuracy of the information contained in this report, but the Ministry of Northern Development and Mines does not assume any liability for errors that may occur. Source references are included in the report and users may wish to verify critical information.

Parts of this publication may be quoted if credit is given. It is recommended that reference be made in the following form for individual papers:

Reford, S.W., and Paterson, N.R.
1986: Testing and Demonstration of Interpretation Software for Magnetic, EM and Spectrometry Inversion; Grant 089, p.65-75 *in* Exploration Technology Development Program of the Board of Industrial Leadership and Development, Summary of Research, 1985-1986, edited by V.G. Milne and R.B. Barlow, Ontario Geological Survey, Miscellaneous Paper 131, 145p.

2000–86–Thorn Press

Contents

Introductory Remarks iv

Grant 039 — Single Receiver, Frequency Scanning Fixed Source Electromagnetic System, *A. Rogozinski* 2

Grant 052 — Production of a Seven-Frequency Helicopter Electromagnetic System, *Paul Wessler* 7

Grant 058/101 — Portable Broadband Multiple Geometry HEM System, *R.L.S. Hogg* 14

Grant 068 — Isotope Ratios and Trace Elements in Gold and Base Metal Occurrences in Ontario: An Application of Plasma/Mass Spectrometry, *E.J. Brooker and T.E. Eagles* 20

Grant 072 — A Microprocessor-Based Digital Receiver Console for the DIGHEM$^{III/IV}$ System, *S.J. Kilty* 25

Grant 079 — Seismic Full Waveform Logging and Seismic Geotomography, *J. Wong* 30

Grant 080 — High Resolution EM Developments, *Y. Lamontagne and A.E. Wieckowski* 36

Grant 081 — Computer Software for the Maglog Borehole Logging System, *S.J. Balch* 42

Grant 084 — Helicopter Borne High Sensitivity Magnetometer Intridirectional Gradiometer Based on Overhauser Effect, *Ivan Hrvoic* 49

Grant 087 — High Resolution Investigations Using Radar And Seismic Techniques, *A.P. Annan and F. Glass* 52

Grant 089 — Testing and Demonstration of Interpretation Software for Magnetic, EM and Spectrometry Inversion, *S.W. Reford and N.R. Paterson* 65

Grant 091 — The Development of a Pocket Digital-Reading Induced Polarization-Resistivity Meter, *M.G. Roman-Barber and C.L. Elliot* . 76

Grant 093 — Software and Hardware Design of Controlled Source Audio-Frequency Magneto-Telluric (CSAMT) System and Test Surveys, *Philip G. Hallof and Mitsuru Yamashita* 83

Grant 097 — Gold in Peat and its Relevance to Mineral Exploration, *R.D. Thomas, C.F. Gleeson, V.N. Rampton, S. Paradis and S.G. Corden* 95

Grant 105 — Processing of Airborne Imagery for Geobotanical Stress Associated with Subsurface Mineralization, *J.R. Miller, D.R. Sturgeon, N.T. O'Neill and R.A.H. Buxton* 117

Grant 109 — The Prospect I AEM System, *A.P. Annan* 124

Grant 112 — Development of Geobotanical Remote Sensing Technology, *D.N.H. Horler, J.A. Ostrowski and D.R. Melling* 130

Introductory Remarks

EXPLORATION TECHNOLOGY DEVELOPMENT PROGRAM

Exploration in Ontario has reached a point where most mineral deposits located at or near the surface have been detected and tested for their economic viability. Therefore, future exploration must concentrate on locating mineral deposits at some depths below the surface. In order to resolve deeper deposits more effectively, new instrumentation must be developed. The Exploration Technology Development Program was created in late 1981 to facilitate this need for more precise instrumentation and techniques required in modern exploration programs.

With the establishment of the Ontario Geoscience Research Grants Program in the late 1970s, the Ontario Geological Survey developed a program to encourage geoscience research at Ontario universities. This program was viewed as the first step towards defining geological parameters and determining possible areas of high mineral potential in Ontario. The Exploration Technology Development Program was conceived as an important second step towards bringing these ideas and concepts to the private sector and ensuring the development of new technology through them.

The Exploration Technology Development Program was initiated to encourage the advancement of exploration geophysics and geochemistry by providing joint venture funding to Ontario companies leading to the development of innovative technology, specifically in those areas which support the mineral exploration industry in Ontario. The program supports applied research and development to seven areas of exploration activity:

1. mineral deposit and overburden, physical and chemical characterization studies
2. development of new or modified airborne systems for improved detection of mineral deposits
3. development of new ground equipment for better detection and dissemination of mineral deposits
4. development of concepts and techniques in exploration geochemistry
5. development of borehole logging systems and related drilling techniques
6. development or implementation of laboratory support equipment not presently available in Ontario for the purpose of offering improved analytical service to mineral exploration companies
7. development of data acquisition and signal processing hardware and software for real–time and part–time collection and interpretation of field data.

The Exploration Technology Development Program awards grants for any one project for up to three years in duration, with the Ontario Government financing 60% of all activities to a maximum contribution for an individual project of $150 000 per year.

Research proposals are reviewed and ranked by a Review Committee according to their scientific merit and relevance to the Program.

The members of the 1985–86 Committee included:

L.S. Collett, Chairman	Geological Survey of Canada
Dr. R.B. Band	Falconbridge Ltd.
R.B. Barlow	Ontario Geological Survey
J. Dowsett	Inco Limited
Dr. J.P. Greenhouse	University of Waterloo
Dr. G.E.M. Hall	Geological Survey of Canada
Dr. W.O. Karvinen	Karvinen and Associates
R.S. Middleton	R.S. Middleton Exploration Services Limited
Dr. I. Nichol	Queen's University
R.H. Pemberton	Noranda Mines Limited
L. Reed	Selco Division – BP Resources Canada Limited
Dr. D.H. Watkinson	Carleton University

During the 1985–86 year, 17 proposals were funded under this program. Grant allocations in support of these projects totalled $905 294.

Final reports for all 1985–86 grants are due six months after termination of funding. These reports will be released as Ontario Geological Survey Open File Reports, and will be available from the Mines Library (Ontario Geological Survey, 77 Grenville Street, Toronto) and from all Regional and Resident Geologists' Offices.

The undersigned would like to thank L.S. (Len) Collett, Chairman of the Review Committee, and the rest of the members and participating companies who gave freely of their time and made the whole program possible. As well, the efforts of the researchers are acknowledged. Thanks are also due to R.B. Watson who acted as Grants Administrator and Secretary to the Committee.

V.G. Milne
Director
Ontario Geological Survey

CONVERSION FACTORS FOR MEASUREMENTS IN ONTARIO GEOLOGICAL SURVEY PUBLICATIONS.

CONVERSION FROM SI TO IMPERIAL				CONVERSION FROM IMPERIAL TO SI		
SI Unit	*Multiplied by*	*Gives*		*Imperial Unit*	*Multiplied by*	*Gives*
			LENGTH			
1 mm	0.039 37	inches		1 inch	**25.4**	mm
1 cm	0.393 70	inches		1 inch	**2.54**	cm
1 m	3.280 84	feet		1 foot	**0.304 8**	m
1 m	0.049 709 7	chains		1 chain	20.116 8	m
1 km	0.621 371	miles (statute)		1 mile (statute)	**1.609 344**	km
			AREA			
1 cm²	0.155 0	square inches		1 square inch	**6.451 6**	cm²
1 m²	10.763 9	square feet		1 square foot	**0.092 903 04**	m²
1 km²	0.386 10	square miles		1 square mile	2.589 988	km²
1 ha	2.471 054	acres		1 acre	0.404 685 6	ha
			VOLUME			
1 cm³	0.061 02	cubic inches		1 cubic inch	**16.387 064**	cm³
1 m³	35.314 7	cubic feet		1 cubic foot	0.028 316 85	m³
1 m³	1.308 0	cubic yards		1 cubic yard	0.764 555	m³
			CAPACITY			
1 L	1.759 755	pints		1 pint	0.568 261	L
1 L	0.879 877	quarts		1 quart	1.136 522	L
1 L	0.219 969	gallons		1 gallon	**4.546 090**	L
			MASS			
1 g	0.035 273 96	ounces (avdp)		1 ounce (avdp)	28.349 523	g
1 g	0.032 150 75	ounces (troy)		1 ounce (troy)	**31.103 476 8**	g
1 kg	2.204 62	pounds (avdp)		1 pound (avdp)	**0.453 592 37**	kg
1 kg	0.001 102 3	tons (short)		1 ton (short)	**907.184 74**	kg
1 t	1.102 311	tons (short)		1 ton (short)	**0.907 184 74**	t
1 kg	0.000 984 21	tons (long)		1 ton (long)	**1016.046 908 8**	kg
1 t	0.984 206 5	tons (long)		1 ton (long)	**1.016 046 908 8**	t
			CONCENTRATION			
1 g/t	0.029 166 6	ounce (troy)/ ton (short)		1 ounce (troy)/ ton (short)	34.285 714 2	g/t
1 g/t	0.583 333 33	pennyweights/ ton (short)		1 pennyweight/ ton (short)	1.714 285 7	g/t

OTHER USEFUL CONVERSION FACTORS

1 ounce (troy) per ton (short)	20.0	pennyweights per ton (short)
1 pennyweight per ton (short)	0.05	ounces (troy) per ton (short)

Note. Conversion factors which are in bold type are exact. The conversion factors have been taken from or have been derived from factors given in the Metric Practice Guide for the Canadian Mining and Metallurgical Industries, published by the Mining Association of Canada in cooperation with the Coal Association of Canada.

Exploration Technology Development Program of the Board of Industrial Leadership and Development

Summary of Research 1985-1986

---

edited by
V.G. Milne[1] and R.B. Barlow[2]

[1] Director, Ontario Geological Survey, Toronto.
[2] Section Chief, Geophysics/Geochemistry Section, Ontario Geological Survey, Toronto.

Grant 039 — Single Receiver, Frequency Scanning Fixed Source Electromagnetic System

A. Rogozinski

Androtex Limited, Mississauga

ABSTRACT

During the last decade the search for mineral deposits has tended toward greater depths and more complex geological environments, and consequently interest in electromagnetic methods using large fixed source transmitter loops considerably increased.

The development of a single sensor receiver is a new version of the Turam fixed source electromagnetic method, which is based on the automatic frequency scanning Elfast system. Instrumentation consists of:

- high power transmitter with stabilized output current, programmable frequency pattern and cycle time synchronized with receiver,
- microprocessor–controlled digital receiver provided with solid state memory and serial port for transferring recorded data to the field computer,
- down hole logging attachment adapted to the receiver.

The measurement of the two parameters, amplitude and phase of the electromagnetic field can be made at any combination of five frequencies, 25, 75, 225, 675 and 2025 Hz. Due to automatic cycling time programmed individually for each frequency, internal data recording, simplicity of operation, and portability of the receiver, considerable improvement in productivity and cost effectiveness is possible.

The new system provides much better capabilities in terms of flexibility in the field and accuracy of measured parameters, as well as significant improvement in down hole logging surveys. Moreover, parametric and/or geometric sounding by varying the frequency and/or distance from the transmitting loop is simplified.

Surveys with the new single sensor receiver Turam system provided with memory bank for recording measured parameters can be carried out by one operator only, rather than the present two man crew, further increasing field productivity and cost effectiveness.

INTRODUCTION

In its standard version the Turam electromagnetic method consists of a large fixed transmitting source and two receiver coils which are moved in tandem at a fixed separation. To assure coherence, measurements of amplitude and phase of the electromagnetic field at each sensor are made in the gradient mode, i.e. in the form of field strength ratios and phase differences.

In the latest developed Turam system, based on advanced electronics, the receiver operates with single coil and memory, so that measurements at each frequency are directly compared with previous readings. Coherence is maintained by means of constant amplitude of an energizing electromagnetic field and a high stability of transmitted frequencies. This is achieved by a stabilized transmitting current–amplitude to 0.1%, and presynchronized temperature–compensated crystal–controlled frequency clocks in the transmitter and receiver to have a phase tolerance of 0.1°.

Considerable improvement in the accuracy of the measurements, particularly at large distances from source and lower frequencies, are due to the high power of a new transmitter as well as stable output current and frequencies. Also, two–channel asymmetry in the receiver has been removed. The analogue input signal is transferred and processed in digital form (stacked), further improving the signal to noise ratio.

Particularly in down hole surveys, the single sensor receiver overcomes many problems that have, until now, limited application of frequency domain drillhole measurements using the Turam method, mainly due to the errors resulting from the variable distance and different conditions (temperature) between logging probe and reference sensor located at the surface; furthermore, the large values of phase differences and amplitude ratios with increasing depth. A new system with single sensing coil receiver overcomes the above mentioned problems, and accurate amplitude as well as phase measurements are obtained, independent of depth.

INSTRUMENTATION

To ensure proper operation of the system with single coil receiver, the transmitting loop must be energized with a stable current at each frequency providing a constant electromagnetic field throughout the survey. Variation of the transmitting loop parameters or ground resistance when galvanic mode is used, as well as change of input voltage from motor generator set, have to be compensated by the transmitter's current regulator.

Accurate phase measurements are accomplished by using high stability temperature–compensated crystal–controlled presynchronized clocks in the receiver and transmitter.

TRANSMITTER

The high power transmitter consists of three solid state relays acting as the main ON/OFF switch at the input of the three–phase transformer. Secondary is connected to six silicon controlled rectifiers which are operating as high efficiency current regulators by means of phase modulation. The output voltage via LC filter supplies the main output converter connected in bridge configuration. Current in the input and output is monitored by protection circuits to disconnect output power in case of excessive input voltage, overload or open loop. Output current is also connected to control module providing synchronized phase control of main current regulator. Low power section of the transmitter is microprocessor controlled and consists of oscillator synchronization circuits, programming of output frequencies and cycle time module, and communication system with receiver during data transfer to the receiver. The processor also monitors standby battery voltage and protection circuits.

Output frequencies can be pre–set at any combination for a given duration of time from 5 to 60 seconds in 5 second increments. Usually the lower the frequency, the longer stacking time at receiver will be required to maintain the same accuracy of measured values at each frequency.

The transmitter is provided with separate "Sync" output for connecting the receiver to synchronize both clocks, transfer the timing and frequency preprogrammed parameters and to power–up the receiver. When both units are connected as shown on Figure 039.1 and self test routines are completed, a ten minute warm–up time for both oscillators is required, which is indicated by a countdown timer at the receiver. After acknowledging clocks synchronization, the frequencies and duration times can be programmed at the transmitter. When data are verified by the transmitter and receiver display indicates "READY", then the "Sync" cable can be disconnected.

Changes in parameters are not possible without connecting both units via the "Sync" cable to protect pre–set program.

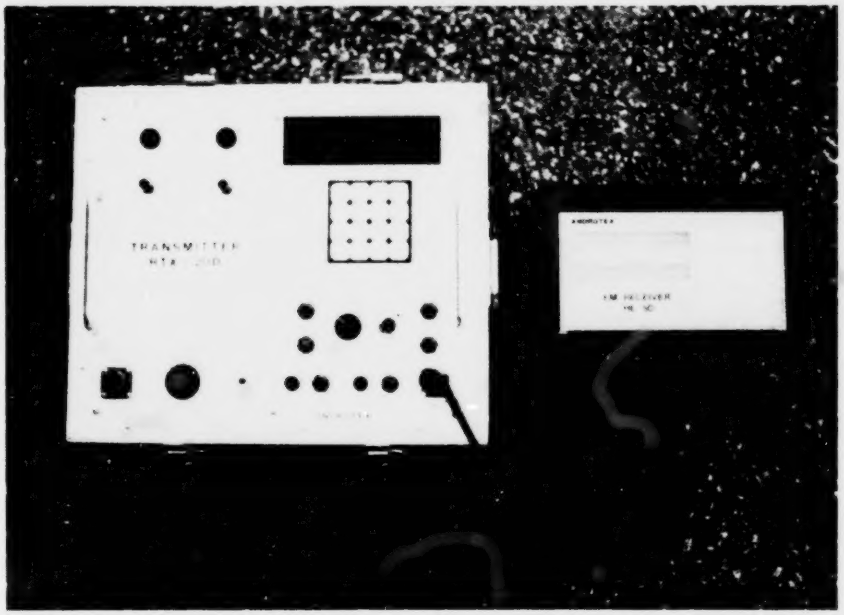

Figure 039.1. Synchronizing receiver with transmitter.

To guarantee continuity of full synchronization with the receiver, when, for any reason, the motor generator stops operating, an internal standby rechargeable battery automatically takes over supply of all digital circuits; i.e. crystal oscillator, programmer and timer system. Thus, both units will still be in initial synchronization and do not require corrections. Even if the output power is turned off by a signal from the protection circuitry (overload, open loop, etc.) additional synchronization is not needed. After a period of approximately 2–1/2 hours, the timer disconnects the standby internal supply system and the transmitter's clock stops.

All diagnostic values, such as input or output voltage current, frequencies, cycle time and faults indicated by protection circuits, are displayed on a 16 character LCD module, giving the operator a clear indication of the transmitter's state of operation.

RECEIVER

The initial idea of the single sensor receiver shown on Figure 039.2 incorporates high sensitivity, simplicity of operation, solid state memory as an internal data storage, portability and low power consumption. The receiver design is based on the same type of 8 bit low power CMOS type microprocessor as the transmitter.

The main console consists of a low noise input amplifier, active band–pass high–Q filter, analogue to digital conversion section with signal processing circuitry, stacking module incorporating surge and excessive noise features, microprocessor unit with ROM memory, RAM memory, as a data storage, interface with the keyboard, display and frequency–cycle duration board. Synchronization of the internal clock incorporates digital phase–lock loop.

The serial port RS232C similar to the one in the transmitter allows two way communication between receiver and transmitter during synchronization of both units, programming and later data transfer to the field computer. Sensor's sensitivity with automatic gain control amplifier in steps of four and frequency setting are controlled by microprocessor in main console in serial mode via interconnecting shielded cable.

Control processing unit – CPU controls all receiver functions. Simple operation using 4 by 4 keyboard minimizes data entry, mainly due to software subroutines. Continuous communication with operator is indicated on a dual 16 character dot matrix LCD display which allows readings of "Present" and "Previous" results from the last station for verification. Both parameters, i.e. amplitude and phase are shown. An operator can also preset, in increments of 0.1%, tolerance of measured values individually at any time.

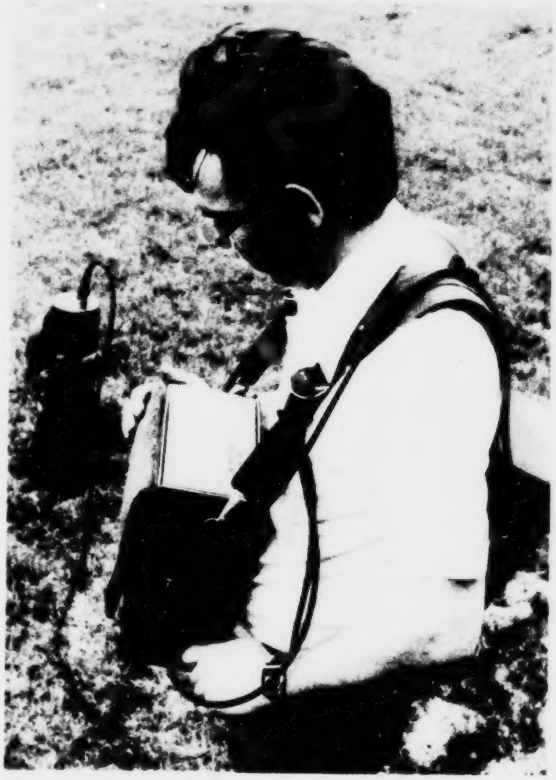

Figure 039.2. Receiver HL–50 with sensor.

When measurements are completed and are in the range of preset tolerance at first position, a station number will automatically advance according to the preprogrammed "Step" station separation. The operator is also able to repeat measurements by erasing an existing record in the memory using "Repeat" key, return to the previous station – "Back", recall measurements stored in the memory – "Recall" or change "Step" – station separation forward or back at any time.

An internal real time clock is also built in and recorded at each reading throughout the entire survey. Access to date or time change requires key–in of password.

All above mentioned functions give an operator full control of measured results during the sur-

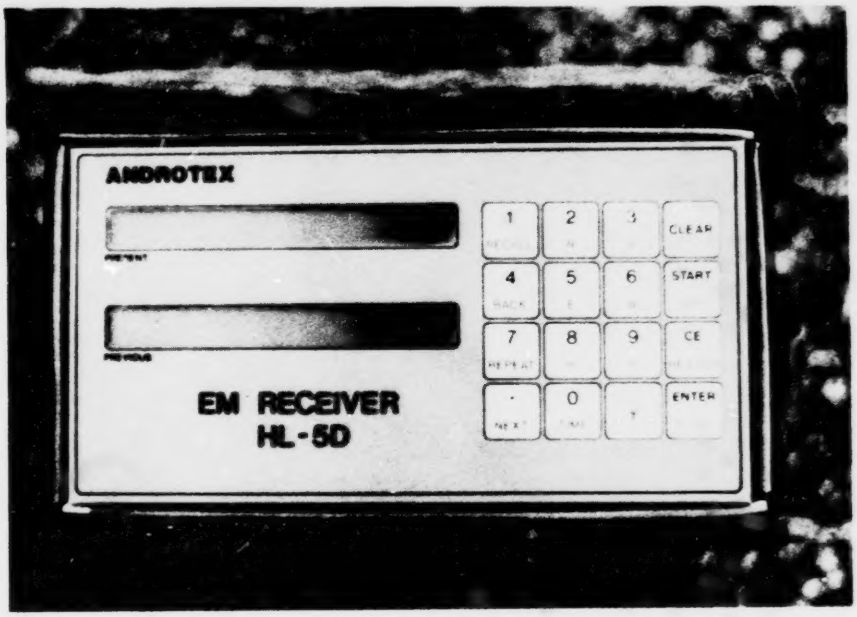

Figure 039.3. Front panel of single sensor receiver.

vey as well as flexibility in terms of station separation, direction of the survey and tolerance of measurements.

The receiver front panel is shown on Figure 039.3.

A rechargeable battery, as a power source is placed in separate compartment at the back of the operator (Figure 039.2).

DOWN HOLE LOGGING ATTACHMENT

The down hole attachment shown on Figure 039.4 consists of a measuring probe, cable and winch. Sensing coil, low noise preamplifier with automatic gain control and transmission circuitry are driven from receiver console and are included in probe assembly. The receiver's microprocessor controls sensitivity setting and frequency.

The probe is powered from the receiver's main battery and is connected to the same input as the sensing coil used for surface surveys.

Supply, control and measured signals are sent using standard two wire shielded cables reinforced with kevlar.

CONCLUSIONS

A newly developed single sensor version of the Turam fixed large source electromagnetic exploration system combines improved field productivity, simplified data processing and plotting, features high spatial resolution and conductivity discrimination, as well as greater exploration depth capabilities. In down hole logging surveys it provides consistent accuracy independent of depth.

By minimizing operator's involvement during the survey, and because of its flexibility and simplicity of operation, the new instrumentation has become a highly cost effective exploration system.

ACKNOWLEDGMENTS

The company is grateful to the Ontario Geological Survey for their support of this project.

REFERENCES

Rogozinski, Andrew

1984: Grant 039 Single Receiver, Frequency Scanning Fixed Source Electromagnetic System; p. 61 - 65 in Exploration Technology Development Program of the Board of Industrial Leadership and Development, Summary of Research 1983 - 1984, edited by V.G. Milne and R.B. Barlow, Ontario Geological Survey, Miscellaneous Paper 120.

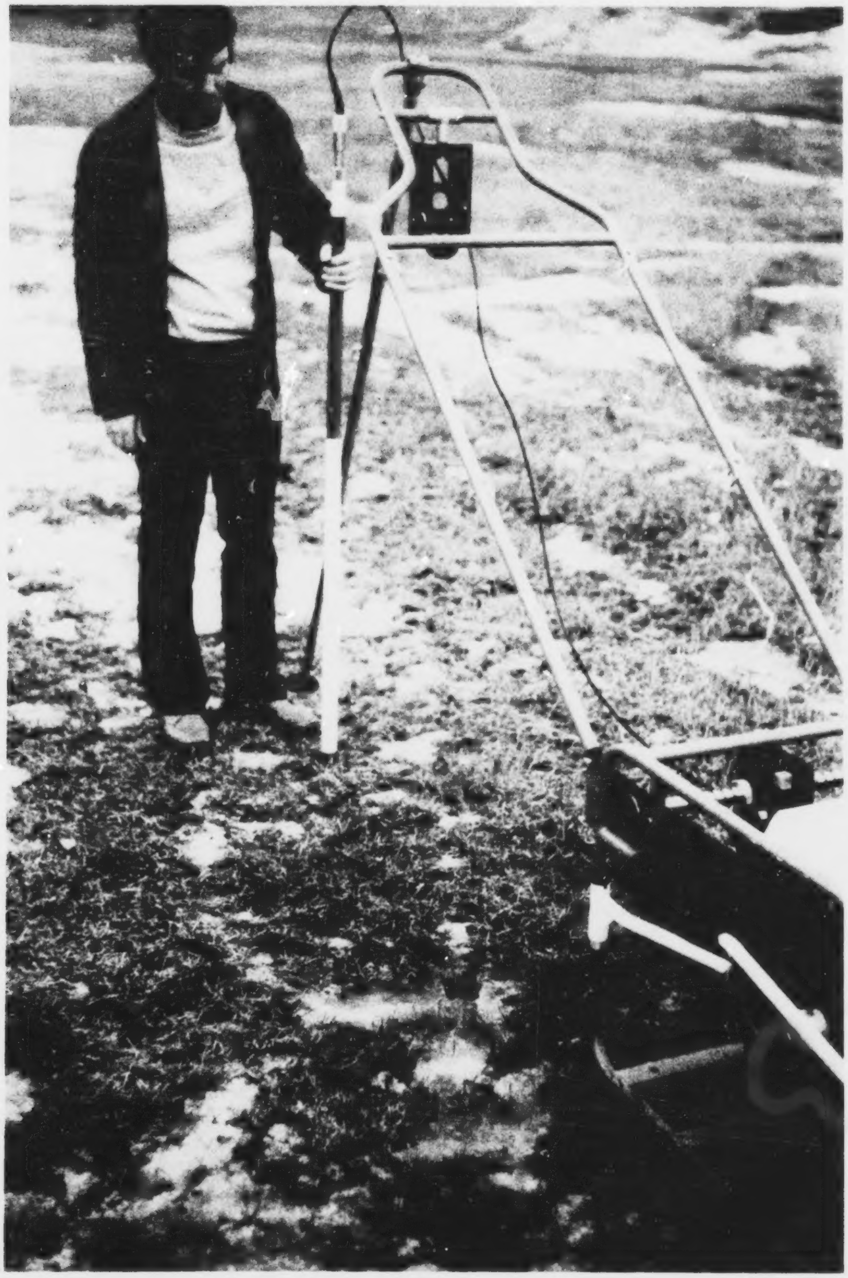

Figure 039.4. Downhole logging attachment DHE-100, winch with probe.

Grant 052 — Production of a Seven–Frequency Helicopter Electromagnetic System

Paul Wessler

Geotech Ltd., Markham

ABSTRACT

During 1985 – 1986 Geotech has continued to refine the EMEX–2 seven–frequency system. Numerous design parameters have been revised since work was originally begun in late 1983, resulting in totally new printed circuit boards and improved system performance.

In keeping with the advancement of EM technology, Geotech is continuing to expand on the capabilities of the seven–frequency system by incorporating the latest techniques developed by Geotech for other projects. Original design frequencies covered the range from 190 Hz to 12 kHz transmitted on three coil geometries. During 1986, Geotech has successfully demonstrated the ability to further extend this frequency range from an ultra low 45 Hz to an upper level in excess of 50 000 Hz. HEM systems can thus be configured to suit virtually all of our clients' applications.

A laser altimeter and bird motion monitors have been successfully installed and tested in our EMEX series of airborne exploration systems. Survey flying that has been done to date shows it is feasible to incorporate these ancillary devices internal to all of our EM systems. Qualitative measurements of bird motion and accurate sensor terrain clearance information are thus available for the first time to aid in post–flight data processing. Through the addition of the laser and motion sensors, it is now possible to use HEM systems for such unique applications as sea–ice thickness measurements.

The addition of an accurate bird sensor height measurement extends the usefulness of the HEM system into areas of groundwater exploration in arid areas as well as airborne bathymetry over coastal waters. The seven–frequency system with its three coil geometries and broad frequency spectrum will be ideally suited for areas of complex geology typical of many of the gold–bearing areas of Ontario.

INTRODUCTION

In 1981 Geotech Ltd. began development of a "state–of–the–art" helicopter–towed Electromagnetic Exploration System. This work culminated the following year in the successful field trials of the system. The EMEX–1 four–frequency system is currently being flown in Canada by independent contractors serving the mining community. Since the inception of this development program, Geotech has become heavily involved in new applications of airborne EM technology beyond those of mineral exploration and mapping. The seven–frequency EMEX–2 system development has allowed us to cross fertilize this latest technology into other areas of engineering endeavour. The EMEX–2 system is currently being offered for sale at the international level complete with a suite of interpretation software.

The seven frequencies have been arranged in such a fashion as to provide widely spaced frequencies transmitting on three independent coaxially coupled coils, two horizontal coplanar coils (whaletail) and two vertical coplanar coils (fishtail). All coils are maintained with an 8 m coil separation, although other coil separations are possible on special order. The coil geometry is represented pictorially in Figure 052.1. The removable transmitter and receiver modules are contained in a 9 m Kevlar composite shell. Geotech has produced its own custom designed mandrel for the production of these bird shells in order to maintain a consistent mechanical integrity. The unique construction of the 9 m shell has been tested to demonstrate adequate strength and dimensional stability while at the same time providing weight savings that are critical in helicopter work. Only one prototype 9 m bird has been produced and test flown to date. Results have shown that the mechanical integrity of the structure is satisfactory to obtain airborne noise levels better than 2.0 ppm.

The following nominal frequencies are incorporated into the standard system (upper frequency available to 32 kHz):

1. 190 Hz horizontal coplanar (whaletail)
2. 870 Hz horizontal coplanar (whaletail)
3. 380 Hz vertical coaxial
4. 918 Hz vertical coaxial

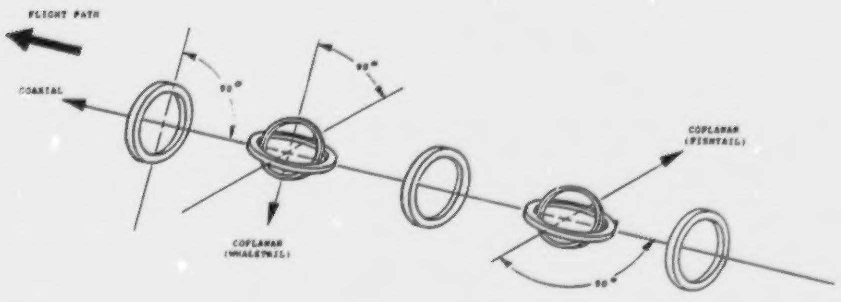

Figure 052.1 Pictorial representation of coil geometry.

5. 2200 Hz vertical coaxial
6. 5000 Hz vertical coplanar (fishtail)
7. 12 000 Hz vertical coplanar (fishtail)

Note that the selection of coil orientation allows for three coaxial geometries that can be nominally tuned for any frequency within the range of 190 Hz to 12 kHz. This also applies to the whaletail and fishtail configurations. As an example of the versatile nature of the design, the whaletail coils could be configured with operating frequencies of 190 Hz and 5000 Hz. The only restriction on the final selection of the frequencies is that the harmonic relationship between transmitter frequencies must be considered for coils having similar geometries.

Thus 14 channels of geophysical information are provided by the EMEX–2 System, along with power line monitors for each frequency should they be required. This configuration of frequencies and coil orientations should provide specific information in areas where the geology was previously unknown. Post–flight processing of this large amount of data can accomplish overburden stripping, multi–layered earth interpretation and resistivity mapping, along with dip and strike interpretations. Optional are laser altimeter and bird motion detectors.

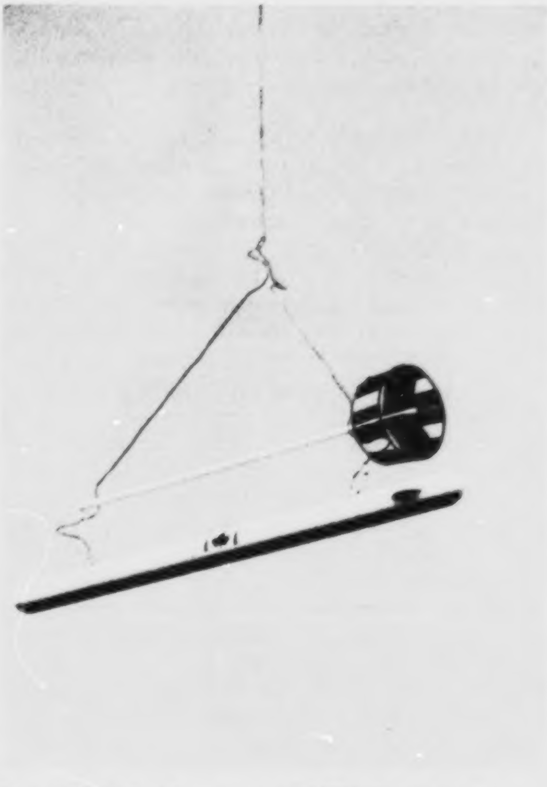

Figure 052.2. Nine metre EMEX–2 prototype bird in flight.

Figure 052.2 shows the 9 m EMEX–2 prototype bird in its normal flying attitude. Note that the low frequency transmitter coil protrudes beyond the extremities of the main Kevlar shell. Since Geotech uses only air core coils, in order to achieve the dipole moments that are required to overcome atmospheric noise in the low end of the frequency spectrum, the cross sectional area of the low frequency (less than 150 Hz) coils must be increased. Optionally if the transmitter current were increased to achieve the required NIA, the overall capability of the helicopter to supply the required power would become a limiting factor. The EMEX–2 system has been designed for small helicopters such as the Astar 350 D.

INSTRUMENTATION DEVELOPMENT

Client feedback has demonstrated the need for a wider range of transmitted frequencies. The recent emphasis on gold exploration and structure delineation has produced the need for higher frequencies than were previously available. In keeping with this need, Geotech embarked on a program to provide a range of frequencies that should suit most geophysical applications, and was initially successful in producing a transmitter design that allows the efficient transmission of frequencies from 45 Hz to an upper limit of about 16 kHz. The possibility also existed to produce a transmitter coil system that could produce the required dipole moment at frequencies well beyond the current 16 kHz upper limit. A 32 kHz transmitting system was produced and successfully test flown in 1985. During 1986 continued development produced yet another new transmitter design that is capable of operating at frequencies in excess of 50 000 Hz. The use of this ultra high frequency has applications in sea–ice thickness measurements (Holladay et al. 1986) and other engineering applications, and in geological mapping (cf. Fraser 1979; Sengpiel 1983).

During 1986 Geotech performed a number of helicopter borne geophysical surveys that utilized various pieces of instrumentation that have been developed under this ETDF grant. The main EMEX–2 analog EM console modules have been flown under a variety of conditions during 1986. Bathymetry surveys have been conducted on behalf of the Canadian Hydrographic Service using some of the technology that was developed under this grant (Macdonald 1986). Figure 052.3 shows some of the results obtained off the coast of Nova Scotia in late 1985 over an extremely rough ocean bottom. The first field trials of this electromagnetic system were conducted over open ocean near Halifax with the help of Atlantic Region hydrographers from the Bedford Institute of Oceanography. A conventional survey by boat took three days: an HEM survey of the same area was done in three and a half hours, with encouraging results. Figure 052.4 shows a comparison of the Geotech Through

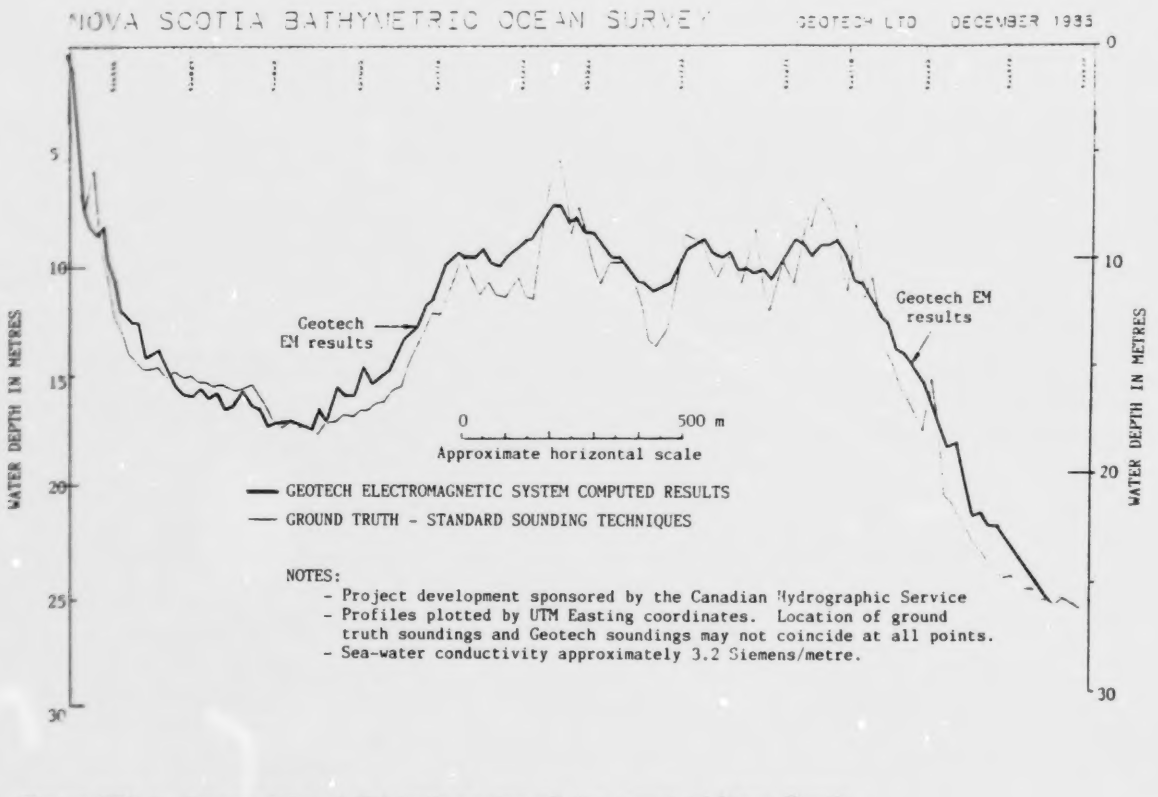

NOTES:
- Project development sponsored by the Canadian Hydrographic Service
- Profiles plotted by UTM Easting coordinates. Location of ground truth soundings and Geotech soundings may not coincide at all points.
- Sea-water conductivity approximately 3.2 Siemens/metre.

Figure 052.3. Comparison of EM bathymetry off the coast of Nova Scotia.

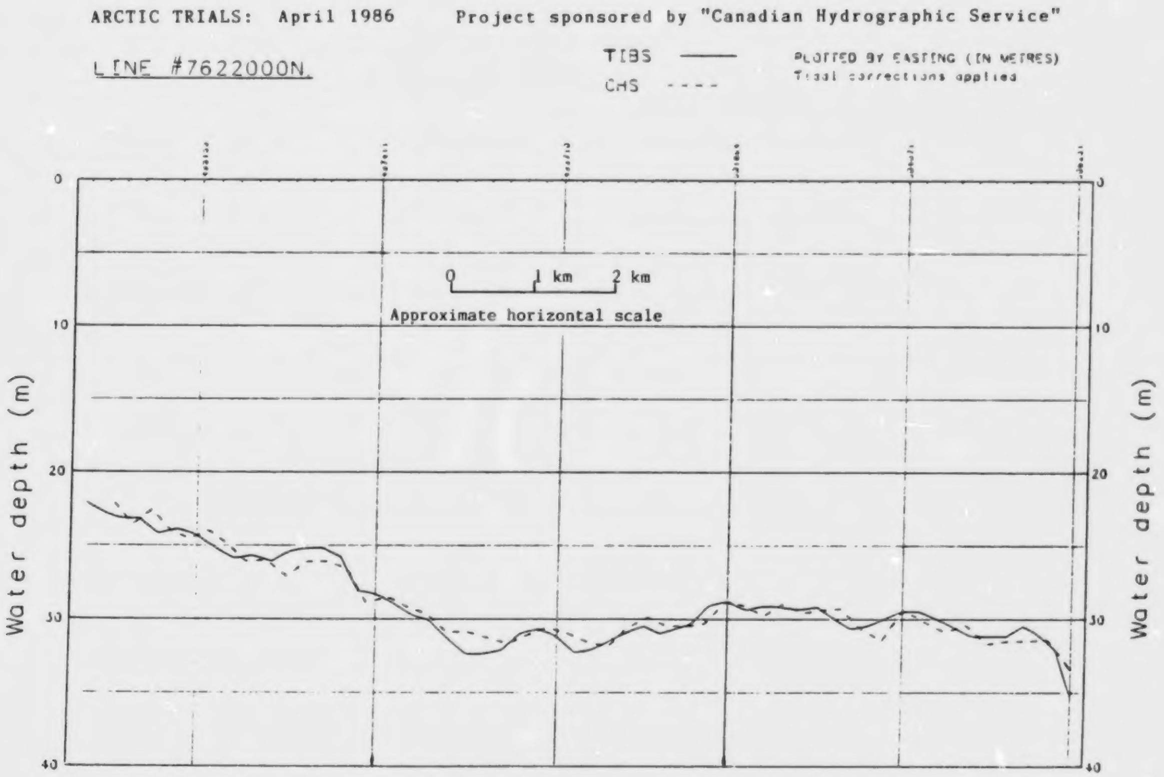

Note: Spatial shift may be due to navigation system positional errors.

Figure 052.4. Arctic bathymetry survey results comparison.

Ice Bathymetry System (TIBS) vs the ground truth provided by the Canadian Hydrographic Survey over a relatively flat ocean bottom in the Canadian Arctic. The excellent agreement of airborne data compared to conventional soundings has clearly demonstrated that new and unique applications of electromagnetic technology are forthcoming.

Figure 052.5 shows a computer–generated graph of the ability of an EM system to resolve sea–ice thickness. This graph shows the almost linear relationship between EM response and ice thickness for a range of frequencies. The addition of an accurate laser altimeter is necessary to achieve sea–ice thickness measurements. Appropriate selection of frequencies can provide information on water depth as well. The laser is used to detect the top of the ice while the EM system measures the bottom of the ice or the top of the water. Figure 052.6 is an actual plot of sea–ice thickness combined with sea–water bathymetry using the TIBS system. Data was obtained in the Canadian Arctic in April 1986. All information provided is reproduced with the permission of the Canadian Hydrographic Service.

In addition to the improvements that have been incorporated in the main console, a significant amount of effort has gone into the bird itself. Special attention has been given to reducing weight while at the same time maintaining the required integrity of the mechanical structure. Weight restrictions become quite severe at lower transmitter frequencies. Various techniques have been used to reduce the possibility of motion of the transmitter coils relative to the receiver coils and the bucking coils. Mechanical design for an EM system requires rigid coupling between the receiver and transmitter coils. A 1 ppm change in coil separation will result in a 3 ppm change in signal amplitude. Temperature gradients in excess of 10 degrees Celsius can be encountered from the start to

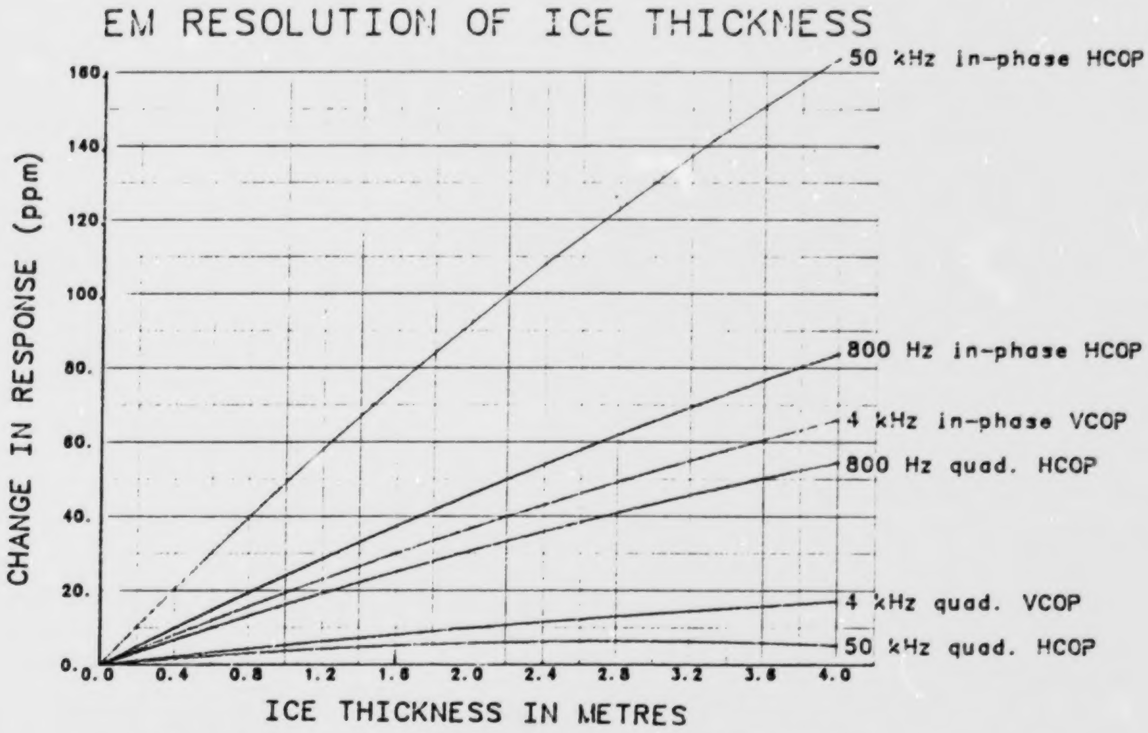

MODEL: Ice conductivity 0.02 S/m, Water thickness 10 m and cond. 3 S/m, bottom cond. 0.1 S/m. Flight height 30 m above ice surface.
EM SYSTEM: Transmitter-receiver separation 4 m, three EM frequencies shown here; VCOP = vertical coplanar configuration, HCOP = horizontal coplanar configuration.

Figure 052.5. Graph showing ability of EM to resolve sea ice thickness.

the end of a typical survey flight, thus the temperature coefficients of materials becomes important to the airborne performance of the system. Geotech has investigated the addition of temperature sensors within the bird to monitor and record transmitter and receiver coil temperatures as well as the ambient temperature that the bird experiences.

Complications for the electrical tow cable arise because of the addition of these extra sensors. Geotech's attention to detail in all aspects of bird design should result in improved performance. Additional airborne testing is required before the benefits of this effort can be finally assessed. It has been observed that the base line drift is somewhat dependent on the actual transmitter frequency as well as the coil geometry.

SOFTWARE DEVELOPMENT

As well as continuing to refine an automated method for the interpretation of multifrequency airborne EM data, Geotech is continuing to develop a suite of interpretational aids for the EMEX–2 System. A suite of phasor diagrams for all three coil configurations will be produced. These diagrams would take into account dipping plates of various sizes, spheres of various sizes, orientations, etc. Also to be developed is an overburden stripping program for the various coil orientations. Included will be such items as dip estimation, consideration of conductive host rock and estimation of body extent using profile information for all three coil geometries. These interpretation aids will be invaluable to the end user of the EMEX–2 System.

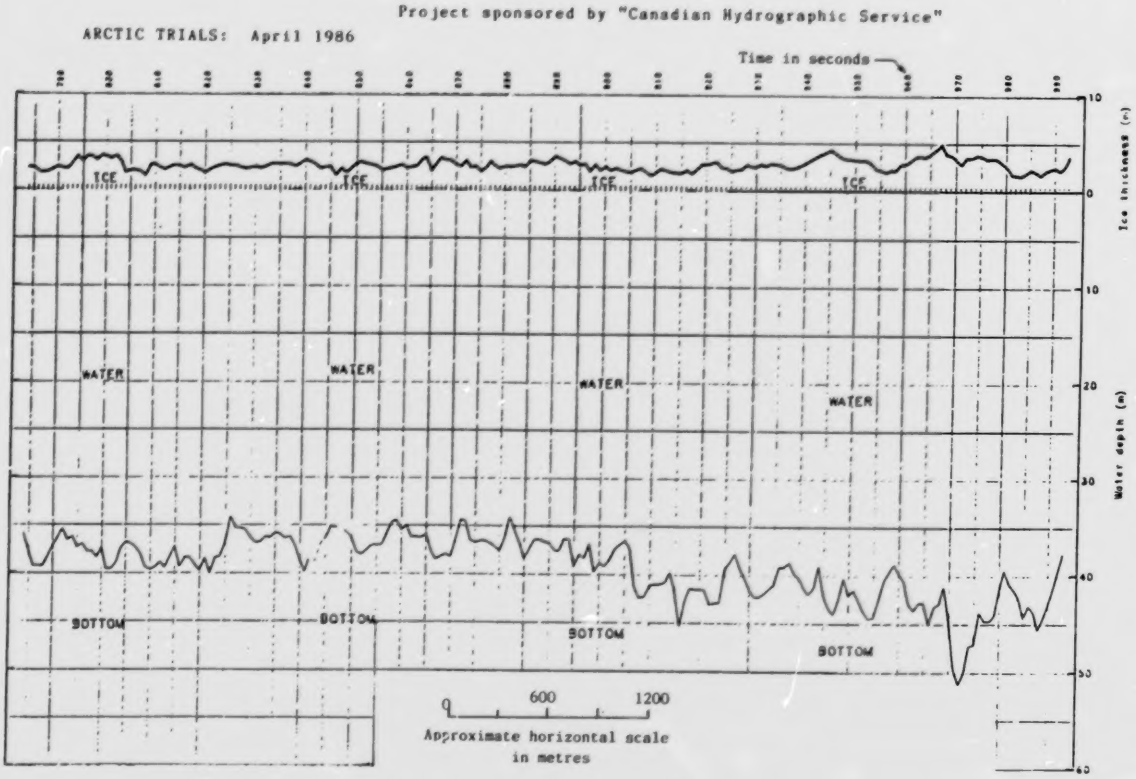

Figure 052.6. Example of simultaneous measurement of ice thickness and water depth.

Due to the overall interaction of interpretive software with raw field data, it is one of our goals to produce a completely digital receiver to replace the analog version that has been developed under this ETDF grant. We foresee the possibility of real-time processing of airborne geophysical data once this has been done. Realistically this latter phase of product development is still quite a few years off. Alternatively we will orient our forthcoming digital receiver to the possibility of telemetering airborne data directly to a ground based computer for field processing of results. Both of these techniques will be complemented by the total system package that would be configured for our client's requirements.

FUTURE PLANS AND CONCLUSIONS

It was hoped that as part of this Grant 052 that Geotech would execute a small airborne survey over known geological targets within Ontario. To date this has not occurred. It is our intention to complete the final development of the seven frequency system and execute the required field testing program. This will be done in conjunction with other flying programs that we presently have scheduled for the coming year. It is also hoped that through the coming years the EMEX-2 system with its full complement of seven independent frequencies operating on three different coil geometries will be operating totally under software control.

The EMEX-2 System has been reasonably well documented, with the production of complete artwork and associated schematics as required. Attention must now be paid to the total HEM survey package including such items as data acquisition systems, radar altimeters, and electronic navigation system integration.

This analog version of the EMEX-2 seven-frequency helicopter electromagnetic system will find immediate application in Earth science applications that extend beyond the more traditional mineral exploration surveys for which the system was originally designed. Geotech will continue to attempt to advance and expand the variety of engineering applications of helicopter–borne survey systems.

We at Geotech feel that the ETDF program has been invaluable to our company. Without this type of funding, our company would not have been able to undertake a system development such as the EMEX–2 Seven Frequency HEM System. Through programs such as the ETDF program, the funds provided will continue to keep Ontario, and indeed Canada, in the forefront of geophysical instrumentation and services throughout the world.

REFERENCES

Fraser, D.C.

1979: The Multicoil II Airborne Electromagnetic System; Geophysics, Volume 44, p. 1367–1394.

Holladay, J.S., Valleau, N. and Morrison, E.

1986: Application of Multifrequency Helicopter EM Surveys to Mapping of Sea–Ice Thickness and Shallow Water Bathymetry; *in* Airborne Resistivity Mapping, edited by G.J. Palacky, Geological Survey of Canada, Paper 86–22, in press.

Macdonald, G.

1986: Airborne Electromagnetic Bathymetry System; *in* Proceedings of 5th Biennial International Symposium, Hydro '86, Southampton, England, Dec. 1986.

Sengpiel, K.

1983: Resistivity/Depth Mapping with Airborne Electromagnetic Survey Data; Geophysics, Volume 48, p. 181–196.

Grant 058/101 — Portable Broadband Multiple Geometry HEM System

R.L.S. Hogg

Aerodat Limited, Mississauga

ABSTRACT

A "multi–geometry, broadband" helicopter electromagnetic system has been developed by Aerodat Limited and preliminary flight testing began in March 1986. The transmitter consists of two concentric coils, 6 m in diameter; one with its axis vertical, the second with its axis in the direction of flight. The receiver, located at the centre of the transmitter loops, consists of 3 orthogonal coils to measure secondary magnetic field strength as well as direction. Both the transmitter and receiver are mounted in a bird towed 30 m below the helicopter. The two transmitter loops are energized with a transient pulse on a time shared basis to provide contrasting inductive geometries of the primary field with the underlying geology. The mark/space ratio as well as the pulse length of the primary field transient is digitally controlled to provide a variable bandwidth.

INTRODUCTION

Aerodat began the development of the HEM system in 1983 with ETDF support. The development of the transmitter and general system design were reported in the 1984 Summary of Research, Grant 058. In 1984, work continued on both bird design and the receiver. In 1985 the bird was built and test flown and the receiver largely completed.

The overall objective of the research program was to develop a button–on helicopter EM system with the following features:

1. wide response band.
2. 2 axis transmitter.
3. 3 axis vector receiver.

The first objective was met with a transient or pulse methodology. The second two objectives required a radical bird design.

SYSTEM DESIGN

BROADBAND CHARACTERISTICS

The resistivity of the ground typically varies over many orders of magnitude, from highly conductive sulphides and graphites through less conductive electrolytic conductors such as faults and shears to poorly conductive bedrock lithologies. Airborne systems originally evolved with the rather narrow band requirements of massive sulphide detection, but inductive electromagnetic systems can be made capable of a more generalized mapping application. To be effective for a wide range of geologic targets, the system must be wide–band and able to energize a broad range of conductivities.

The foundation of a broadband HEM system is the transmitter; it must radiate power over a wide range of frequencies. For a transient or pulse system, the high frequency content is governed by the sharpness of the pulse truncation and the low frequency content by the pulse duration. The abruptness of pulse termination is limited by the power of available electronic switching devices and the pulse duration by the practical consideration that the helicopter is moving and the observation must be completed within a fraction of a second.

The Aerodat waveform is illustrated in Figure 058.1. The pulse duration TON has a minimum duration of 730 microseconds but may be extended to any length by a digital control. The pulse truncation is fixed with a fall from 200 amperes to zero in 70 microseconds. In conductive terrain,

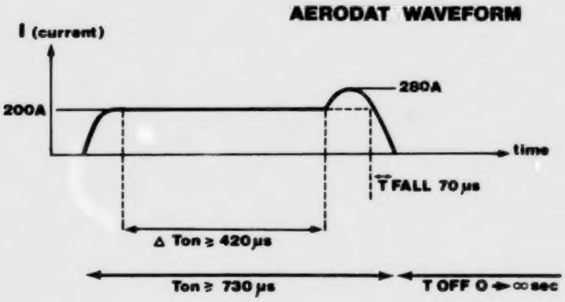

Figure 058.1. Aerodat transmitter current pulse waveform.

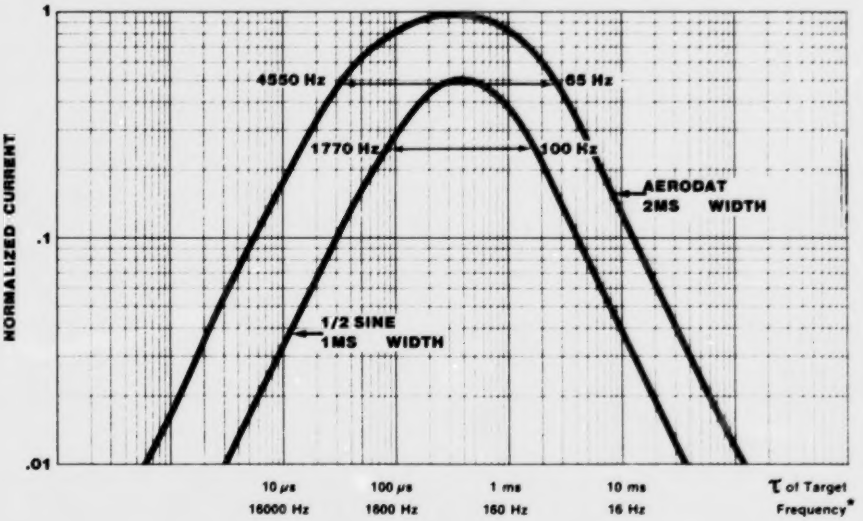

Figure 058.2
Peak current (at pulse termination) plotted as a function of target time constant τ for both the Aerodat waveform as well as a 1/2 sine waveform. The frequency* values shown are equal to 1/2 π τ.

the pulse duration may be lengthened to increase the low frequency response. Alternatively in resistive terrain, the pulse may be shortened to increase the pulse repetition rate with an ensuing increase in the signal to noise ratio for the higher frequency content.

A transient electromagnetic system induces a current to flow in the geologic target. The secondary magnetic field is directly proportional to the amplitude of this current and is a measure of the response band of the system. A ground target may be approximated by a simple R–L circuit (resistive inductive loop).

The time constant τ of such a target is equal to L/R; and hence the rate of decay of the secondary field increases with increasing resistivity. The starting value of the induced ground current immediately following pulse truncation, is significant as an indicator of the potential signal to noise ratio. In Figure 058.2 the induced ground current is plotted as a function of τ for the Aerodat waveform as well as for the 1/2 sine pulse. Using the relationship

$$\frac{WL}{R} = 1$$

for the centre of the response band of an L–R circuit, the related frequency is also indicated. Arbitrarily defining the principal response band as the zone within 50% of peak amplitude, a bandwidth of 65 Hz to 4550 kHz is indicated. Useable signal will certainly exceed these limits, however, actual limits will only be identified after flight testing.

The receiver consists of 3 orthogonal antennae with the input from each handled independently. The voltage induced in the receiver coils is integrated to provide a measure of the secondary field rather than its derivative, this reduces the dynamic range of the output and reduces the dependence of signal amplitude on the τ of the target. The receiver averages the signal over a series of widening time gates in a conventional fashion. Tests to date have indicated that the earliest time gate may start in the vicinity of 50 microseconds.

MULTI–GEOMETRY CHARACTERISTICS

The adjective "multi–geometry" is used to describe the incorporation of two transmitter axes with three receiver axes. The two transmitter axes, one aligned in the direction of flight and the other vertically are operated on a time–shared basis. The ground is energized from two directions, completely avoiding potential blind spots and allowing the geometrical form of buried targets to be interpreted with minimal ambiguity. The advantage of the two transmitter coils is analogous to the improvement in three dimensional shape recognition than can be achieved when an object can be illuminated from different directions.

The receiver is located at the centre of the transmitter, this places both transmitter and receiver in the closest proximity to the ground providing optimum spatial resolution. The symmetry of the configuration also ensures that the response is the same on reciprocal flight line directions.

In order to provide an indication of what may be expected from the system, computer modelling has been carried out using the University of Toronto Plate program. Figures 058.3a, b, c and d illustrate the response in six arbitrary time channels for a conductive plate, 300 m in strike length by 150 m in depth extent. In each illustration, the top row is for the transmitter axis aligned in the direction of flight and the bottom row for the vertical axis transmitter. The graphic amplitudes of the profiles have been normalized.

A thin sheet is characterized by a response peak over the conductor for the TxRx combination and a null for the TzRz coil combination, as illustrated in Figure 058.3a. As the dip changes from vertical, Figure 058.3b, the same peak and null persists; however, a pronounced asymmetry of the TxRz, TzRx and TzRz profiles develop, thus providing an excellent interpretive dip indicator.

In Figure 058.3c, the conductor is flat lying and edge effects are pronounced in early channels. In the later channels and the central zone of a wider conductor, the TxRx and TzRz combination settle down to a similar response form and constant amplitude ratio.

In Figures 058.3a, b and c, the conductor axis was perpendicular to the flight direction and no response is generated in the Ry receiver. Figure 058.3d illustrates the sensitivity of Ry to strike direction and its potential benefit for interpretation.

BIRD CHARACTERISTICS

The design of a bird for the system was a major undertaking. The optimum antennae for a sharp pulse truncation with large dipole moment is a single turn loop of large area. A practical limit of 4 turns and a 6 m diameter was set for the bird. Design work was carried out by a team of aeronautical engineers associated with the University of Toronto, Institute for Aerospace Studies. Computer modelling was followed by wind tunnel testing of a selected design. Aerodynamic stability with minimum weight and drag were the key objectives.

Construction of the bird began in the summer of 1985 and was completed in March 1986. The bird is made up of 4 ring sections with cross members supporting the central receiver pod.

The main elements of the structure are 4 inch diameter fibreglass tubes with specially reinforced joints. The transmitter cable is fastened, in formed channels, on the outside wall of the pipe. A fairing to reduce drag is added over the pipe sections.

Test flights were carried out in late March 1986 at Cherry Beach in Toronto. The bird was flown at speeds ranging from 30 km/h to 180 km/h and no instability was noted. Drag was minimal and will be less than that introduced by the tow cable. Figures 058.4a, b and c illustrate the bird in flight.

The assembly of the receiver was not yet complete at the time of the test flights and hence only the aerodynamics have been verified to date. It is expected that the fully operating system will be completed this summer and comprehensive testing of the total system begin thereafter.

RESULTS AND FUTURE PLANS

The design, fabrication and independent testing of the major elements of a new multi–geometry wide band HEM system have been completed and a fully operational system is anticipated in the near future. The system is expected to provide comprehensive information for exploration and mapping in a wide variety of geological environments.

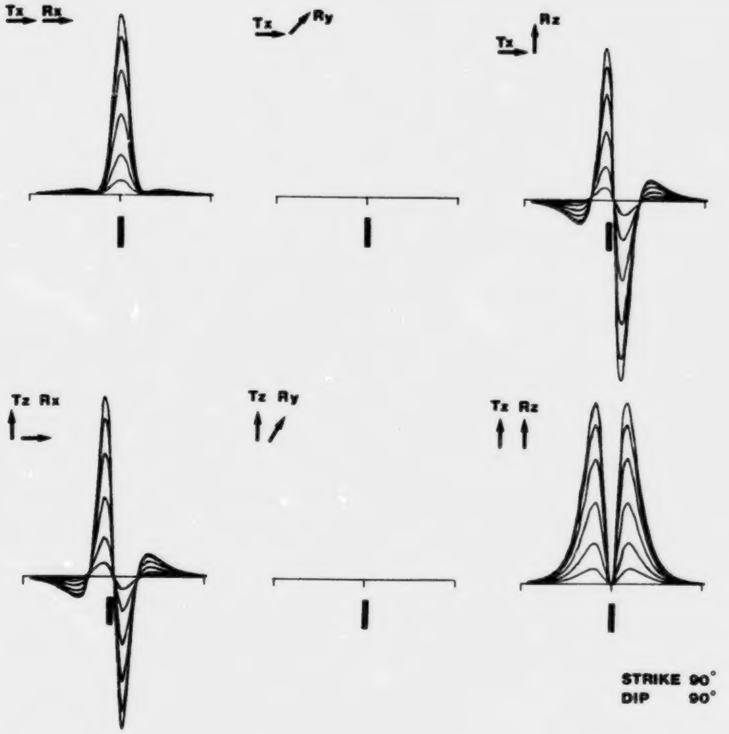

Figure 058.3. Normalized response profiles over a 300 x 150 m conductive plate for 6 arbitrary time gates, rnodelled by the University of Toronto Plate Program.
(a) Strike 90°, dip 90°.

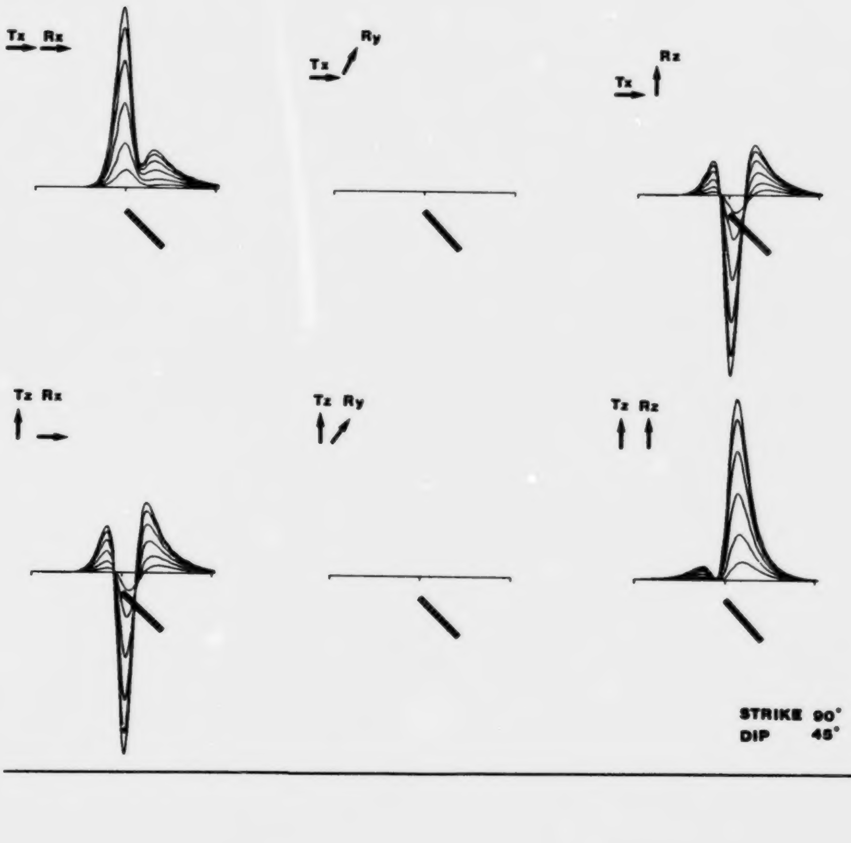

Figure 058.3 (b). Strike 90°, dip 45°.

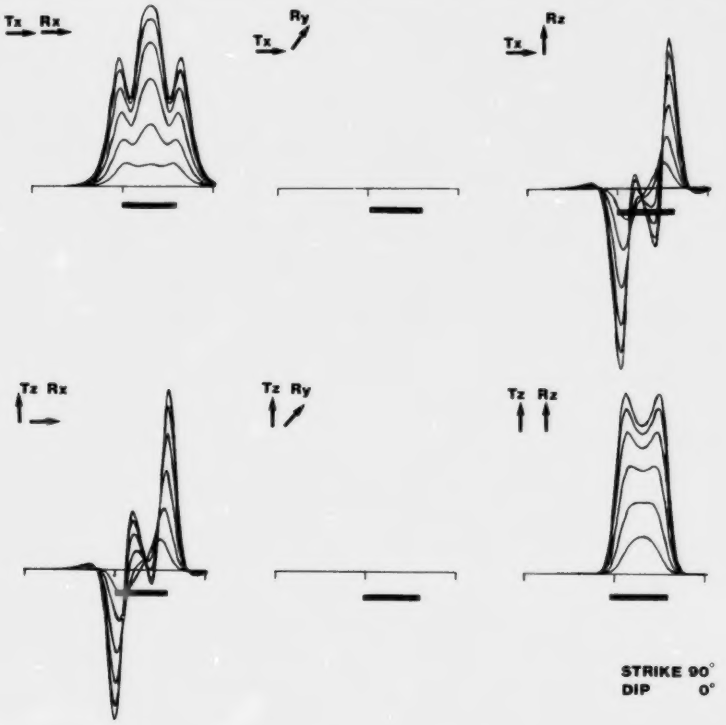

Figure 058.3 (c).
Strike 90°, dip 0°.

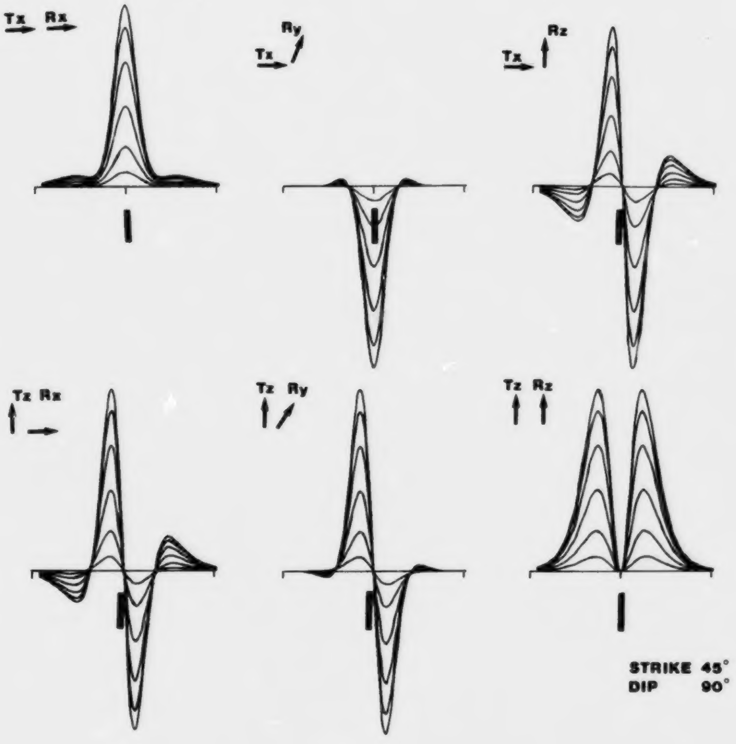

Figure 058.3 (d).
Strike 45°, dip 90°.

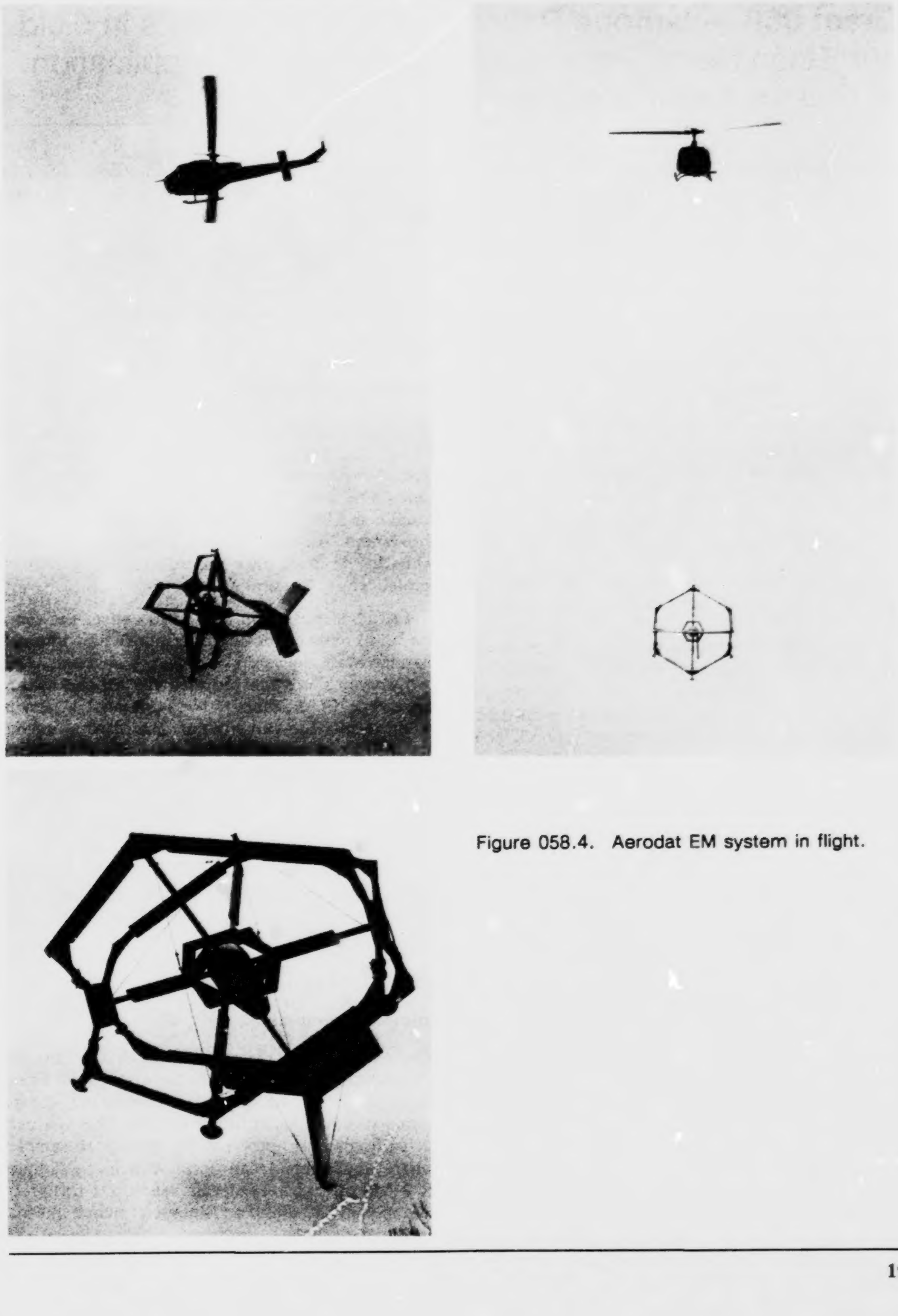

Figure 058.4. Aerodat EM system in flight.

Grant 068 — Isotope Ratios and Trace Elements in Gold and Base Metal Occurrences in Ontario: An Application of Plasma Mass Spectrometry

E.J. Brooker and T.E. Eagles

X–Ray Assay Laboratories, Don Mills

ABSTRACT

The plasma mass spectrometer has been referred to as the greatest advance in analytical spectroscopy since the introduction of inductively coupled plasma. In the late spring and early summer of 1984 the first commercial plasma mass spectrometers became available. The objective of this research program is to assess the potential of the plasma mass spectrometer for solving analytical problems relevant to exploration and mining activities in Ontario.

INTRODUCTION

Inductively coupled plasma mass spectroscopy (ICP–MS) has been available as a commercial instrument since mid 1984. This instrumentation combines the superior sensitivity of inductively coupled plasma atomic emission spectroscopy (ICAP) with the isotope capability and simple spectra of mass spectroscopy. Inorganic mass spectra tend to be quite simple with very predictable interferences. (The profusion of molecular species of argon, oxygen, chlorine and sulphur make it more difficult to interpret the ICP–MS spectra and often degrade the detection limits.) Nevertheless the detection limits are still superior to conventional ICAP. Elements with isotopes above mass 80 are not as seriously affected by this problem.

Recent modifications in the quadrupole mass spectrometer and in the ion optics have greatly enhanced the capabilities of this instrument. The introduction of a new lens system has greatly reduced the swings in sensitivity experienced in earlier versions of this instrument. In addition to the improved stability the drifting that still occurs tends to be in the same direction – that is, the sensitivity of all elements will tend to drift upward or downward in time. Thus it is possible to do analysis using internal standards. Our experience and those of other users (J.W. McLaren, National Research Council, Ottawa, personal communication, 1985) indicates that the best internal standard has a mass very similar to that of the isotope being analyzed. Improvements in the multichannel capabilities of the software have improved the quality of isotope ratios.

In this report consideration will be given to applications of ICP–MS to determine rare earth, platinum group elements and lead isotope ratios. A brief discussion of multi–element analysis will also be provided.

INSTRUMENTATION

All experimental work was carried out on an ELAN 250 inductively coupled plasma mass spectrometer manufactured by Sciex, Thornhill, Ontario. The nebulizer is a Meinhard C–type. The torch is the long style which was delivered with the instrument. All three argon gas flows are regulated with Brooks mass flow controllers. All gas flows quoted are at atmospheric pressure.

A peristaltic pump is used to deliver the sample and to pump the drain. Samples and internal standards are delivered on separate channels. The two channels are merged at a tee on the instrument side of the pump. No additional action is taken to mix the two streams. Standard additions are also made using the second channel. Sample uptake on each channel is about 1 ml/min. Unless stated otherwise plasma power is 1.1 kilowatts, plasma gas 14 litre/min, auxiliary gas 2 litre/min and nebulizer gas 1 litre/min.

Data was transferred to a DEC PDP 11–44 via the printer port of the instrument computer. Data reduction was done using custom built Fortran and Basic programs.

EXPERIMENTS AND RESULTS

Internal Standards

The ability to do isotope analysis has eliminated one fundamental problem in the application of internal standards, namely the possibility that the internal standard exists in the sample. This is a particularly difficult problem in geological samples where any element can occur in a given sample. ICP–MS offers a very elegant solution to this problem namely the use of an isotopic enriched internal standard.

TABLE 068.1. OXIDE AND ISOTOPES INTERFERENCE FACTORS.

Element	Int.	STD	10^{-N}	Apr 24	Apr 25	May 6	May 8	May 9	May 12	May 22
^{151}Eu	^{137}BaO	G	3	2.38	6.73	6.68	7.29	5.40	4.79	5.74
^{159}Tb	^{141}PrO	G	5	7.00	8.27	7.07	6.61	6.97	5.92	6.67
	^{143}NdO	I	2	3.84	4.51	4.20	4.22	4.51	4.78	4.22
^{160}Gd	^{140}CeO	H	5	1.15	1.53	1.69	1.56	1.68	1.83	2.22
	^{143}NdO	I	2	6.44	7.11	6.02	6.40	6.34	5.32	5.85
	^{147}SmO	H	3	0.663	3.41	1.89	2.19	1.94	2.75	2.96
	^{163}Dy	G	2	9.33	9.64	9.02	9.06	9.17	8.89	9.19
^{163}Dy	^{143}NdO	I	5	5.61	5.14	5.00	5.08	5.06	4.25	4.96
	^{147}SmO	H	3	5.26	8.52	2.27	2.69	5.34	5.90	2.37
^{165}Ho	^{147}SmO	H	3	5.25	6.18	3.28	2.49	4.37	1.77	3.41
^{167}Er	^{147}SmO	H	5	1.05	1.25	0.669	0.509	0.892	0.362	0.696
	^{157}EuO	H	3	0.433	1.29	0.889	0.360	0.162	0.196	0.295
^{169}Tm	^{157}EuO	H	3	1.31	1.29	0.646	0.785	0.646	0.523	1.43
^{174}Yb	^{160}GdO	I	2	2.20	2.53	1.98	1.87	1.96	1.64	1.70
	^{163}DyO	G	5	2.90	3.80	1.39	1.79	1.62	1.42	1.35
	^{177}Hf	F	3	7.56	6.56	8.59	9.32	9.72	9.06	8.09
^{175}Lu	^{159}TbO	H	2	2.15	2.38	1.91	1.80	1.95	1.60	1.83
	^{160}CdO	J	5	2.87	3.27	2.59	2.44	2.56	2.14	2.27

Provided the isotopic ratios of the internal standard are known for the sample, the counts obtained can be corrected for those coming from the sample itself. For the majority of elements these ratios are known to several significant figures and are the same for samples collected anywhere on the earth. This technique has been employed throughout this work. In each case the apparent isotopic ratio has been determined experimentally at the beginning of the sample run rather than using established ratios. This eliminates the problem of lens and quadrupole mass discrimination.

Rare Earth Elements

For these experiments 0.5 g of sample was digested in 30 ml of 1:1:1 H_2O, $HClO_4$ and HF in a teflon beaker. The digest was taken to dense fumes of $HClO_4$ then made up to 50 ml with 10% HNO_3. A 1 ml aliquot was further diluted to 10 ml in 10% HNO_3, resulting in a final dilution factor of 1:1000. Plasma conditions were selected to reduce oxide formation. The following plasma conditions were used: RF power 1.15 kilowatts, plasma gas 14 litre/min, auxiliary gas 2 litre/min and nebulizer gas 0.9 litre/min. It was found that these conditions reduced rare earth oxide peaks to less than 4% of the parent peak.

At the beginning of each run a series of 5 mixed rare earth solutions were run. The elements in each solution were selected so that there were no oxide or isobaric overlaps. These solutions were used to calculate isobaric and oxide interferences. These factors are presently determined daily. Table 068.1 shows typical values for these factors determined over a period of several weeks. Once enough information has been accumulated, it should be possible to predict these factors from a few representative solutions which would be run daily.

Table 068.2 lists the isotopes analyzed along with potential oxide and isobaric interferences. The rare earths were separated into two groups for calibration purposes. These groups were made up so that no member of the group produced a significant interference on any other member of that group. The two groups are labelled A and B in Table 068.2. The two internal standards used were ^{125}Te on the low mass side and ^{196}Pt on the high mass side. Standards were run periodically throughout the sample run. Ten repeats of 1 second/element were carried out. The total sample throughput was 13 samples/hour. After the data had been collected it was transferred to the main laboratory computer via the printer port of the instrument computer.

Concentration numbers were produced by an in–house computer program which calculated the interference factors from the interference standards run at the beginning of the run. These factors are in turn used to correct the counts obtained for each isotope. The magnitude of the corrections are stored in the computer memory and are converted to concentrations and displayed on the final output. The standard deviation from the ten 1 second repeats are also converted to concentration units and displayed on the final output. The final output includes the concentration, an estimate of the precision and the magnitude of any known interferences.

TABLE 068.2. ISOTOPES USED FOR RARE EARTH ANALYSIS.

Element	Mass	Standard	Interferences
Ba	137	B, G	
La	139	A, G	
Ce	140	A, H	
Pr	141	A, G	
Nd	143	A, I	
Sm	147	B, H	
Eu	151	A, H	BaO
Tb	159	B, H	PtO, NdO
Gd	160	B, J	Dy, CeO, NdO, SmO
Dy	163	A, G	NdO, SmO
Ho	165	A, J	SmO
Er	167	B, J	SmO, EuO
Tm	169	B, I	EuO
Yb	174	A, H	Hf, GdO, DyO
Lu	175	A, I	TbO, GdO
Y	89	B	
HF	177	F	
Te-Io	125		
Te-II	128		
Pl-II	195		
Pl-Io	196		

Both a high mass and a low mass internal standard are run. Once the data has been reduced the results from the standard analyzed throughout the day are considered in selecting the more effective internal standard. The success of an internal standard varies slightly from day to day. The general trend is that the low mass standard is very good for the low and middle mass rare earths while the high mass internal standard or an average of the low and high result works best for the high mass rare earths (^{165}Ho and up). During a typical sample run from 4 to 6 hours it is found that the internal standards compensate for any instrument drift. The calibration curve is based on the average corrected count rates obtained throughout the run. On occasions, when instrument drift could not be corrected by internal standards, the data set was broken into smaller subsets and re-analyzed. In a sense the instrument was recalibrated using software.

Table 068.3 shows the mean of 10 replicate analysis of SY2 and SY3. The second column shows the percent relative standard deviations for this study. The high standard deviation for Eu reflects the uncertainty in the BaO correction to the isotope.

Platinum Group Elements

The platinum group elements were extracted from 25 g samples using the nickel sulphide procedure (Hoffman 1978). The sulphide precipitate obtained by this procedure was dissolved in 10 ml of aqua regia and diluted to 25 ml. The samples were analyzed using ^{151}Eu as an internal standard. The isotope analyses are given in Table 068.4. There are no interfering peaks. It should be noted that ^{102}Ru has a NiAr+ interference such that 1000 ppm Ni produces an interference of 2 to 4 ppb Ru. It should be noted that a number of argon–metal molecular species might cause interference with the calibration lines selected. The metals must be present in concentrations in excess of 1000 ppm to be a serious problem. Cobalt, copper and zinc are three potential problem elements. Fortunately these elements are unlikely to be found in the solution in sufficient concentration to be of concern.

TABLE 068.3. REPLICATE RARE EARTH ANALYSES USING ICP-MS.

	SY2			SY3		
	ICP-MS	Rel. STD	Other	ICP-MS	Rel. STD	Other
La	75.1	1.6	73–88	1336	6.3	1350–1365
Ce	169	1.8	164–210	2114	5.5	2290–2435
Pr	21.7	1.8	21	225	5.4	239–255
Nd	86.9	2.3	70–80	756	4.7	760–821
Sm	16.6	3.5	15–16.5	116	3.9	126–134
Eu	2.1	8.0	2.4–3	17.0	5.6	16–18
Tb	3.2	4.3	2–3	19.7	3.7	15–23
Gd	17.8	3.1	17	113	3.2	117–123
Dy	22.1	2.1	20–21.3	131	4.2	138–151
Ho	4.7	3.0	5	28.1	2.6	29–30
Er	15.2	3.6	12–16	85.3	2.6	88–96
Tm	2.5	5.1	2–2.6	11.8	3.5	12–13
Yb	18.5	2.7	17–18.4	69.6	2.7	71–75
Lu	3.1	4.7	3	8.7	3.0	8.6–10
Y	109	3.0	126–131	615	4.5	716–740

TABLE 068.4. ISOTOPES ANALYZED FOR PLATINUM GROUP ELEMENTS.

Element	Mass	Element	Mass
Ru	99	In	193
Rh	103	Pt	195
Pd	105	Au	197
Re	185	Eu–IO	151
Os	189	Eu–II	153

Lead Isotope Ratios

It has already been mentioned that the sensitivity of the instrument is a function of mass. These small changes in sensitivity result in the isotopic ratios determined by ICP–MS being slightly different from the true isotopic ratios. Previously the authors (Brooker and Eagles 1985) suggested a correction procedure which involved periodically running a certified standard. A correction factor was generated using the observed and certified ratios. These factors were used to adjust the observed ratios.

This procedure had two major disadvantages, namely, the large number of extra control samples required and the blind extrapolation of control factors between standards. In addition the large error on the 204/206 ratio was compounded by the large error on the 204/206 correction factor. Recent work which resulted in sample on–line internal standard addition, has lead to the trial of an internal standard approach to calibrate the efficiency of the quadrupole mass spectrometer.

The element selected as an internal standard for lead isotopes is thallium. Thallium has two isotopes of mass 203 and 205. The relative abundance of these isotopes are 29.524 and 70.476 respectively. Since thallium is not fractionated, the true ratio for any thallium solution should be $^{205}Tl/^{203}Tl = 2.38707$. Any deviation from this ratio can be attributed to mass discrimination by the quadrupole. If the pass efficiency of the quadrupole is defined as E_0 at mass 203 and if it is assumed that the efficiency changes linearly with mass then the change in efficiency with mass is given by equation 1,

$$\gamma = \frac{E_{203}(r-R)}{2R} \tag{1}$$

where γ is the change in efficiency per unit mass from mass 203, r is the isotope ratio of thallium determined by the ICP–MS and R is true thallium 205/203 ratio (2.38707). Equation 1 can be used to generate the expressions given in equations 2, 3 and 4.

$$R_{\frac{204}{206}} = r_{\frac{204}{206}} \frac{(3r-R)}{(r+R)} \tag{2}$$

$$R_{\frac{207}{206}} = r_{\frac{207}{206}} \frac{(3r-R)}{(4r-2R)} \tag{3}$$

$$R_{\frac{208}{206}} = r_{\frac{208}{206}} \frac{(3r-R)}{(5r-3R)} \tag{4}$$

The advantage of this procedure is that these factors can be determined simultaneously as the lead isotope data is collected. It is not necessary to extrapolate correction factors in time or even to rely on a control sample where the potential of contamination is always a concern.

Multi–element Analysis

Under ideal conditions approximately 65 to 70 elements can be detected by ICP–MS. In fact the only elements that cannot be detected are those that fall very close to the main argon peak at mass 40 and a few elements that form negative ions in the plasma (F,S,Cl). In practice, the presence of molecular species often seriously degrades detection limits. Usually there is a secondary isotope which can be analyzed.

In single element analysis each of these problems can be considered separately and appropriate action taken. For multi–element analysis it is not possible to select the best set of conditions for each element. In addition, the interaction of all the elements must be understood before a reliable multi–element analysis can be produced. At the time of writing semi–quantitative multi–element analyses are being done at X–Ray Laboratories using ICP–MS.

The Sciex software is used to identify the major constituents of the sample and then the concentrations of these elements are determined on an individual basis. This procedure is labor intensive but as more data are accumulated a great deal of this burden can be shifted to a computer. One of the major problems is establishing reliable lower limits of detection. The approach currently being explored is to use multi–element standard addition at the 0.5 or 0.1 ppm level to determine if the spike can be distinguished from the background.

DISCUSSION

In the past year ICP–MS instrumentation has undergone some major changes. The new ion optic has dramatically improved the stability of the instrument. Not only has the stability improved but the residual drift is predictable in the sense that all elemental drift is in the same direction. Thus it is possible to use internal standards. The ability to use internal standards results in about an 80% improvement in efficiency over standard addition methods used in the past.

In this report two analytical problems were considered in detail. Both the rare earth element procedure and the platinum metal procedures have produced detection limits equal to or better than currently available techniques. However, it is sample throughput not detection limits where the most impact will be noticed. We have chosen to discuss two major developments but ICP–MS has been applied to a number of analytical problems. Some of the elements which have been successfully analyzed by ICP–MS are Sn, Gd, Ga, Tl, Th, U, In and Pb. In addition to this short list there are another 20 to 30 elements which have been determined on difficult samples where the conventional methods have failed.

The routine production of reliable lead isotopic ratios to a precision of 0.1% has not been accomplished. The technique described in the lead isotope section of this report offers the potential of producing accurate ratios but first the precision of the raw ratios must be improved. Our effort at this time is concentrated on improving the precision of the ratios.

ICP–MS is by no means the ultimate analytical tool for all elements in every sample. However, there is probably no other single method with as wide a possibility for applications as ICP–MS.

REFERENCES

Brooker, E.J. and Eagles, T.E.

1985: Isotope ratios and trace elements in gold and base metal occurrence in Ontario; p.23–28 *in* Exploration Technology Development Program, Summary of Research 1984–1985, Ontario Geological Survey, Miscellaneous Paper 125.

Hoffman, E.L.

1978: The Platinum Group Element and Gold Content of Some Nickel Sulphide Ores; unpublished Ph.D. Thesis, University of Toronto, Department of Geology, Toronto, Ontario.

Grant 072 — A Microprocessor-Based Digital Receiver Console for the DIGHEM$^{III/IV}$ System

S.J. Kilty

Dighem Surveys & Processing Inc., Mississauga

ABSTRACT

Dighem Surveys & Processing Inc. commenced work on the development of a digital receiver for its helicopter-borne EM system in December of 1983. This project has resulted in a system capable of providing high resolution, spheric-free electromagnetic data.

The basic premise of the system is high speed sampling and subsequent filtering of electromagnetic data which has undergone limited analog filtering. The system yields high resolution data which has had the high frequency noise removed.

INTRODUCTION

Dighem Surveys & Processing Inc. is a geophysical company specializing in helicopter-borne electromagnetics. Dighem has always been in the forefront of HEM technology as witnessed by its history of technological firsts, including DIGHEM^{I} (Fraser 1972, 1973), the first system to measure the three-dimensional electromagnetic field, and DIGHEM^{II} (Fraser 1978, 1979), which was the first system to utilize two orthogonal primary fields such that the system was coupled well to both vertical and horizontal conductors. In 1982, Dighem began a research and development program to upgrade the DIGHEM^{II} system to technology more appropriate to the 1980s.

In June of 1982, Dighem began the development of the DIGHEM^{III} system that featured a third coil-pair operating at 7200 Hz. This program was partially financed by the Exploration Technology Development Fund under Grant 025 (Kilty 1983). The DIGHEM^{III} development was completed by the end of March 1983. As a result of this program, Dighem is now operating four DIGHEM^{III} systems worldwide with three in North America and one that floats between Australia and Europe. The higher frequency of 7200 Hz has allowed Dighem to use the system for several new applications that include geological mapping for engineering purposes, resistivity mapping for the location of Extra Low Frequency military transmitter sites, bathymetric mapping, and geological mapping for the location of gold-bearing formations.

As a natural continuation of the DIGHEM^{III} program, we also developed a four coil HEM system with operating frequencies between 900 and 56 000 Hz. This program was partially funded by the Federal Industrial Research Assistance Program. This system is primarily used for engineering applications requiring the accurate inversion of EM data.

The above two programs were both oriented around the electromagnetic sensor: that is transmitting a primary field and measuring the resulting secondary field response. No attempt was made in these programs to improve upon the electromagnetic receiver electronics. The signal analysers utilized by all HEM companies are based on an original design by Barringer Research Limited in the 1960s. Since then, the analog processors have undergone upgrading in 1972 and once again in 1978 but have never been redesigned. As well, no attempt has been made to utilize an on-board microprocessor to enhance system response.

On December 1, 1983, Dighem commenced a program to correct this deficiency under a four-month seed grant from the Exploration Technology Development Fund.

This development program was defined in the Summary of Research 1984–1985 (Kilty 1985). The following is an update of the information presented in that publication.

THE DEVELOPMENT PROGRAM

HARDWARE DESCRIPTION

Figure 072.1 illustrates the digital receiver configuration. This two unit system consists of an integrated analog processor/primary nulling system and a Hewlett-Packard 1000, A600 series microcomputer. The analog front end is a custom designed unit manufactured by Dighem and the A600 is readily available from Hewlett-Packard agents worldwide. This combination allows for easy servicing and repair of the hardware under field conditions.

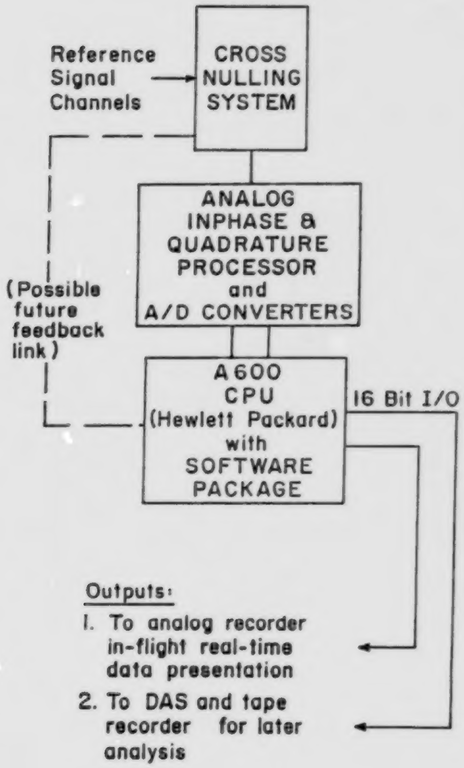
Reference
Signal
Channels
CROSS
NULLING
SYSTEM
ANALOG
INPHASE & QUADRATURE
PROCESSOR
and
A/D CONVERTERS
(Possible future feedback link)
A600
CPU
(Hewlett Packard)
with
SOFTWARE
PACKAGE
16 Bit I/O
Outputs:
1. To analog recorder in-flight real-time data presentation
2. To DAS and tape recorder for later analysis

Figure 072.1. Receiver console package.

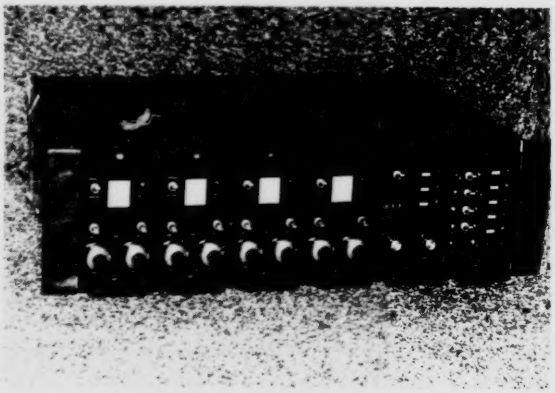

Figure 072.2. Analog console.

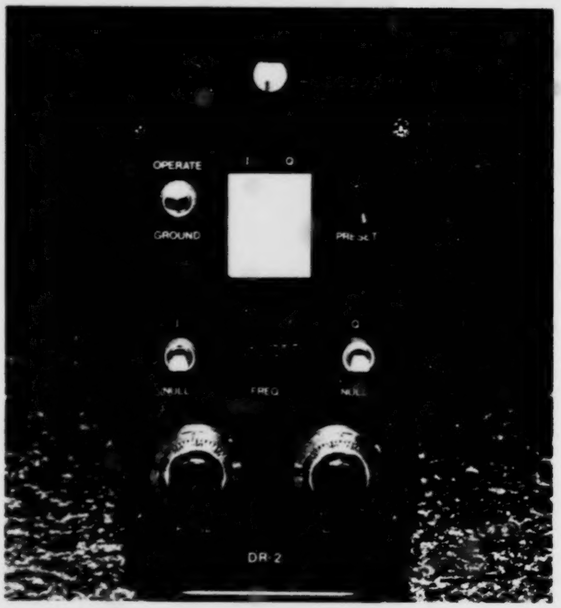
OPERATE
I
Q
GROUND
PRESET
I
Q
NULL
FREQ
NULL
DR-2

Figure 072.3. EM module.

ANALOG FRONT END

The analog section of the digital receiver project was designed in a modular fashion to allow for greater flexibility in a simplified design. The analog console contains an EM module for each frequency, a transmitter control unit and a system monitor (Figure 072.2). This packaging provides a direct link between the bird signal and the processing module, thus eliminating any possibility of the signal being affected by electromagnetic radiation as it passes through intermediate buffering.

The EM modules (Figures 072.3 and 4) have been redesigned with extensive use of large scale integration technology, especially with regard to the frequency dependent components. Care was taken to ensure that the system would be reliable and easy to use over a long period of time under harsh field conditions.

The most important changes in this design involve the analog filtering and the data output of the module.

Filtering within the module has been reduced from present industry rise–time standards of 0.1 – 0.5 seconds to 0.04 seconds. This rapid rise–time allows the resolution of short time events such as spherics, and virtually eliminates spectral overlap between such noise and valid EM anomalies. This increased sensitivity provides improved resolution with regard to bedrock anomaly definition.

Output of the modules includes two additional channels to monitor gain and phase of the primary field. These are used for real time control of long term drift. The primary field signal gain at the transmitter is monitored to detect any changes in the dipole moment due to small changes in current in the transmitter coil. The phase signal is monitored to measure any possible phase drift. Control of both gain and phase provides a far more stable output allowing more accurate and reliable calculation of resistivity values.

THE DIGITAL PROCESSOR

All six outputs from each module are transferred directly to a Hewlett–Packard 1000 microprocessor (Figure 072.5) via a 16 bit A/D converter at a sample rate of 100 Hz.

The digital operations performed on the data can be broken into three basic modes: calibration, survey and filter definition.

The first is the calibration mode where the electromagnetic base level and the system calibration (i.e., millivolts–to–ppm conversion) is carried out. Also, during this time period, the processor provides statistical information on the amount of spheric activity.

In the survey mode, the receiver acquires and processes the raw inphase, quadrature and primary field signals from the analog modules. At this point, several operators are applied to the data.

First, one second of incoming data from each of the 16 inputs is stored in a buffer for a total of 1,600 data points. The eight basic EM channels (inphase and quadrature from four coil–pairs) are first examined for spheric activity. Figure 072.6 illustrates a typical spheric after passing through the analog module. The 100 Hz sample rate allows the 70 millisecond wide pulse to be readily recognized and subsequently chopped. Following this, the EM channels are passed through a 81–point digital filter to remove unwanted high frequency content in the signal. Next, signal amplitudes are normalized relative to the primary field strength. This latter correction removes any long term drift caused by fluctuations in the dipole moment. That data stream is processed through a digital filter to eliminate all frequencies higher than 0.4 Hz. The resulting data stream is then sampled at 5 times a second, and these are sent to the recording devices. This data is recorded on magnetic tape and also displayed on a digital graphics plotter. This output is the normal field product.

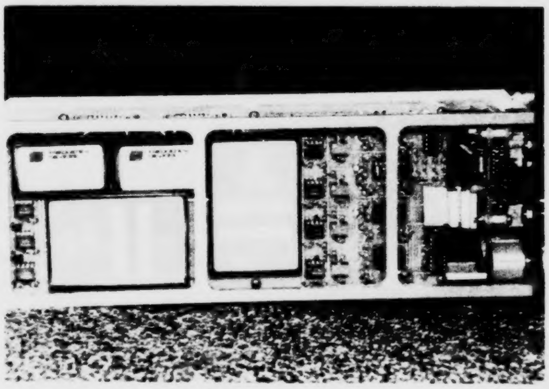

Figure 072.4. EM module.

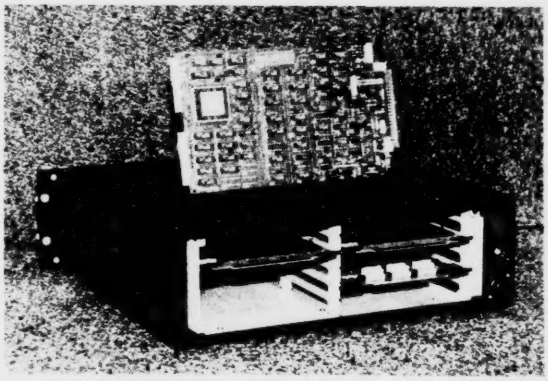

Figure 072.5. Microprocessor.

The filter definition mode allows modifications to the spheric rejection and filter operators. Here it is possible to modify the real–time filtering. It is anticipated that some changes will be made to filter routines as experience is gained when utilizing the system under survey conditions.

SURVEY EXAMPLE

Figure 072.7 shows the output of the digital receiver over the Night Hawk Lake geophysical test site (Barlow 1981). Illustrated here are four of the eight EM channels of the DIGHEM^{IV} system. These channels are the inphase and quadrature responses from the coaxial and coplanar coil–pairs

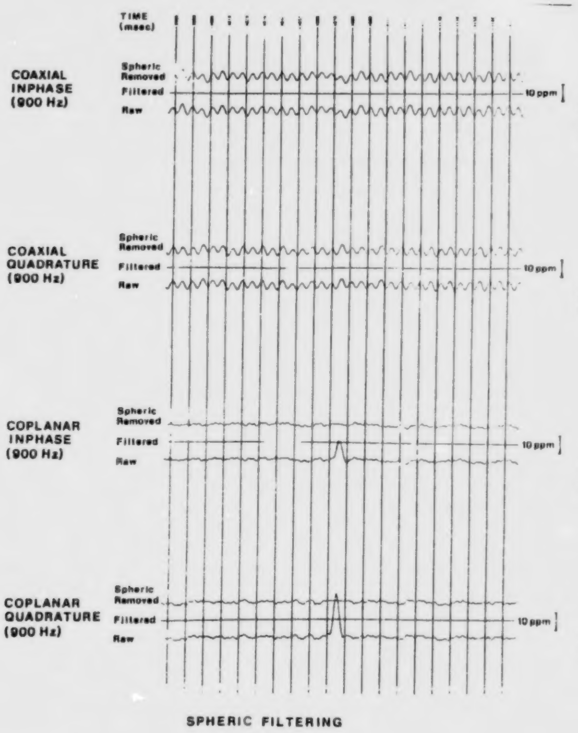

Figure 072.6. Spheric filtering.

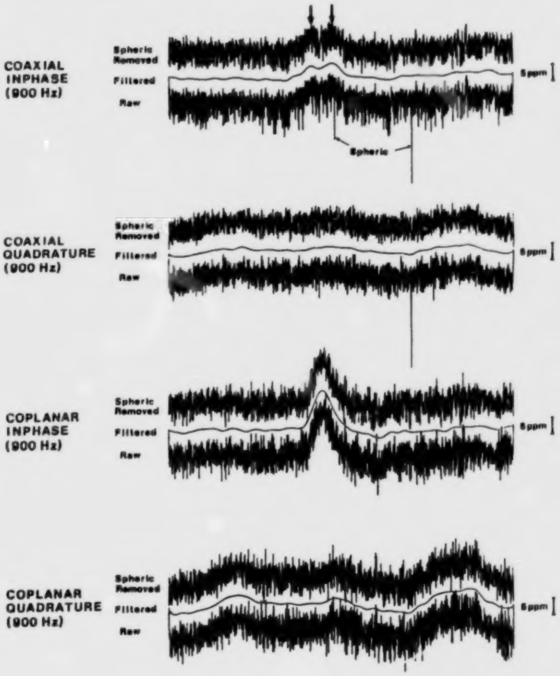

Figure 072.7. Digital receiver response over Night Hawk Lake test site.

operating at approximately 900 Hz. This profile shows the 100 Hz unfiltered raw data, the raw data with response from spherics clipped, and the final data after application of a filter operator for each of the four data channels.

The high frequency noise seen here is typical of EM data acquired with a fast rise–time, and includes beating of the approximately 900 Hz frequency which is transmitted on the two orthogonal coil–pairs. This noise is readily removed by digital filtering because its wavelength is considerably shorter than that of the desired signal. Of particular interest on this profile are the well defined double peak on the coaxial inphase channel over the Night Hawk Lake conductor and the ability to remove spherics without altering the shape of the anomaly.

DISCUSSIONS AND CONCLUSIONS

The majority of desired benefits expected to be derived from the digital receiver have been achieved. Figure 072.7 illustrates the improved signal–to–noise and increased resolution of the system. Improved ease of operation, reliability and increased stability can only be judged after extensive experience with the system has been obtained.

Extensive field trials are still being carried out to ensure the integrity of the data and to provide examples of system response over a number of varying situations. Data acquired to date has been evaluated and some modifications have been made to the processing hardware.

Major improvements have been made to the actual hardware. This has resulted in an electronics package that is inherently more stable and less prone to electronic drift. In addition, auto nulling and a much wider phase range have been incorporated to allow for various operating conditions.

REFERENCES

Barlow, R.B.

1981: Night Hawk Geophysical Test Range Results Using Two Electromagnetic Systems, District of Cochrane; p.152– 159 in Summary of Field Work, 1981. by the Ontario Geological Survey, edited by John Wood. O.L. White, R.B. Barlow, and A.C. Colvine, Ontario Geological Survey, Miscellaneous Paper 100, 225p.

Fraser, D.C.

1972: A New Multicoil Aerial Electromagnetic Prospecting System; Geophysics, Volume 27, p.518-537.

1973: Magnetite Ore Tonnage Estimates from an Aerial Electromagnetic survey: Geoexploration, Volume 11, p.97-106.

1978: Resistivity Mapping with an Airborne Multicoil Electromagnetic System; Geophysics, Volume 43, p.144-172.

1979: The Multicoil II Airborne Electromagnetic System; Geophysics, Volume 44, p.1367-1394.

Kilty, S.J.

1983: GR 025 The Development of an Omni-Directional Multi-Frequency Airborne EM System; p.99-105 in Exploration Technology Development Program of the Board of Industrial Leadership and Development, Summary of Research 1981-1983, edited by E.G. Pye and R.B. Barlow, Ontario Geological Survey, Miscellaneous Paper 115, 135p. Accompanied by 2 charts.

1984: GR 072 Microprocessor-Based Digital Receiver Console for the DIGHEM$^{III/IV}$ Helicopter Airborne Electromagnetic System; p.173-176 in Exploration Technology Development Program of the Board of Industrial Leadership and Development, Summary of Research 1983-1984, edited by V.G. Milne and R.B. Barlow, Ontario Geological Survey, Miscellaneous Paper 120, 176p.

1985: GR 072 Microprocessor-Based Digital Receiver Console for the DIGHEM$^{III/IV}$ Helicopter Airborne Electromagnetic System; in Exploration Technology Development Program of the Board of Industrial Leadership and Development, Summary of Research 1985, edited by V.G. Milne and R.B. Barlow, Ontario Geological Survey, Miscellaneous Paper 125.

Grant 079 — Seismic Full Waveform Logging and Seismic Geotomography

J. Wong

JODEX Applied Geoscience Limited, Toronto

ABSTRACT

Substantial progress has been made in the development of the crosshole seismic instrumentation as well as in the implementation of processing and display techniques for crosshole seismic data. The electronic and mechanical components of the prototype piezoelectric transmitter and multi-detector receiver subsystems have been built and assembled into a field-testable configuration. Hardware and software interfacing of these subsystems to a high-performance 16-bit microcomputer for system control and digital data acquisition has been achieved. Cross-correlation seismograms using PRBS references have been collected in a small-scale field survey. Clear P and S arrivals are observed, and the S arrival times have been used to create a color geotomograph of shear velocities showing the presence of a cavity between two boreholes. The full waveform logging system has been designed, and benchmark tests have been done in the laboratory to verify the major concepts. However, logger development has not advanced as yet to the point of in-hole testing.

INTRODUCTION

Crosshole seismic tomography is a procedure by which subsurface geology is imaged using information gained from transmission seismograms between boreholes (Wong et al. 1983). Successful implementation of the technique requires seismic instrumentation suitable for scanning between boreholes and computer-based algorithms for creating and displaying the images.

With support from the Ontario Geological Survey Exploration Technology Development Fund, JODEX Applied Geoscience Limited has undertaken to produce instrumentation and computer software which will make seismic geotomography easily accessible for application to a variety of geological and engineering activities in which detailing between boreholes may be important. As well, a high-frequency full waveform seismic logging system which operates within single boreholes is being designed and built for making *in situ* measurements of seismic rock properties. Such measurements can be correlated with core logging and will facilitate the interpretation of the geological significance of seismic geotomographs. More discussion on the reasons and goals of this project may be found in Wong (1985). The present report summarizes the progress made during the second year of the project, covering design and construction of equipment, implementation of computer software for system control and data analysis, and initial field results obtained with the prototype crosshole system.

INSTRUMENTATION

Figure 079.1 is a schematic diagram of the equipment designed for crosshole seismic scanning. Figure 079.2 is a photograph of the prototype system showing the desktop microcomputer, the surface electronics modules, and the downhole transmitter and detector probes.

The transmitter subsystem consists of a high-voltage driver module and a single downhole pie-

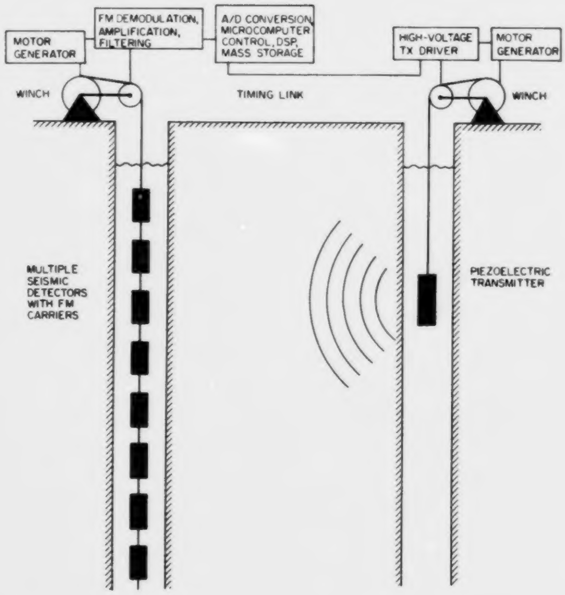
MOTOR GENERATOR
FM DEMODULATION, AMPLIFICATION, FILTERING
A/D CONVERSION MICROCOMPUTER CONTROL, DSP, MASS STORAGE
HIGH-VOLTAGE TX DRIVER
MOTOR GENERATOR
WINCH
TIMING LINK
WINCH
MULTIPLE SEISMIC DETECTORS WITH FM CARRIERS
PIEZOELECTRIC TRANSMITTER

Figure 079.1. Function blocks for the crosshole seismic scanning system.

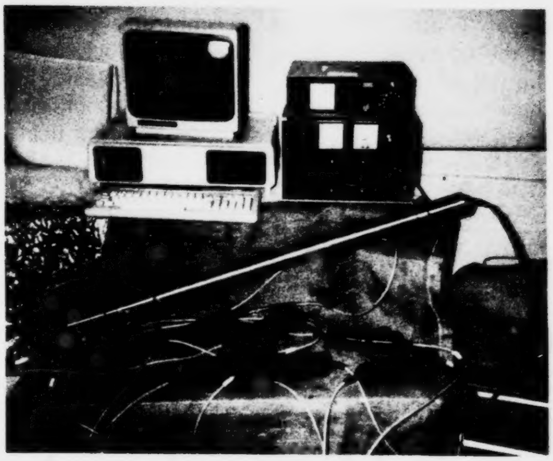

Figure 079.2. Components of the prototype crosshole seismic instrumentation.

zoelectric seismic source connected by a 500 m four–conductor cable on an electric winch. When high voltages are switched across the piezoelectric transducers, they generate vibrations with adjustable dominant frequencies in the range 800 to 5000 Hz. When the source is placed in a water–filled borehole, the vibrations are coupled into the rock as seismic waves. The high–voltage waveforms (and hence the seismic vibrations) can be controlled by a signal link from the receiver subsystem.

The receiver subsystem consists of eight high–sensitivity downhole detectors which use piezoelectric transducers to convert seismic vibrations to electrical signals. Downhole electronic circuits within a pressure–proof stainless steel housing, buffer and pre–amplify the detected signals and use them to modulate eight FM carriers with centre frequencies in the range 2.5 to 8 MHz. The carriers take the multi–channel seismic signals uphole along a twin–conductor balanced line in a four–wire cable. The use of FM carriers decreases cable weight and thus enhances system portability. The other conductors in the cable carry 12–volt power from the surface down to the pre–amplifier–modulator circuits.

At the surface, the FM carriers are separated by tuned circuits, demodulated to recover the audiofrequency seismic signals, and filtered with a passband of approximately 500 to 5000 Hz. Each of the eight seismic signals is then digitized with eight–bit precision at a rate of one sample per 50 or 100 microseconds. The A/D module is designed to interface with and be controlled by desktop microcomputers via a parallel port. In the prototype system, the microcomputer is a Tandy 2000 with an Intel 80186 processor, an 8 MHz system clock, and an MS–DOS operating system. After digitization, vertical stacking of repeated waveforms is done to increase both dynamic range and signal–to–noise ratios. The stacked waveforms are then stored on floppy disks in the microcomputer for post–survey processing and analysis.

Further improvements in dynamic range and signal–to–noise ratios can be obtained by using a cross–correlation technique to acquire seismograms. Usually, seismograms are obtained by generating an impulse–like burst of pressure at the source. In the present instrumentation, the source is driven, not by an impulse, but by a special, continuous–wave periodic signal known as a pseudo–random binary sequence (PRBS). Seismograms are then obtained from the stacked detected data by digital cross–correlation with the PRBS. Although this procedure involves an extra processing step (cross–correlation), the effort is well justified as it results in large gains (of at least 36 dB) in signal–to–noise ratios.

A typical stacked and cross–correlated seismogram recorded with the prototype seismic scanner contains 2047 digital samples with 32–bit precision at 100 microsecond intervals. Digitization, stacking, and cross–correlation are all done within the Tandy 2000 microcomputer running assembly–language programs developed by JODEX Limited. The sampling interval, amount of stacking, and PRBS and seismogram length can be adjusted under software control.

TESTING OF HARDWARE AND SYSTEM CONTROL

During various stages of its development, the crosshole seismic scanner has been tested in the laboratory and under field conditions to ensure the proper operation of its mechanical and electronic components. The downhole probes have withstood hydrostatic pressures equivalent to depths in water of 500 m, and we plan to use pressure chamber testing to verify their integrity to depths of 1 km. The electronic circuits and system control software now function as required, but optimization will continue to be done to improve the technical specifications of the system and to increase the ease of use by field operators.

PROCESSING SOFTWARE FOR CROSSHOLE SEISMIC DATA

In addition to the design and construction of the crosshole equipment shown in Figure 079.1, JODEX Limited also was engaged in the production of computer software for tomographic interpretation of crosshole seismic data. In this regard, processing routines for spectral analysis and filtering of seismograms, for plotting and display of seismic fans, and for interactive time–picking have been written. In addition, image–creation algorithms based on algebraic reconstruction techniques (ART) and back–projection, procedures for two–dimensional interpolation, and routines for the generation of color–coded maps on CRT display have been implemented in FORTRAN or BASIC. Most of these computer programs are presently operational on the Tandy 2000. However, much optimization remains to be done to increase efficiency and decrease CPU times.

FULL WAVEFORM SEISMIC LOGGER

Most of the effort during the project year was concentrated on building the crosshole seismic scanner and implementing processing and interpretational software for tomography. Consequently, progress in the development of the full waveform logger did not advance to the stage of field–testing. Nevertheless, the main design concepts for the system (Wong 1985) were verified and specific components were constructed for laboratory testing. Figure 079.3 shows the function blocks for the full waveform logger. It will be noted that these are similar to the function blocks of the crosshole scanner shown in Figure 079.1. This similarity has enabled us to adapt circuits already proven sound during development of the scanner for use in the logger. Figure 079.4 shows seismograms collected in the course of testing a laboratory mock–up of the full waveform logger. The sampling interval for these seismograms is 10 microseconds. Continued development of the logger should result in a field–testable prototype before the end of 1986.

CROSSHOLE SEISMIC TOMOGRAPHY: A FIELD EXAMPLE

The prototype crosshole seismic scanner was used in a test survey at an underground mine in the Sudbury area operated by Inco Limited. The boreholes used were 76 mm in diameter and about 34 m deep, drilled about 14 m apart at the collars but not quite parallel (see Figure 079.5). Scanning took place with the detectors in Hole A and the source in Hole B, with probe placements at 1 m intervals along the holes. The resulting seismic coverage is depicted schematically in Figure 079.5 as a dense network of about 700 rays criss–crossing the rock section under study. Also shown on the Figure is an open cavity which extends into the scanned area near the bottom of the boreholes.

Figures 079.6a–c show typical seismic fans recorded during the survey. The sampling time for these digital seismograms is 50 microseconds. Stacking, cross–correlation, and the short transmission paths made it possible to obtain good seismograms despite strong mine noise. Clear P and S direct arrivals are observed, and interactive time–

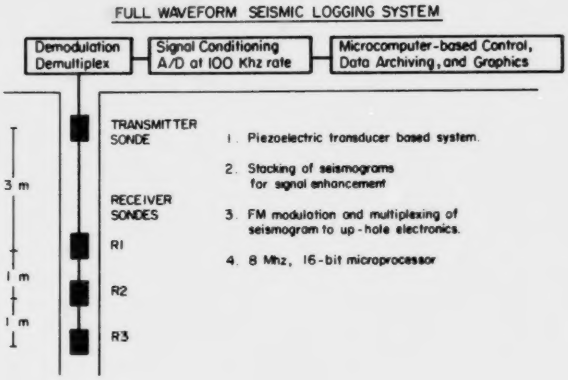
FULL WAVEFORM SEISMIC LOGGING SYSTEM
Demodulation Demultiplex
Signal Conditioning A/D at 100 Khz rate
Microcomputer-based Control, Data Archiving, and Graphics
TRANSMITTER SONDE
RECEIVER SONDES
R1
R2
R3
3 m
1 m
1 m
1. Piezoelectric transducer based system.
2. Stacking of seismograms for signal enhancement
3. FM modulation and multiplexing of seismogram to up-hole electronics.
4. 8 Mhz, 16-bit microprocessor

Figure 079.3. Function blocks for the full waveform seismic logger.

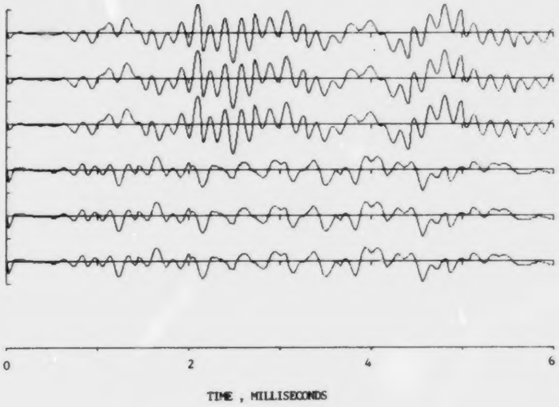

Figure 079.4. Test full waveform seismograms recorded in the laboratory.

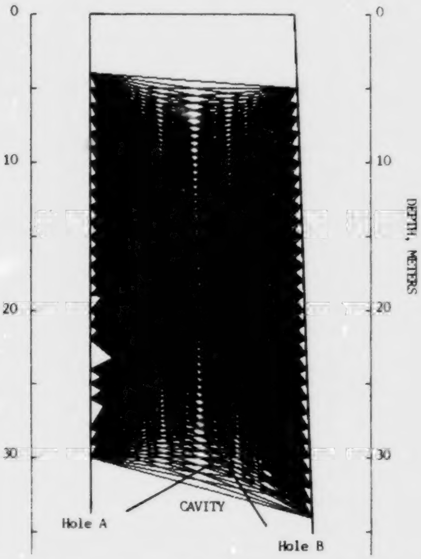

Figure 079.5. Raypath diagram showing the seismic coverage between two boreholes in the test survey.

picking using the high-resolution CRT display of the Tandy 2000 microcomputer can be done without difficulty. The source-detector separation associated with each seismogram can be calculated using survey data for the holes. Back-projection of the average velocities based on the transmission times and probe locations for all the seismograms reconstructs an estimate of the seismic velocity field within the scanned area.

Figure 079.7 is a color-coded tomograph (reproduced here in black and white) created by back-projection of the S information from the survey. The two-dimensional distribution of shear velocities indirectly represents the geology between the two boreholes. Near the top of the map, apparent S velocities are relatively low (3.25 to 3.35 km/s, green-yellow), suggesting either weakened rock due to cracking or metallic ore of greater density than the surrounding rock. In the central portions of the map, the apparent S velocities lie in the range 3.40 to 3.50 km/s (orange-red) and are characteristic of the host rock. At the bottom of the map, the apparent S velocities are significantly lower (3.10 to 3.20 km/s, dark blue-blue), indicating the presence of the cavity.

CONCLUSION

The development of the crosshole seismic scanning instrumentation has advanced very satisfactorily, and a working prototype system now exists. As well, essential software running on MS-DOS microcomputers has been written for processing crosshole data and for creating and displaying color images of seismic velocities. The field equip-

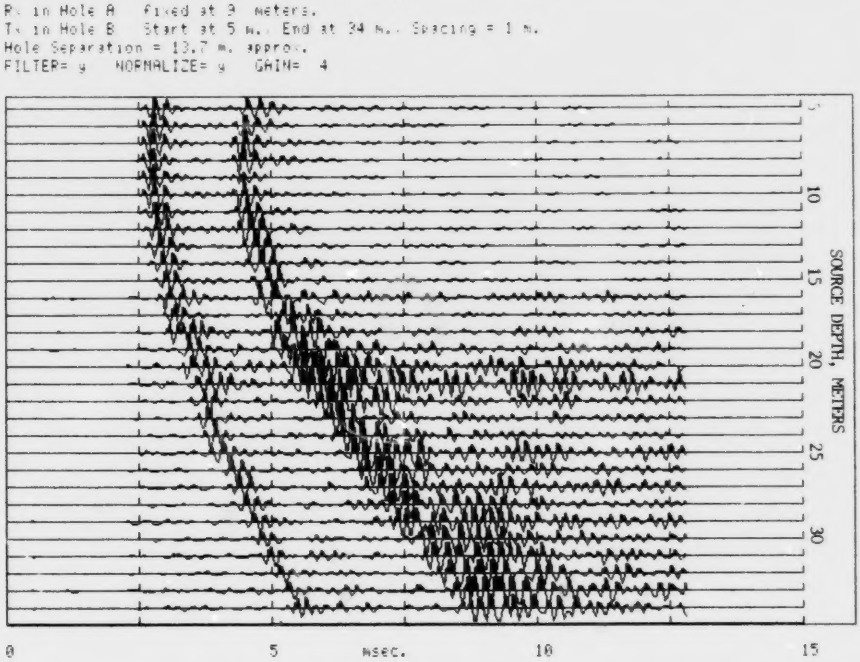
```
Rx in Hole A   Fixed at 9  meters.
Tx in Hole B   Start at 5 m., End at 34 m., Spacing = 1 m.
Hole Separation = 13.7 m. approx.
FILTER= y   NORMALIZE= y   GAIN=  4
```

Figure 079.6. (a) Seismic fan with detector fixed at 9 m depth in Hole A.

```
Rx in Hole A   fixed at 12  meters.
Tx in Hole B   Start at 5 m., End at 34 m., Spacing = 1 m.
Hole Separation = 13.7 m. approx.
FILTER= y   NORMALIZE= y   GAIN=  4
```

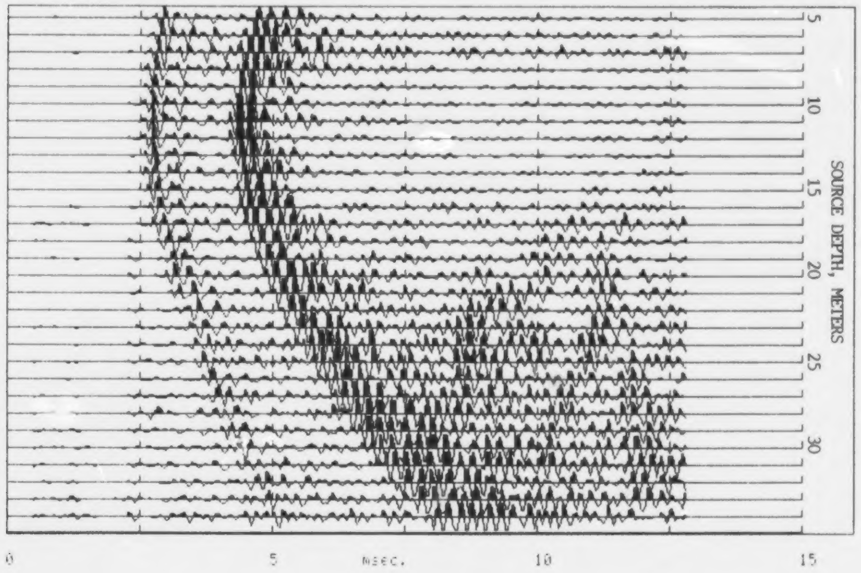

Figure 079.6. (b) Seismic fan with detector fixed at 12 m depth in Hole A.

```
Rx in Hole A   fixed at 29  meters.
Tx in Hole B   Start at 5 m., End at 34 m., Spacing = 1 m.
Hole Separation = 13.7 m. approx.
FILTER= y   NORMALIZE= y   GAIN=  4
```

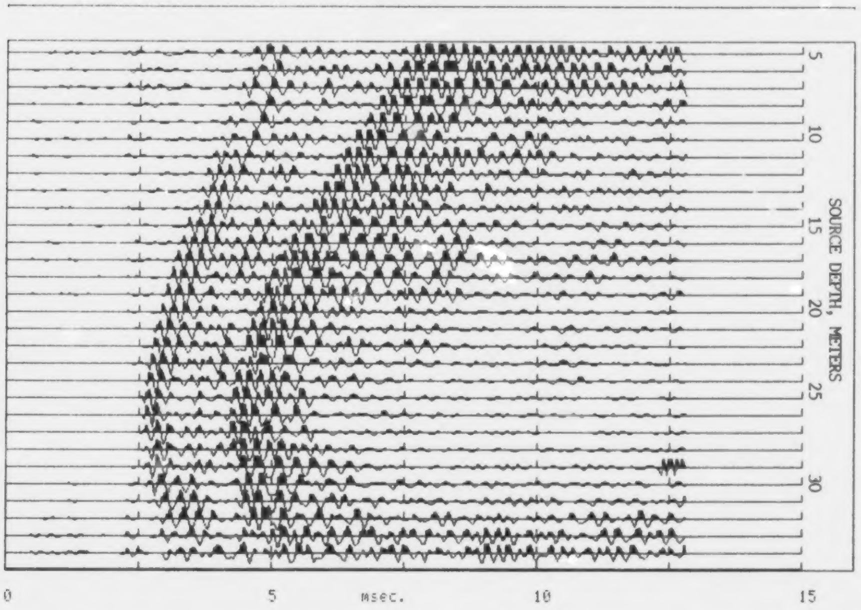

Figure 079.6. (c) Seismic fan with detector fixed at 29 m depth in Hole A.

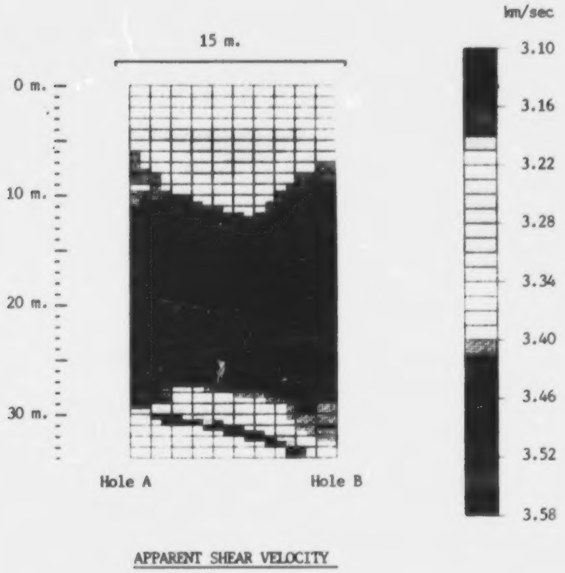

Figure 079.7. Back–projection tomograph of S velocities for the rock section of Figure 079.5. Note that the low velocities at the bottom of the map coinciding with the open cavity.

ment and data analysis software have been used in a test survey in which a cavity between two boreholes was imaged successfully in a tomograph of shear velocities.

As of May 1986, development of the full waveform seismic logger has progressed only to the point of being tested as a mock–up system in the laboratory. It is anticipated that instrumentation fully configured for in–hole logging operation will be completed before the end of 1986.

Further development in instrumentation for in–hole and crosshole seismology will involve optimization of the electronics for both the scanner and the logger. Improvements will also be made to the processing and imaging software required for tomographic interpretation. Finally, the major activity in the continuation of this project will be the generation of more case histories under a variety of geological conditions. Such case studies, in both seismic tomography and full waveform logging, will be essential for guiding the upgrading of the technical specifications of the field equipment and for adding to our expertise in interpretation.

ACKNOWLEDGMENTS

JODEX Applied Geoscience Limited expresses its appreciation to Inco Limited and the Geological Survey of Canada for access to test boreholes. This project has been supported in part by the Ontario Geological Survey through the Exploration Technology Development Fund.

REFERENCES

Wong, J.

1985: Grant 079 Seismic Full Waveform Logging and Seismic Geotomography; p.37–44 in Exploration Technology Development Program of the Board of Industrial Leadership and Development Summary of Research 1984–1985, edited by V.G. Milne and R.B. Barlow, Ontario Geological Survey Miscellaneous Paper 125, 110 p.

Wong, J., Hurley, P. and West, G.F.

1983: Crosshole Seismology and Seismic Imaging in Crystalline Rocks; Geophysical Research Letters, Volume 10, p.686–689.

Grant 080 — High Resolution EM Developments

Y. Lamontagne and A.E. Wieckowski

Lamontagne Geophysics Limited, Toronto

ABSTRACT

A project was initiated in 1984 to improve the effectiveness of wideband EM measurements with developments in both hardware and software. The hardware development is the design and field testing of an effective current regulated high power transmitter. The hardware design was reported on earlier. The emphasis of this report is on the last stage of our laboratory development: the use of high speed signal processing techniques to achieve very high current fidelity while using efficient switch–mode regulation. The software development consisted in two parts, both aimed at displaying processed multi–channel EM data in the form of apparent conductivity sections more easily related to the underlying conductivity structure. One of these processes, 'Depth Image Processing', which is suitable for quasi–layered structures, has been finalized and reported on earlier. The other process, 'Matched Filter Processing', is still in development. It transforms the data into correlation densities which are functions of the model parameters. Algorithms are being developed to turn these multi–dimensional tables into apparent conductivity sections.

INTRODUCTION

To respond to the need for more effective exploration tools for mineral exploration, a major effort was undertaken by Lamontagne Geophysics to pursue geophysical hardware and software developments for mineral exploration. These comprise the design and testing of an effective high power EM source with regulated current, and of software for processing and display of multichannel EM data.

There are thus two sub–projects in this development which started in 1984, and was scheduled to continue until 1987:

A. High Power Transmitter

B. EM Data Processing Techniques:

  B1. Matched filter processing

  B2. Depth image processing

A first report (Lamontagne et al. 1985) reported on earlier progress on these projects, and in particular, on the completion of the depth image processing development, which is a processing system for transforming quasi–layered earth responses into approximate images of the causative conductivity structure.

Recent developments have been on the sub–projects A and B1 which are now nearing completion.

HIGH POWER TRANSMITTER

The analysis leading to an optimized high power wideband transient EM source was given in Lamontagne et al. (1985). The implementation of this design in the form of a field usable instrument has been an ongoing project for 2–1/2 years.

In summary, the unique characteristic of this EM transmitter is to regulate the current to a high precision and over a high bandwidth to allow measurements during the "on" time at a much higher power level than the present UTEM 3 transmitter: 15 kW vs 1.5 kW. This feature, together with a judicious choice of waveform, can make such an EM source considerably more effective for the same power level than a more conventional transient EM source. This is why the development of such a device is well justified in spite of its much greater complexity.

HARDWARE REVIEW

The block diagram of the prototype transmitter presented in Lamontagne et al. (1985) is reproduced in Figure 080.1. The main blocks of this diagram are visible in the bench assembled prototype shown in Figure 080.2. The switch–mode regulators power components (SMPR and 4QSM) are in the main frame assembly supporting the two visible circuit boards. The circuit board on the left is the switch–mode controller (SMC), and the large circuit board is the microcomputer and the two high speed signal processors. The separate module is the waveform measuring module (WFM) linked to the processors by two fiber optic cables. The main frame also includes a D.C. power supply (DCPS) for up to 5 kW operation. An external D.C. voltage source is required for high power operation.

In Figure 080.3, the final prototype components are shown in the transmitter case incorporating elaborate shielding partitions to protect sensitive circuits from high voltage switching within the output stage. The WFM shown in its guarded box is actually mounted on the main output frame and floating at the output voltage for operation. The high voltage isolation required in this arrangement is achieved by the fibre optic cables and use of digitally coded signals.

The size of the field case is 54 cm x 49 cm x 40 cm. Protective ventilation baffles and filters (not shown in Figure 080.3) add 12 cm to the length. This prototype is relatively heavy (47 kg), in good part as a result of magnetic shielding material used in partitions. However this is not excessive in comparison to the 450 kg of the 20 kW generator set which will be needed as a power source in operation, and the estimated 100 L of fuel which it will consume daily.

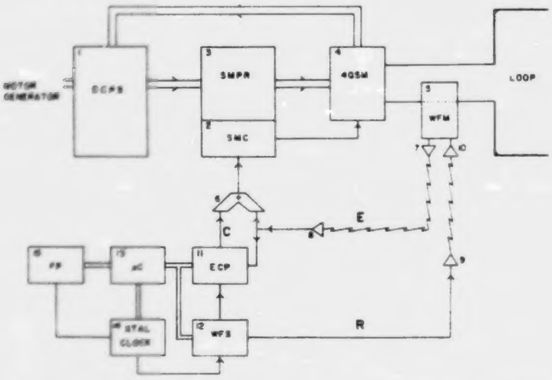

Figure 080.1. Block diagram of the prototype transmitter:

1	DCPS	D.C. power supply
2	SMC	Switch-mode controller
3	SMPR	Switch-mode preregulator
4	4QSM	Four quadrant switch mode regenerative regulator
5	WFM	Waveform measuring module
6		High speed digital adder
7,8,9,10	Optical transducers	
11	ECP	Error correction processor
12	WFS	Waveform synthesizer
13	C	Microcomputer circuit
14		Precision crystal controlled clock
15	FP	Front panel

The paths labelled are the digitally coded signals referred to in the text:

R : reference waveform
E : error waveform
C : correction waveform

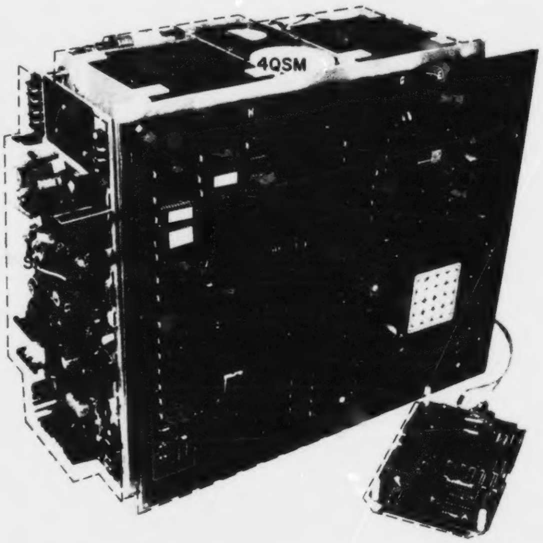

Figure 080.2. The assembled prototype on the bench with locations of the main components shown.

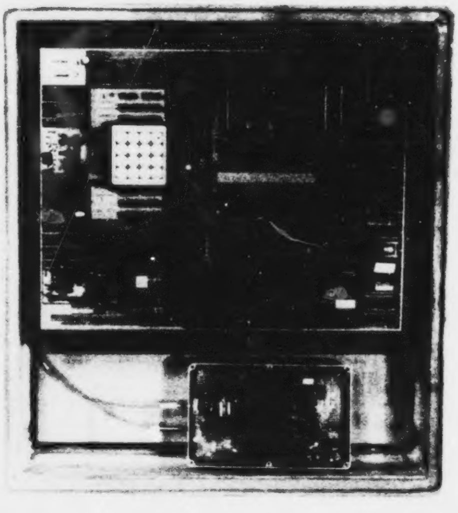

Figure 080.3 Transmitter components mounted in the field case with its front panel removed.

CURRENT REGULATION TECHNIQUES

Recent developments in this project have been centered on the difficult problem of regulating the current to the desired accuracy by refinement of the switch-mode regerative regulator, and particularly by use of digital signal processing techniques. The processing power for this purpose is provided by two high speed digital processors marked ECP and WFS on Figure 080.4 coupled to the controlling processor marked µC. The signal processors implemented with TMS320 processors and high speed support circuitry are capable of 10 million filtering operations per second and 32 bit accuracy.

Two techniques were originally considered to achieve the high current fidelity needed for high resolution EM measurements:

A. Transmitter current waveform sampling and recording.

B. Automatic current waveform correction.

Both of these options were considered only as digital processing enhancements of the regulation level achieved by electronic regulation. Option A was considered feasible only if the correction required is a minor perturbation of the raw waveform. Otherwise, fine time sampling of the waveforms and complete deconvolution of the receiver measurements would be necessary.

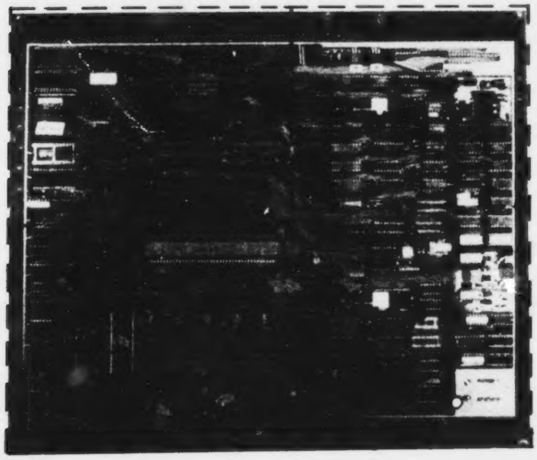

Figure 080.4. The main digital circuit board and its functions.

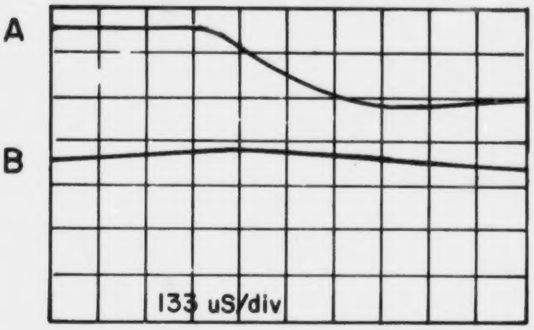

Figure 080.5. Response of the switch-mode regulators for a load simulating a large loop. A: voltage waveform; B: current waveform; The reference waveform is triangular. The time window displayed is near a peak of the refernce waveform.

It was soon realized that, although the switch-mode regulator can be tailored to have an accuracy better than 1% for slow signals, the output response with a very inductive load (simulating a transmitter loop) is too slow for reasonable regulation within up to 1 ms. One reason for this is that the regulator must be conservatively stabilized to handle a variety of load impedances.

This is illustrated in Figure 080.5 which shows the output voltage (a) and current (b) around a slope transition of the reference triangular wave for a load with 15 mH inductance (simulating a 1500 m square loop). Because of the inductive load, the voltage (a) shows the step response of the current regulator. It has a rise time of 250 µs and a 15% overshoot at 400 ms delay. These times are to be compared with the design objective of 20 µs rise time.

After these characteristics were determined, the main emphasis was turned towards option B: the use of automatic waveform correction techniques.

AUTOMATIC WAVEFORM CORRECTION ALGORITHM

This technique is based on digital processing of the error E in the output current waveform, which is the difference between the desired reference waveform R and the measured current M. The aim of this processing is to produce an estimate of a correction waveform C to add to the input waveform on later cycles to obtain the desired output.

The original error with no correction applied E0 is:

$$E0 = M0 - R \qquad (1)$$

where M0 is the original current waveform. If a process G{E} can be found which can produce an estimate of the correction C to apply to correct an error E, then the first correction C1 is:

$$C1 = G\{E0\} \qquad (2)$$

Using this correction, a new measured current M1 is obtained. Then,

$$E1 = M1 - R \qquad (3)$$

The new correction becomes:

$$C2 = C1 + G\{E1\} \qquad (4)$$

The Nth iterate is recursively defined as:

$$Cn = Cn{-}1 + G\{En{-}1\} \qquad (5)$$

For this algorithm to converge to the exact output, the RMS error waveform must decrease for every iteration, whereas, if the process G was perfectly designed, only one iteration would be necessary.

The process G is actually the inverse transfer function of the regulator. A number of least square formulations were tried to estimate this function as a convolution filter from output responses representative of various loads. The main objective was to find the form which produced a good estimate while being computationally economical.

A good approximation was found to be:

$$I(t-e) = A\ D(t;k) + B\ D'(t;k) + C\ D''(t;k) \qquad (6)$$

involving the density function D and its derivatives where D(t;k) is:

$$D(t;k) = \begin{cases} \exp(-tk) & t \geq 0 \\ 0 & t < 0 \end{cases} \qquad (7)$$

The delay e is a system constant which is not load dependent. The correction is estimated by convolving the error waveform with the inverse filter I. In practice this can be done in the signal processor by a simple three point filter with recursion. Depending on how well determined the error waveform is (over how many cycles it is averaged), damping factors less than 1 can be applied, particularly to the higher terms of (6) to prevent over estimating the correction waveform.

So far inverse filter calculations have been studied experimentally on a development station, but the latest formulation is simple and well behaved enough that it is being programmed into the error correction processor to be determined adaptively for every new load and to adjust for non linear variations in the response.

In the present implementation, the error is sampled every 2 μs near waveform transitions and more coarsely at long delay after these. The number of cycles over which the error waveform is averaged will remain variable until enough experience is gained by field use in the presence of power lines and other noise sources which will introduce errors in the waveform estimate.

Our objective is to achieve current regulation of better than 0.1% for delay times greater than 1 ms, and better than 1% for delay times as short as 50 μs. These specifications would apply to the average of several hundred waveforms at least because of the statistical nature of the switch–mode regulation techniques. Proper testing of the actual transmitter performance will be done in the field using the UTEM 3 digital stacking receiver.

CONCLUSION

The use of adaptive waveform correction techniques promises to open new geophysical applications for high power signal sources combining high efficiency and very high waveform accuracy. These would be particularly suited for use with the new generation of digital stacking receivers. This development constitutes the last stage in the development of a current regulated 15 kW, 800 V wideband EM transmitter.

MATCHED FILTER PROCESSING

The formalism of automatic interpretation using 'matched filter' processing was presented in Lamontagne et al. (1985). In summary, the process consists of forming correlation functions between measured data and filters matched to models of varying parameters. The two types of correlation density functions described are:

R, the result of matched filter correlation,

S, semblance function.

The function R is amplitude dependent in the sense that if the input is doubled, R is halved, whereas S is not amplitude dependent, being devised as a measure of shape similarity without regard to amplitude.

PROCESS IMPLEMENTATION

The process described in the above reference has been partially implemented by means of building blocks which are either independent programs or major subprograms.

Model response generation

smodel: generate a suite of elementary dipole responses of varying positions and orientation for use in matched filter calculation.

sdec: generates a set of sphere model decays in form suitable for matched filter calculation.

mloopl: generates a suite of quasi–plate responses of varying positions, depths, dips, and conductances for use in matched filter calculation.

pplate: generate the response of multiple interacting quasi–plates each made of several concentric ribbons for use as synthetic data for processing.

Matched filter design

wdat: select a data window for filter design around point of interest, set up special treatment near data boundaries, apply cosine taper.

wcorr: generates a windowed multidimensional correlation matrix.

wpar: generates a windowed parameter covariance matrix.

dlequ: fast damped matrix inversion routine, linear equation solver with lag taper.

rfil: generates R function 'filters'.

mfil: generates intermediate result for S 'filters'.

pmpy: multidimensional matrix multiplication for correlation matrices.

Analysis of results

vscan: scans R for dips of maximum correlation.

xscan: scan correlations for instability in x.

ssiz: estimate effective size function using smoothed ratio of S and R, using the sphere model as reference.

cfill: add densities to circular and elliptic 'areas of influence'.

Data display

plot3d: 3–D perspective screen display package.

occlud: screen display package with opaque surfaces and hidden lines.

The main difficulties in designing the filters has been in achieving reasonable speed, considering the large number of matrix inversions. This was done by restricting the number of lags in the autocorrelations matrices to a minimum without smearing the results unduly.

In the cases treated so far, no y variation was considered such that the correlations are functions of:

x, position along profile

z, depth

T, time constant

d, dip angle of dipole.

The only problems with instability have been as a function of the x parameter, which have been identified as being caused by insufficient damping (excessive number of lags). Lateral averaging with a simple three point filter has been used on poorly behaved functions, rather than critically adjusting the data window width and lag taper with almost equivalent results. The iterative use of smoothing filter to remove local instabilities has resulted in a considerable improvement in performance because iterative matched filter recalculations have been mostly eliminated. The processing time ranges from 0.5 to 5 s per point in parameter space depending on the filter width which varies according to model depth.

The difficulty in displaying intermediate results which are large matrices, and in searching for which parts to display has been addressed with the recent design of three–dimensional display programs and data scanning routines.

TOWARDS AN APPARENT CONDUCTIVITY SECTION

An essential step in presenting the processed data as a useful section is the reduction of the number of parameters. An obvious choice in parameter reduction is the dip of the reference model, but this has proved more difficult than anticipated. After experimenting with a simple method scanning for maxima as a function of the dip parameter which produced spurious results, the method now under trial is one using a least square sine/cosine fit of each complete set of S correlation values as a function of dip. The estimated maximum correlation as a function of dip will then be a function with one less parameter. A more meaningful measure of effective size can then be obtained which is equivalent to the radius of a sphere. This is proportional to the cubic root of the smoothed ratio S/R.

The apparent conductivity is estimated with reference to the sphere model:

$$\sigma = \pi^2 T/(\mu_0 a2) \qquad (8)$$

where a is the effective size and T the time constant.

The planned final processing as outlined in Lamontagne et al. (1985) is in the form of correlation sections for a number of conductivity classes.

CONCLUSION

A processing system for multichannel EM data was implemented which converts these data to tabulated correlation densities of two types each a function of four parameters. It is hoped that further analysis of these data by reduction and combination of parameters will result in a system for automatic preliminary interpretation of multichannel wideband EM data in the form of approximate conductivity sections.

ACKNOWLEDGMENT

The authors wish to thank the Ontario Geological Survey for partial funding of this project through the Exploration Technology Development Program.

REFERENCES

Lamontagne, Y., Macnae, J.C., Wieckowski, A.E., Huxter, R.

1985: High Resolution EM Developments; Grant 080, p.45-56 *in* Exploration Technology Development Program, Summary of Research 1984-1985, Ontario Geological Survey Miscellaneous Paper 125.

Grant 081 — Computer Software for the Maglog Borehole Logging System

S.J. Balch

Morris Magnetics Inc., Lucan

ABSTRACT

A suite of computer software has been developed to assist in the acquisition, processing and interpretation of data acquired by the MAGLOG system – a multi–parameter borehole logging probe and digital data acquisition unit. This software, designed for borehole or line profile data, provides the user with the capability of obtaining presentation quality plots on site soon after surveying. Special consideration has been given to the problem of dealing with the large volume of recorded data which can exceed the capabilities of the microcomputer. Some programs have been designed to be independent of the number of recorded data points while other programs allow the data to be broken down into smaller segments that can be handled by the interpretation routines. With the advent of the transportable microcomputer and the cost effectiveness of performing more processing and interpretation during the field survey, the advantages of this design approach become apparent. Through software control the geophysicist moves quickly to the interpretation phase without having to directly manipulate or reformat the data.

INTRODUCTION

Geophysical surveys generally involve the acquisition of data in the field followed by data processing and any subsequent interpretation. We include under data acquisition any processing, through data file manipulation or reformatting that is required to make the field tapes useful while still preserving the "raw" data. Within data processing we include procedures for smoothing data, removal of data spikes and any regional/residual or drift removal techniques that do not relate measured parameters to geological ones. Interpretation, which often involves quantitative statistical techniques, empirical formulae or iterative modelling of data based on specific geometries, is the last step in exploration, putting into physical terms what is indicated by anomalous responses from the different physical rock property measurements. A typical MAGLOG survey can be illustrated by a flowchart as shown in Figure 081.1.

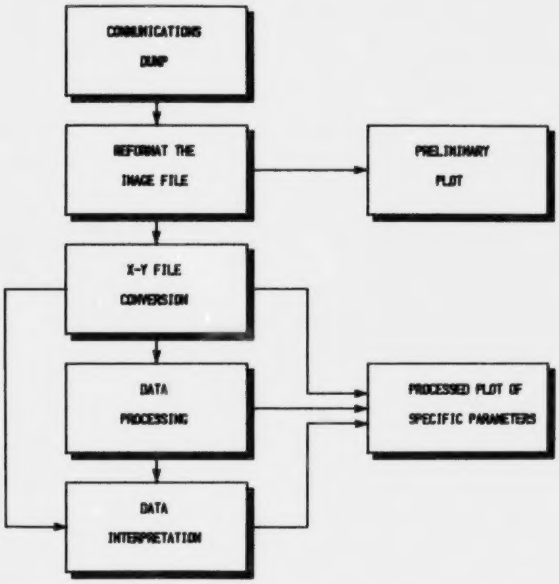

Figure 081.1. A typical MAGLOG system survey is outlined by this simple flowchart.

The MAGLOG system is a field portable borehole logging unit capable of simultaneous measurement of up to 5 physical rock properties:

- Total magnetic field
- Bulk magnetic susceptibility
- Temperature
- Self potential
- Fluid conductivity

With the use of an onboard high speed microprocessor, the probe can measure and transmit readings to the surface console four times every second. This high sampling rate provides a very detailed record of subsurface features with a resolution on the order of a few centimetres thickness. Field tapes commonly contain 10 megabytes or more of recorded information. Software programs currently available for microcomputers are usually unable to cope with such a large data set since a single borehole may contain 5000 or more points per parameter.

The surface control unit contains a 1/4 inch tape drive for data storage, a 40 column LCD display, a keyboard and a small thermal printer, useful for trouble–shooting during logging. This unit contains enough software (in ROM) to allow a flexible field setup and includes a program for dumping data through an onboard RS232 serial port.

The software developed under this grant includes programs for processing, plotting and interpretation and a communications link between the MAGLOG system and an IBM PC/AT compatible microcomputer running under MS DOS. System requirements for processing include a hard disk (10 megabytes or more of storage) and a floating–point math coprocessor.

DATA ACQUISITION

The MAGLOG system consists of the probe, the surface console, a cable/winch assembly and a portable generator. The information recorded on tape is dumped to the microcomputer through the serial port at a rate of 9600 baud. The information transfer is controlled through the microcomputer with the program CDUMP which displays the information on the microcomputer's screen while concurrently writing it to a disk file – which we refer to as the image file. This procedure can occur while logging, or the field tapes can be dumped at a later time. A second program RTPLOT, when completed, will allow real time plotting of the parameters on the graphics screen of the microcomputer during the logging phase.

Once the image file has been created it is reformatted using the program REFORM. This program generates a new file in a simple column–row format of ASCII characters with each recorded parameter occupying a separate column and each successive measurement occupying a new row. The use of standard ASCII format ensures compatibility, allowing easy transfer between different computer systems (microcomputer to mainframe, MS DOS to CP/M) and permits the use of popular software programs like Lotus 1–2–3. REFORM also checks the image file for transmission or write–to–tape errors.

An option to produce a preliminary plot of any combination of parameters vs depth is provided with the program PRELIM which supports a graphics screen, printer and plotter. These plots (see Figure 081.2) provide a quick way of examining all the data so that parameters which may benefit from further processing or interpretation can be identified. Once identified, these parameters are reduced to X–Y data files (parameter vs depth) with the program XYDUMP. Data for any parameter from any section of the borehole may be saved

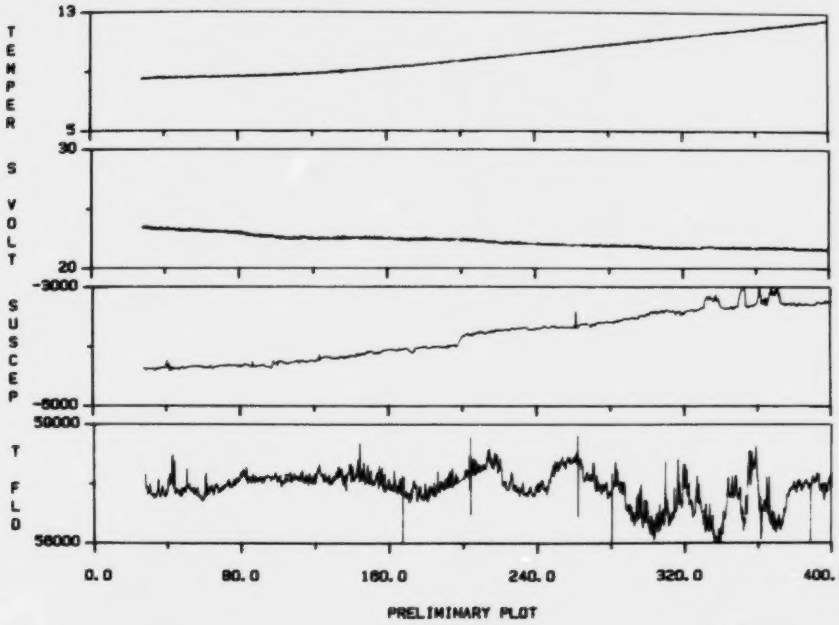

Figure 081.2.
Any combination of parameters may be plotted vs depth with the program PRELIM.

to a disk file with a preview option that allows you to zoom in on small depth segments of the borehole.

DATA PROCESSING

The processing of the raw data is possible once the files have been converted with the program XYDUMP. Many processing techniques, common to geophysical applications, have been combined into a single program DATAPRO. Its capabilities include frequency filtering (low pass, high pass and band pass), spike removal, trend removal with low order polynomials, splining, moving average and moving median filters and so on. All options are available through interactive menus with options for plotting or saving data to a disk file. Processed plots can be plotted with the graphics package MPLOT which allows five different plot types including log or linear scales for both axes and histograms. MPLOT also provides three different plot formats. A series of profiles can be combined on a common set of axes (Figure 081.3a), profiles may be stacked above a common X-axis (Figure 081.3b) or up to four separate plots may be displayed in quadrants (Figure 081.3c).

Instrument drift, a problem common to borehole susceptibility measurements, is removed with the interactive program DETREND. Drift in the probe shows itself in the form of a near linear or gently sloping curve. This curve is often removed by fitting a low order polynomial to all measurements in a least-squares approach. In lithologies characterized by large susceptibility contrasts this method proves feeble since the resulting curve cuts through all lithologies with little regard for the actual probe drift. The preferred approach is to choose points on the profile which properly characterize the drift of the probe and to fit a low order polynomial to these points only. The resulting curve is subtracted from the original data to remove the effects of drift. DETREND allows points on a curve to be selected or removed and fits either a low order polynomial or a cubic spline to these points allowing the detrended data to be saved to a disk file. DETREND operates in high resolution graphics mode using the CGA (colour graphics adapter) of the microcomputer, incorporating both the arrow and function keys for ease of use.

INTERPRETATION

TOTAL MAGNETIC FIELD

Measurements of the total magnetic field are commonly approximated by geometric models of specified physical and magnetic property characteristics.

In forward modelling, a theoretical total field curve, derived from fixed model parameters, is compared with the observed field curve. By repeating this process the interpreter can decide on parameter limits and can examine parameter sensitivity. Two forward modelling programs, FMMAG2D and FMMAG3D have been developed to model the total magnetic field with either 2 or 3 dimensional models respectively. Parameters are chosen through a parameter file and each parameter may be changed at any time through an interactive menu. Options within this menu include displays for showing the system of models in perspective, theoretical vs observed profiles (or just the theoretical curve if you have no data) and saving the theoretical field values and the final parameters to separate disk files.

Inverse modelling algorithms control the changes of the model parameters through an iterative process until the theoretical and observed profiles match to within some acceptable error margin. The programs IMMAG2D and IMMAG3D used for inverse modelling of 2 and 3 dimensional models allow complete control over the iteration process, both using the Marquardt algorithm (Marquardt 1963) to control the inversion. Options selected through menus include displays which show the models in perspective (Figure 081.4a), the theoretical vs observed profiles (Figure 081.4b) and the sum of squares deviation vs iteration (Figure 081.4c).

The 3 dimensional modelling routines (Plouff 1976; Hjelt 1972) allow both borehole and surface magnetic readings (grid or profile) to be modelled simultaneously. Modelling also is possible within the geometric body in boreholes that may have any known orientation.

BULK MAGNETIC SUSCEPTIBILITY

Magnetic susceptibility provides a measurement of the average oxide content in a given volume of rock. The variation in these measurements can be used to determine the degree of alteration which is characterized by a reduction of magnetic susceptibility through an oxidation of the primary oxide magnetite to hematite. Magnetic susceptibility has

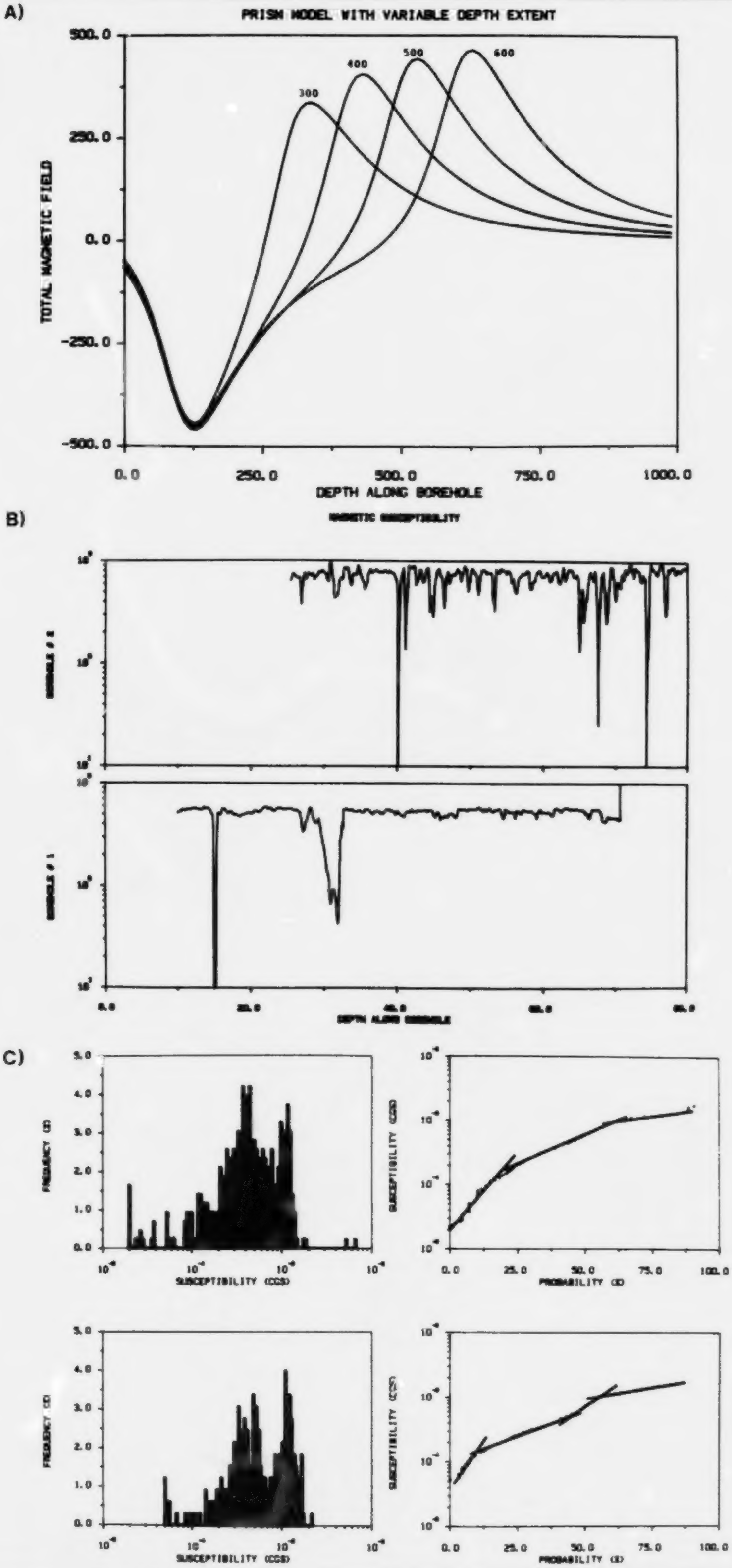

Figure 081.3. MPLOT allows three different plot types which are selected from an interactive menu.
(a) Multiple curves on a common set of axes.
(b) Stacked profiles over a common X-axis.
(c) Quadrant plots.

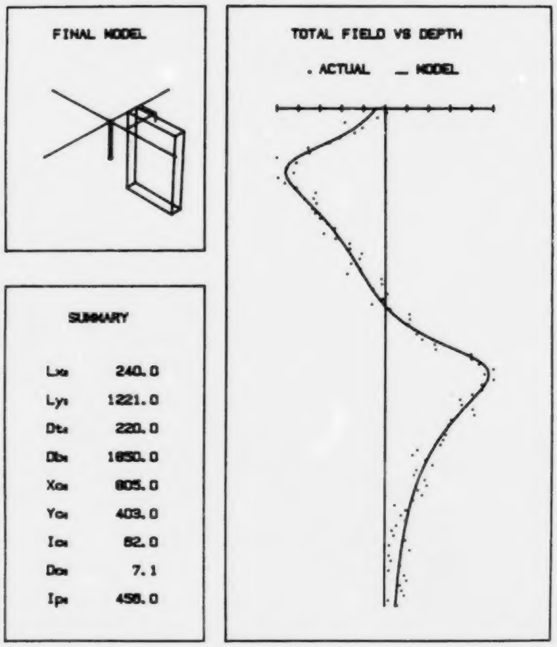

A

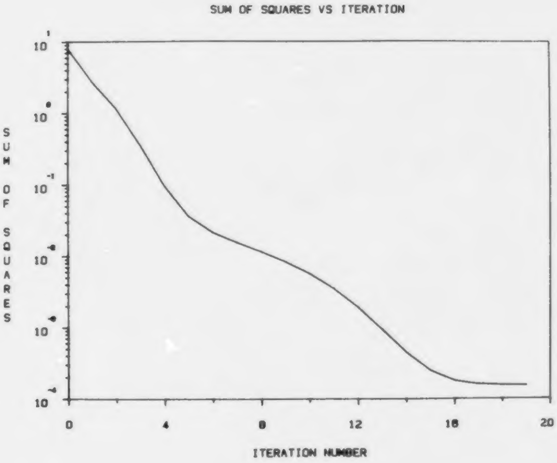

C

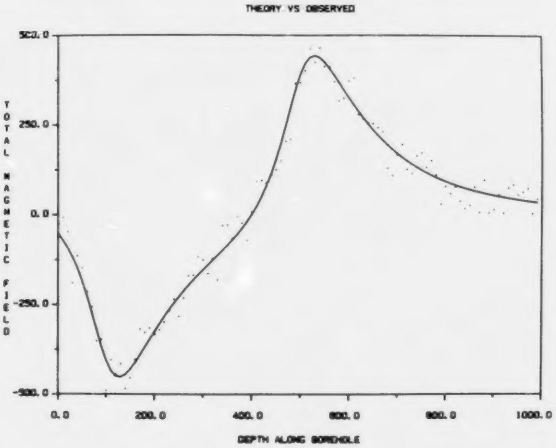

B

Figure 081.4. IMMAG3D plotting options include: (a) The final model(s) in perspective together with a parameter summary and theory vs observed profile. (b) The theoretical vs observed profile is plotted separately with annotations. (c) The sum of squares error between observed and theory fields can be plotted after any iteration.

a log10–normal distribution. Populations which characterize different geological environments as reflected in the core log can be separated using frequency and cumulative frequency diagrams on the basis of bulk magnetic susceptibility using the program HIST (see Figure 081.3c). Work is continuing on a program which will automatically define these populations using a non–linear least–squares decomposition of mixtures of normal distributions, with the result being a pseudo–lithologic log.

TEMPERATURE

Temperature logs can be used in mapping lithological detail (Conaway and Beck 1977; Kayal 1981) although their usefulness has not yet been clearly demonstrated in mineral exploration. Temperature measurements require a borehole in which the borehole fluid has reached equilibrium with its surroundings. Temperature sensors must be sensitive to very small changes in the temperature of borehole fluids. Sensors with very small delay constants permit continuous rather than incremental logging. The initial temperature sensor on the MAGLOG probe was sensitive to temperature changes on the order of a few hundredths of a degree although its delay constant was unacceptable. Recent improvements in the temperature sensor are expected to reduce the delay constant down to the order of a few seconds. Currently programs exist to reformat the temperature data into degrees per kilometre vs depth. Work is continuing on a program which models temperature disturbances in a borehole using a plane crack model (Carslaw and Jaeger 1959).

SELF POTENTIAL

The MAGLOG probe measures the self potential difference between two lead electrodes in the probe spaced 40 cm apart. Unlike conventional SP surveys which measure self potentials arising between a fixed reference electrode and a second electrode which is moved along the survey line, both electrodes in the borehole probe are always encountering new geological features with associated varying self potential differences. These difference measurements cannot simply be integrated to give the common SP log, nor can the derivative of the common SP log be used to obtain the SP difference as it is measured in a borehole with a fixed electrode spacing. The SP difference anomalies appear to be promising although their geological relevance is not quite understood. To take advantage of the literature and interpretation techniques available for common SP logs, the MAGLOG probe is being modified to allow both types of SP measurements by incorporating a fixed reference electrode at the surface. A computer program for the forward and inverse modelling of SP data in a borehole based on a thin dipping sheet model is currently under development.

SUMMARY

The MAGLOG system has now been tested in many different geologic settings including the Sudbury Basin and the Oil Sands of Alberta. Currently the probe measures the total magnetic field, magnetic susceptibility, temperature and self potential difference with excellent uphole–downhole repeatability. Recent interest in the MAGLOG system by both oil and mineral exploration companies may result in the construction of a second probe that measures new rock properties including borehole resistivity and natural radiation.

ACKNOWLEDGMENTS

The author wishes to thank R.T. Graydon of Morris Magnetics for his work in the development of the program DATAPRO and W.A. Morris for his continued support on this project. Morris Magnetics is grateful to the Ontario Geological Survey for its financial assistance through the Exploration Technology Development Fund. Detlef Bluhm of IFG, the designer of the MAGLOG system made many contributions to the design approach of the systems software. Bill Thuma of Geotech has also made many valuable contributions. Falconbridge Ltd. and Syncrude Canada supported much of the field survey work and we are grateful for permission to publish their data.

REFERENCES

Carslaw, H.S. and Jaeger, J.C.

1959: Conduction of Heat in Solids; Clarendon Press, 2nd Ed., Oxford.

Conaway, J.G., and Beck, A.E.

1977: Fine Scale Correlation Between Temperature Gradient Logs and Lithology; Geophysics, Vol. 42, No. 7, p.1401–1410.

Drury, M.J., Jessop, A.M. and Lewis, T.J.

1984: The Detection of Groundwater Flow by Precise Temperature Measurements in Boreholes; Geothermics, Vol. 13, No. 3, p.163–174.

Hjelt, S.E.

1972: Magnetostatic Anomalies of Dipping Prisms; Geoexploration, Vol. 10, p.239–254.

Kayal, J.R.

1981: Correlation of T–log with E–log in Coal Bearing Formations; Pageoph, Vol. 119, p.349–355.

Lawson, C.L. and Hanson, R.J.

1974: Solving Least Squares Problems; Prentice Hall Inc.

Marquardt, D.W.

1963: An Algorithm For Least Squares Estimation of Non-Linear Parameters; Journal of the Society of Industrial Applied Mathematicians, Vol. 11, p.341-441.

Plouff, D.

1976: Gravity and Magnetic Fields of Polygonal Prisms and Applications to Magnetic Terrain Corrections; Geophysics, Vol. 41, No. 4, p.727-741.

Society of Exploration Geophysicists

1985: Engineering and Groundwater Applications of the Self Potential Method; p.152-168 *in* Abstracts of 1984 Annual General Meeting of the Society of Exploration Geophysicists held in Atlanta, 302p.

Grant 084 — Helicopter Borne High Sensitivity Magnetometer Intridirectional Gradiometer Based on Overhauser Effect

Ivan Hrvoic

GEM Systems Inc., Don Mills

INTRODUCTION

The magnetometer–gradiometer Model GSM – 11GH4 has been described in some detail in the 1985 ETDF report (Hrvoic 1985) and will only be briefly reviewed here.

Four Overhauser effect proton oscillators have been mounted in a special bird, one in the bird body, and three others in the three fins, placed radially from the bird body at 120 degree mutual angles and at the front end of the bird (Figure 084. 1). The magnetic field is measured synchronously at 4 points in space and three differences calculated and divided by appropriate distances from the sensors. Vertical, along and across the track gradients are calculated as well as fourth differences. The results are displayed and presented at the output ports in analog, BCD, serial RS232 or parallel GPIB form.

RESULTS

Upon assembly of the system, numerous ground tests and bench tests were conducted in order to minimize noise and achieve adequate reliability. A

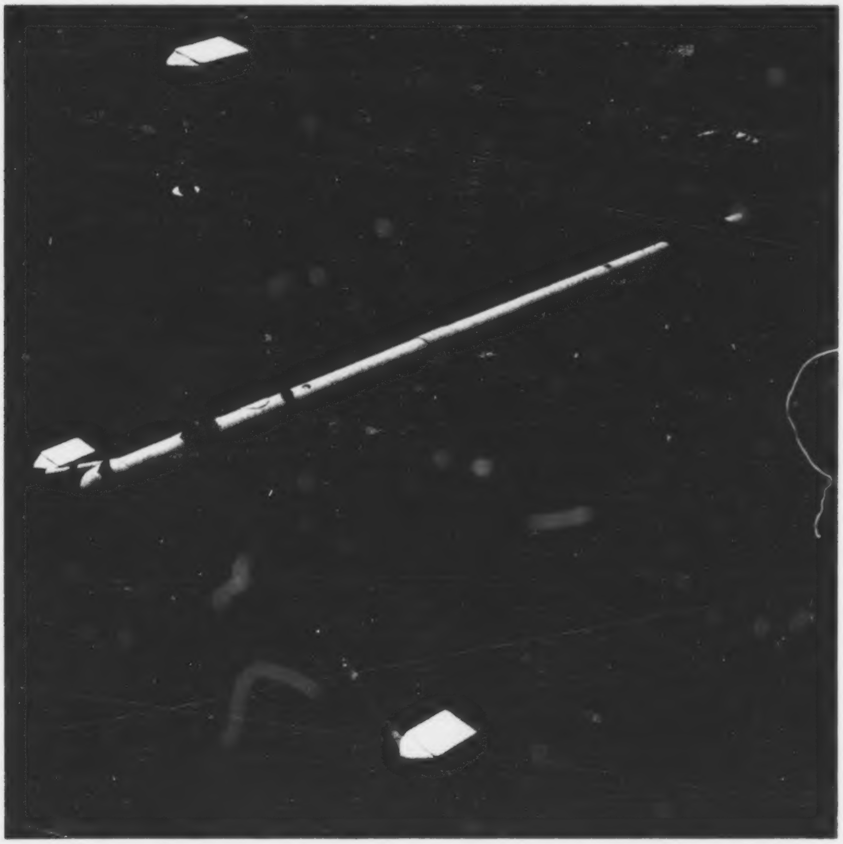

Figure 084.1. Overhauser effect proton oscillators mounted in a special bird, one in the bird body, and three others in the three fins.

new improved fully deuterated free radical was used in all four sensors, improving the precession signal strength by some 30%. Special care was taken to synchronize all four readings and eliminate errors caused by phase differences in the precession signals.

During the year, several improvements were made to the electronics. For example, a common RF source for all 4 channels was built and tested. Automatic gain control was introduced to replace clipping of the signal, etc.

Upon completion, the system was installed in a Bell Jet Ranger helicopter. Radar altimeter, data acquisition system, tape deck, power distribution unit and video camera were rented from Geotech Limited of Toronto.

A small test survey was conducted in the Bowmanville area in early March of 1986. Flight parameters were the following:

- Bird height above ground 500 feet or 150 m to comply with standard heights required by Federal–Provincial contracts
- Speed 60–80 mph
- 2 readings/sec, 0.5 Hz bandwidth of data collected, constant delay (linear phase) digital filter.

A sample of in–flight data is shown in Figure 084. 2; parameters and scales are: across–track 58 pT/m per division, vertical 67 pT/m per division and along–track 55 pT/m per division.

The system noise envelope appears to be in the range of 25 pT/m. This noise level set for the Federal–Provincial Vertical Gradiometer Survey

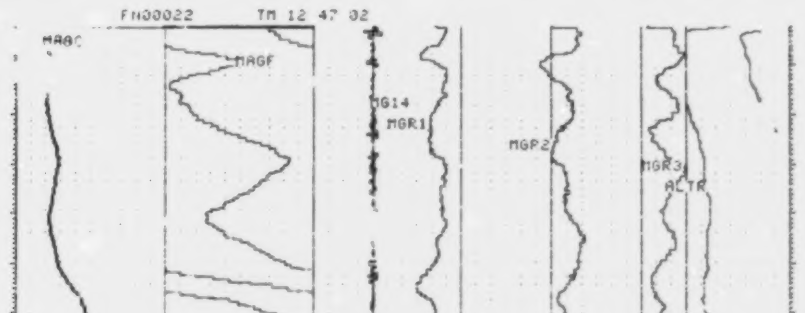

Figure 084.2. Sample of in–flight data.

Program will be further reduced in the upcoming improvements based on the first test flight experiences.

Total field map of the area as well as three gradient maps and total gradient map are now being produced by Urquhart–Dvorak of Toronto. The area is inhabited and many man–made magnetic anomalities can be expected.

The use of data and interpretation remains somewhat an open question. Total gradient and its direction can be determined. Interpolation of total field and vertical gradient values between flight lines and better reconstruction of profiles is possible from the across–track and the along–track gradients respectively. The first derivative of total field will give some insight into cleanliness of the sensor heads, i.e. of the heading error due to local contamination. From the profile in Figure 084. 2 one can estimate the discrepancy between zero gradient total field (points A and B) and reading of along–track gradient as about 0.8 nT.

Positioning system to keep track of in–flight position and orientation of the bird will be developed in the near future.

REFERENCE

Hrvoic, Ivan

1985: Helicopter Borne High Sensitivity Magnetometer Tridirectional Gradiometer Based on Overhauser Effect; Grant 084, p.64–67 *in* Exploration Technology Development Program of the Board of Industrial Leadership and Development, Summary of Research 1984–1985, edited by V.G. Milne and R.B. Barlow, Ontario Geological Survey, Miscellaneous Paper 125, 110p.

Grant 087 — High Resolution Investigations Using Radar And Seismic Techniques

A.P. Annan and F. Glass

A–Cubed Inc., Mississauga

ABSTRACT

This paper presents geophysical data from two controlled test areas in southern and eastern Ontario that were selected by A–Cubed Inc. for the execution of high resolution shallow soundings for mapping the overburden stratigraphy and bedrock profile. The principal survey techniques employed were pulseEKKO® electromagnetic reflection profilers (radar) and multi–fold coverage high resolution engineering seismic surveys.

Detailed geological information is available for the two test sites and is summarized in this report. A–Cubed Inc. has established a geophysical data base for each area with which to correlate data from present and future surveys conducted at these sites. The two test areas described meet the objectives established at the outset of this project, namely, to set up test sites for high resolution surveys and to develop integrated site investigation techniques which employ radar, seismic, as well as other geophysical methods.

The results presented here demonstrate that high resolution profiling of shallow stratigraphy can be attained with radar and seismic methods. In general, the two techniques are complementary.

INTRODUCTION

One of the main areas of endeavor at A–Cubed Inc. is research and development of new equipment and practical field instrumentation and techniques for high resolution shallow mapping of the overburden stratigraphy and bedrock profile. The two most applicable techniques are high resolution engineering seismic and electromagnetic reflection profiling (also known as ground probing radar). Some examples of data from two test areas are presented which compare the results of the different techniques used and also illustrate the technical advances achieved with new equipment.

A–Cubed* Inc. has developed special equipment and has adopted consistent field procedures for the execution of detailed seismic and radar surveys. These techniques and the field procedures have been described in greater detail in a previous ETDF Summary Of Research (Davis and Annan 1985). The present paper presents an overview of examples of data from selected test areas at Base Borden and Chalk River. These sites are excellent areas for carrying out shallow soundings and have well documented geological information with which to correlate the geophysical results. A–Cubed Inc. now uses both these control test sites routinely as a basis of evaluating new equipment developments.

SITE DESCRIPTIONS

BASE BORDEN

The Borden test site is situated within the Borden Military Reserve of the Canadian Armed Forces, about 80 km NNW of Toronto, Ontario. The test site is situated in ranges I and II of the NW corner of Essa Township, Simcoe County. Figure 087.1, taken from NTS map sheet 31D/5, shows the general survey area. The specific test area is within the boxed zone on the map. The site was selected primarily because previous investigations in the area had been conducted by the University of Waterloo for ground water studies (Cherry 1983). The site is quite close to Toronto and thus readily accessible for quick instrument and method testing field trips.

The Quaternary deposits of the test site and the area around the Borden Military Reserve consist of glaciofluvial outwash sand and minor gravel (Burwasser and Cairns 1974). The principal sequence in the test area consists mainly of sand that has been reworked by shallow waters of a former glacial lake underlain by glacial till. The drift thickness within Base Borden varies from about 60 to 68 m and the general relief of the bedrock topography varies from a high of about 160 m above M.S.L., southwest of Base Borden, to a local low of about 105 m above M.S.L., northeast of Borden. The bedrock topography appears to vary gradually but this may be a result of the scarcity of wells that reach the bedrock rather than a smooth bedrock surface.

No bedrock outcrops in the area of Base Borden. The area is underlain by argillaceous and shaley limestones of Middle and Upper Ordovician ages.

® Trademark of A–Cubed Inc.

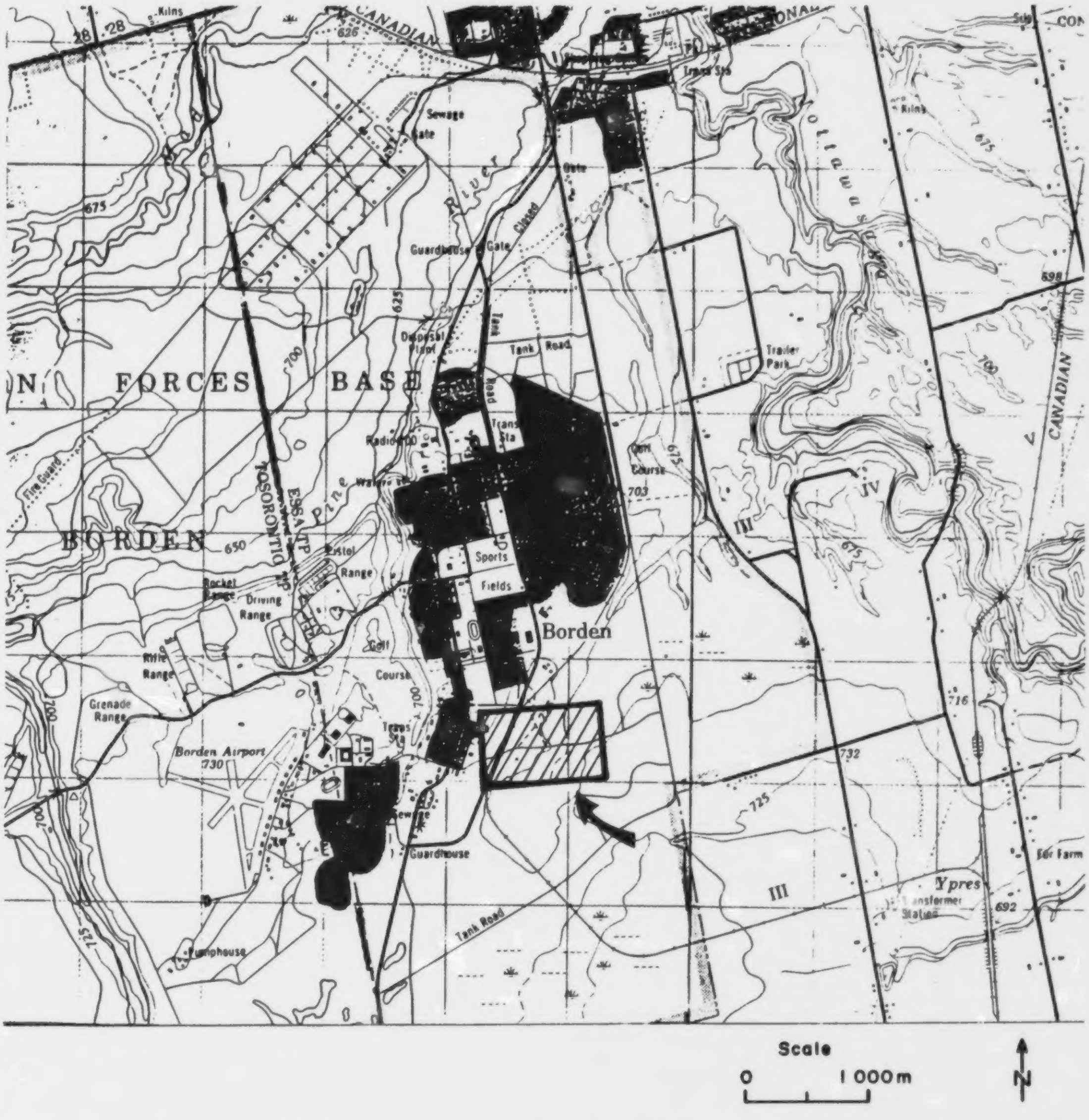
FORCES BASE
BORDEN
Borden
Borden Airport
730
Sports
Fields
Golf
Course
Rifle Range
Grenade Range
Rocket Range
Driving Range
Pistol
Range
Tank Road
Guardhouse
Sewage
Trailer Park
Ypres
Transformer Station
Fur Farm
III
IV
V
675
700
725
Scale
0
1 000m
N

Figure 087.1. Area map showing the location of the geophysical test area at Canadian Forces Base Borden. The test area is the area boxed in the lower centre portion of the map.

CHALK RIVER

The test areas near Chalk River are situated within the Chalk River Nuclear Laboratories (CRNL) site of the Atomic Energy of Canada Limited (AECL). The CRNL site is about 180 km northwest of Ottawa and is situated within the town limits of Deep River, Buchanan Township, Renfrew County. The test surveys completed were carried out with the permission of AECL. The area was selected for a test range because of the widespread and great variety of geophysical, geological and hydrogeological investigations which have been carried out in the area over the past decade (Thomas and Dixon, in press).

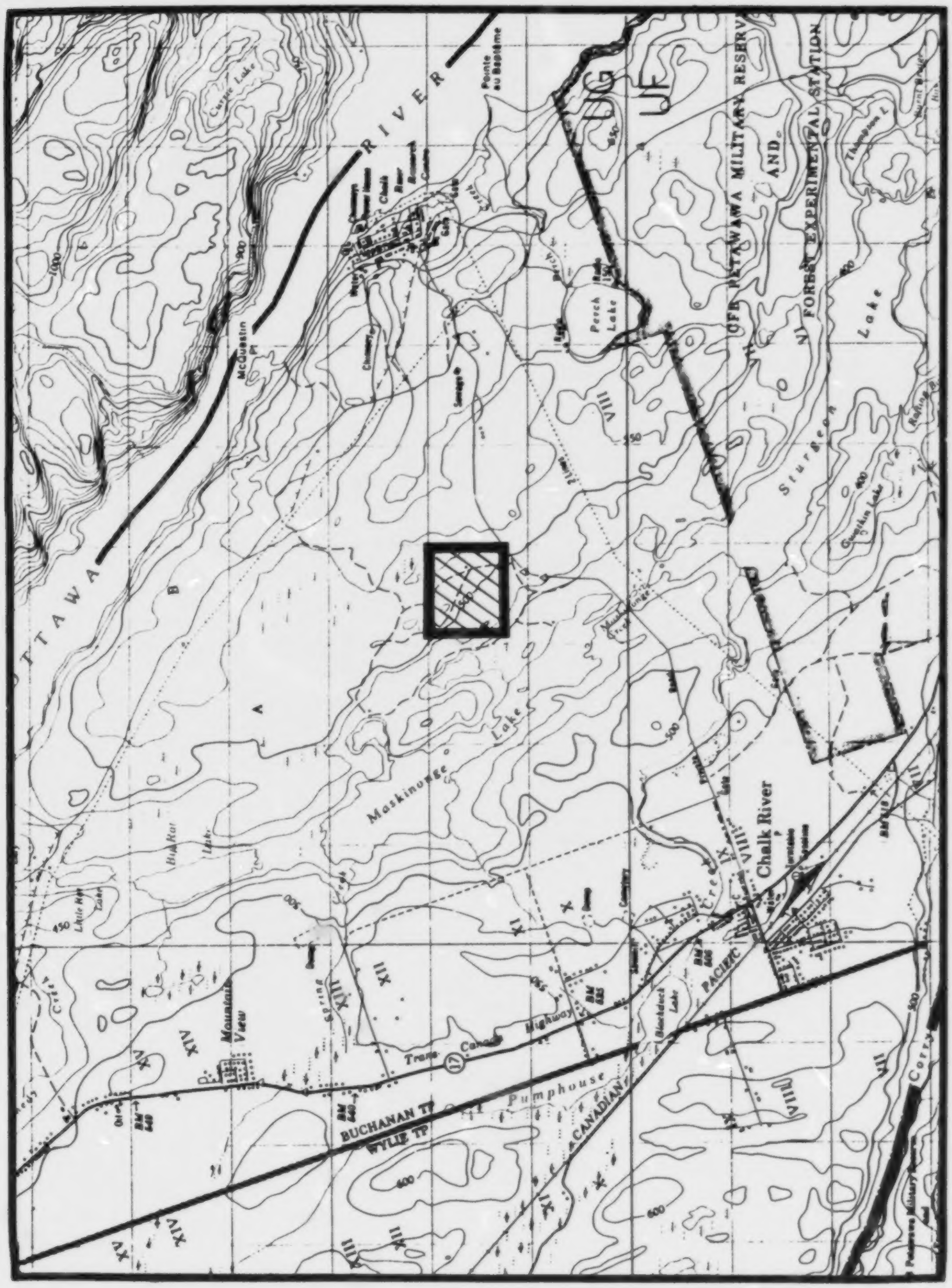
OTTAWA RIVER
McQuestin Pt
Pointe au Baptême
Chalk River
Perch Lake
Maskinonge Lake
Sturgeon Lake
Thompson L.
PETAWAWA MILITARY RESERVE AND PETAWAWA FOREST EXPERIMENTAL STATION
Little Rat Lake
Big Rat Lake
Mountain View
Trans Canada Highway
17
Pumphouse
CANADIAN PACIFIC
BUCHANAN TP
WYLIE TP
Spring
Creek
Corry
UG
UF
A
B
450
500
550
600
900
1000
VIII
IX
X
XI
XII
XIII
XIV
XV

Figure 087.2. Site location map for the Chalk River area survey sites. The field test areas are located within the zone boxed in the central part of this map area.

The principal area of interest within the CRNL site addressed in this report is outlined in the boxed area on Figure 087.2. The Quaternary geology of the CRNL area has been described by Catto et al. (1981) and a very brief summary follows. The bedrock of the CRNL area consists principally of an anorthositic suite of intrusive rocks of monzonitic to granitic composition of Late Precambrian age (Lumbers 1976). Above bedrock, the statigraphic section starts with a glacial till layer of about 12 000 BP age. A period of deglaciation was followed by a marine incursion of short duration and regressing nature resulting in the deposition of marine silts and clays. This marine incursion was of low salinity because of the small area of the marine body and its restricted contact with the open ocean. At the same time a large influx of fresh water from glaciofluvial run–off provided a high proportion of non–clay minerals in the clay–sized fraction of the marine sediments.

The upper surface of the marine sediments was modified by erosion caused by subsequent fluvial activity as the marine sea regressed and a second period of glaciation commenced. As glaciation advanced, the marine silts and clays were overlain by nearshore beach and deltaic sands followed by the deposition of a second till layer. With the last deglaciation, a sequence of varved lacustrine silts and clays, loess, fluvial sands and gravels followed.

The maximum known elevation of the marine clay sequence at Chalk River is at 139 m. This is lower than most of the deepest sections discussed in this report which means that only the upper sequences of varved silts, loess and fluvial sands are being mapped.

FIELD PROCEDURES & EQUIPMENT

EM SURVEYS

Fixed frequency electromagnetic surveys using the Geonics EM31 were conducted at Base Borden. The surveys were completed with the EM31 at waist height with the coil axes vertical. An operating frequency of 9.8 kHz and a intercoil separation of 3.66 m were used. The objective of this work was to provide ground conductivity estimates for comparison with observed radar signal attenuation and to correlate the field data to previous geophysical work carried out by the University of Waterloo (Greenhouse and Harris 1983).

EM REFLECTION PROFILING (RADAR)

The ground probing radar surveys were completed using the A–Cubed Inc. pulseEKKO I, II, III series of electromagnetic reflection profilers. The pulseEKKO I equipment is analog. For the results presented here, the unit operated at a centre frequency of 100 MHz with a window range of 500 ns.

The pulseEKKO II equipment is a prototype digital system with a window range of 4000 ns operating at a centre frequency of 30 MHz. The antenna systems for the pulseEKKO I surveys were operated mostly in the continuous mode while those for the pulseEKKO II survey were operated in the discrete step mode. Station intervals of 4 or 5 m were employed for the survey results presented in this report.

The new pulseEKKO III high performance digital electromagnetic reflection profiler developed by A–Cubed Inc. for the Geological Survey of Canada has programmable range window, sampling interval and stacking times. The data from this system shown in this paper are from Base Borden and were obtained using an antenna system with a centre frequency of 100 MHz. Discrete data collection at 2 m steps and 2 m antenna separation was the survey method utilized.

SEISMIC SURVEYS

For the seismic surveys, a Geometrics 1210 F (Nimbus) recorder was employed with direct digital read–out to a HP 9836 computer. Both units were truck mounted for these tests. Spreads of 12 geophones each with a 5 m geophone interval and 5 m shot source offset were used. Data with 1200% coverage were collected using an efficient roll–over technique for the spread layouts. Figure 087.3 illustrates typical multifold shot–geophone configurations. Geophones were 50 Hz, 710 ohm coils with 60% damping and were implanted into the frozen soil. The shot source was a 7 kg hammer impacting directly on frozen soil (Borden, mid–January) or on a damped steel plate (Chalk River, early spring). Both surveys were carried out in winter periods at times when crew and equipment were available.

High pass filtering using 100 Hz cut points on the standard Nimbus control panel were employed. Digital recording permitted either reflection or refraction interpretation and processing approaches.

EXAMPLES OF FIELD RESULTS

At each of the test areas there are a number of individual locations which have been investigated

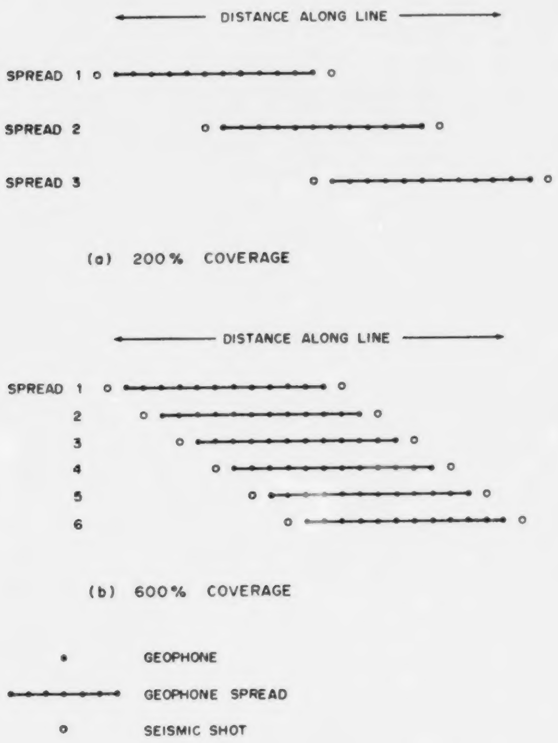

Figure 087.3. Multi-channel engineering seismographs can be used to collect multifold coverage data in survey operation. The above illustrations indicate how 200% and 600% coverage can be obtained in a rolling shot measurement manner.

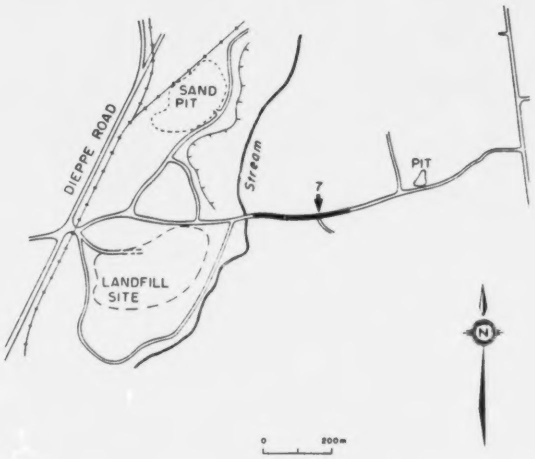

Figure 087.4. Detailed site map for the survey area at Base Borden. The section of the road profiled is shaded in. The marker with pointer 7 is a reference point on the data sections shown in Figures 5 through 8.

to varying degrees. In some instances the objective was to define the comparison between radar and seismic methods. In other instances the objective was to define the comparative performance of different radar systems which have been evolved by A-Cubed Inc. over the past three years. The following presents a few selected examples which illustrate some interesting points at each of the test areas. More detailed information on both areas can be obtained from A-Cubed Inc.

BASE BORDEN

At Base Borden, radar, seismic and EM31 profiling have been carried out over a number of sections of road. One section of road which has proven to be a good test line for radar systems is indicated in Figure 087.4. This section of road which is about 450 m in length runs up a gradual slope rising about 8 m in the 450 m length of line. At the west end of the line there is a small stream. The east end of the line terminates at the crest of the hill.

In Figure 087.5 the EM31 conductivity profiling data is presented. The average ground conductivity is about 9 mS/m. The EM31 data provides a background basis for understanding radar penetration at the site. This level of ground conductivity assuming a homogeneous half space would result in a radar penetration depth of about 15 m assuming a system performance of 120 dB. The radar signal attenuation rate for the soil is estimated to be 2.6 dB/m.

There are minor fluctuations in the EM31 data. The explanation of these localized peaks is not obvious. The higher conductivity at the west end of the line could be associated with contaminated ground water. The other peak in the data might be associated with a localized clay pocket. The radar data shows a lot of scattering in this area indicating a heterogeneous subsurface.

Three radar sections over this line are presented in Figures 087.6, 7 and 8. Figure 087.6 shows the data from the pulseEKKO I system. This unit is totally analog and uses a burnt paper line scan recorder for data display. Data

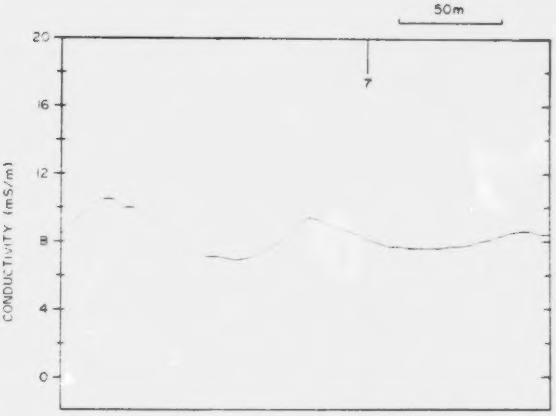

Figure 087.5. EM conductivity versus position along the section of road shown in Figure 4.

were collected using a 2 m antenna separation with continuous profile attained by towing the antenna system behind a truck.

The data in Figure 087.7 were obtained using the pulseEKKO II system. The pulseEKKO II system operating with a centre frequency of about 30 MHz was the precursor unit to the pulseEKKO III digital radar system. This particular line was surveyed in discrete step mode using an antenna separation of 4 m and a 5 m step interval. Historically, ground probing radars have been continuous profilers generating data as shown in Figure 087.6. The pulseEKKO II is the first step towards the discrete step mode of radar system. This type of system is much more useful in rough terrain as it allows profiling in a controlled manner. One of the major questions with radar sounding is what should the step interval be on a particular site. There are obviously some situations where sounding on a 5 m step interval is fine. In other situations sounding on a 0.5 m interval is required. The main feature of the pulseEKKO II data was that it demonstrated a superior performance in terms of depth penetration. The lower operating frequency, however, combined with the large step interval employed resulted in lower resolution of sub-surface features.

Figure 087.8 shows the data along the same line collected with the pulseEKKO III radar system. These data were collected using 100 MHz antenna systems with a 2 m antenna separation and a 2 m step interval in discrete profiling mode. It is quite evident from these data that the system has achieved comparable resolution to that obtained with the continuous profiler pulseEKKO I but the performance capabilities of the pulseEKKO III system are superior to the pulseEKKO I.

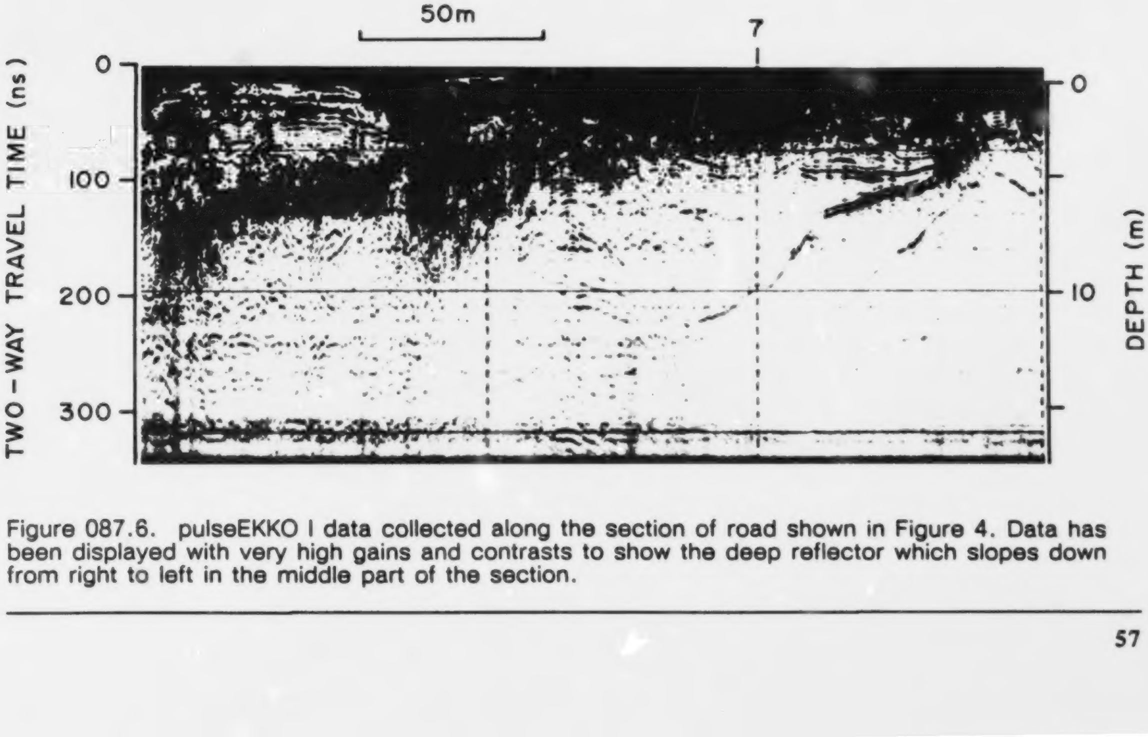

Figure 087.6. pulseEKKO I data collected along the section of road shown in Figure 4. Data has been displayed with very high gains and contrasts to show the deep reflector which slopes down from right to left in the middle part of the section.

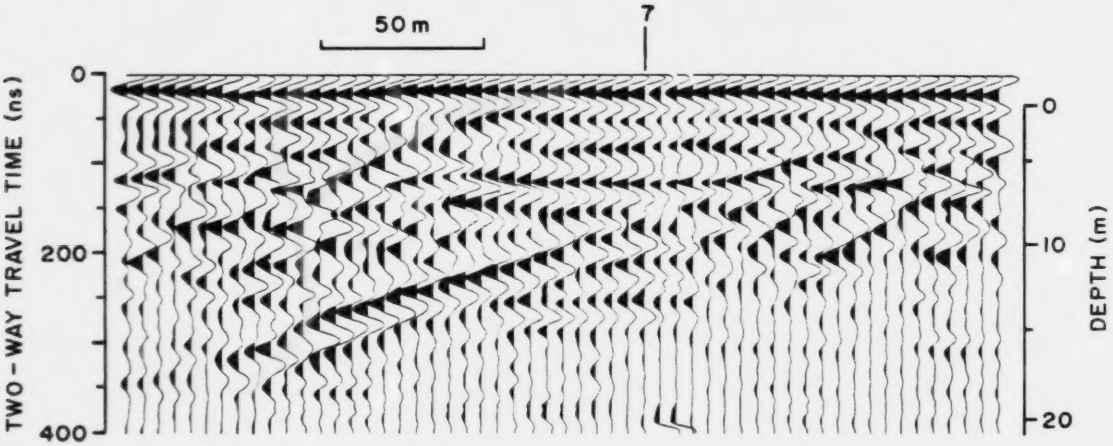

Figure 087.7. pulseEKKO II digital discrete mode radar data section for the area highlighted in Figure 4. These data are plotted on the same scale as that for the pulseEKKO I shown in Figure 6. An antenna separation of 4 m and a step interval of 5 m was employed for this survey work. The centre operating frequency of the radar was 30 MHz.

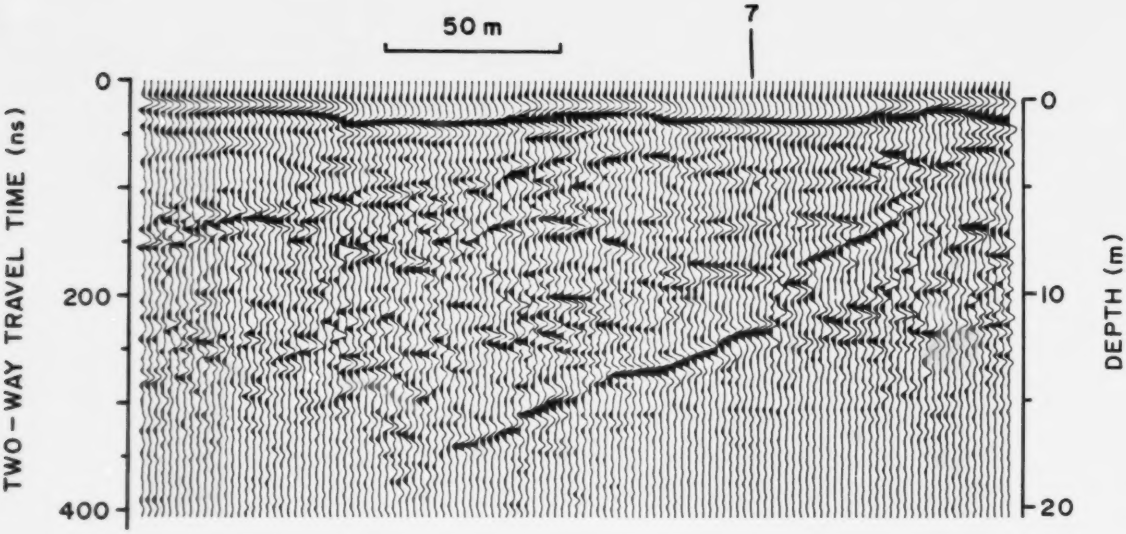

Figure 087.8. pulseEKKO III data section for the test area at Base Borden. These data are from the same area shown in Figures 6 and 7. In this instance, the new pulseEKKO III digital radar unit was employed. Data were collected using an antenna separation of 2 m and a step interval of 2 m. The centre operating frequency was 100 MHz.

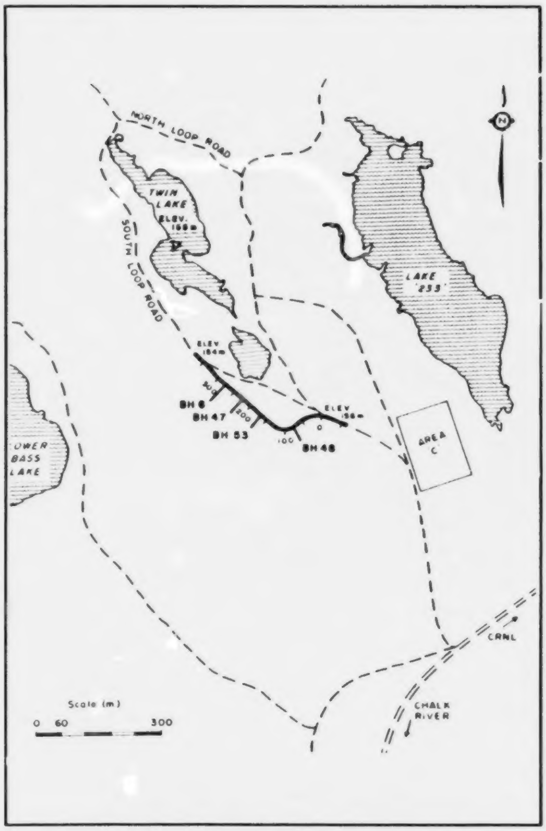

Figure 087.9. The Twin Lake Road test survey area is highlighted in the middle of this section. Refer to Figure 2 for the location of this area with respect to the main Chalk River site map.

The section of line described here has been surveyed many times with the various radar units and the same response has been consistently observed. The area can now be used as a standard site for regular testing of equipment. Extension of this line to the west is covered by both radar, seismic and EM31. The pulseEKKO I data continues about 0.5 km to the east following the road system.

CHALK RIVER

As with the Camp Borden site there are numerous areas which have been investigated in the Chalk River area using radar, seismic and other geophysical techniques. Data from two localized test areas denoted as the Twin Lake Road and the Area C Main Road zones are presented here.

Twin Lake Road

The Twin Lake Road survey area is shown in Figure 087.9. Figure 087.9 is an enlargement of the small boxed area shown on Figure 087.2. This particular test area was selected because of its rather abrupt bedrock depth variations. In addition there are a number of boreholes along the road alignment which permit correlation of survey results with sub-surface investigation data. Figure 087.10 shows the pulseEKKO I continuous profiling data along the section of road indicated. This area is an ideal one for radar in that the overburden conductivity is less than 1 mS/m. The radar data clearly defines the bedrock topography and also defines a number of strata in the overburden in the area.

Figure 087.11 illustrates the data from the same section obtained with the pulseEKKO II unit in discrete step mode using an antenna separation of 4 m and a step interval of 4 m. The lower frequency large step profiling information has less resolution than the pulseEKKO I data but clearly defines the major stratigraphic units. Again the system has the advantage that more closely spaced data can be collected if required and data collection in rough terrain is as easy as it is on the road. The main point to be noted is that both systems define the same stratigraphy and correlate well with the borehole data shown in Figure 087.12. This site has been visited regularly and the same results have been obtained with radar over the past decade. Hence this test road makes an ideal area for comparison of equipment performance levels as instrumentation capabilities improve.

Area C Main Road

Figure 087.13 shows the location of another test line which is just to the north and east of the Twin Lake site. This site is of interest because it was used for both radar and seismic testing. The radar section for this area is shown in Figure 087.14. This is characterized by a very strong reflector at a delay time of 50 to 100 ns. A number of strata are faintly visible in the pulseEKKO I data at greater depths but an experienced eye is usually required for identifying these features on the pulseEKKO I data. The bedrock surface is highlighted on Figure 087.14 to draw the readers attention to this event. The interpreted radar section is shown in Figure 087.15. Drilling in the area confirms that many of the identified radar horizons correspond with strata of varying depositional history.

The same section of line was surveyed using high resolution reflection/refraction survey methods. A rolling spread digital acquisition mode of operation was employed along this line. A geophone spacing of 5 m was employed. For

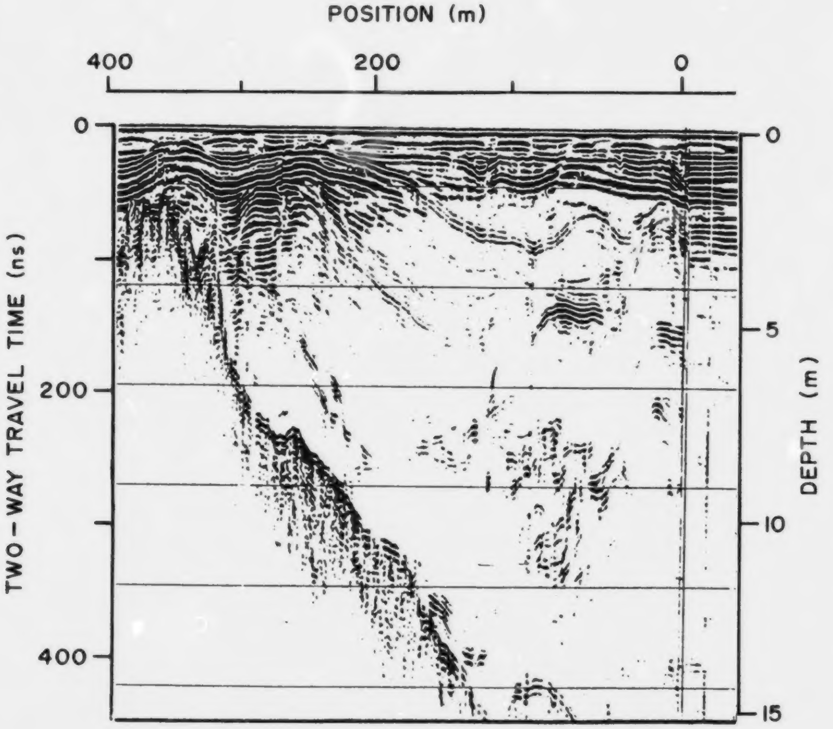

Figure 087.10. pulseEKKO I radar profile along the test section of the Twin Lake Road. Data were collected in continuous profiling mode with a 2 m antenna separation.

every shot a complete 12-channel section was acquired. These data were saved in digital form for future processing. The primary objective of the survey method was to assess whether or not data could be collected routinely without detailed consideration being given to the characteristics of the site as is normally required. The idea was to collect data with considerable redundancy so that the data could be treated with either reflection or refraction processing.

Figure 087.16 shows a set of four shot/spread data sets collected at 5 m intervals along the road. Since these data were acquired in digital form they can be replayed in a number of ways. Figure 087.17 shows the data plotted in the common offset manner with a shot geophone offset spacing of 50 m. While this section looks like the conventional high resolution common offset reflection data such as presented by Hunter et al. (1984), in fact the two main arrivals in the data set are both refraction arrivals. For this offset the first arrival is the bedrock refractor and the second arrival is the water table refractor. Using a simple two layer model for the site it was possible to reconstruct a section which showed the depth to water table and depth to bedrock. This result is presented in Figure 087.18.

The important feature about the collection of refraction data in this manner is that it allows the data to be worked in several forms depending on the precise nature of the site. Since subsurface conditions are not predictable before the survey it is best to collect data in this manner so that there are a number of options in how the data can be processed and interpreted after the fact. This leads to more efficient data collection in the field and a much higher level of confidence in the interpretation after the fact. This particular site proved to be a very interesting one in that the water table refractor was never a first arrival event. In other words it was a hidden layer in the classic sense for seismic refraction work. Data collection in the manner shown here indicates that indeed this event can be accounted for and interpretations carried out in a sensible manner to accommodate a hidden layer by use of second arrival events in the data.

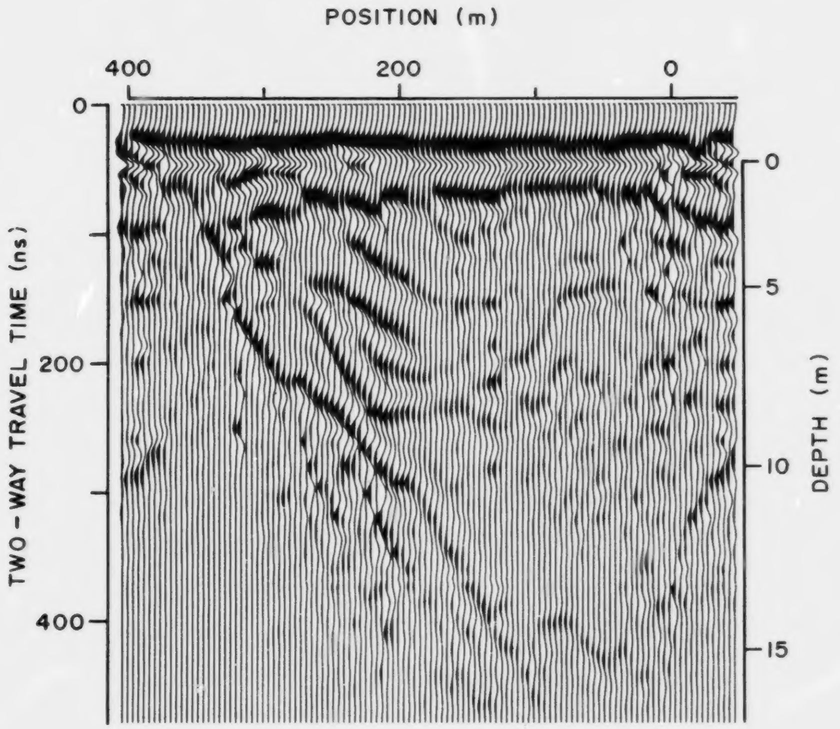

Figure 087.11. pulseEKKO II profile data for the Twin Lake Road section. The data shown were collected with an antenna separation of 4 m and a step interval of 4 m. The centre operating frequency was 30 MHz.

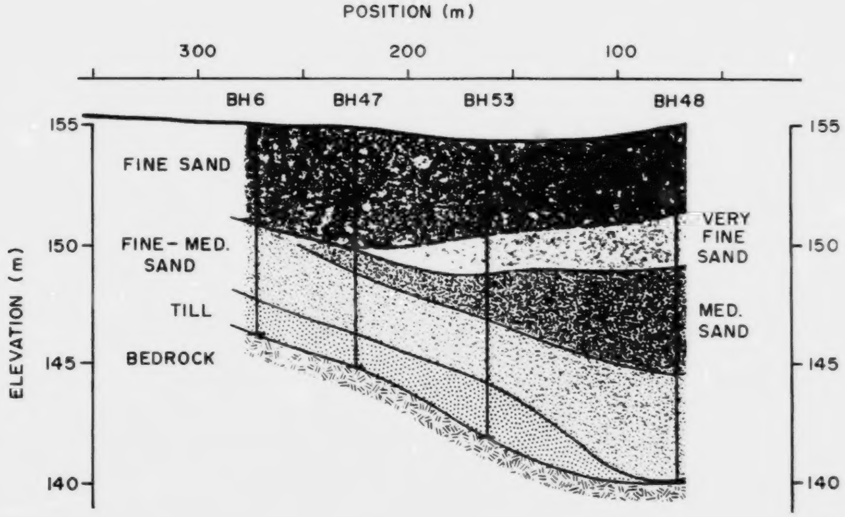
POSITION (m)
300
200
100
BH6
BH47
BH53
BH48
ELEVATION (m)
155
150
145
140
FINE SAND
FINE-MED. SAND
TILL
BEDROCK
VERY FINE SAND
MED. SAND

Figure 087.12. Borehole section for the Twin Lake Road area used for test survey work.

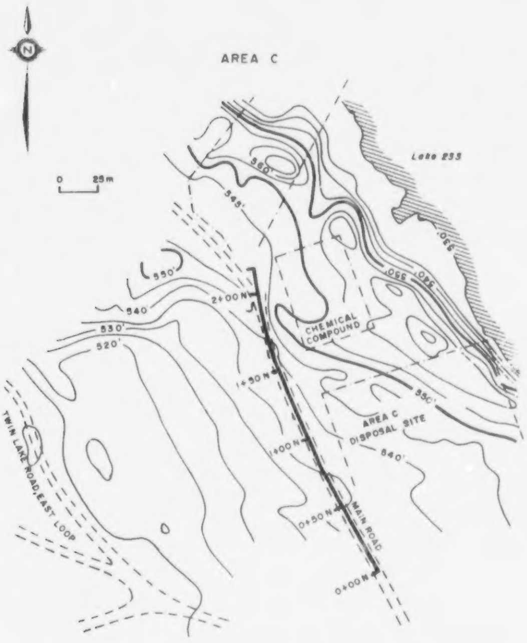
N
AREA C
0 25m
Lake 233
560'
545'
550'
540'
530'
520'
2+00N
1+50N
1+00N
0+50N
0+00N
CHEMICAL COMPOUND
AREA C DISPOSAL SITE
MAIN ROAD
TWIN LAKE ROAD, EAST LOOP
530'
540'
550'
550'
540'

Figure 087.13. Detailed location map for the Area C Main Road test survey line. Refer to Figure 087.2 for the location of this site with respect to the main Chalk River location map.

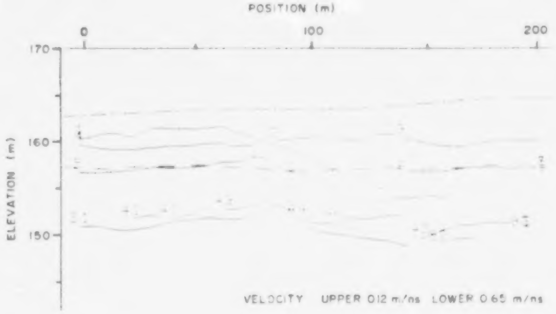
POSITION (m)
0
100
200
170
160
150
ELEVATION (m)
VELOCITY UPPER 0.12 m/ns LOWER 0.65 m/ns

Figure 087.15. The subsurface section inferred from the pulseEKKO I radar data shown in Figure 087.14.

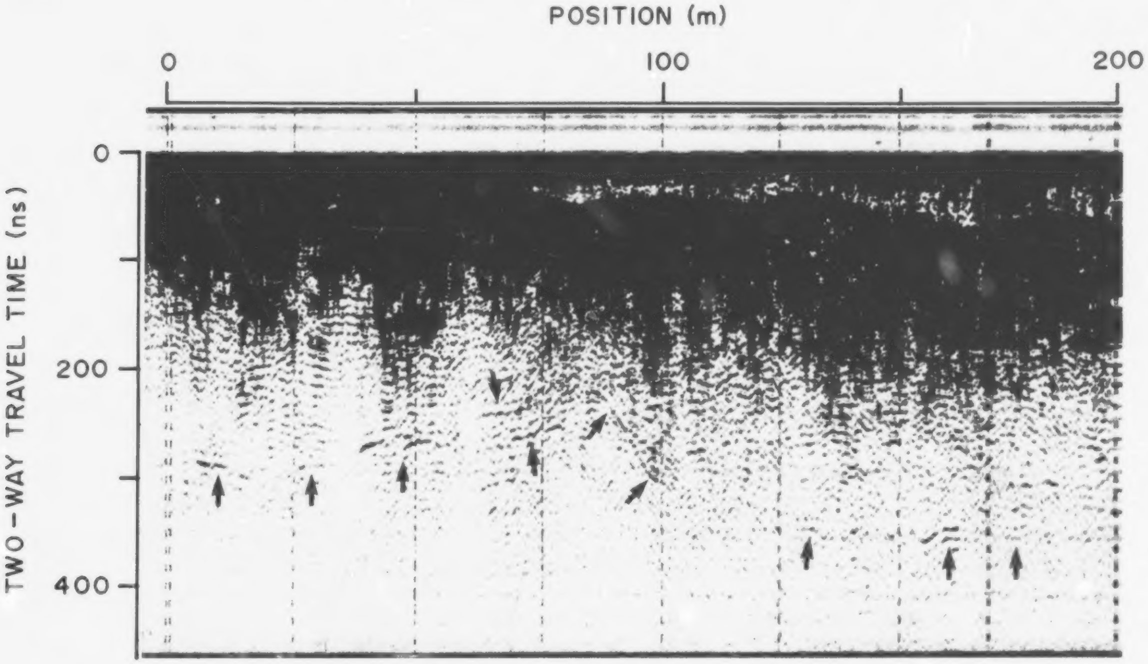

Figure 087.14. pulseEKKO I radar section along the Area C Main Road. Arrows highlight the weak reflection from the bedrock surface.

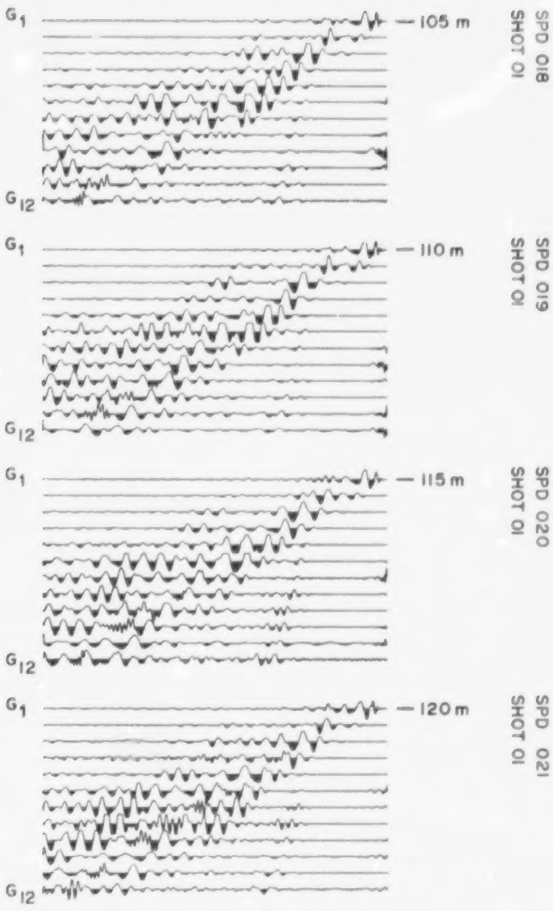

Figure 087.16. A subset of the 12-channel digitally recorded seismic data for a number of shot locations along the Area C Main Road. Each spread of data shown was collected in a rolling data collection procedure with steps of 5 m and a the geophone spacing is 5 m.

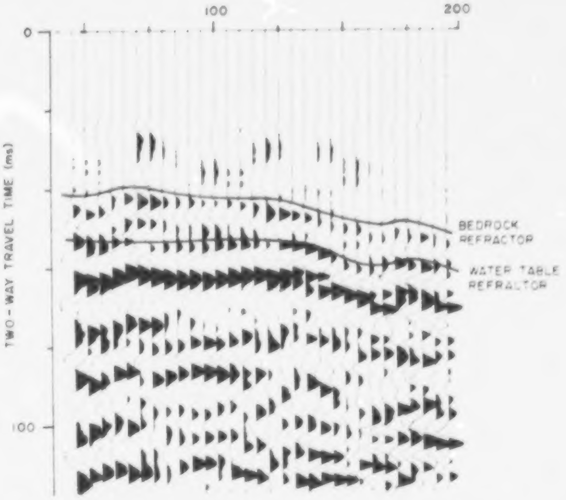

Figure 087.17. The data shown in Figure 087.16 has been compiled into a common offset display using a common offset of 50 m.

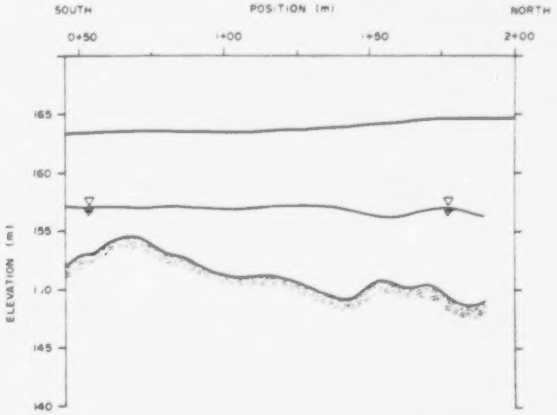

Figure 087.18. The seismic data in Figure 17 have been used to generate this interpreted section for the Area C Main Road. These results compare favourably with the interpretation acquired from the radar data shown in Figure 087.15 (Note that the seismic data do not span the full length of the area surveyed with radar).

SUMMARY AND CONCLUSIONS

This project has permitted the systematic carrying out of test surveys in a number of locations. Several test sites have been defined and controlled information on the geology and geophysical response is now in hand. Some of the areas were described in a previous ETDF report (Davis and Annan 1985). In addition the work carried out on this project has permitted evaluation of several different forms of field methodology for both radar and seismic techniques.

We very much encourage people to use these areas in the future for testing their new instrumentation or techniques. The systematic testing in these areas will continue to improve our knowledge base for the sites. A–Cubed Inc. staff have further information on the test areas and this information is available upon request.

The data examples here clearly demonstrate the evolution of the radar technique. Two major points which should be noted are the evolution from continuous to discrete mode radar. The other is the evolution of radar from an analog measurement system to a totally digital system with data presentation akin to that used for seismic techniques.

Integration of radar and seismic has proven a very powerful combination of methods for high resolution subsurface investigations. In situations where there is high attenuation in the overburden, radar has a limited penetration depth. In such instances radar can be used for the shallow stratigraphy and seismic can be used to map the deeper horizons typically at bedrock depth. Radar has a survey speed and resolution advantage when compared to seismic.

The utilization of redundancy in seismic data for both engineering reflection and refraction survey methods is a very powerful approach to field operations. The one example presented here illustrates the flexibility in handling the data post–survey if a systematic high volume digital data collection scheme is used in the field.

ACKNOWLEDGMENTS

The work on this project has been carried by a number of people at A–Cubed Inc. The authors wish to acknowledge the contributions of all those who have participated in the various field surveys. In addition, the support of Mr. L.S. Collett and Dr. J.A. Pilon of the Geological Survey of Canada is acknowledged; these individuals have been instrumental in support of the development of the new digital pulseEKKO III radar system. The support of the Ontario Geological Survey ETDF program which made many of these field tests possible is also gratefully acknowledged. Field work at Chalk River has been carried out in close proximity to site investigations directed by Mr. R. D. W. Killey of Atomic Energy of Canada Ltd. whose interest and enthusiasm is highly appreciated.

REFERENCES

Annan, A.P., and Davis, J.L.
1976: Impulse Radar Soundings in Permafrost; Radio Science, vol. 11, Number 4, p.383–394.

Burwasser, G.J. and Cairns, B.D.
1974: Quaternary Geology of the Barrie Area (Western Half) Southern Ontario; Ontario Ministry of Natural Resources, Preliminary Map P. 978, Geol. Ser., scale 1:50 000. Geology 1974.

Catto, N.R., Patterson, R.J. and Gorman, W.A.
1981: Late Quaternary marine sediments at Chalk River, Ontario; Canadian Journal of Earth Sciences, vol. 18, p.1261– 1267.

Cherry, J.A., Guest Ed.
1983: Migration of Contaminants in Groundwater at a Landfill: A Case Study; Journal of Hydrology, vol.63, p.197.

Davis, J.L. and Annan, A.P.
1985: High Resolution Shallow Soundings Using Radar and Reflection Seismic Methods; Grant 087, p.68–79 *in* Exploration Technology Development Program of the Board of Industrial Leadership and Development, Summary of Research 1984–1985, edited by V.G. Milne and R.B. Barlow, Ontario Geological Survey, Miscellaneous Paper 125.

Greenhouse, J.P. and Harris, R.D.
1983: Migration of contaminants in groundwater at a landfill: a case study, 7. DC, VLF, and inductive resistivity surveys; p.177–197 *in* Migration of Contaminants in Groundwater at a Landfill: A Case Study, edited by J.A. Cherry, Journal of Hydrology, vol.63.

Hunter, J.A., Burns, R.A., Gagne, R.M., Good, R.L., MaCaulay, H.A., and Pullen S.E.
1984: Field Experience with "Optimum Window" Hammer Seismic Reflection Technique; Society of Exploration Geophysicists, 52nd Annual Meeting, Abstracts, p.466–468.

Lumbers, S.B.
1976: Mattawa - Deep River Area (Eastern Half), District of Nipissing and County of Renfrew; Ontario Division Mines, Preliminary Map P.1197, Geol. Ser., scale 1:63 360. Geology 1972 to 1975. Compilation 1972 to 1976.

Morey, R.M.
1974: Continuous Subsurface Profiling by Impulse Radar; Proceedings of Engineering Foundations Conference on Subsurface Explorations for Underground Excavation and Heavy Construction, Henniker, N.H., USA, p.213–232.

Thomas, M.D. and Dixon, D.F., Editors
in press: Geophysical and Related Geoscientific Research at Chalk River, Ontario; Proceedings of a workshop held at Ottawa, December 14–15, 1983. AECL–8327.

Grant 089 — Testing and Demonstration of Interpretation Software for Magnetic, EM and Spectrometry Inversion

S.W. Reford and N.R. Paterson

Paterson, Grant & Watson Limited, Toronto

ABSTRACT

Computer software has been developed to assist in the interpretation of airborne magnetometer, ground electromagnetometer (EM) and airborne spectrometer data. Emphasis has been placed on techniques of direct application to exploration problems in Ontario. Work is continuing to further develop these techniques and to test their applicability by means of data sets from a number of well-known areas. Documentation of some of the methods is complete; in other cases, it is nearing completion. The capabilities and applications of the techniques are being presented to the mineral exploration community through publications, case histories, conference presentations and other technical media.

OBJECTIVES

Several geophysical interpretation software programs were developed in 1981–1984 with the aid of Exploration Technology Development Fund (ETDF) grant 011. The overall objective of the current project is to evaluate and demonstrate the effectiveness of these programs by rigorously testing the methods on data sets in areas where the physical properties and geology are adequately known. After necessary modifications to the software, final interpretations will be prepared and published in the form of case histories.

The three essential elements to the project are: testing and evaluation; modifications and final development; final application and publication. All three phases are considered essential if these interpretation tools are to be accepted by the mineral exploration industry and applied effectively to exploration in Ontario.

FIELDS OF STUDY

MAGNETIC INVERSION (SUSCEPTIBILITY MAPPING)

The SUSMAP technique is a spatial domain procedure that iteratively determines the apparent magnetic susceptibility of a grid of sources modelled as vertical prisms of infinite depth extent, each with a specific depth–to–top, from an identical grid of total field values (Paterson et al. 1983). The use of a model with a variable depth to its upper surface produces a more accurate determination of susceptibility, thus enhancing the interpretation and, at the same time, eliminating terrain effect. It is also possible to calculate the total field response on an arbitrary surface from a grid of susceptibility values and depths. This allows for simulation of a barometric–flown aeromagnetic survey from measured drape–flown data, or vice versa.

The technique has been successfully applied to the problem of reducing the terrain effect on aeromagnetic data. A number of examples were prepared for a paper presented at the meeting on Potential Fields in Rugged Topography held in Lausanne, Switzerland (Paterson 1985). Figure 089.1 illustrates the problem in aeromagnetics. Often, the data is acquired over areas with significantly varying topography. For a constant barometric–flown survey, the depth below the sensor of the magnetic sources can change significantly across an area due to steep topography. For drape–flown surveys, one attempts to maintain the height of the sensor above the earth's surface constant. Since this cannot be achieved in practice, variable height is a major source of terrain effect. The diagram also shows that the contribution of

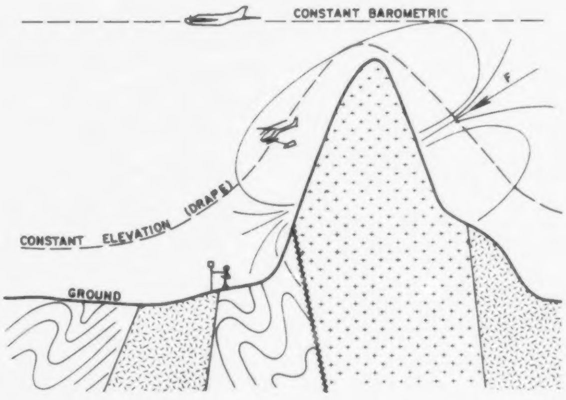

Figure 089.1. Magnetic surveys over variable topography.

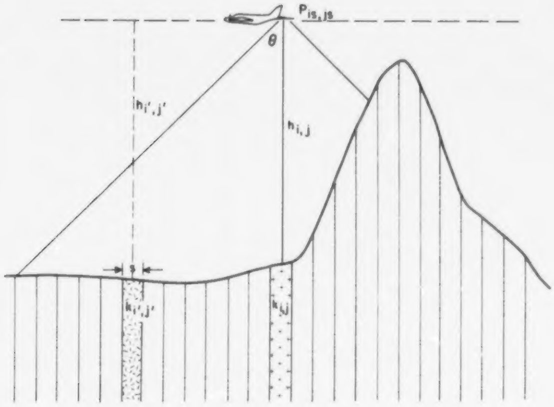
Pis,js
θ
hi',j'
hi,j
s
ki',j'
ki,j

Figure 089.2. The SUSMAP technique's model earth as applied to the variable topography problem.

the sources, situated in the "window" that is "seen" by the sensor, regardless of height, changes with the terrain (a ground magnetometer survey in rough topography contains strong terrain effects). Another factor to consider is that the magnetic sources may or may not correlate with the topography (i.e. a topographical feature may also be a geological feature). Terrain correction methods (e.g. Grauch 1985) that minimize correlation suffer accordingly.

Figure 089.2 shows the model used by the SUSMAP technique as it applies to the problem, for a barometric-flown survey in this case. The earth is modelled by a set of square-ended vertical-sided prisms (of width s), each with a susceptibility k(i,j). The depth to the top of each prism, h(i,j), is calculated as the elevation of the earth's surface (digitized from a topographic map or calculated using the aircraft's altimetry records) subtracted from the measured sensor altitude (not strictly constant in practice). The measured magnetic field, P(i,j), is considered to be the sum of the contributions of all sources (i.e. prisms) lying within a window specified by the angle θ. Although the diagram illustrates the model as a two-dimensional cross-section, the technique operates in three dimensions, with the window taking a square shape.

A data set was treated from a survey measured in the Pleasant Bay area on the northwest coast of Cape Breton Island. The simplified geology of the area is given in Figure 089.3 (taken from Neale 1963). The area is underlain by Devonian paragneiss cut by Devonian syenite. Some inliers of Precambrian mafic schists remain. Near the coast, Mississippian sandstones lie in fault contact with the Devonian rocks. The topography (Figure 089.4) is dominated by a number of hills and two major valleys, striking northeast and southeast. Local relief reaches 400 m. The total field (Figure 089.5) was measured by an aeromagnetic survey, flown at a barometric altitude of 610 m above sea level. The flightlines were oriented east-west, 400 m apart and the resolution of the measured field was 0.01 nT.

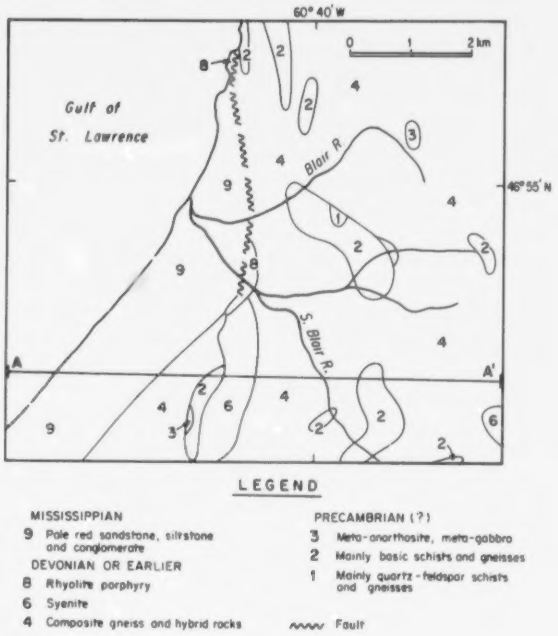
60° 40' W
0
1
2 km
Gulf of
St. Lawrence
Blair R.
S. Blair R.
46° 55' N
A
A'
9
8
6
4
3
2
1
LEGEND
MISSISSIPPIAN
9 Pale red sandstone, siltstone and conglomerate
DEVONIAN OR EARLIER
8 Rhyolite porphyry
6 Syenite
4 Composite gneiss and hybrid rocks
PRECAMBRIAN (?)
3 Meta-anorthosite, meta-gabbro
2 Mainly basic schists and gneisses
1 Mainly quartz-feldspar schists and gneisses
Fault

Figure 089.3. Geology map of the Pleasant Bay area, Cape Breton Island, Nova Scotia.

The total field shows a positive correlation between valleys and negative peaks in the field, and, to a degree, between hills and positive peaks. This is more prevalent in the southern part of the area. The field falls off steadily, moving away from the coast, as the distance between sensor and sources increases. Note that the topography of the ocean floor has not been included in the topography data set, preventing the analysis of the terrain effect from underwater sources.

A pole-reduced version of the measured total field was calculated (Figure 089.6). One effect of this operation is to center anomaly peaks directly

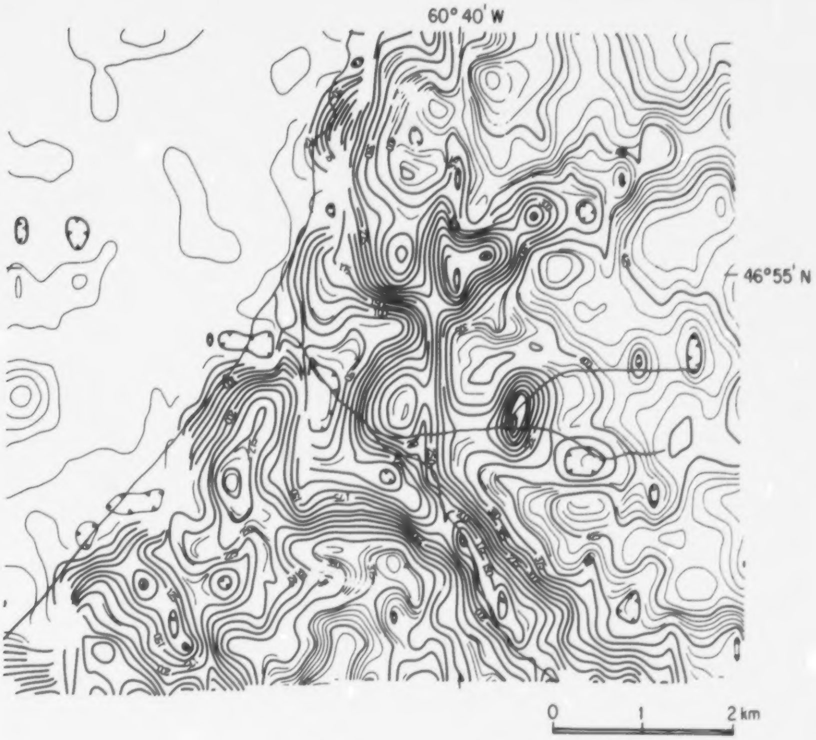
60° 40' W
46°55' N
0
1
2 km

Figure 089.4. Contour map of measured topography (metres above sea level), Pleasant Bay area.

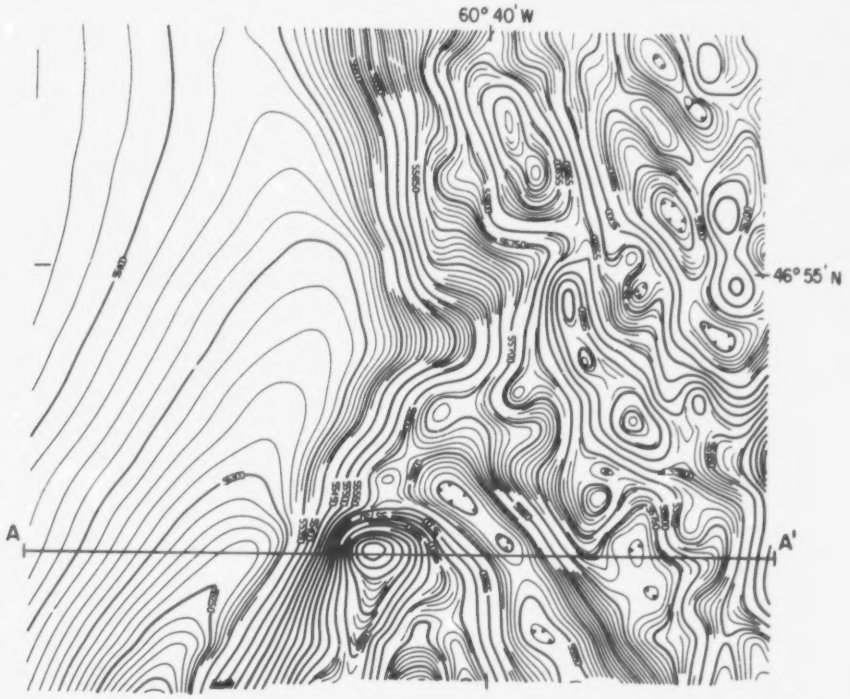
60° 40' W
46° 55' N
A
A'
0
1
2 km

Figure 089.5. Contour map of measured total magnetic field (nT), Pleasant Bay area.

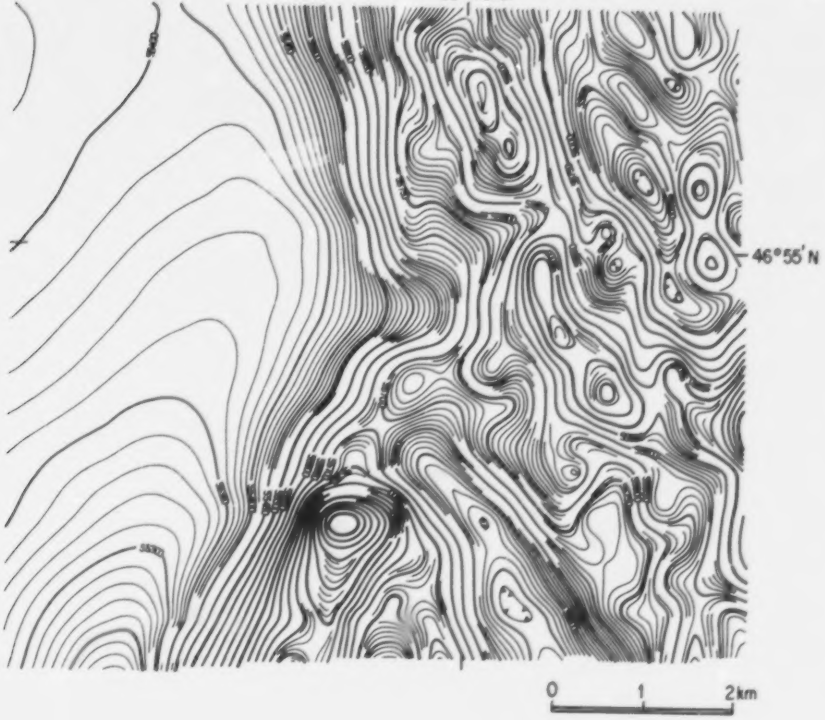
60°40'W
46°55'N
0
1
2 km

Figure 089.6. Contour map of pole-reduced magnetic field (nT), calculated with MAGMAP, Pleasant Bay area.

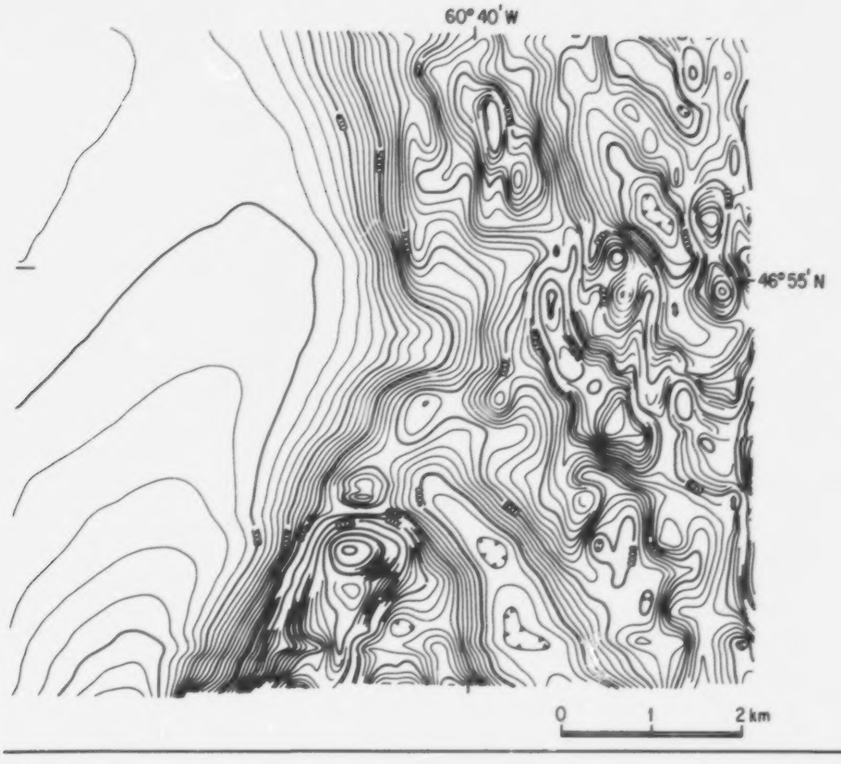
60°40'W
46°55'N
0
1
2 km

Figure 089.7. Contour map of apparent magnetic susceptibility (emu x 10^{-6}) on a level surface 200 m below plane of observation, calculated with SUSMAP Pleasant Bay area.

over their sources. Susceptibility maps are usually generated from pole–reduced data so that they will more accurately reflect the true geology. This map was generated using the MAGMAP software package, a general purpose filtering and processing system that operates in the frequency domain. It shows a minor reduction in the terrain effect since it eliminates the contribution of horizontal terrain polarization. This data set was used to produce all subsequent susceptibility maps.

Figure 089.7 shows a map of apparent susceptibility calculated, using SUSMAP, on a plane 200 m below the plane of observation. This level is approximately equivalent to the highest level of sources in the area. The map shows increased resolution in the areas of higher ground but no reduction of the terrain effect. Calculating an apparent susceptibility map on a flat surface any lower than this one will result in values that "blow up" where the altitudes of the sources exceed the level of the surface. To obtain accurate susceptibilities and good resolution in the valleys, a variable depth surface is clearly desirable.

Again using the SUSMAP technique, a map of apparent susceptibility on the ground surface was calculated (Figure 089.8). This map shows considerable detail in resolution of the magnetic structure while the terrain effects have been reduced to a minimum. It allows for a geological interpretation more detailed than the existing mapping or than could be derived strictly from the total field data.

Figure 089.9 shows a map of the total field calculated from the ground–level susceptibility on a variable altitude surface situated at a constant 100 m above the ground. The result is a map that simulates the response of a drape–flown survey measured at a flying height of 100 m. Comparison of this map to the previous map shows a small loss of detail and a minor enhancement of the terrain effect, mainly in the areas of extreme topography.

There still remains some correlation between topography and apparent susceptibility in these results: in the vicinity of the large valley to the south for example. This is, in fact, due to a correlation between topographical and geological features. The location of profile A–A′ is noted on Figures 089.3 and 5. The cross–section at the base of Figure 089.10 shows the topography and mapped geology along the profile. Note that the geological units do not have vertically dipping boundaries as plotted. The measured and pole–reduced total fields are plotted immediately above. The two profiles of apparent susceptibility are given at the top of the diagram. We see in the latter two profiles that resolution of the magnetic response has increased but terrain effects are minimized. The profile of ground–level susceptibility shows somewhat more detail, especially in the lower elevation areas. The sources of the two major anomalies are the syenite and mafic schist units, which also coincide with peaks in the topography. The profile of the simulated, drape–flown total field shows a contribution from the topography, with peaks and valleys producing or enhancing positive and negative peaks in the data. These profile results also demonstrate that the greatest minimization of terrain effects is obtained by calculating apparent susceptibility on the variable depth surface of magnetic sources. This also holds for sources buried below the ground surface.

In the process of preparing this and other case histories, some modifications to the SUSMAP software were made. The flexibility for calculation of susceptibility and total field on any arbitrary surface was increased. Initially, a "ringing" effect was observed on the processed maps in areas of steep topography. This problem was alleviated by changing the approach taken in application of the window (Figure 089.1) to the surface of interest.

The previous example also illustrates the technique's capability for continuation of magnetic data between arbitrary surfaces, from a constant barometric– to a drape–flown surface in this case. One application of this feature would be to merge data sets from adjacent areas measured under different survey specifications.

MAGNETIC INVERSION (MAGNETIC MODELLING)

The MAGMOD method, for inversion of discrete magnetic anomalies, utilizes the well–known Marquardt least–squares optimization of the source parameters to provide a geological model for the observed magnetic response. Recently (Reford et al. 1985), work on the application of singular value decomposition (SVD) to MAGMOD commenced. This work continued during the past year. SVD has been implemented in many areas of geophysics (e.g. Paterson et al. 1983) to delineate the contribution and accuracy of each model parameter through the course of an inversion.

The theory, as it applies to MAGMOD, and the inversion algorithm have been completed, and testing of the technique is underway. As well as providing new information on the model parameters and their contribution to the model, the application of SVD will lead to a greater variety of possible model shapes, variable remanence direction, inversion to multiple magnetic bodies and the abil-

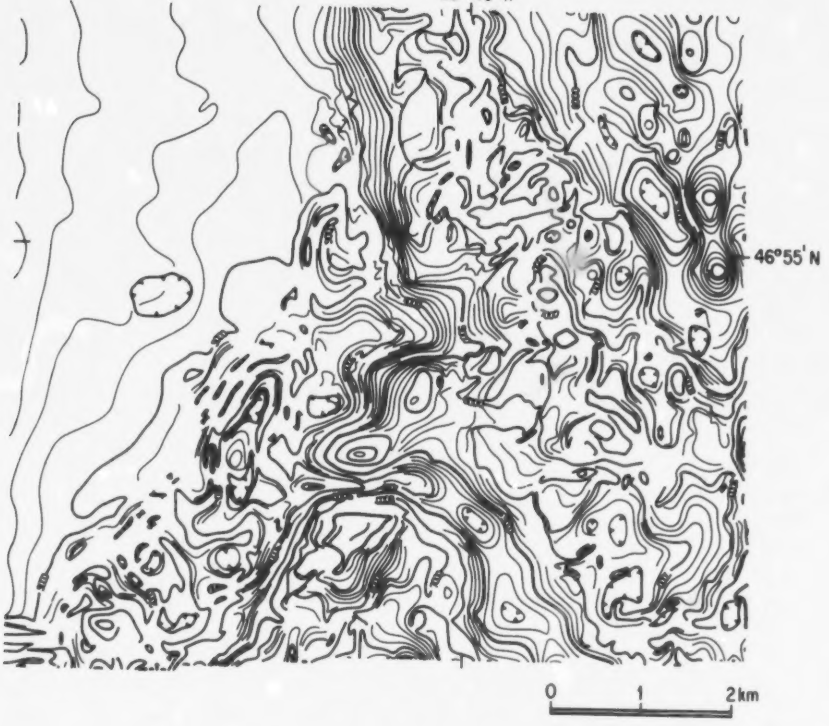
60° 40' W
46°55' N
0
1
2 km

Figure 089.8. Contour map of apparent magnetic susceptibility (emu x 10^{-6}) on the ground surface, calculated with SUSMAP, Pleasant Bay Area.

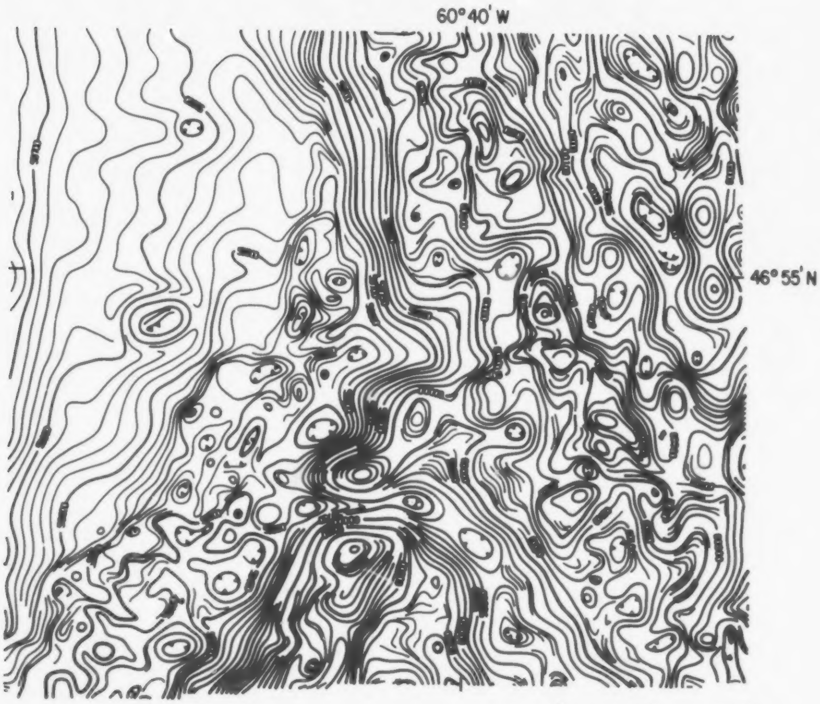
60°40' W
46°55' N
0
1
2 km

Figure 089.9. Contour map of total field (nT, contour labels 4000 nT too high) on simulated drape-flown surface 100 m above ground, calculated with SUSMAP, Pleasant Bay area.

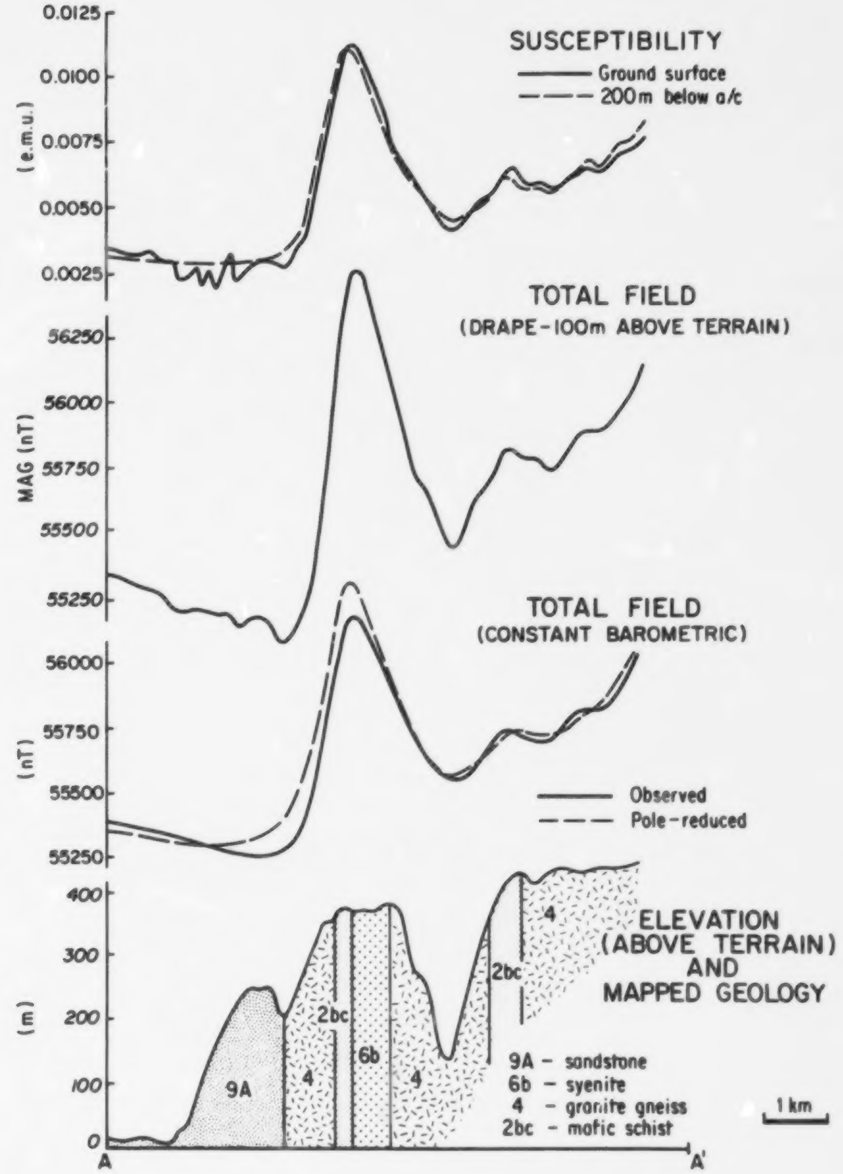

Figure 089.10. Measured magnetic response and SUSMAP inversion results, profile A–A' Pleasant Bay area.

ity to jointly invert multiple data sets, such as total field and vertical gradient.

ELECTROMAGNETIC INVERSION

The inversion of frequency–domain electromagnetic (EM) data to a layered earth model has previously been described for ground (Reford et al. 1984) and airborne (Paterson et al. 1983) systems. Both methods employ SVD as an aid to determination of the model parameters (layer resistivity, thickness and magnetic permeability (ground only)).

In 1984, EM soundings, using an eight–frequency tilt angle/ellipticity system, were measured at a number of sites in Alfred Township. Inversion of the data in terms of parametric soundings (many frequencies measured at a single coil separation) was previously described (Reford et al.

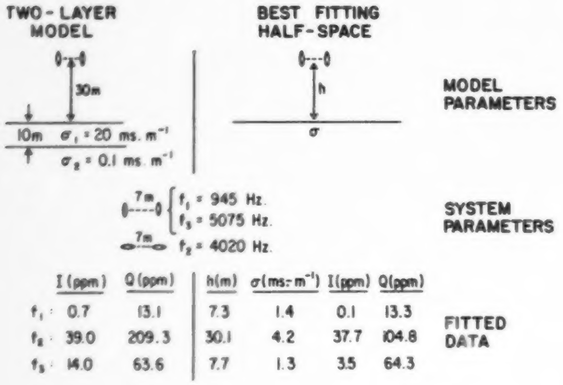
TWO-LAYER MODEL
BEST FITTING HALF-SPACE
30m
h
10m
σ_1 = 20 ms. m^{-1}
σ_2 = 0.1 ms. m^{-1}
σ
MODEL PARAMETERS
7m
f_1 = 945 Hz.
f_3 = 5075 Hz.
7m
f_2 = 4020 Hz.
SYSTEM PARAMETERS
I (ppm) Q (ppm) h(m) σ(ms·m^{-1}) I(ppm) Q(ppm)
f_1: 0.7 13.1 7.3 1.4 0.1 13.3
f_2: 39.0 209.3 30.1 4.2 37.7 104.8
f_3: 14.0 63.6 7.7 1.3 3.5 64.3
FITTED DATA

Figure 089.11. Comparison of actual 2–layer and best–fitting halfspace airborne EM responses.

1984). The data has also been assessed by treating it as a set of geometric soundings (two frequencies, three or four coil separations). SVD analysis shows that the results are, in this particular case, more ambiguous for the geometric sounding configuration. Further testing is required to determine which frequencies give the best results for the geometric soundings.

A paper was presented at the Fifty–fifth Annual Meeting of the Society of Exploration Geophysicists (Reford et al. 1985), strictly devoted to the company's research in EM inversion conducted under the ETDF program. A second paper was presented at the Geological Survey of Canada's Workshop on Airborne Resistivity Mapping (Paterson and Reford 1985). This paper incorporated a number of results from the airborne data inversion technique to demonstrate the advantages of using a two–(three–)layer model, rather than a halfspace, for resistivity mapping.

On the left side of Figure 089.11, we see the response of a frequency–domain airborne system measured over a geological situation typical to Canadian exploration, a conductive overburden overlying a resistive bedrock. On the right are given the model parameters and responses of the best–fitting halfspaces to the data, inverted separately for each frequency. Both coaxial coil pairs (frequencies 1 and 3) give good fits to the quadrature response. The inphase response of the coplanar coil is well–fitted and the depth to the ground surface below the sensor has been properly determined. In all cases, the halfspace conductivities are poor approximations to either layer conductivity in the two–layer model. The depth–to–surface was not properly determined for the two coaxial coil frequencies. At each frequency, one of the two EM component responses did not fit the data. This example demonstrates the need for a multi–layer model in many, if not most, applications of airborne resistivity mapping in Canada.

Figures 089.12 and 13 show the results from inversion of proprietary two–frequency helicopter EM data as applied to a groundwater exploration program. Inversion of the data was conducted on a continuous basis along the flightlines. Contour maps of the depth to the water table (Figure 089.12) and the conductance (Figure 089.13) were among the products generated. The shallower areas include several known springs while the deeper areas do not. The wells are located in areas of high conductance, indicating a thicker water layer or locally higher porosity. Several zones of high conductance, occurring in areas of relatively shallow depth, are of potential importance.

Development of the software for both the ground (GEMINV) and airborne (AEMINV) techniques continues. GEMINV is being upgraded to a status suitable for commercial use. This includes the addition of further EM system configurations to the software's library and the preparation of full documentation. A version specifically tailored to inversion of MaxMin data over a three–layer model earth is under development. It will have particular application to mapping overburden and the bedrock surface with MaxMin, a popular exploration tool. In addition, the feasibility of joint inversion of ground EM and resistivity data is being studied. It is expected that the addition of resistivity data to an inversion will help in resolving EM's ambiguity of separating conductivity from thickness in some situations, and also to improve the resolution of depths to the layers.

AEMINV is in the process of being adapted to inversion of data measured with the INPUT system. This is the first attempt at implementing either inversion technique with a time–domain EM system. If successful, the capabilities of the method will certainly be extended.

A report on the effect of current channeling, as it relates to EM modelling, was prepared (Hanneson 1985). These effects were studied, as the conductivity of the host rock was varied, on data measured by typical frequency–domain systems. This is a significant consideration as the inversion scheme assumes a purely inductive response in the layered earth model. The ability to recognize, and possibly remove, current channelling effects is an

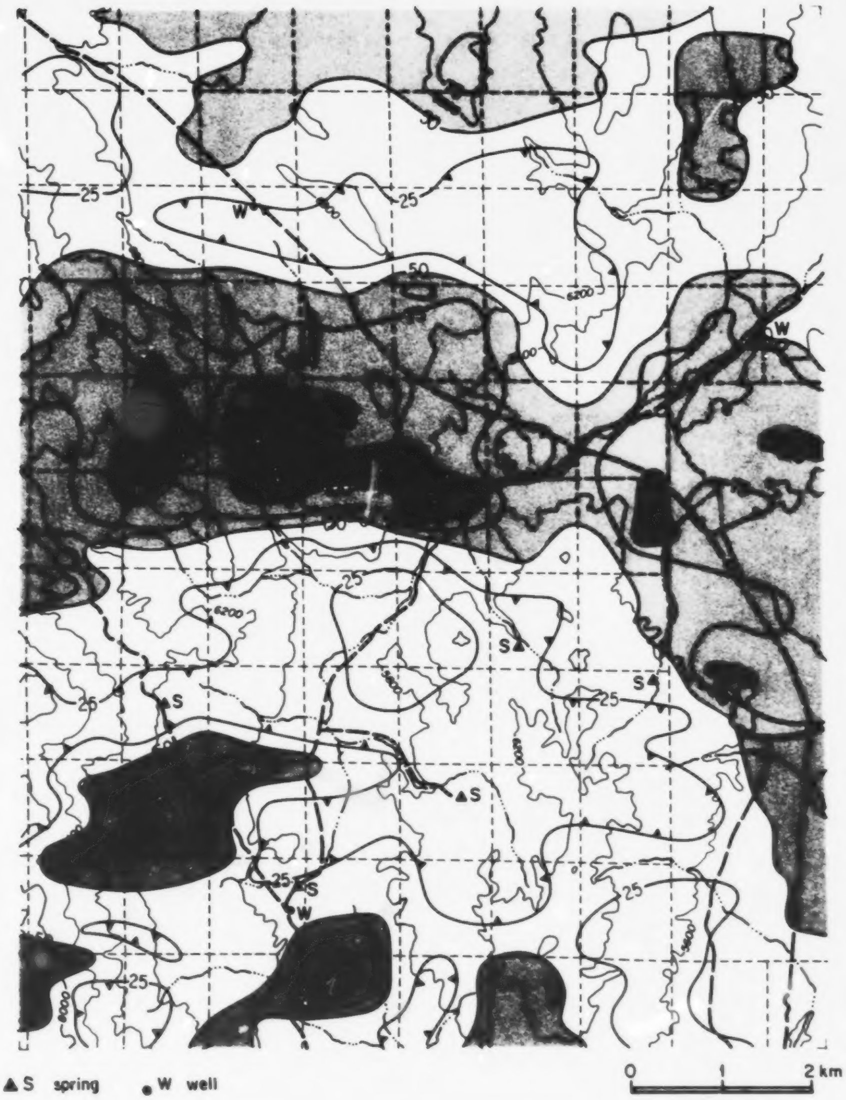

Figure 089.12. Contours of depth to water table (metres) derived by AEMINV from a 2–frequency helicopter EM groundwater exploration survey. Note occurrence of surface springs and seasonal drainage in some areas of shallow water table. Where depth is large, springs are rare.

important component of the EM inversion process under certain geological conditions.

INVERSION OF GAMMA–RAY SPECTROMETRY

The SPECMAP method (Misener et al. 1984) was developed for the presentation of three–element data on a single colour map. It has particular application to plotting three–radioelement (K, U and Th) gamma–ray spectrometric data, or any three elements in a geochemical data set. Such a colour map can be geologically zoned according to colour, intensity and texture, eliminating the need to simultaneously interpret a number of single element and ratio maps. A chart showing colour examples of SPECMAP processing was given by Reford et al. (1984).

Experience in application of this technique and feedback from users in industry have led to some modifications in the SPECMAP software. The input of processing parameters has been simplified, incorporating default values that suffice for standard application. The processing report is more comprehensive, allowing the user to assess

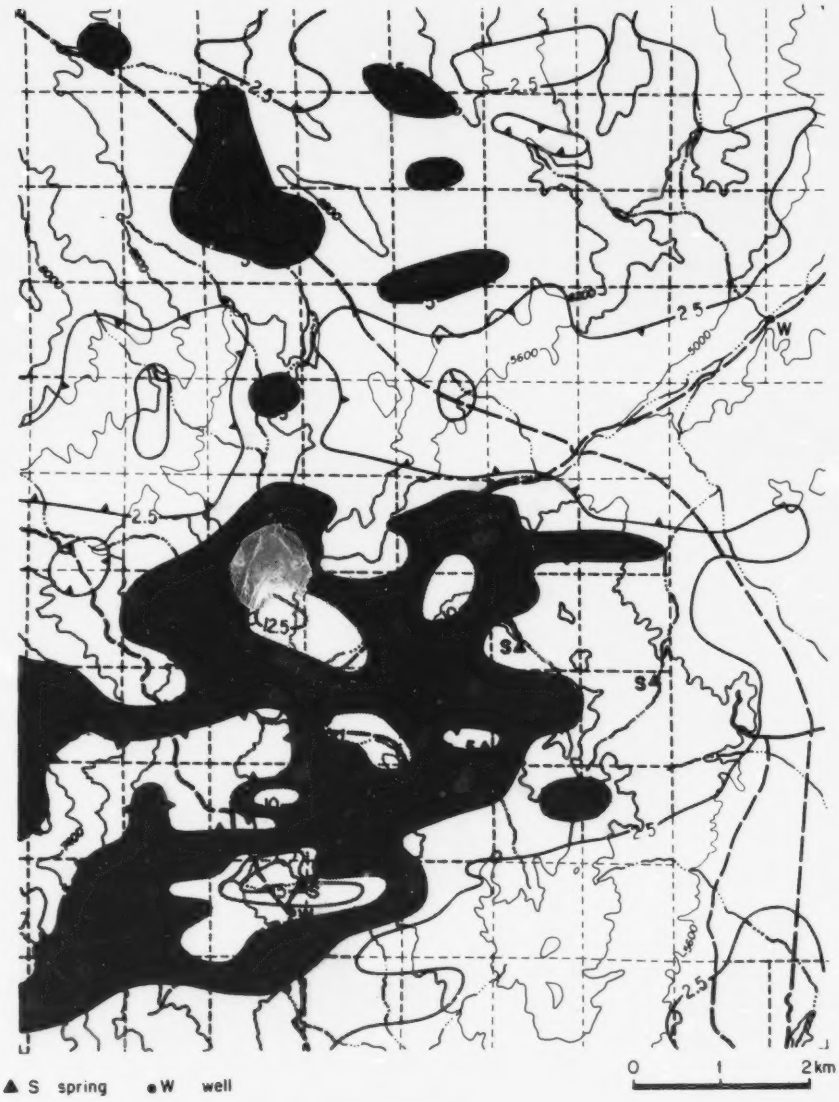

Figure 089.13. Contours of conductance (siemens) of water layer derived by AEMINV from a 2-frequency helicopter EM groundwater exploration survey. Wells are generally close to zones of high conductance, probably indicating a thicker water layer or higher porosity.

the distribution and intensity of colour on a map before it is plotted. The output colour map is produced in a grid format compatible with the plotting software of the colour plotters currently available on the market. Software tailored to the Applicon plotter has been prepared to transform such a grid into an image suitable for plotting. Colour ternary diagrams have also been gridded at different scales to facilitate the plotting of legends to accompany maps.

Full documentation for operation of the software has been completed. It includes guidelines and examples as to the choice of the processing parameters. The various map presentations and the possible statistical distributions of the element data are treated comprehensively. The application of the SPECMAP software to radiometric and geochemical data, both in-house and by users in industry, have demonstrated the many advantages of the technique and the clarity of the documentation.

CONCLUSIONS

The company's five years of research and development under the ETDF program have proven to be very fruitful. A number of new software packages, for both the micro– and mainframe computer environments, have been introduced, while other existing methods have been enhanced. New ground has been broken to aid the Ontario exploration community in the interpretation of magnetic, electromagnetic, radiometric and gravity data. The company will continue with the development of these methods so that they remain as the state–of–the–art in geophysical software. We have found that the ETDF program has given our company and many other companies the opportunity to contribute to Ontario's world–renowned reputation in mineral exploration. We believe that such a program should be continued so that the province will always lie at the leading edge of this ever–evolving field.

ACKNOWLEDGMENTS

The company is grateful to the Ontario Ministry of Northern Development and Mines for its financial assistance, and for cooperation of the staff of the Ontario Geological Survey in various aspects of the work.

The following also made valuable contributions to the work described in this paper: D.J. Misener, E. Baranyi, R.B. Hearst, D.C. Gresham, I.N. MacLeod, J.E. Hanneson and R.N. Edwards.

REFERENCES

Grauch, V.J.S.

1985: A New Magnetic–Terrain Correction Method; p. 14 in Preliminary Abstracts of the International Meeting on Potential Fields in Rugged Topography, University of Lausanne, 32 p.

Hanneson, J.E.

1985: Report on EM Computer Modelling; Prepared for Paterson, Grant and Watson Limited, 26 p.

Misener, D.J., Reford, S.W., Bailey, R.C., and Holroyd, M.

1984: Ternary Colour Plotting of Three Radioelement Spectrometer Data; p. 750–751 in Expanded Abstracts of the Technical Program with Authors' Biographies, 54th Annual Meeting of the Society of Exploration Geophysicists, 914 p.

Neale, E.R.W.

1963: Geology of Pleasant Bay, Cape Breton Island, Nova Scotia; Map 1119A, Scale 1 inch to 1 mile, Geological Survey of Canada.

Paterson, N.R.

1985: Geological Mapping by Airborne Magnetometer in Rugged Topography; p. 16–17 in Preliminary Abstracts of the International Meeting on Potential Fields in Rugged Topography, University of Lausanne, 32 p.

Paterson, N.R., Grant, F.S., and Misener, D.J.

1983: Development of Computer Software for Geophysical Interpretation; Grant 011, p. 53–61 In Exploration Technology Development Program of the Board of Industrial Leadership and Development, Summary of Research 1981–1983, edited by E.G. Pye and R.B. Barlow, Ontario Geological Survey, Miscellaneous Paper 115, 135 p.

Paterson, N.R., and Reford, S.W.

1985: Inversion of Airborne EM Data for Overburden Mapping and Groundwater Exploration; in Proceedings of the Workshop on Airborne Resistivity Mapping, Geological Survey of Canada, in press, preprint available from authors, 15 p.

Reford, S.W., and Paterson, N.R.

1985: Testing and Demonstration of Interpretation Software for Magnetic, EM and Spectrometry Inversion; Grant 089, p. 80–84 in Exploration Technology Development Program of the Board of Industrial Leadership and Development, Summary of Research 1984–1985, edited by V.G. Milne and R.B. Barlow, Ontario Geological Survey, Miscellaneous Paper 125, 110p.

Reford, S.W., Paterson, N.R., and Edwards, R.N.

1985: Inversion and SVD Analysis of Frequency–domain EM Data; p. 251–254 in Expanded Abstracts of the Technical Program with Authors' Biographies, 55th Annual Meeting of the Society of Exploration Geophysicists, 696 p.

Reford, S.W., Paterson, N.R., and Misener, D.J.

1984: Development of Computer Software for Geophysical Interpretation; Grant 011, p. 44–51 in Exploration Technology Program of the Board of Industrial Leadership and Development, Summary of Research 1983–1984, edited by V.G. Milne and R.B. Barlow, Ontario Geological Survey, Miscellaneous Paper 120, 176 p.

Grant 091 — The Development of a Pocket Digital–Reading Induced Polarization–Resistivity Meter*

M.G. Roman–Barber[1] and C.L. Elliot[2]

[1]EDA Instruments, Inc., Toronto

[2]Elliot Geophysical Company, Inc., Tucson, Arizona

*Funded in 1984–85 fiscal year.

ABSTRACT

Induced polarization and resistivity surveys are common geophysical methods used in Canada in the exploration for mineral deposits. Measurements of the electrical parameters of samples can have a significant impact on geophysical survey programs to maximize the chance of ore discovery.

A meter to measure IP–resistivity physical properties is essential to obtain reliable estimates of the electrical response parameters. Such a pocket IP–resistivity meter is useful to the explorationist for survey planning, geophysical feasibility studies, confirmation of anomaly drill tests, refining data interpretations, geological/geophysical correlations, and determination of properties without sample contamination or destruction.

A pocket–size digital–reading IP–resistivity meter for electrical parameter measurements has been developed that offers:

- Direct and rapid measurement of IP and resistivity parameters in the field;
- Simple to operate with minimum sample preparation;
- Lightweight pocket–size for ease in field use;
- Operator–controlled keyboard for instrument control;
- Battery powered for remote field operation with low power microprocessor and state–of–the–art analog/digital electronics.

For physical property measurements there has not been any pocket–size digital–reading IP–resistivity meter in world markets. EDA Instruments perceived the need and has developed such an instrument.

INTRODUCTION

Induced polarization and resistivity surveys are principal geophysical methods used in Canada as well as in the rest of the world in the exploration for mineral deposits. These methods can also be used in water exploration, and in geologic structural studies. Throughout the years, these methods have been some of the most used geophysical methods and will continue to be so used in the foreseeable future.

Physical property data pertaining to these electrical methods is fundamentally very useful information. As a result, several physical property measuring instruments have been available on the world market, but except for instruments for the measurement of the magnetic properties of samples and drill cores, none of these instruments are small pocket digital models for rapid measurements under field conditions. Excellent field survey IP–resistivity instruments have been readily available on world markets, but companion physical property instruments, particularly for the measurement of induced polarization and resistivity parameters have not been as available and certainly not in a small size.

All known crustal rock units have finite resistivities and induced polarization responses. Therefore, measurement of the electrical parameters of samples can have a significant impact on geophysical survey planning, supervision, and interpretation of geophysical survey data. A small physical property meter to measure the induced polarization and resistivity parameters is an essential instrument in that visual observation of samples, even by experts, can rarely yield estimates of the electrical response parameters that are so important in electrical geophysical surveys.

There are many laboratories with sophisticated instruments of laboratory quality for the measurement of induced polarization and resistivity parameters. Such facilities exist at many academic institutions, government laboratories, and commercial facilities. While these laboratory services are reliable, the typical turn–around time is too long to be acceptable for many explorationists, who require immediate physical property answers to guide survey planning or anomaly drill testing.

A small pocket size digital reading IP–resistivity meter is extremely useful to the geophysicist who deals with physical property data in survey planning and data interpretation. He therefore would utilize such a meter in planning geophysical surveys, to aid in enhanced data interpretation from electrical method surveys, and particularly to use at a drill site when drill testing induced polarization anomalies. In this latter application, rapidly obtained data is most important so that immediate results can be decisive in continuing or stopping the drill tests. Quantitative interpretation of induced polarization and resistivity data cannot be performed, even with utilization of sophisticated computer modelling procedures without good control of the physical property parameters. These parameters must be measured on the rock units in the survey area and cannot for the most part be obtained from tables and handbooks.

Similarly, such a pocket digital reading IP–resistivity meter is also handy for the geologist, who can use it in geological mapping, as an aid in distinguishing similar rock units that often have dissimilar electrical properties, and mapping of sulphide materials and magnetite which can be of economic interest.

Major uses of IP–resistivity physical property data can be summarized:

- Planning geophysical surveys;
- Geophysical feasibility studies;
- Confirm anomaly drill tests;
- Refine geophysical data interpretation;
- Geological–geophysical correlations;
- Determine properties prior to core assay without sample contamination or destruction.

Rapid field determinations of IP–resistivity parameters can have a significant impact on the efficiency and effectiveness of an exploration program. They can materially aid the explorationist in guiding an exploration program to maximize the chance of discovery of mineralized bodies while minimizing the cost. With these obvious benefits in mind, EDA Instruments perceived the important need for such a small pocket sized IP–resistivity meter for physical property measurements, and proceeded to develop such an instrument.

PROJECT OBJECTIVES

The objective of this research and development project was to design and develop a small pocket size physical property meter for the measurement of induced polarization and resistivity data. Heretofore, there has been no known pocket digital reading IP–resistivity meter available anywhere on the world market. It has already been shown that such an instrument does have an important utilization for the modern day explorationist.

This research project is in actuality an electronic instrumentation development, using modern state–of–the–art electronics available today from the rapidly expanding electronic technology industry. In order to insure reaching the desired goals, EDA Instruments employed the consultation of C.L. Elliot of Elliot Geophysical Co., Inc., Tucson, Arizona, who is well respected in the geophysical industry and has been responsible for the development of several physical property testing instruments. It was believed that a technological combination of this expertise in such instrumentation with EDA's expertise in microprocessor technology, circuit miniaturization, and marketing experience could result in the development of an interesting new range of physical property testing instrumentation. Of this new family of physical property instruments, the IP–resistivity physical property meter is one of the group of products that was designed and developed under this research grant.

The objective that has been accomplished in this research and development project is an instrument whose salient features are:

1. Digital display of IP and resistivity parameters in appropriate units;
2. Direct and rapid measurement of IP and resistivity parameters in the field;
3. Microprocessor based design using state–of–the–art analog/digital electronics;
4. Lightweight for ease in transportation to field site or core shack;
5. Unitized construction with no separate external sample holders or electrodes;
6. Keyboard entry by operator for instrument control, parameter selection, battery testing, etc.;
7. Principal utilization in measuring drill core samples;
8. Simple to operate;
9. No sample preparation required for drill cores;
10. Diamond sawing preferred but breaking core for a flat surface required to read properties of surface (grab) samples;
11. Battery powered for remote field operation;
12. No critical time delay waiting for laboratory turnaround of physical property data;
13. Low current densities to simulate actual field conditions;
14. High input impedance buffer amplifier to prevent electrical loading of the sample;

15. LCD display for clear readability in bright sunlight;
16. Handy size for operator convenience which fits readily into a pocket;
17. Low power consumption design using CMOS digital logic and comparable low power analog circuitry;
18. No manipulation of operator keyboard can damage instrument;
19. All solid state circuitry for dependability.

SPECIFICATIONS

The induced polarization meter for physical property investigations that has been developed operates in the conventional time domain mode, commonly used in induced polarization surveys in the field. The instrument has specifications that are compatible for an instrument that must operate under adverse field conditions. Table 091.1 lists the principal specifications of the physical property instrument.

TABLE 091.1. PRINCIPAL SPECIFICATIONS.

1. Ambient operating temperature: -20 to +60°C
2. Constant current output: 0.1, 1, 10, and 100 μA
3. Maximum allowable load impedance:
    - 100 megaohm @ 0.1 microamps
    - 10 megohms @ 1.0 microamp
    - 1 megohm @ 10 microamps
    - 0.1 megohms @ 100 microamps
4. Time cycle: Symmetrical period with 1/4 period of 2.0 seconds
5. Accuracy of output current: ± 5%
6. Accuracy of waveform period: ± 1%
7. Power supply: Replaceable batteries
8. Power line rejection frequency: 50 or 60 Hz
9. Receiver input impedance: > 1000 megohms
10. Input primary voltage maximum: ± 2.5 volts
11. Input primary voltage resolution: ± 1.0 millivolts
12. Self potential buckout range: ± 2.0 volts
13. Accuracy of primary voltage measurement: ± 5%
14. Induced polarization response range: 1-1000 millisecs
15. Accuracy of induced polarization response: 5%
16. Weight complete with case: < 2 kg
17. Dimensions of meter: 20 x 7 x 4 cm (Approx.)

SYSTEM DESCRIPTION

The pocket digital-reading induced polarization-resistivity system is a physical property measurement system designed to measure the IP response and resistivity of drill core or otherwise prepared samples. The type of drill core samples measureable with this system can be from conventional diamond drilling operations in mineral exploration or small cores or diamond sawed samples taken from surface or underground samples.

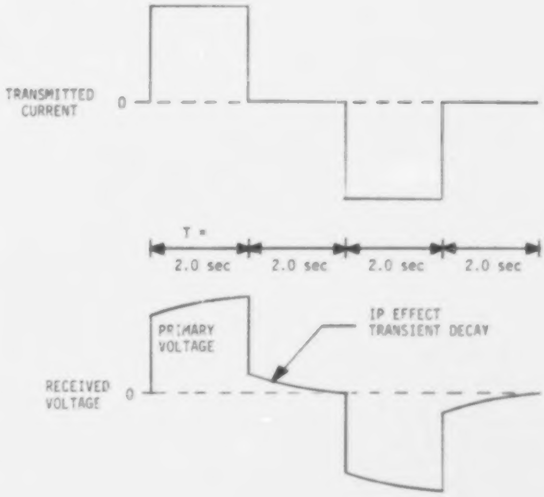

Figure 091.1. Time domain transmitter and receiver waveforms.

The system was designed to operate in the conventional time domain mode of operation. Therefore as depicted in Figure 091.1, the current waveform will be a symmetrical waveform consisting of an ON period of T seconds, an OFF period of T, an ON period with current flow in the reverse direction for T seconds and finally another OFF period for T seconds, where T = 2.0 seconds.

Thereby, the overall period will be 4T or 8.0 seconds. The output current waveform will be coupled to the sample by means of non-polarizing electrodes for the measurement,

The electrode system consists of four electrodes mounted on the sample end of the instrument and spaced 2.5 cm apart inline. The current electrodes are on the outside with the potential electrodes in between the current electrodes. These electrodes are non-polarizing types made of Pb-PbS that are cloth padded in order to provide good galvanic contact to the rock sample under test. This electrode system (Figure 091.2) is commonly referred to as the Wenner array, as used in field induced polarization-resistivity operation. The general resistivity equation for this array is:

$$\rho = \frac{4 \pi V a}{I}$$

Where

ρ = resistivity

V = primary received voltage in volts,

I = injected current in amps,

a = electrode separation in distance units.

For the specific case of this instrument, a = 2.5 cm and for the resistivity data in conventional ohm–metres, the above equation reduces to:

$$\rho = \frac{0.3142\ V}{I} \quad \text{in ohm–metres}$$

A block diagram of the instrument is shown in Figure 091.3. In general the instrument is a digitally controlled system using a microprocessor CPU with associated program plus scratch memory as the controller. The CPU is the heart of the system and handles keyboard input from the operator, controls display for the LCD presentation on the front panel of the instrument, and provides necessary instrument timing. It also performs the calculations of resistivity and induced polarization response for presentation of the data to the operator.

The system is powered by internal replaceable batteries with appropriate battery test functions to alert the operator when the batteries need replacing. All of the electronic construction is with solid–state circuitry, including low power operational amplifiers and logic circuits for minimum battery drain. All of the electronic circuits have been designed to be completely foolproof so that no combination of operator action can cause internal damage to the instrument.

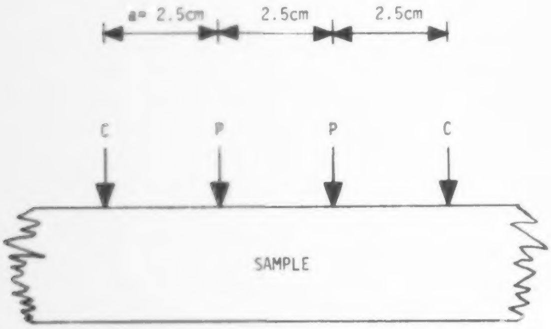

Figure 091.2. Electrode system (Wenner array). C = current electrode, P = potential electrode, a = electrode separation.

Mechanically, the system has been designed in an aluminum case that is rugged and sealed. All of the active electronic circuits are mounted on printed circuit boards for stability. Conservative designs have been employed for the circuitry in order to guarantee its reliability and dependability under normal field conditions.

Considering in more detail the instrument block diagram (Figure 091.3), the CPU processor communicates with the various circuits by means of address, data and control buses. The transmitter time base is a free running clock with appropriate divider signals to generate necessary timing of the transmitted current waveform. The time base provides control of a constant current source, which in turn is multiplexed by the current waveform generator. The output current is coupled to the core sample by means of non–polarizing current electrodes. A reference signal from the transmitter time base is sent to the signal processor for timing reference. Output currents are keyboard selectable at constant current levels of 0.1, 1.0, 10.0, and 100.0 microamps to simulate as well as possible normal current densities in field IP–resistivity exploration.

The potential signal is received from the sample by means of non–polarizing potential electrodes. Because the impedance of this signal can be very high for very resistive samples, coupling of the signal from the sample is by means of a very high input impedance buffer amplifier. Following this, the signal is further amplified and filtered to provide a clean signal for the signal processor. The signal processor is under control of the CPU, and consists primarily of an analog–to–digital function, thereby generating a digital representation of the analog signals for proper digital processing by the microprocessor CPU.

Sampling of the received signal is done both while the transmitter is on and while it is off, as depicted in the expanded scale presentation of Figure 091.4. The primary voltage signal (VP) is sampled 1800 milliseconds into the waveform when the transmitter is turned on or some 200 milliseconds before turn off of the transmitter. After turn off of the transmitter at time (T0), a delay of 500 milliseconds is made and a sample of the secondary decay voltage is taken for purposes of instrumental gain control. Following this gain adjustment, a further delay of 200 milliseconds is real-

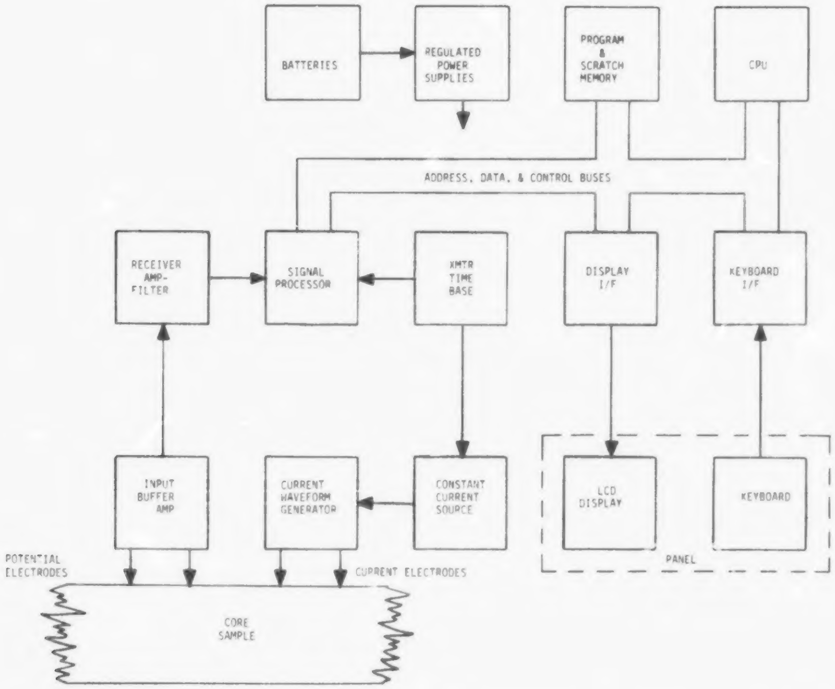
BATTERIES
REGULATED POWER SUPPLIES
PROGRAM & SCRATCH MEMORY
CPU
ADDRESS, DATA, & CONTROL BUSES
RECEIVER AMP-FILTER
SIGNAL PROCESSOR
XMTR TIME BASE
DISPLAY I/F
KEYBOARD I/F
INPUT BUFFER AMP
CURRENT WAVEFORM GENERATOR
CONSTANT CURRENT SOURCE
LCD DISPLAY
KEYBOARD
PANEL
POTENTIAL ELECTRODES
CURRENT ELECTRODES
CORE SAMPLE

Figure 091.3. Instrument block diagram.

ized. After this, 12 samples of the decay voltage are taken at a 100 millisecond repetition rate.

Calculation of the induced polarization effect is performed by discrete–time integration of the 12 decay voltage samples, using the well–known trapezoidal rule. Normalization of the integrated decay voltage for calculation of the true induced polarization response is done in accordance with:

$$C = \frac{\int V(t)\,dt}{K\,VP}$$

Where

C = chargeability (IP Effect)

V(t) = decay voltage,

K = calibration constant,

VP = measured primary voltage.

For the chargeability C in milliseconds, it is necessary to calibrate the instrument against a known standard. We have elected to follow the fine research of Newmont Exploration Ltd., who were pioneers in the development of the time domain induced polarization method. General descriptive material has been presented in Wait (1959), and more particularly, the calibration system is presented in Dolan (1967) and McLaughlin (1967). Research by the Newmont staff has shown that a very acceptable analog of the true induced polarization response can be realized, utilizing a geometric RC ladder network. This working model is ideal for purposes of calibrating this instrument. For calibration a log ladder network has been utilized containing 26 RC elements with a geometric ratio = 2.0. Newmont has found this to be a very acceptable simulation network for the decay interval from 700 to 1800 milliseconds, after transmitter turnoff. The factor K = 0.4279, as calculated from the log ladder simulation network. This factor has been used in the internal computations of the instrument to present true chargeability in milliseconds on the display for the operator.

BASIC OPERATION

Proper operation of the IP–resistivity physical property meter requires carefully prepared samples in order to assure reasonable measurements of the electrical response parameters. Drill core samples or grab samples that have reasonably flat surfaces must be selected, cleaned, and surface dry. Once a selected suite of samples are ready, the instrument may be turned on and battery test procedures per-

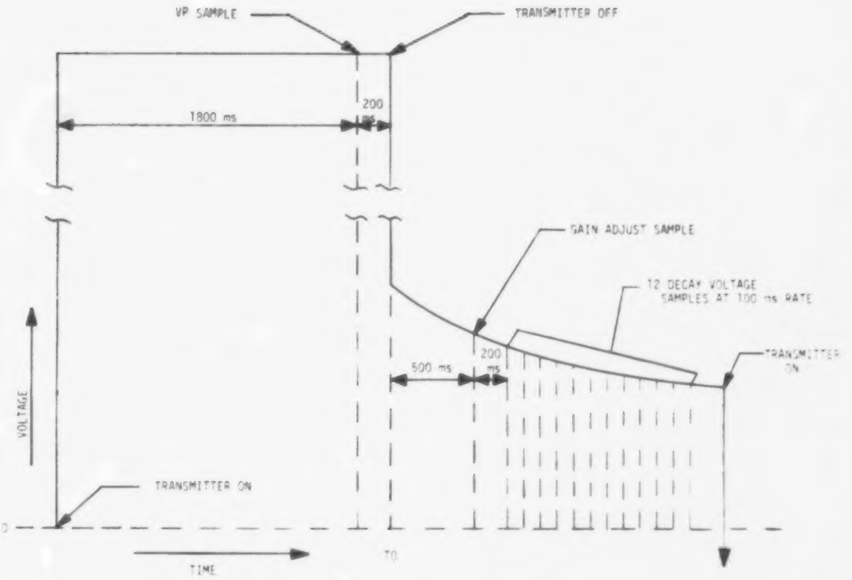

Figure 091.4.
An expanded scale presentation of the secondary transient decay showing sampling points.

formed. Following this, the basic steps in making the measurement of induced polarization and resistivity parameters on the sample are outlined below.

1. Select the SP mode of operation by means of the keyboard. Adjust the DC offset voltage due to the natural self potential of the sample. During this adjustment the transmitter is off.
2. Select the CURRENT mode of operation. Transmitter is turned on and an appropriate current is selected from the four current possibilities: 0.1, 1.0, 10.0 and 100 microamps.
3. Select the GAIN mode of operation. With the transmitter running, the primary voltage gain is set in order to provide appropriate signal levels for accurate operation of the measurement part of the circuitry. During this phase it may be found that the selected current in step 2 above is insufficient for providing an appropriate signal level. Therefore return to step 2 and advance current selection to the next higher step. Following this, the primary voltage gain adjustment is repeated. Interactively, steps 2 and 3 need to be performed to guarantee appropriate signal levels.
4. Readjust the self potential offset, alter the current, or primary voltage gain as required to obtain balanced signals of an appropriate level for measurement.
5. Select the RUN mode of operation. Measurements are performed over four complete cycles of the transmitter current waveform. This step after initialization takes 32 seconds. After the measurement, the data is reduced internally by the instrument software to provide the operator with readouts of average physical property parameters of the four cycles that were measured. The instrument display will present to the operator induced polarization response of the sample in milliseconds and the resistivity of the sample in ohm–metres.
6. Repeat above step 5 for additional measurements on the same sample, or repeat as might be required steps 1, 2, or 3, followed by the repeat of step 5 for measurement of a sample.
7. Re–orient sample and repeat a measurement. This allows the operator to obtain a better average electrical parameters for a specific sample by reading multiplie sets of data from various orientations of the specific sample. Once a sample is re–oriented, then the above steps 1 through 6 will need to be repeated.

The instrument has been designed to be user–friendly, and only simple step–by–step procedures need to be followed by the operator. The design of the instrument has been to make it foolproof, so that no action by the operator can damage the instrument, and if the operator follows the prescribed procedures, as presented in the operation manual, then accurate electrical parameters can be measured.

FUTURE PLANS AND CONCLUSIONS

EDA Instruments perceived the important need for a small pocket sized induced polarization–resistivity meter for the measurement of the physical properties of drilled cores. EDA subsequently developed such an instrument under this research development grant and this instrument has the desirable measurement functions for use in metallic mineral exploration. Such an instrument has a very important utilization for mineral explorationists both in Canada and elsewhere in the world. The instrument has met or exceeded the proposed design parameters and as a result it should find a ready market for use in worldwide metallic exploration projects.

This induced polarization–resistivity instrument for physical property measurements is the second in a family of physical property equipment under development by EDA Instruments. Already in production is a companion magnetic susceptibility meter (EDA Model K–2). This instrument has a similar use in exploration for measuring the magnetic properties of drill cores and rock samples. Oftentimes in exploration, magnetic measurements go side by side with electrical measurements, and therefore these two instruments can be used in a comparable sense to aid the explorationist in understanding the physical properties of the rock units in his project area.

Other physical property instruments are currently under consideration for development to further expand the family of physical property instruments. These instruments will measure other physical property parameters of drill cores and rock samples, such as electromagnetic properties of general interest in Canadian exploration for massive sulphide deposits. We at EDA hope that this family of physical property instruments will find their place in every exploration project, both in Canada and worldwide.

ACKNOWLEDGMENTS

We wish to acknowledge the consultation and support of the staff of Elliot Geophysical Co., Inc., Tucson, Arizona, in the development and successful conclusion of this research project. Their extensive knowledge of physical property systems was extremely valuable, particularly in the initial development stages.

REFERENCES

Dolan, W.M.

1967: **Considerations Concerning Measurement Standards and Design of Pulsed I.P. Equipment, Part I; Symposium On Induced Electrical Polarization, University of California, Berkeley, p.2–16.**

McLaughlin, G.H.

1967: **Considerations Concerning Measurement Standards and Design of Pulsed I.P. Equipment, Part II; Symposium On Induced Electrical Polarization, University of California, Berkeley, p.17–31.**

Wait, J.R.

1959: **Overvoltage Research and Geophysical Applications; International Series of Monographs on Earth Sciences, Vol.4.**

Grant 093 — Software and Hardware Design of Controlled Source Audio-Frequency Magneto-Telluric (CSAMT) System and Test Surveys

Philip G. Hallof and Mitsuru Yamashita

Phoenix Geophysics Limited, Markham

ABSTRACT

A controlled source audio-frequency magneto-telluric (CSAMT) system had been developed by Phoenix Geophysics Limited under the Exploration Technology Development Fund Grant from the Ontario Geological Survey in 1984–1985. This grant was extended to the second year 1985–1986, for further improvement of the hardware and software as well as more data processing programs.

The systems were successfully used for contract surveys and test surveys in various applications and various areas, including overseas countries. Six systems have been already sold and delivered. Several systems are soon going to be delivered to various countries, such as China, Japan and Indonesia.

The system, the software and some case histories were described in the ETDF Summary of Research for 1984–1985.

Under the second year of the extended grant, additional test surveys, software development and a number of system improvements have been achieved. These are summarized as follows:

1. System Improvements

(a) The frequency range and the number of frequencies available, were expanded to 34 frequencies, from 0.0625 to 8192 Hz, in steps of approximately $\sqrt{2}$.

(b) An improved noise rejection function was added.

(c) A signal pre-conditioning adaptor was provided for use at the electrodes.

(d) A high power transmitter consisting of T-30 and MG-30 motor generator has been developed.

2. Software Development

A finite element 2D modelling program, executable with a desk-top computer, has been developed.

3. Test Surveys

A number of test surveys were carried out for oil exploration, geothermal exploration, uranium exploration, and waste-disposal study.

INTRODUCTION

The details of the CSAMT equipment (Figure 093.1), and its method of operation, were described completely in last year's "Summary of Research, 1984–1985". Also included was a complete discussion of the near-field correction procedure that has been developed. The CSAMT method has been found to be very useful, in a wide variety of exploration problems, in which there are electrical parameter contrasts in the subsurface.

A few of these field data examples were included in the previous report. In the extended program, the hardware and software developments have been continued. Further examples of field data are also now available.

SYSTEM HARDWARE IMPROVEMENTS

As might be expected, continued field experience with the V-4, CSAMT system has suggested that improvements are warranted.

(a) The frequency range of the entire system has now been extended to cover the range from 0.06125 to 8192 Hz. There are now approximately 34 frequencies that may be chosen by the geophysicist. The smallest frequency step available is $\sqrt{2}$.

(b) A greatly improved electrical noise rejection function has been introduced into the V-4. This circuitry is a combination of hardware and software that will reject a bad sample, before it is averaged into the "stacked" answer. This rejection is either automatic, at a pre-set level, or manual, when the operator sees the need.

(c) In order to improve the data quality, in the situation in which a poorly grounded potential electrode has been prepared, a signal pre-conditioning adaptor has been designed to be used at the potential electrodes. This pre-amplifier can also give additional gain in situations in which poor current electrodes result in low sig-

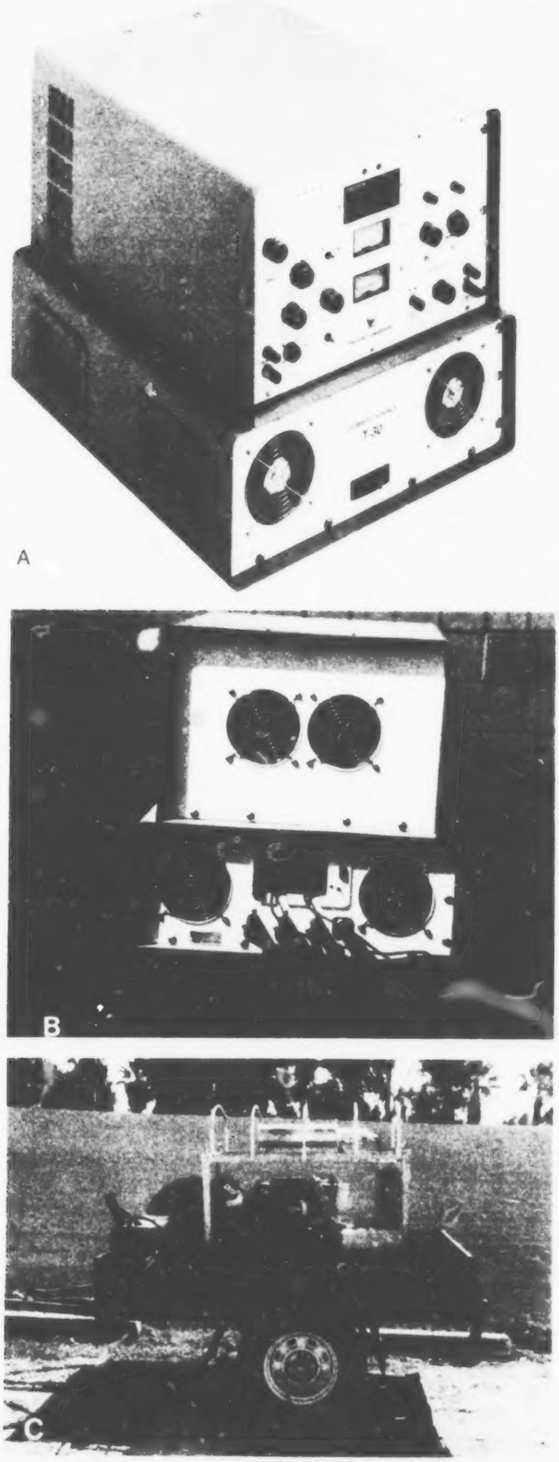

Figure 093.1. (a) T–30 transmitter: front panels. (b) T–30 transmitter: rear view of instrument. (c) MG–30 motor generator.

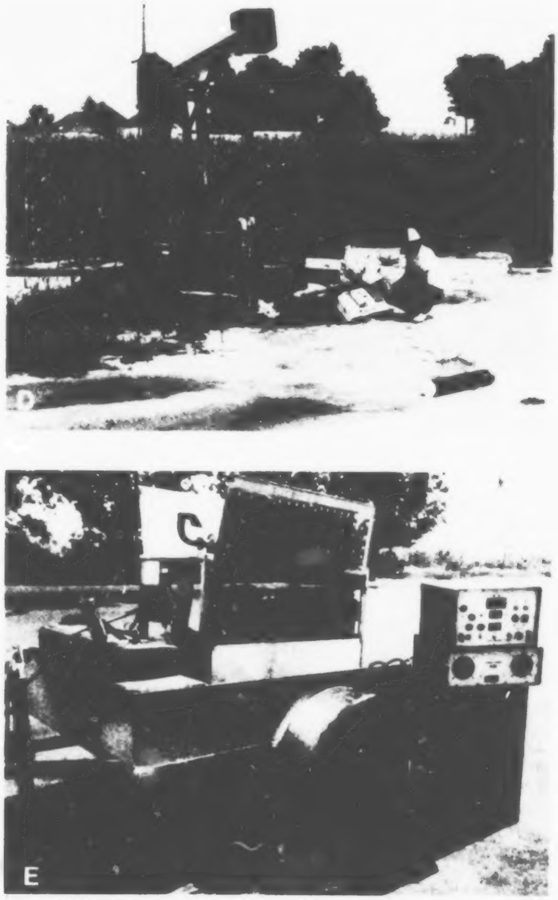

Figure 093.1. (d) V–4 and coil at test site, Sarnia, Ontario. (e) T–30 and MG–30 set-up for preliminary testing.

nals. A special high–pass filter becomes operative at frequencies above 500 Hz, resulting in better signal/noise ratios at the higher frequencies. The signal adaptor (pre–amplifier) permits measurements to be made with high grounding impedance at the E–field electrodes. This also permits metal stakes to be used, for instance, in deep snow conditions.

(d) In the previous field surveys, the Phoenix IPT–1/MG–3 combination was used. This resulted in a maximum power output of approximately 3.0 Kva. We have now designed, manufactured and field–tested a current source that has an order of magnitude greater power output. The T–30/MG–30 combination (Figure 093.1) has an output of approximately 30 Kva. The specifications are:

	T-30	MG-30
Weight:	80 kg	365 kg
Frequency:	0.06125 - 8192 Hz	400 Hz
Max:	30 amperes 2000 volts	30 Kva

SOFTWARE DEVELOPMENT

The CSAMT technique is relatively new, and there is little information concerning the type of anomaly to be expected in certain exploration problems. In order to help the geophysicist with the interpretation of field data, we have developed the CSAMT forward problem calculation, using a finite element model.

The software can be used in the following desktop computers:

HP 9845

HP 9000 - Model 217

HP 9000 - Model 310

Several examples are given in Figures 093.2a–d, to give some feeling for what types of problem can be calculated.

ADDITIONAL FIELD SURVEY EXAMPLES

The field work with the Phoenix CSAMT system has continued throughout the year. The results to be shown below are from short test surveys, as well as more lengthy paid contract surveys. In these latter cases, the results are being included with the permission of the original client.

A. Geothermal Exploration Problem, Hatchobaru, Japan (Figures 093.3a,b)

One line of CSAMT results from this geothermal area was included in last year's report. Due to the initial success of the measurements, the survey has been extended. The results shown here are for Line C. This line passes several hundred metres from the line shown in last year's report.

These results are much more complex; they clearly do not approximate a "layered" earth. For this reason the one–dimensional interpretation of the CSAMT results does not agree well with the one–dimensional interpretation of the previous MT and Schlumberger soundings.

The region of very low resistivities, at the east end of Line C (at a depth greater than 500 meters), could be traced for a considerable distance. Two drill holes have recently intersected the geothermal cell that is the source of these low resistivities. A 55 megawatt geothermal electric power plant will be built at the site.

B. Sulphide Mineralization with Gold, Estrades Township, Quebec (Figures 093.4a,b)

The Golden Hope–Teck Exploration gold ore zone recently discovered in Estrades Township, Quebec, is typical of several gold zones that have been located in recent years in western Quebec and eastern Ontario. Some of these zones of sulphide mineralization are conductive enough to be detected using electromagnetic methods; others are not.

This is confirmed at the Golden Hope Zone, where Line 24W (Main Zone) results in a CSAMT anomaly. The forward problem solution attached confirms the type of anomaly to be expected.

C. Uranium Exploration, Wollaston area, Saskatchewan (Figures 093.5a,b on Chart, back pocket, and Figure 093.5c)

The geometry of the uranium ore zones in the Athabaska area are well known. An extensive survey was completed; as part of the exploration survey, a test survey was completed over the McLean Lake ore zone.

The porous regolith at the top of the Precambrian lies beneath 350 to 500 m of Athabaska sandstone. The uranium–sulphide ore zones occur at the intersection of the regolith with near–vertical basement faults. These intersections result in approximately horizontal, "pipe–like" zones of increased alteration, porosity and mineralization.

The near–field corrected results clearly show the deep conductors from the McLean Lake North Zone (12+50N to 13+50N) and the McLean Lake South Zone (8+50S to 7+50S).

The forward problem solution attached gives an excellent confirmation concerning the shape of the anomaly to be expected.

D. Gas Exploration from Buried Reef, Sarnia, Ontario (Figures 093.6a,b)

The buried reef structures in southwestern Ontario have produced gas for many years. There is almost no information available concerning the subsurface resistivity structure. However, the CSAMT pseudosection attached shows a definite, complex resistivity pattern at the position of the reef.

E. Oil Exploration, Zhou Xiang Oil Field, Hebei Province, P.R.C. (Figure 093.7 on Chart, back pocket)

The structure at this location is much simpler. A porous clastic sedimentary band lies between a non-porous clastic sediment above and a non-porous limestone beneath. The petroleum accumulations are controlled by topographic highs and lows in the limestone.

It was for this application, that the lowest frequency was reduced to 0.065125 Hz. At the low frequency, the higher resistivity basement lime-

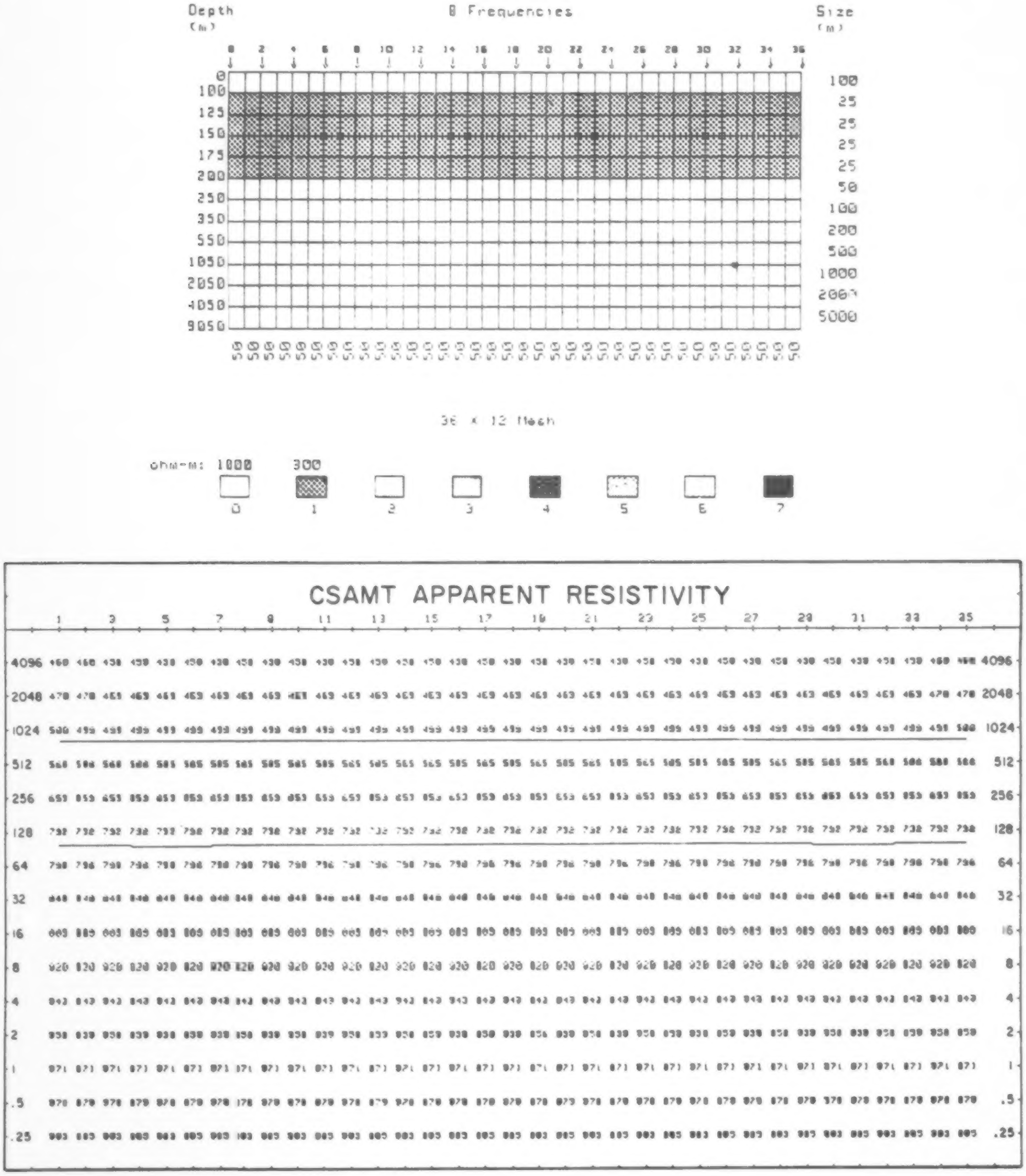

Figure 093.2a. CSAMT modeling case showing flat response over layered earth.

stones can be mapped, even at a depth of 1.0 to 2.0 km.

EMPLOYMENT OF CSAMT

At this time, Phoenix has three V-4/CSAMT Systems that are used to conduct contract surveys. Six systems have been sold and are in use by the purchasers. Further, we currently have a back-log of four additional systems to be delivered in the next few months (all overseas).

From these facts, it appears to us that interest in the CSAMT Method is increasing.

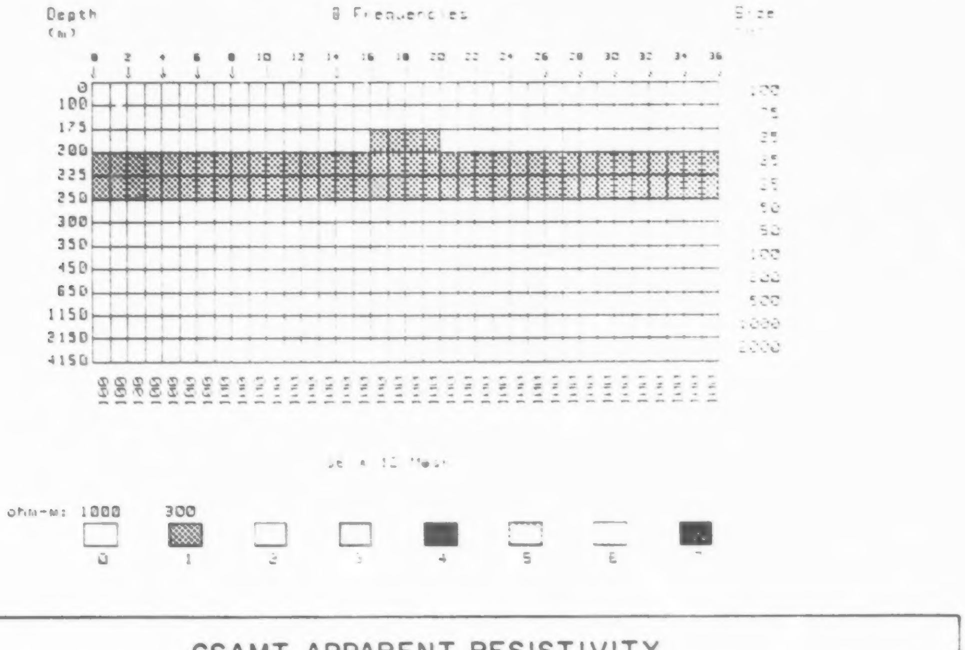

Figure 093.2b. CSAMT modeling case showing reconnaissance location of source in host rock.

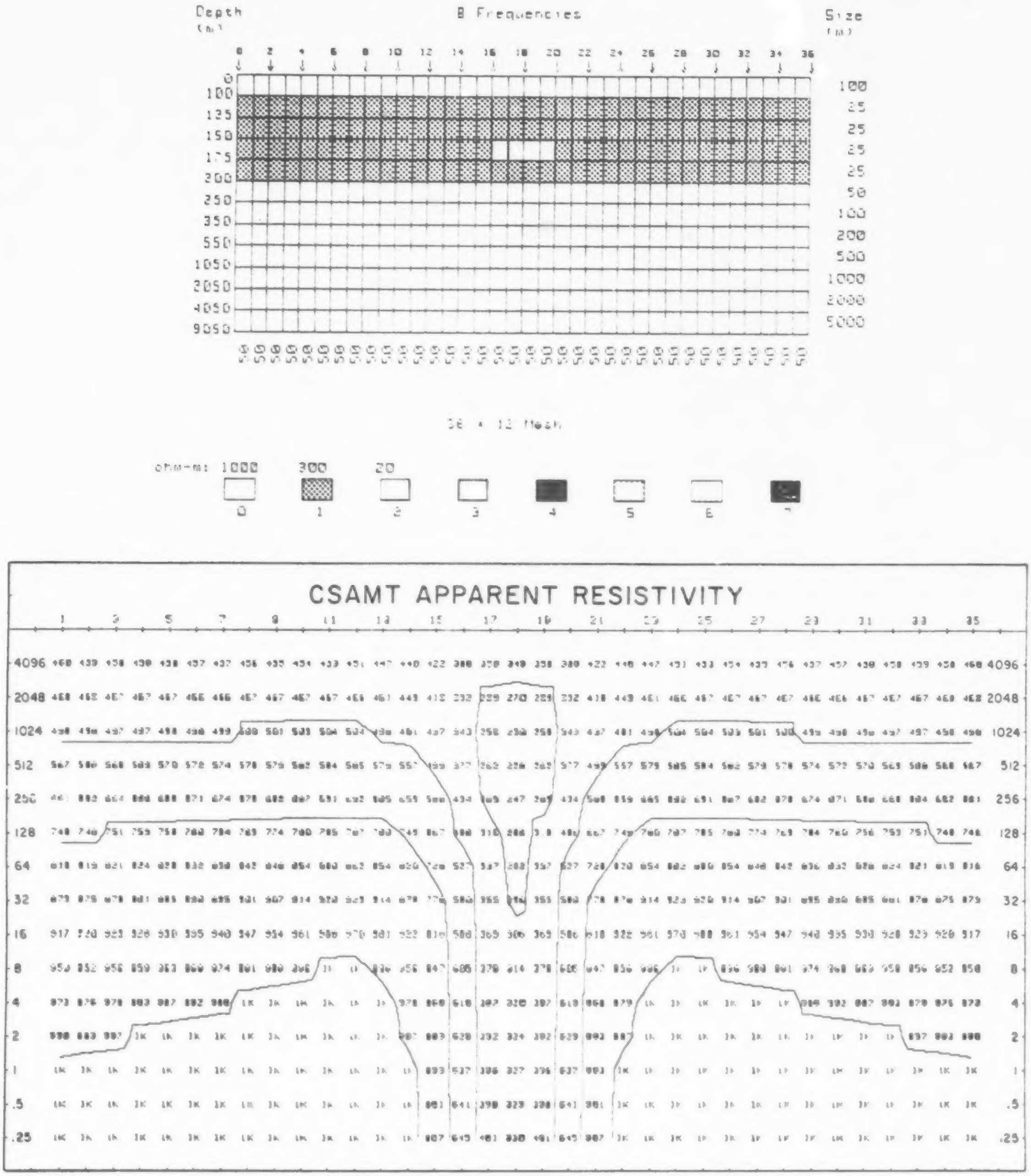

Figure 093.2c. CSAMT modeling case showing verified source at depth.

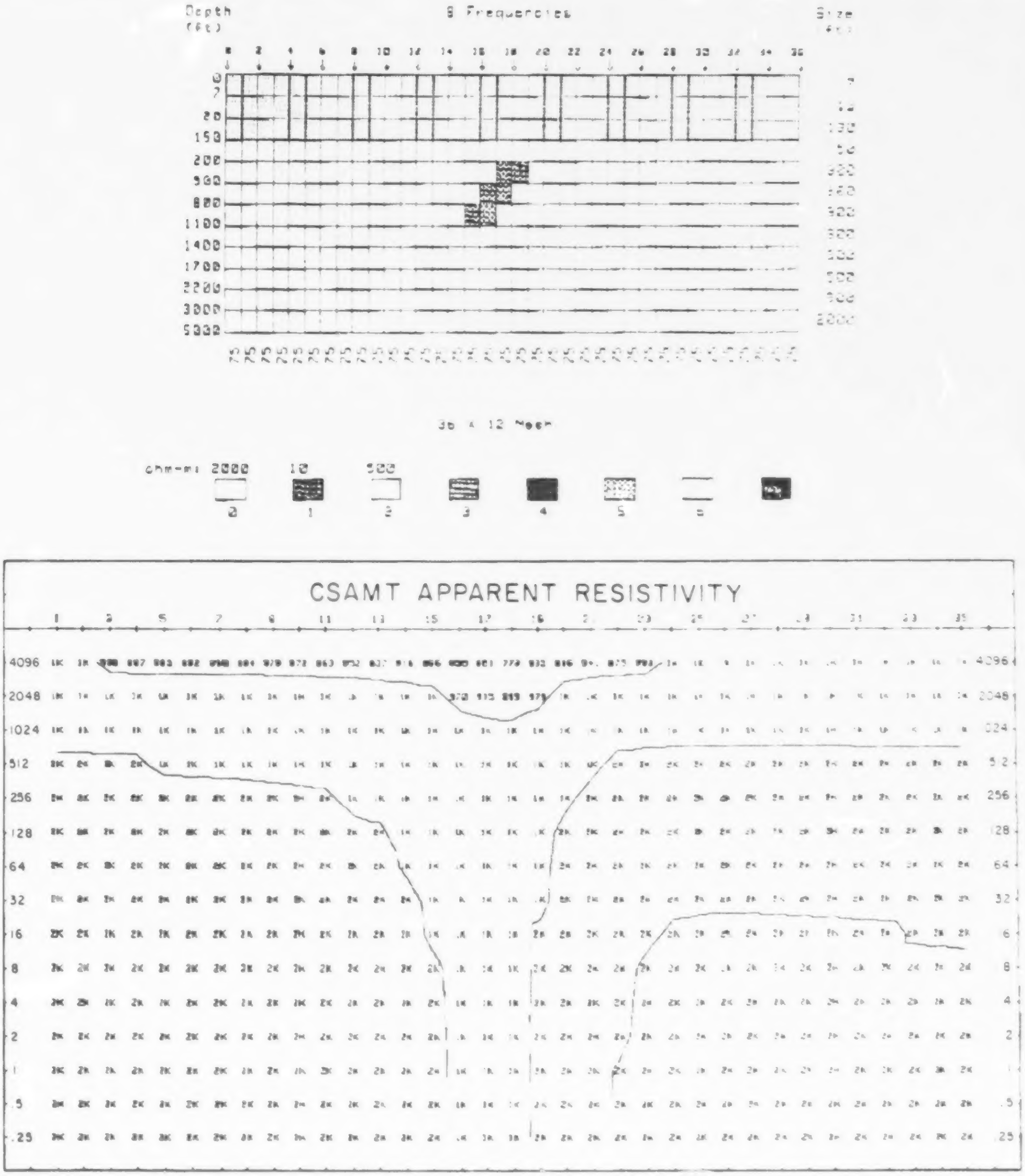

Figure 093.2d. CSAMT modeling case showing conductor in high resistivity host rock.

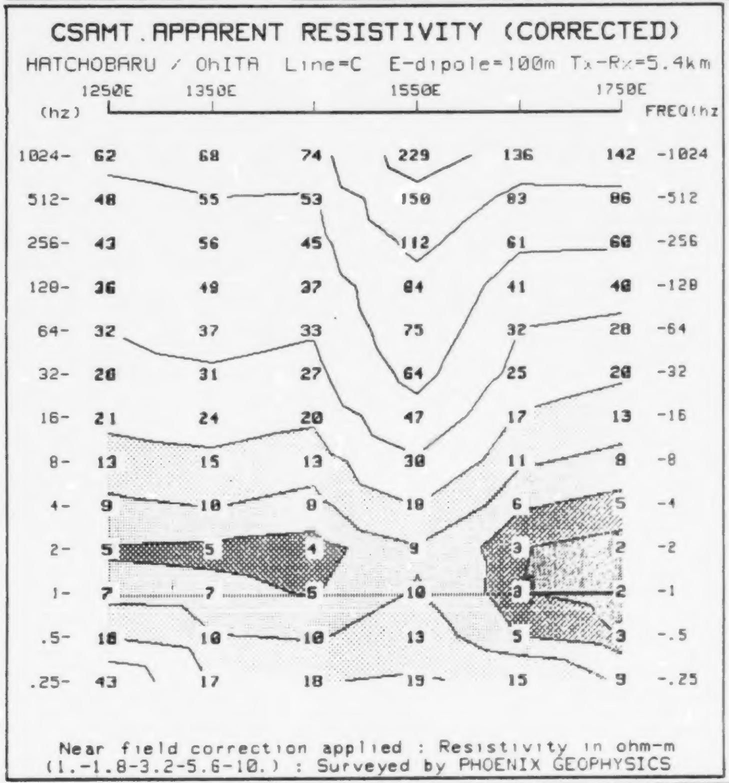

Figure 093.3a. CSAMT apparent resistivity pseudo-section vs. frequency on Line-C, Hatchobaru, Japan.

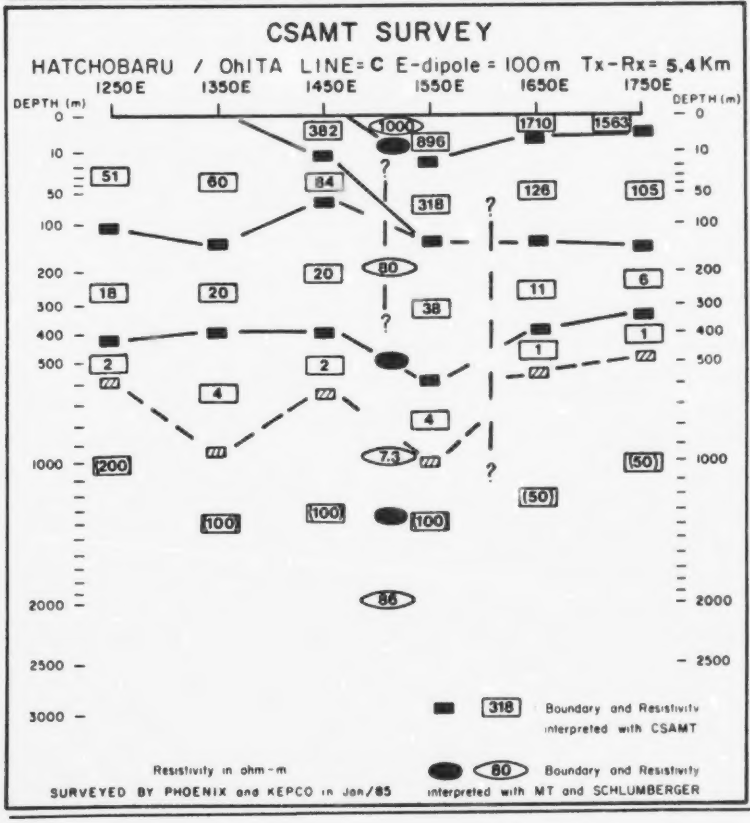
CSAMT SURVEY
HATCHOBARU / OhITA LINE=C E-dipole=100m Tx-Rx=5.4Km
1250E 1350E 1450E 1550E 1650E 1750E
DEPTH (m)
0 10 50 100 200 300 400 500 1000 2000 2500 3000
318 Boundary and Resistivity interpreted with CSAMT
80 Boundary and Resistivity interpreted with MT and SCHLUMBERGER
Resistivity in ohm-m
SURVEYED BY PHOENIX and KEPCO in Jan/85

Figure 093.3b. True resistivity section interpreted form corrected CSAMT apparent resistivities on Line-C, Hatchobaru, Japan.

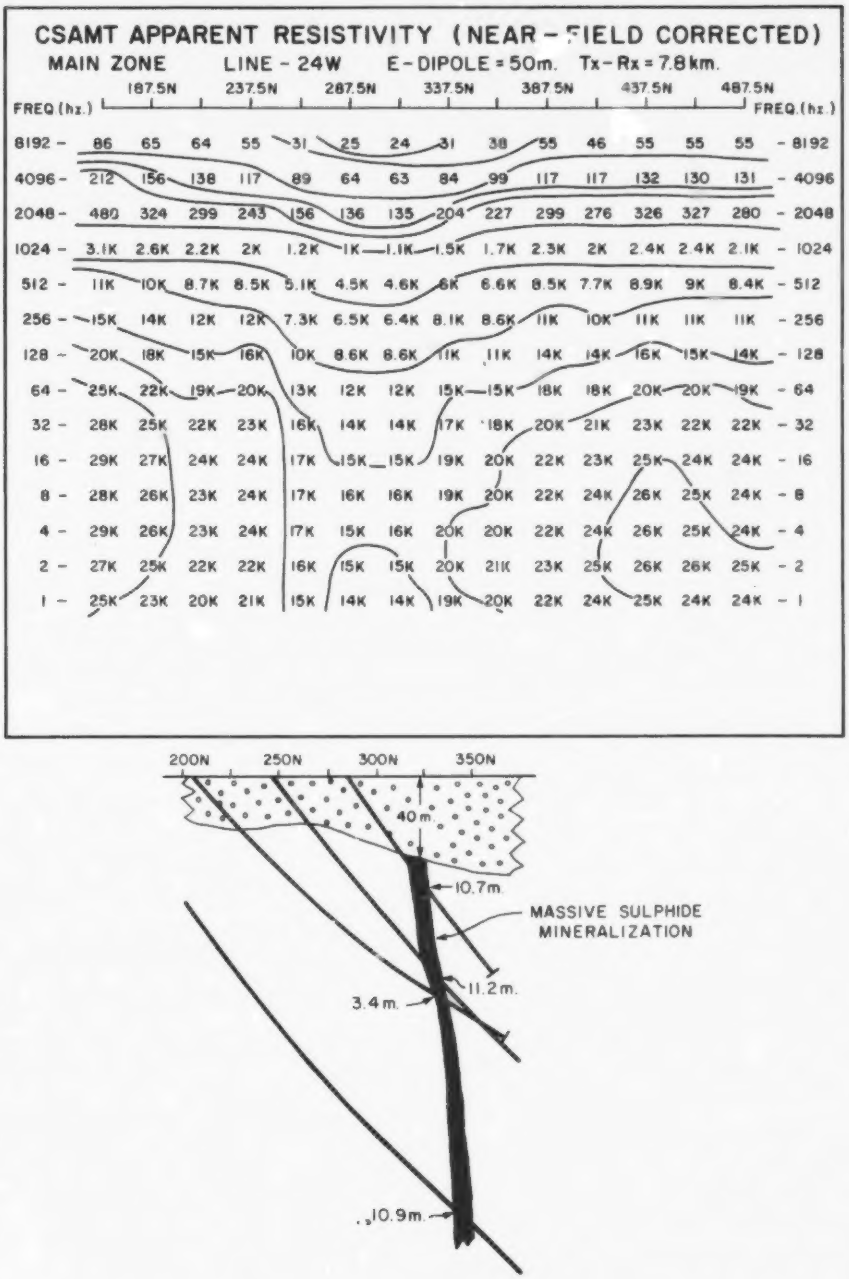

FREQ (hz.)		187.5N		237.5N		287.5N		337.5N		387.5N		437.5N		487.5N	FREQ. (hz.)
8192	86	65	64	55	31	25	24	31	38	55	46	55	55	55	8192
4096	212	156	138	117	89	64	63	84	99	117	117	132	130	131	4096
2048	480	324	299	243	156	136	135	204	227	299	276	326	327	280	2048
1024	3.1K	2.6K	2.2K	2K	1.2K	1K	1.1K	1.5K	1.7K	2.3K	2K	2.4K	2.4K	2.1K	1024
512	11K	10K	8.7K	8.5K	5.1K	4.5K	4.6K	6K	6.6K	8.5K	7.7K	8.9K	9K	8.4K	512
256	15K	14K	12K	12K	7.3K	6.5K	6.4K	8.1K	8.6K	11K	10K	11K	11K	11K	256
128	20K	18K	15K	16K	10K	8.6K	8.6K	11K	11K	14K	14K	16K	15K	14K	128
64	25K	22K	19K	20K	13K	12K	12K	15K	15K	18K	18K	20K	20K	19K	64
32	28K	25K	22K	23K	16K	14K	14K	17K	18K	20K	21K	23K	22K	22K	32
16	29K	27K	24K	24K	17K	15K	15K	19K	20K	22K	23K	25K	24K	24K	16
8	28K	26K	23K	24K	17K	16K	16K	19K	20K	22K	24K	26K	25K	24K	8
4	29K	26K	23K	24K	17K	15K	16K	20K	20K	22K	24K	26K	25K	24K	4
2	27K	25K	22K	22K	16K	15K	15K	20K	21K	23K	25K	26K	26K	25K	2
1	25K	23K	20K	21K	15K	14K	14K	19K	20K	22K	24K	25K	24K	24K	1

Figure 093.4a. CSAMT apparent resistivities locating mineralized zone on Line–24W, Estrades Township, Quebec.

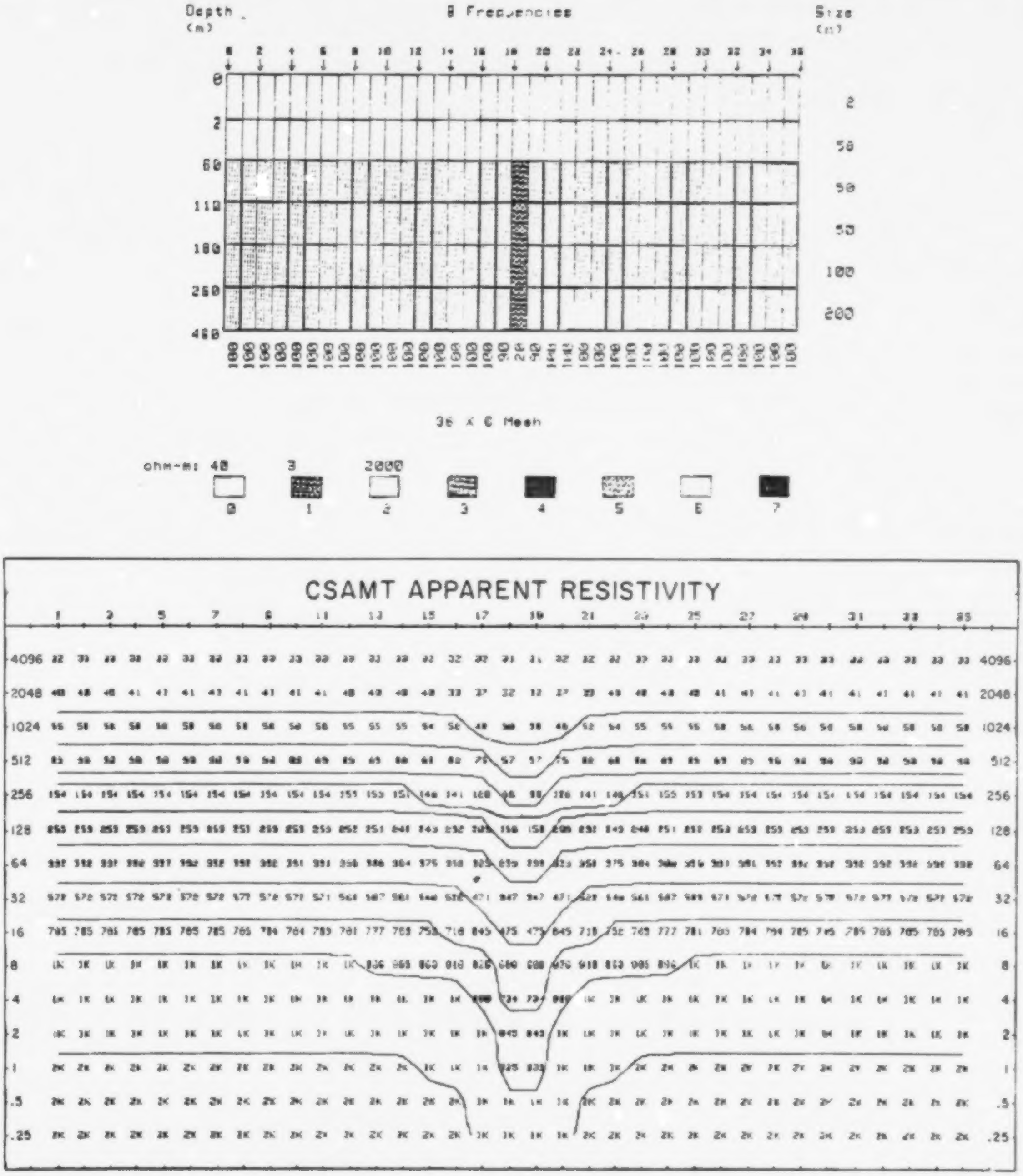

Figure 093.4b. CSAMT modeling case showing type of anomaly expected.

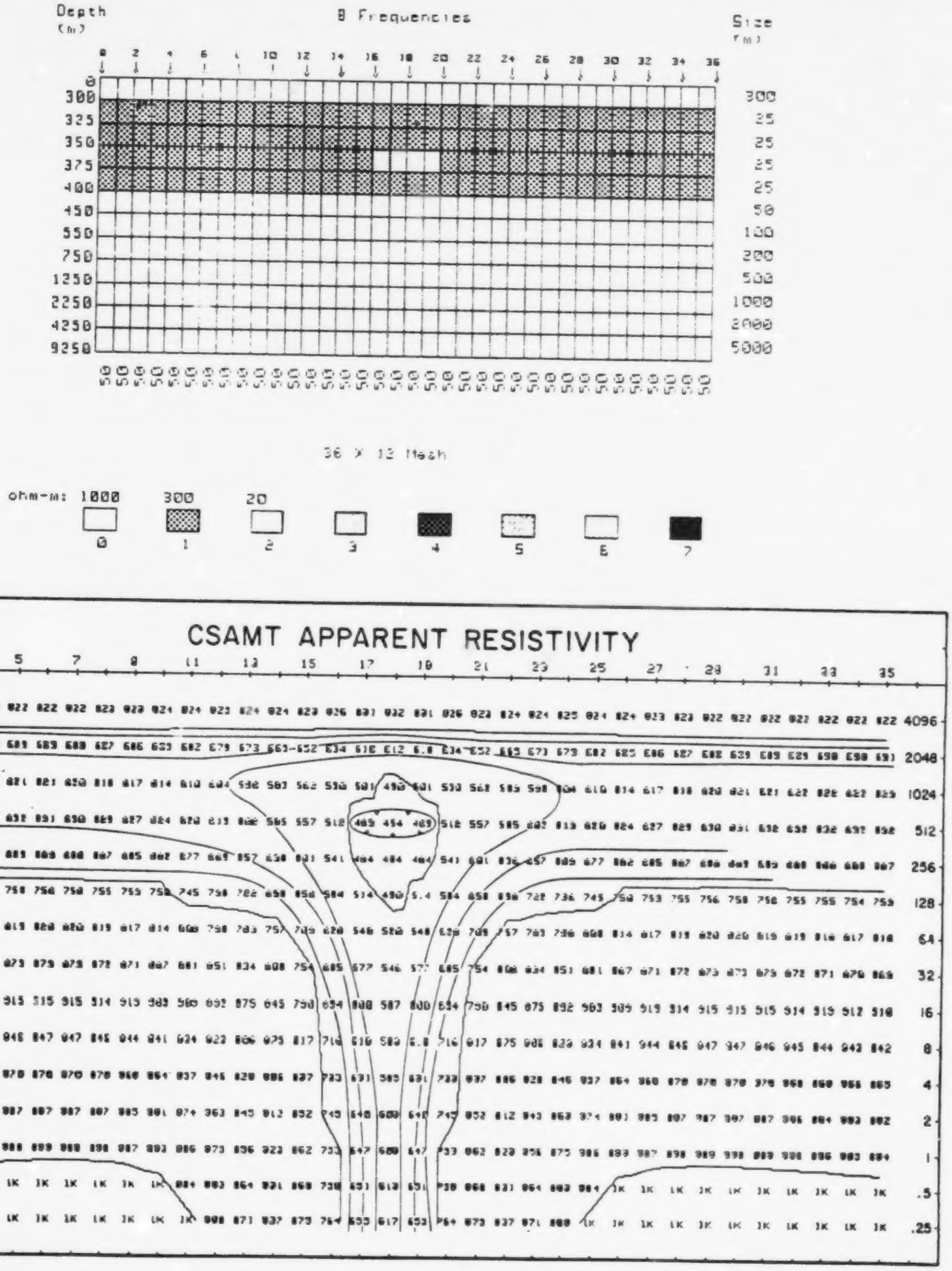

Figure 093.5c. Forward problem solution confirms shape of anomaly.

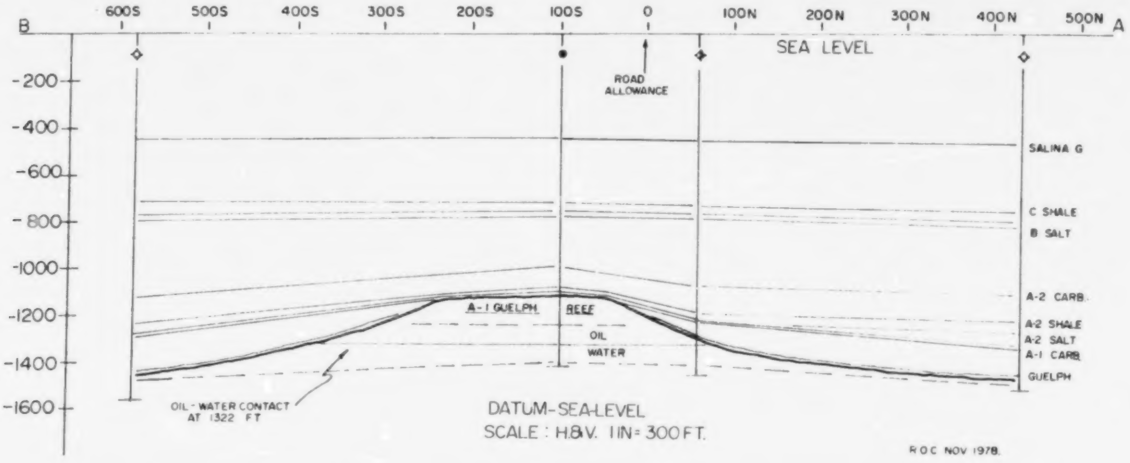
B
600S
500S
400S
300S
200S
100S
0
100N
200N
300N
400N
500N
A
SEA LEVEL
ROAD ALLOWANCE
-200
-400
-600
-800
-1000
-1200
-1400
-1600
SALINA G
C SHALE
B SALT
A-2 CARB.
A-2 SHALE
A-2 SALT
A-1 CARB.
GUELPH
A-1 GUELPH
REEF
OIL
WATER
OIL-WATER CONTACT AT 1322 FT
DATUM-SEA-LEVEL
SCALE: H.&V. 1IN=300FT.
ROC NOV 1978.

Figure 093.6a. Structural cross-section at Corey East Pinnacle Reef, Sarnia, Ontario.

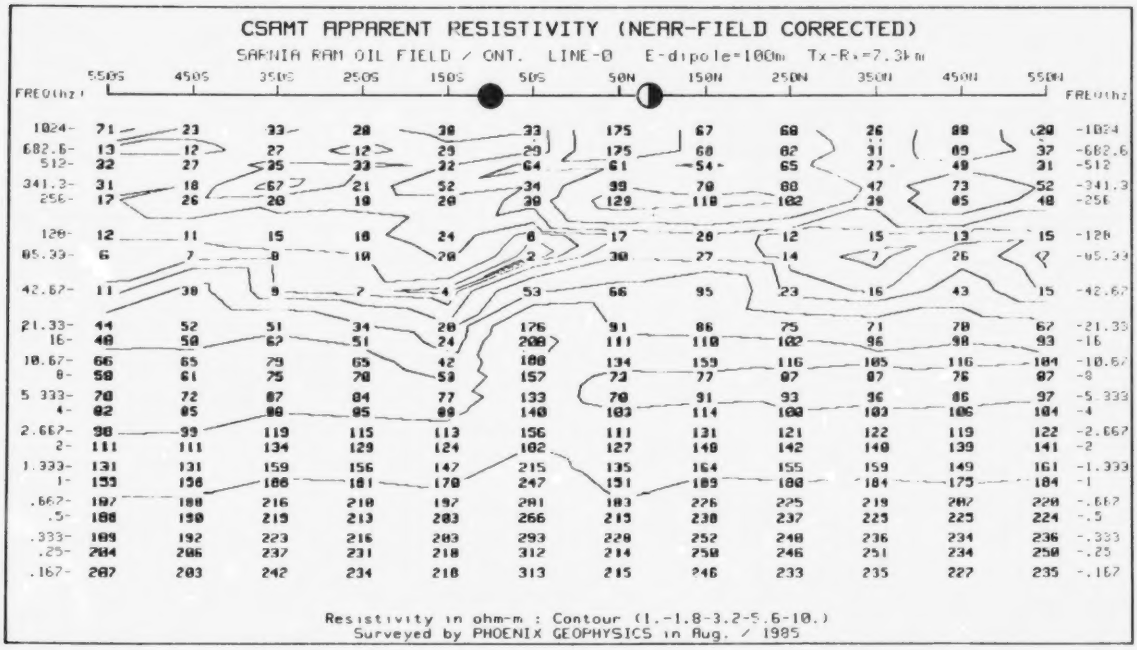

Figure 093.6b. CSAMT pseudo-section shows a definite, complex resistivity pattern at the position of the reef.

Grant 097 — Gold in Peat and its Relevance to Mineral Exploration

C.F. Gleeson[1], R.D. Thomas[2], V.N. Rampton[2], S. Paradis[2] and S.G. Corden[1]

[1]C.F. Gleeson and Associates Ltd., Iroquois, Ontario

[2]Terrain Analysis and Mapping Services Ltd., Carp, Ontario

ABSTRACT

Gold anomalies in near–surface peat in two bogs on glaciolacustrine sediments near Kirkland Lake appear related to underlying till or bedrock sources. The horizontal and vertical patterns of conductivity, hydrogen ion concentration, gold and other element values support an electrochemical model of dispersion from their source to the surface of the bogs. Gold and selected elements are concentrated at the bedrock–till interface, the clay–peat interface and the F–layer due to changes in physical and chemical conditions at these horizons. Concentration of gold in the F–layer is believed to be related to the position of the water table. Its relative concentration is controlled by climatic conditions prior to sampling. Further research is required to detail the source and dispersion of gold and other elements in peat.

INTRODUCTION

During 1985 and 1986 laboratory and field investigations were completed to assess and develop sampling strategies for geochemical gold exploration in peatlands. Peat and overburden were systematically sampled from surface to bedrock in two areas to determine the variations of gold and other elements, conductivity and H+ with depth. The two areas selected covered gold anomalies in near–surface peat that had been located during a program completed in 1983.

Both areas are in Morrisette Township northeast of Kirkland Lake (Figure 097.1). The Alfie Creek area is 11 km northeast of Kirkland Lake. The Lahaie Lake area is located 16 km northeast of Kirkland Lake. Both are accessible via logging trails from the Esker Lakes Park Road.

PREVIOUS WORK

Metal–rich peat has been reported by numerous authors (cf. Townsend 1824, Percey 1875, Lovering 1927, Forrester 1942, Eckel 1949, Cannon 1955, Ermengen 1957, Boyle and Cragg 1957, Webb 1958, Webb et al. 1959, Boyle 1977). Generally the enrichment was due to precipitation of these elements from metalliferous waters entering the bogs.

Successful geochemical prospecting in peatlands was initiated by Salmi (1950) in Finland. Salmi (1955, 1956, 1958, 1967) studied the distribution of numerous metals in peat bogs relative to known orebodies. Salmi found that some elements, e.g. vanadium and titanium, were commonly concentrated in the base of the peat; some elements, e.g. iron, molybdenum and lead, were concentrated at the surface of the peat; metallic elements showed anomalous concentrations in peat over orebodies even where the ore was overlain by 10 m of sand and till; and pH values of peat were affected by underlying bedrock types. Geochemical studies on bogs in Canada have been numerous (Gleeson 1960, Hawkes and Salmon 1960, Gleeson and Coope 1967, Fortescue and Hornbrook 1967, 1969, Hornsnail and Elliott 1971, Gunton and Nichol 1974, Bradshaw 1975, Fortescue 1975, Hornsnail 1975, Lett and Fletcher 1979 and DiLabio and Coker 1982). For the most part these studies involved enrichment in peat of such metals as copper, lead, zinc, molybdenum and uranium that moved hydromorphically down freely drained slopes into the bogs. Similar studies have also been carried out in Europe, especially in Scandinavian countries (Bolviken and Gleeson 1979).

Little information is presently available on the gold content of peats. Borovitskii (1976) noted anomalous values of gold in peats over gold deposits in permafrost regions of Russia. Dissanayake and Kritsotakis (1984) noted gold values of 159 to 882 ppb in a peat deposit in Sri Lanka. In 1983, Gleeson and Rampton (1983a) noted some well defined gold anomalies in a peat bog near Kirkland Lake. The latter lead to the research project herein being reported.

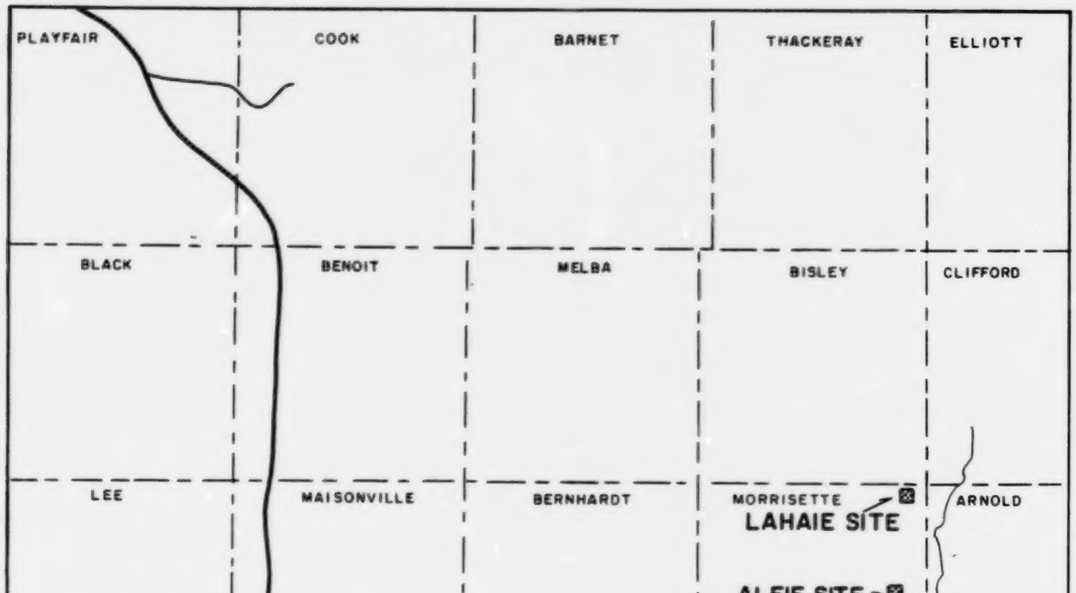
PLAYFAIR
COOK
BARNET
THACKERAY
ELLIOTT
BLACK
BENOIT
MELBA
BISLEY
CLIFFORD
LEE
MAISONVILLE
BERNHARDT
MORRISETTE
LAHAIE SITE
ARNOLD
ALFIE SITE
KIRKLAND LAKE AIRPORT
BOMPAS
GRENFELL
Sesekinika L
TECK
LEBEL
Victoria L
King Kirkland
KIRKLAND LAKE
11
66
GAUTHIER
BURT
Kenogami L.
OTTO
BOSTON
McELROY
N
0
5
10 km
EBY
GROSS
BLAIN
MARQUIS
Round L.
PACAUD
CATHARINE

Figure 097.1. Location map.

METHODOLOGY

The near-surface peats of the study areas were sampled at 100 foot (30 m) intervals on lines spaced at 400 feet (122 m) in 1983 as part of an exploration program covering a larger area. Details of the sample depth, slope, vegetation and material sampled were recorded. Samples were prepared for analysis and analyzed by Bondar-Clegg and Company Ltd., Ottawa, Ontario. The peat samples were dried and sieved through a 50 mesh screen, and 10 gram splits were analyzed for gold using a by fire assay carbon–rod atomic absorption spectrometric technique.

Anomalies located during 1983 were resampled. The anomalies were reproduced, although values were lower. These samples were analyzed by fire assay carbon–rod atomic absorption as in 1983. Two areas for detailed investigation were selected following this resampling program. The area of detailed investigation at Alfie Creek was resampled and redescribed at 25 m intervals on lines newly cut and spaced at 125 m intervals. Eight grams of minus 50 mesh material was briquetted, shrink wrapped and analyzed for gold and twenty other elements by Direct Irradiation Instrumental Neutron Analysis (INAA). One–half of the samples were analyzed by fire assay carbon–rod atomic absorption spectrometry to determine the variability between techniques.

On selected lines transecting gold anomalies located during 1983, peat profiles were sampled at 15 m intervals using a hiller peat borer. The underlying lacustrine and glacial deposits were sampled in section at 30 m intervals using a Pionjar percussion drill with a flow–through sampler. Alder leaves from the overstory were also sampled along these profiles. Generally, a sample of the living layer (O–layer), a sample of partially decomposed organic material (F–layer) and the peat profile, which was described according to peat type and humification, were sampled. The peat was sampled in 50 cm lengths or according to peat type. Samples were split with one portion being submitted for analysis by INAA for gold plus 20 elements, one portion being retained for measurement of pH and conductivity, and in some instances one portion being retained for radiocarbon dating by the laboratory at Brock University. If adequate material was not available from one boring, multiple holes were utilized. The lacustrine and glacial deposits were sampled at relatively uniform intervals not exceeding 6 m. Samples, 25 cm in length, were obtained using the flow–through sampler. Portions of samples were retained for trace element analysis and portions for pH and conductivity measurements. Ten to twenty gram splits were encapsulated and analyzed by INAA for gold plus 18 elements following sieving through a 250 mesh screen. In addition, a heavy mineral separate (S.G. >2.9) of the plus 250 mesh material of the tills was encapsulated and similarly analyzed.

Copper, lead, zinc and silver were analyzed by atomic absorption spectrometry using an aqua regia dissolution for all samples collected during 1985.

Conductivity and pH were measured for most samples using techniques described by Govett (1975). Generally, 100 ml of de–ionized water was added to 1 gram of moist sample. The conductivity of this slurry was measured by a Radiometer Coperhagen (type CDM 2e) conductivity meter with probe model PP1042, and the pH by a Canlab pH meter (model H5503–1) with a combination electrode. For the leaves and samples of the O–layer and F–layer, 100 ml of de–ionized water was added to 1 gram of dried and screened material. A few samples of similarly dried and screened peat were also measured and it was discovered that the dried and screened samples had conductivities 6 to 10 times the conductivities of the moist samples. Obviously the amount of dry material introduced to the slurry significantly affects the conductivity of the slurry. The pH measurements were converted to hydrogen ion concentrations, and measured conductivities were corrected in all cases for H+ concentration as recommended by Govett (1976). For a further discussion of the problems inherent in measuring the conductivities and pH's of soils reference is made to Govett (1976) and Thomas et al. (in prep.).

SETTING

The areas investigated in detail were relatively flat and poorly drained (Gleeson and Rampton 1983a,b). One small bedrock–controlled knob rises 4 m above the swamp near the southeast corner of the Alfie Creek area, and a ridge, presumably bedrock–controlled, borders the south edge of the Lahaie Lake area. Some areas at the north edge of the Lahaie Lake grid along a creek are affected by flooding from beaver dams.

Much of the Alfie Creek area is covered by alder swamp, although sawn stumps attest to a more mature forest in some areas. Black spruce, tamarack and birch are scattered throughout the area. At the west edge of the area, dense tall spruce grows on the surface of the bog. Mosses, sedges and herbs form a continuous ground cover. Spruce and alder cover most of the Lahaie Lake area; on the ridge along its south edge tamarack, birch and sumac are also present; other deciduous trees are present on the better drained part of the ridge. The poorly drained area has a ground cover similar to the Alfie Creek area, but the better drained areas are covered by caribou moss.

The Alfie Creek area is underlain by a dacite–andesite unit of the Blake River Group in contact to the south with basaltic volcanic rocks of the Kinojevis Group. The contact strikes east and dips

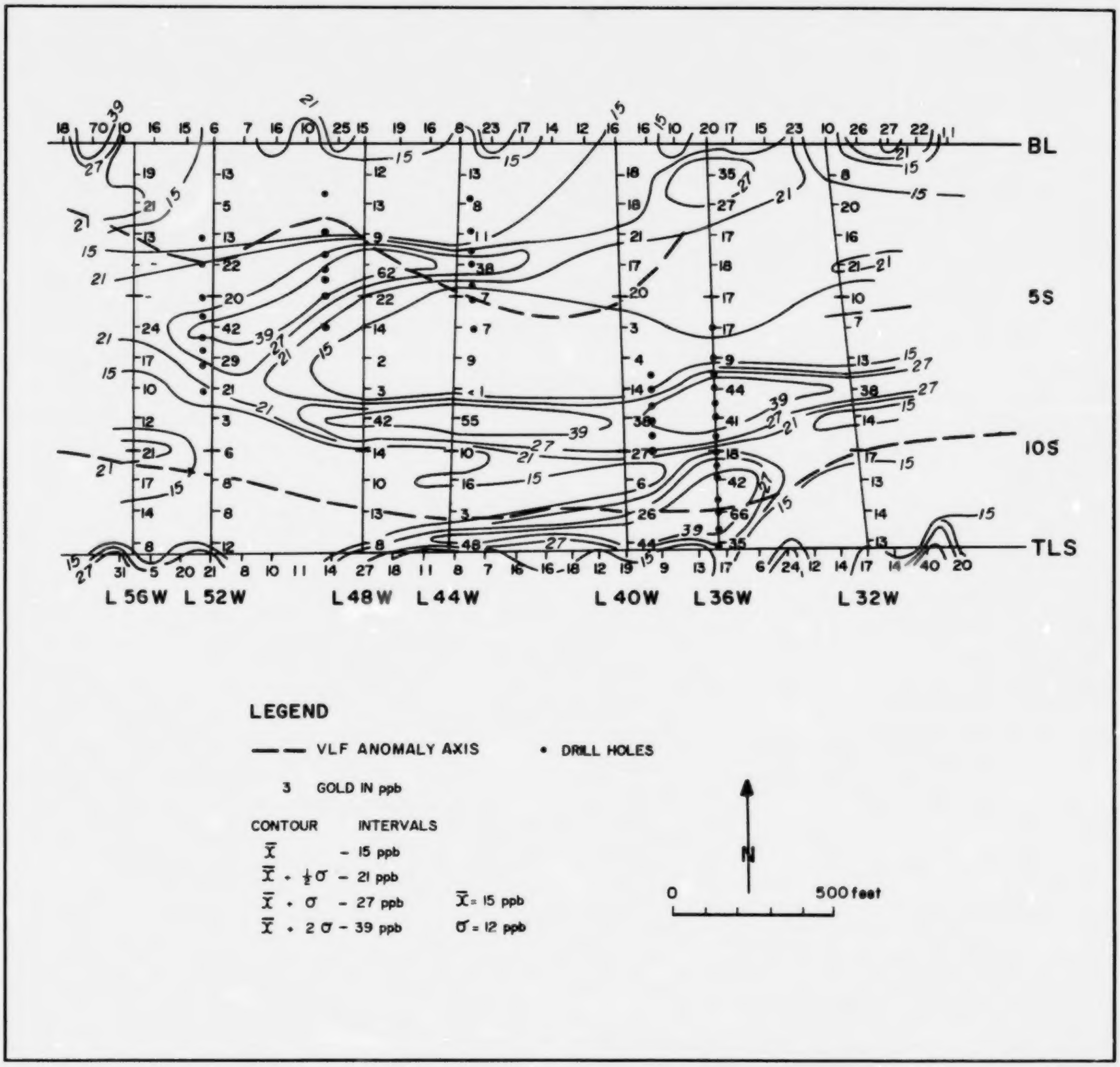
BL
5S
10S
TLS
L 56W
L 52W
L 48W
L 44W
L 40W
L 36W
L 32W
LEGEND
VLF ANOMALY AXIS
• DRILL HOLES
3 GOLD IN ppb
CONTOUR INTERVALS
X̄ - 15 ppb
X̄ + ½σ - 21 ppb
X̄ + σ - 27 ppb
X̄ + 2σ - 39 ppb
X̄ = 15 ppb
σ = 12 ppb
N
0
500 feet

Figure 097.2. Gold in near-surface peat: Alfie 1983 grid.

steeply to the north. The Lahaie Lake area is interpreted to be underlain by an east-striking dacite-andesite unit in contact with andesite to the south; both units are part of the Black River Group.

Thin till was deposited over the area during Lake Wisconsin glaciation, primarily by southeastward flowing ice. Sand from subaqueous outwash fans appears to have been deposited over part of the Lahaie Lake grid. The remainder of the silty and clayey deposits were deposited in a glacial lake, which covered the area until about 8000 years B.P. Paludification and the accumulation of peat appears to have began shortly afterwards, although in some areas it may have been delayed until about 4000 B.P.

RESULTS

Geochemical analyses, conductivities and hydrogen ion concentrations for both the near-surface peats and the drill hole samples were plotted and contoured in plan and profile respectively (Thomas et al. in press). For comparative purposes both the gold results of the near-surface peat samples for the 1983 and 1985 surveys on the Alfie grid also were plotted and contoured (Figures 097.2 and 3). A number of contoured plans and profiles of the analysis from both the Alfie and

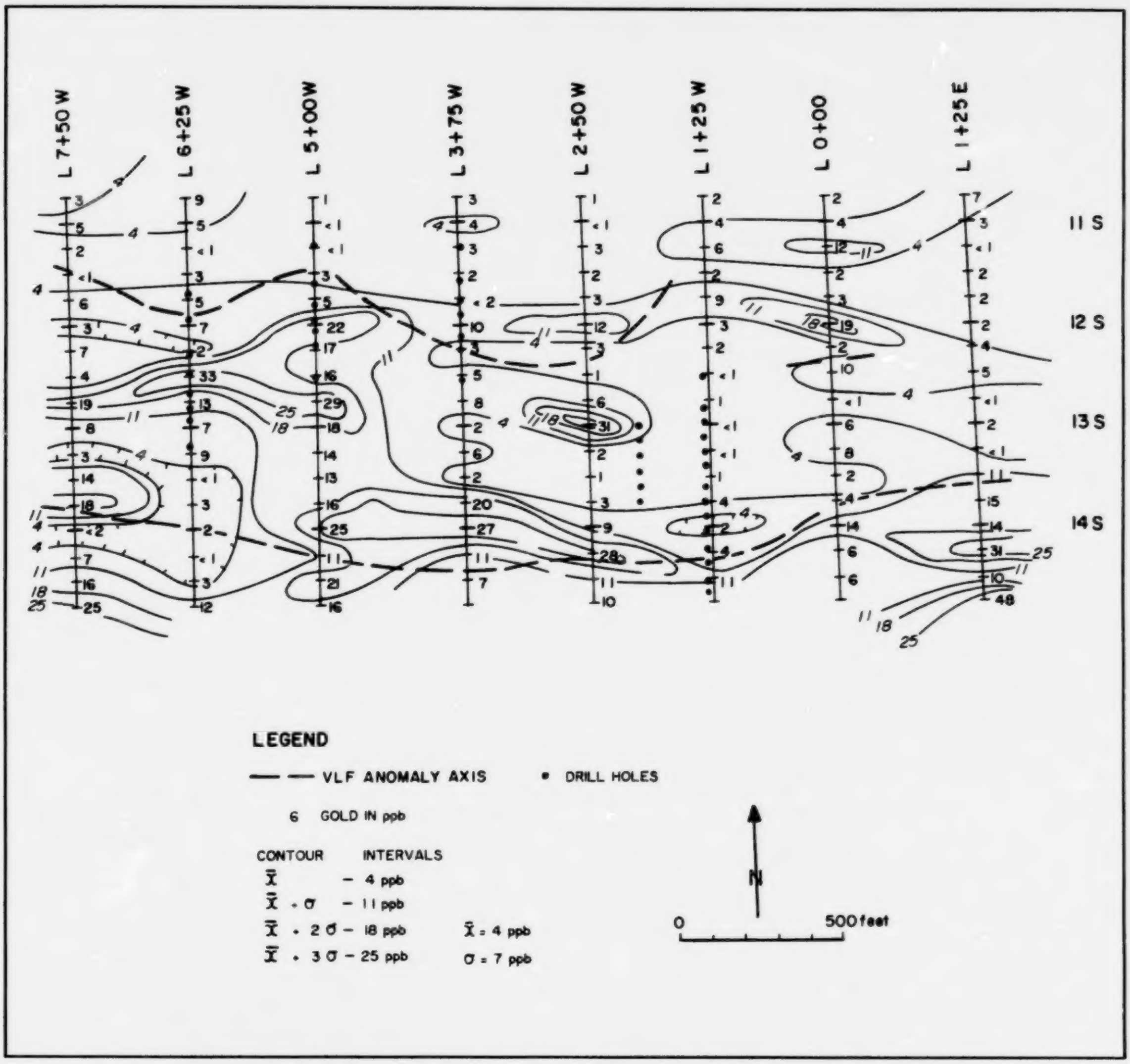
L 7+50 W
L 6+25 W
L 5+00 W
L 3+75 W
L 2+50 W
L 1+25 W
L 0+00
L 1+25 E
11 S
12 S
13 S
14 S
LEGEND
VLF ANOMALY AXIS
DRILL HOLES
6 GOLD IN ppb
CONTOUR INTERVALS
x̄ – 4 ppb
x̄ + σ – 11 ppb
x̄ + 2σ – 18 ppb
x̄ + 3σ – 25 ppb
x̄ = 4 ppb
σ = 7 ppb
N
0
500 feet

Figure 097.3. Gold in near–surface peat: Alfie 1985 grid.

Lahaie grids (Figures 097.2 to 15) are included in this paper to illustrate the results and facilitate an abbreviated interpretation of the results.

DISCUSSION

GOLD IN NEAR–SURFACE PEAT, ALFIE GRID

It was apparent from selected resampling during 1985 of gold anomalies defined in 1983 that both background and anomalous values were lower in 1985. Thus the entire study area was resampled on a grid to verify the original anomalies and to establish background values. The contoured results of both surveys (Figures 097.2 and 3) show a number of anomalous zones, which although parallel, show some lateral shift in position. The variations in the 1983 and 1985 gold data may be due in part to (a) the depth at which the samples were taken, and (b) differences in seasonal climatic conditions prior to and during sampling. The gold content of plants has been demonstrated to vary seasonally (Aripova and Talipov 1966, Schiller et al. 1973, Dunn 1984, 1985) as has the metal content of peats (Kokkola 1977, Salminen and Kokkola 1984). Annual precipitation prior to the 1983 sampling was greater than prior to the 1985 sampling. Perhaps this resulted in loosely bonded metals being flushed from the living plants into the bog, thus resulting in the relatively high gold values in near–

surface peat for 1983. Kovalevkii (1978) has shown that element concentration may decrease in plants by up to one-fifth during rains. Also, moisture conditions and depth of sampling may combine to affect metal values as the exact positioning of metal concentrations in peat profile may be related to the position of the water table. Damman (1978) found that during periods of high water levels, elements in the zone of water level fluctuation can be reduced and immobilized. In times of lower water levels, oxidation will mobilize previously reduced metals.

OTHER ELEMENTS IN NEAR-SURFACE PEAT, ALFIE GRID

The contoured plans for a number of metals, e.g. arsenic (Figure 097.4a), antimony (Figure 097.4b), copper, lead and zinc, and to a lesser degree silver showed similar anomaly patterns to those of gold. These patterns suggest a common source for these metals.

Barium (Figure 097.5b), chromium (Figure 097.5a), cobalt (Figure 097.6b) and nickel (Figure 097.6a) show similar anomaly patterns with their highest values being concentrated in the southwest part of the grid where a magnetometer survey (Walker 1985) showed increasing magnetism. They could reflect the presence of kimberlitic rocks, which are present in the area.

CONDUCTIVITY AND HYDROGEN ION CONCENTRATION IN NEAR-SURFACE PEATS, ALFIE GRID

The conductivity (Figure 097.7a) and hydrogen ion concentration (Figure 097.7b) of near-surface peat generally varies inversely. Hydrogen ion peaks and conductivity troughs flanked by highs (producing "rabbit-ear" anomalies; Govett 1976 and Smee 1983) commonly coincide with VLF-EM anomaly axes. These are all phenomena considered to be indicative of buried conductive sulphide bodies. In plan there is some correlation between "rabbit-ear" conductivity anomalies, hydrogen ion peaks, VLF-EM axes, gold and associated metal anomalies. The incomplete correlations may be caused by such factors as the effect on the transfer of metals and hydrogen ions to the near-surface peats because of variability in peat or overburden thicknesses. Where conductivities, hydrogen ion concentrations and gold values in near-surface peats from closely spaced drill holes have been plotted in profile, the relationship between conductivity "rabbit-ears" anomalies, hydrogen ion and gold peaks is even more apparent (Thomas et al. in press) than in plan view.

GOLD AND OTHER ELEMENTS IN NEAR-SURFACE PEAT, LAHAIE GRID

Although the Lahaie grid covered a relatively small area, near-surface peat (F-layer) anomalies trending east-southeast and east were established for gold (Figure 097.8a) and other related elements, e.g. arsenic (Figure 097.8b), copper (Figure 097.9b), silver, molybdenum, lead (Figure 097.9a), antimony and zinc. Barium, thorium and uranium also had similar anomalous distributions. "Rabbit-ear" conductivity anomalies and hydrogen ion highs were noted to coincide with anomalies in gold and related metal values (Thomas et al. in press).

ELEMENT DISTRIBUTION IN PROFILES

A number of generalities became obvious concerning the distribution of gold and other elements in the sampled profiles:

1. copper and zinc are invariably concentrated in alder leaves. Locally, gold, silver, chromium and lead may also have increased values;
2. the F-layer is commonly a horizon where gold (Figure 097.10), arsenic (Figure 097.11), antimony, lead and zinc are concentrated. Less commonly, copper (Figure 097.13), silver, cobalt and molybdenum may be concentrated here. In some cases, the values are not highly anomalous, but are elevated relative to the underlying peat;
3. upper peats locally can be relatively enriched in gold, copper, lead, zinc, molybdenum, chromium, nickel and thorium;
4. basal peats commonly show large concentrations, at least relative to the overlying peat, of copper, uranium, chromium (Figure 097.12), molybdenum and thorium. Locally, it is also enriched in gold, silver, cobalt and barium;
5. nickel is commonly enriched throughout the peats;
6. elements such as barium, thorium, uranium, gold (Figure 097.10), and chromium (Figure 097.12) show relatively high values in the clays immediately underlying the peat; zinc, nickel and cobalt may also be locally concentrated at this horizon;
7. zones of anomalous values can be found within the glacial sediments underlying the peats. Commonly, these zones show multi-element

anomalies (cf. gold and chromium at the base of AR85–35 on Figures 097.10 and 12);

8. in addition to the concentration of elements in certain horizons, some elements clearly have vertical or inclined components as can be seen in Figure 097.10 for gold and Figure 097.12 for chromium.

In summary, trends in element values are not necessarily related to depth of sample. Anomalous values of many elements are concentrated along certain horizons such as the F–layer, the clay–peat interface and the till–bedrock interface. Inclined or vertical zones of above normal values of some elements can also be present. Commonly these zones have the highest values in the F–layer and in the above interfaces. Although horizontal patterns for conductivity (Figure 097.14) and hydrogen ion concentration (Figure 097.15) predominated, inclined or vertical components in places reflect those shown by elements.

SOURCE OF GOLD AND OTHER ELEMENTS IN PEAT

Two sources for the gold and other elements, especially near–surface peats, seem most likely:

(a) airborne contamination; and

(b) migration from a source at depth.

Airborne contamination seems to be an unlikely source for gold and other element concentrations in the near–surface peats, as the distribution patterns of the elements are not properly oriented relative to the prevailing winds and locations of tailings and smelters in surrounding areas. The metal patterns are too complex to be related to distant wind transport of elements, unless some secondary biologic or hydrologic process is immediately redistributing the elements. Different groupings of elements with common distribution patterns around probable sources at depth also argue against an airborne source. For example, chromium, cobalt and nickel (Figures 097.5 and 6) have concentrations in near–surface peat near a magnetically high zone on the Alfie grid. Also, gold, arsenic, antimony and copper concentrations occur over a basal till anomaly on L6 + 25W, Alfie grid (cf. Figure 097.10).

Migration from a source at depth is suggested by general vertical and inclined zones of increased values from depth for some elements (Figures 097.10 and 12). It is probable that some physical, biological, chemical or electrochemical process or processes are affecting transfer of the elements from depth to the near–surface. Vertical and inclined perturbances to the general horizontal patterns of conductivity and hydrogen ion concentration (Figures 097.14 and 15), which coincide with similar trends of increased values of gold and other elements, suggest that the dispersion of elements, through the glacial sediments may be by an electrogeochemical process. According to Skvartsev (1978) the part played by electrochemical dissolution in enriching waters with heavy metals increases in importance under reducing conditions. Conditions at depth in glaciolacustrine environments of the shield are reducing (Gleeson 1960). Dispersion may also be assisted by diffusion of ions (Smee 1983) through the water saturated column of overburden. Hence the release and dispersion of metal cations may be totally electrogeochemical (Nuutilainen and Peuraniemi 1977) with plants or humus (peat) picking up metal cations directly from the electrogeochemical circulation path, or the mechanism could involve a combination of electrogeochemical dispersion and diffusion.

During the course of their general movement from depth, elements may become concentrated at horizons or interfaces, such as the peat–clay interface at the base of the bog or the F–layer near the top of the bog. These are horizons where rapid changes in the physical, biological, chemical or electrogeochemical conditions occur.

The ultimate source of the gold and other elements is believed to be the local bedrock as suggested by coincident VLF–EM anomalies and a value of 380 ppb gold in rock along strike to the east of the Alfie study area (Routledge et al. 1981, Gleeson and Rampton 1983a).

The mechanism for concentration of gold and other elements in the F–layer involves the transfer of the elements from the base of the bog through biological action, capillary action (Sillanpaa 1972), or electrogeochemical circulation (Nuutilainen and Peuraniemi 1977). Finally, plants growing on the surface of the bog probably absorb the elements through their root system. Their element–enriched leaves then are returned to the bog system and incorporated into the organic material. Final enrichment at the F–layer may be related to oxidation–reduction changes that occur at the water table. Some concentration of elements may occur in this environment simply from elements moving upward through capillary or electrogeochemical processes. The zone of element concentration may follow changes in the water table, either seasonal, annual or longer (Dammon 1978). The above model is most effective on mineratrophic bogs such as the Alfie and Lahaie bogs.

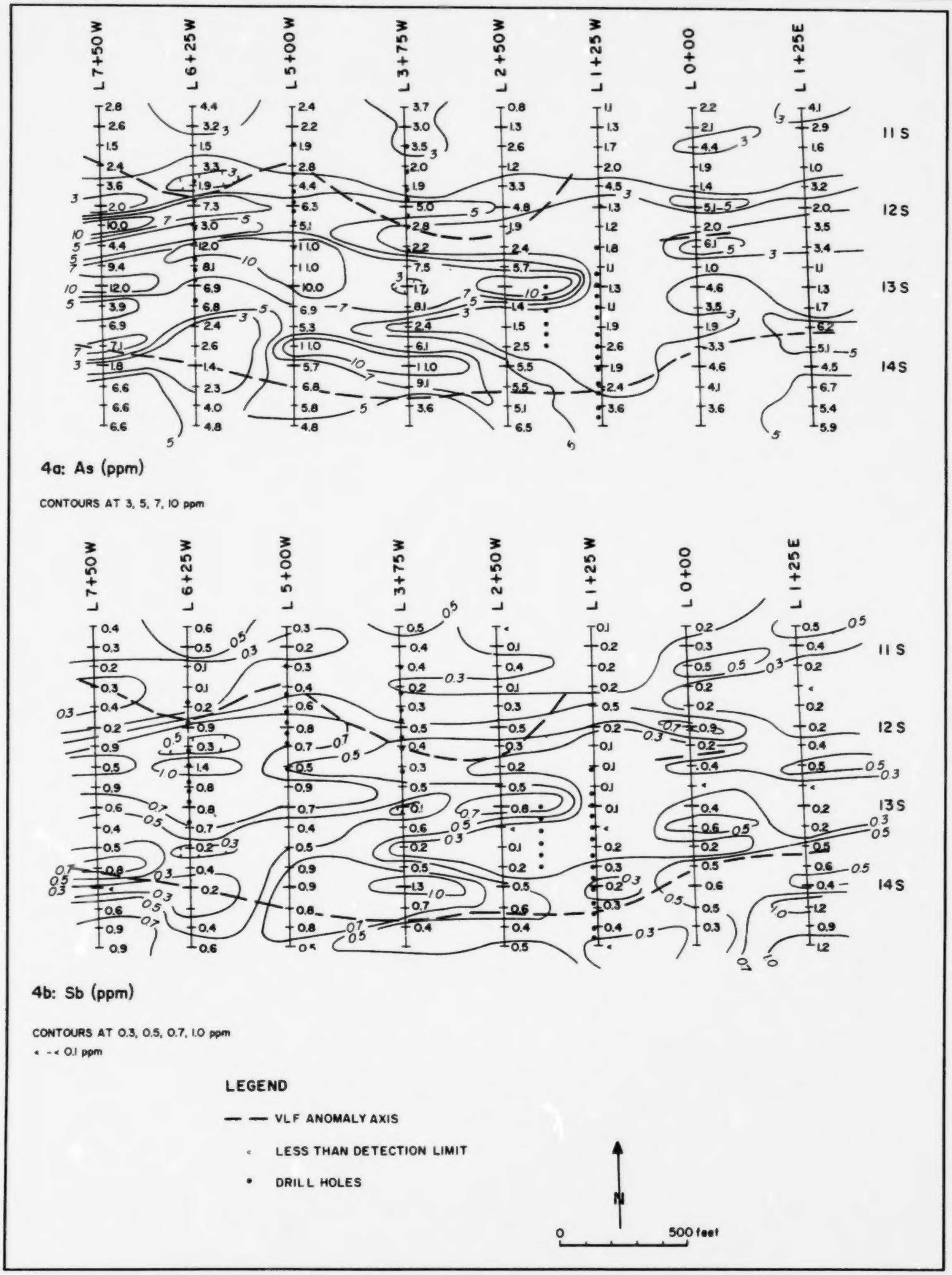
L 7+50W
L 6+25W
L 5+00W
L 3+75W
L 2+50W
L 1+25W
L 0+00
L 1+25E
11 S
12 S
13 S
14 S
4a: As (ppm)
CONTOURS AT 3, 5, 7, 10 ppm
4b: Sb (ppm)
CONTOURS AT 0.3, 0.5, 0.7, 1.0 ppm
< - < 0.1 ppm
LEGEND
VLF ANOMALY AXIS
< LESS THAN DETECTION LIMIT
• DRILL HOLES
N
0
500 feet

Figure 097.4. Arsenic (a) and antimony (b) in near-surface peat: Alfie 1985 grid.

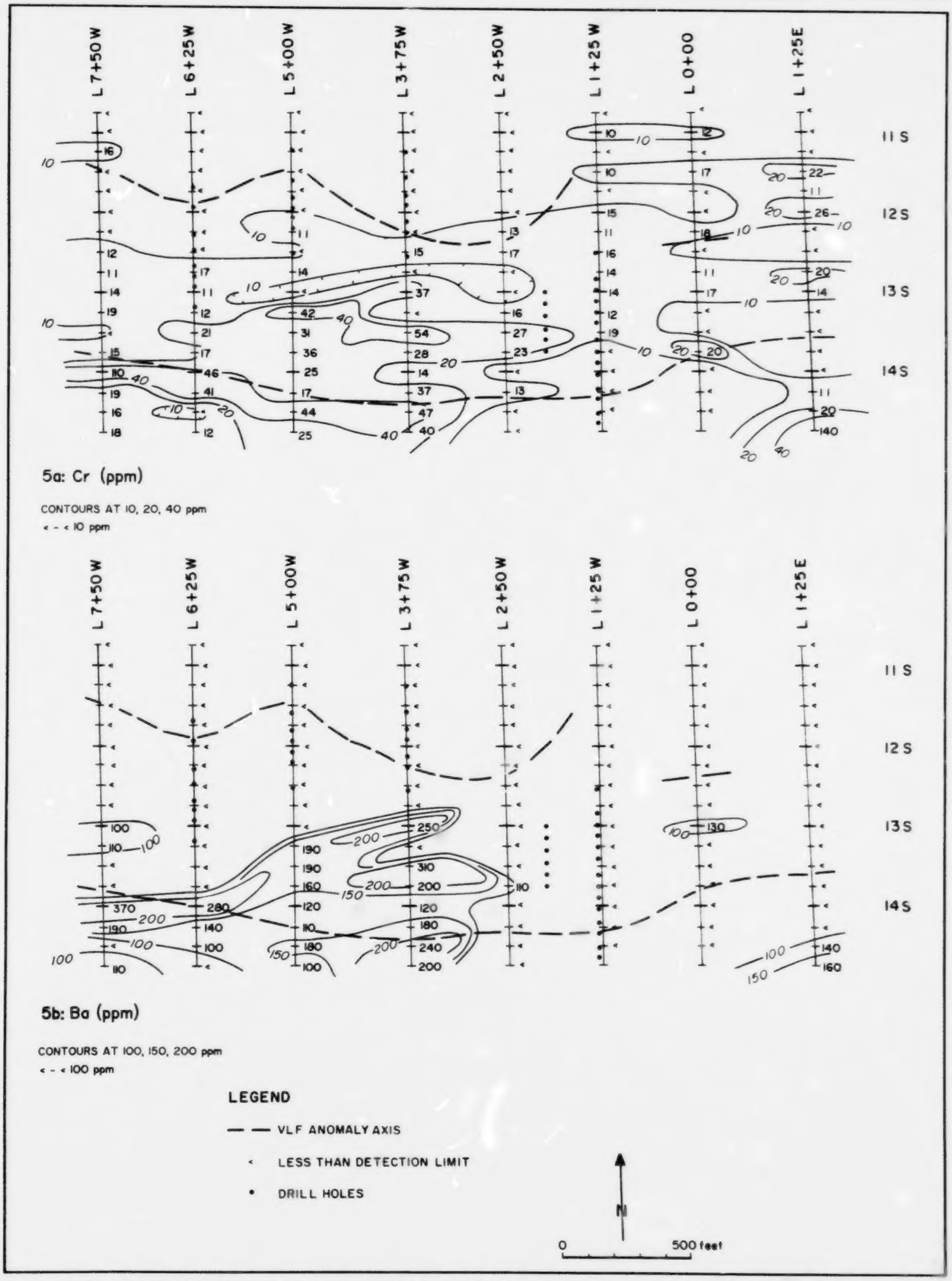
L 7+50W
L 6+25W
L 5+00W
L 3+75W
L 2+50W
L 1+25W
L 0+00
L 1+25E
11 S
12 S
13 S
14 S
5a: Cr (ppm)
CONTOURS AT 10, 20, 40 ppm
< - < 10 ppm
5b: Ba (ppm)
CONTOURS AT 100, 150, 200 ppm
< - < 100 ppm
LEGEND
VLF ANOMALY AXIS
< LESS THAN DETECTION LIMIT
• DRILL HOLES
N
0
500 feet

Figure 097.5. Chromium (a) and barium (b) in near-surface peat: Alfie 1985 grid.

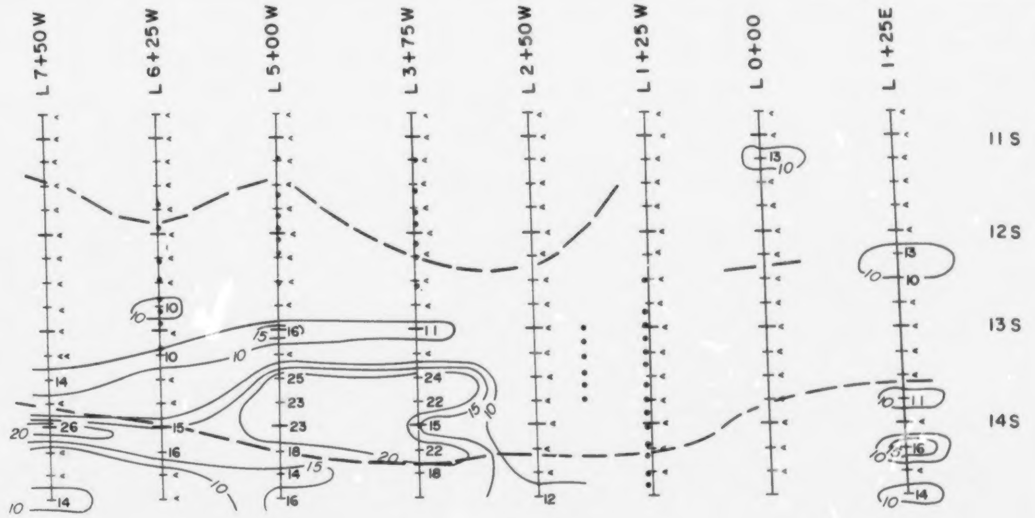
L 7+50 W
L 6+25 W
L 5+00 W
L 3+75 W
L 2+50 W
L 1+25 W
L 0+00
L 1+25 E
11 S
12 S
13 S
14 S

6A: Ni (ppm)

CONTOURS AT 10, 15, 20 ppm
< - < 10 ppm

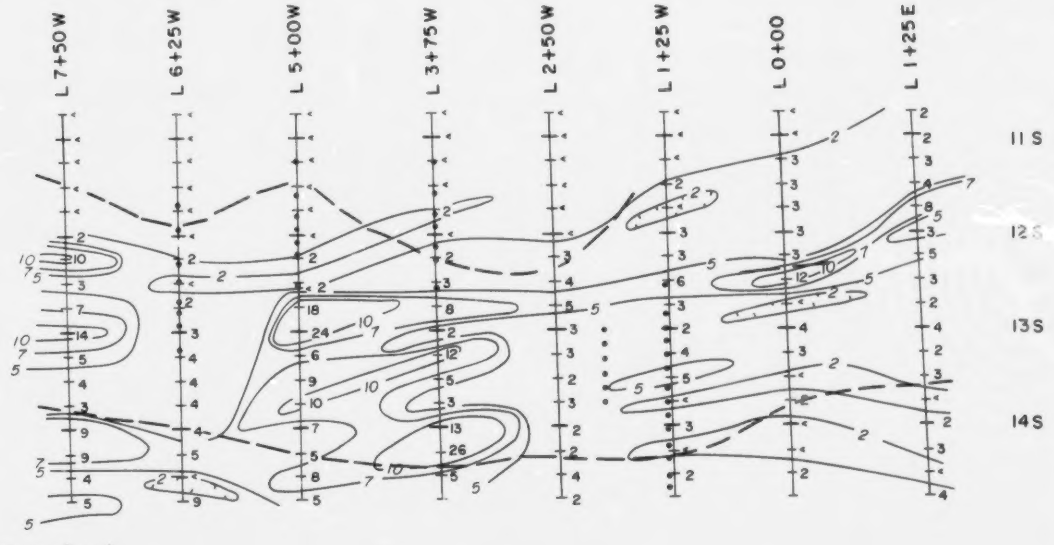
L 7+50 W
L 6+25 W
L 5+00 W
L 3+75 W
L 2+50 W
L 1+25 W
L 0+00
L 1+25 E
11 S
12 S
13 S
14 S

6B: Co (ppm)

CONTOURS AT 2, 5, 7, 10 ppm
< - < 2 ppm

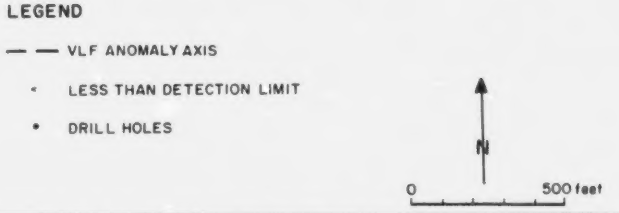
LEGEND
— — VLF ANOMALY AXIS
< LESS THAN DETECTION LIMIT
• DRILL HOLES
N
0
500 feet

Figure 097.6. Nickel (a) and cobalt (b) in near-surface peat: Alfie 1985 grid.

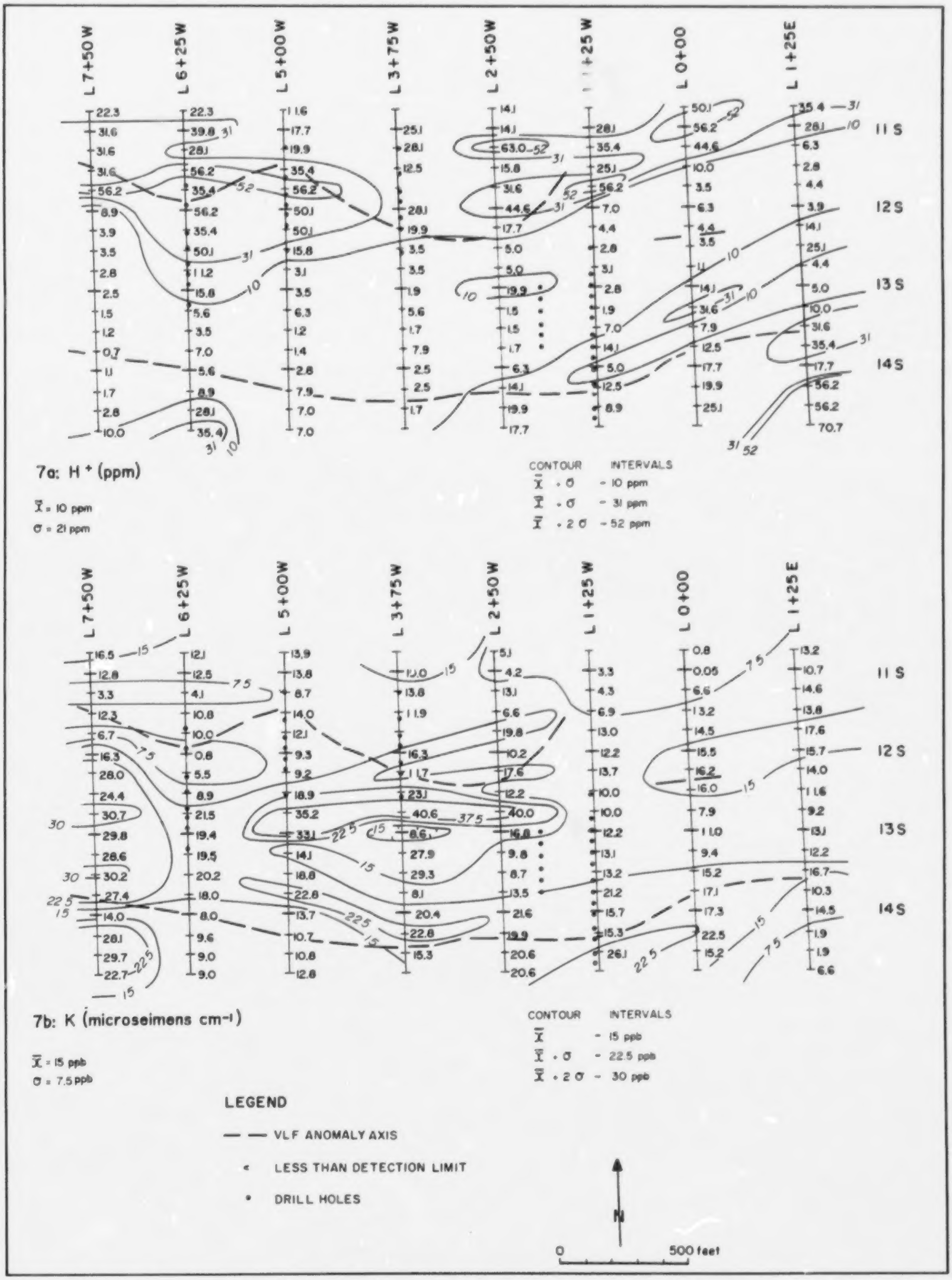
L 7+50W
L 6+25W
L 5+00W
L 3+75W
L 2+50W
L 1+25W
L 0+00
L 1+25E
11 S
12 S
13 S
14 S
7a: H⁺ (ppm)
X̄ = 10 ppm
σ = 21 ppm
CONTOUR INTERVALS
X̄ + σ - 10 ppm
X̄ + σ - 31 ppm
X̄ + 2σ - 52 ppm
7b: K (microseimens cm⁻¹)
X̄ = 15 ppb
σ = 7.5 ppb
CONTOUR INTERVALS
X̄ - 15 ppb
X̄ + σ - 22.5 ppb
X̄ + 2σ - 30 ppb
LEGEND
VLF ANOMALY AXIS
LESS THAN DETECTION LIMIT
DRILL HOLES
N
0
500 feet

Figure 097.7. Hydrogen ion concentration and conductivity in near-surface peat: Alfie 1985 grid.

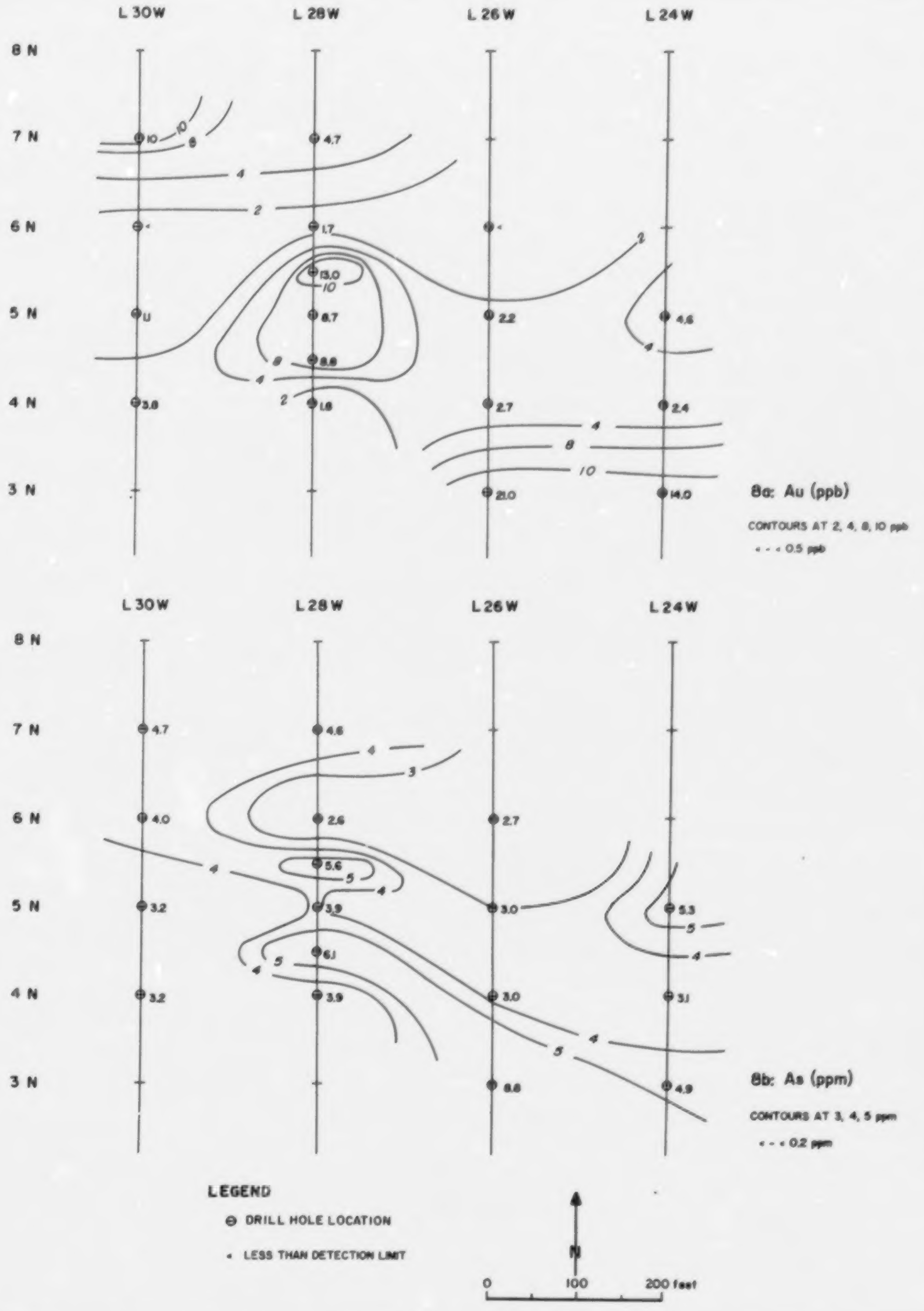
L 30W
L 28W
L 26W
L 24W
8 N
7 N
6 N
5 N
4 N
3 N
10
4.7
1.7
13.0
8.7
8.8
1.8
3.8
2.2
4.6
2.7
2.4
21.0
14.0
8a: Au (ppb)
CONTOURS AT 2, 4, 8, 10 ppb
< - < 0.5 ppb
L 30W
L 28W
L 26W
L 24W
8 N
7 N
6 N
5 N
4 N
3 N
4.7
4.6
4.0
2.6
2.7
5.6
3.2
3.9
3.0
5.3
6.1
3.2
3.9
3.0
3.1
8.8
4.9
8b: As (ppm)
CONTOURS AT 3, 4, 5 ppm
< - < 0.2 ppm
LEGEND
DRILL HOLE LOCATION
< LESS THAN DETECTION LIMIT
N
0
100
200 feet

Figure 097.8. Gold and arsenic in near-surface peat: Lahaie grid.

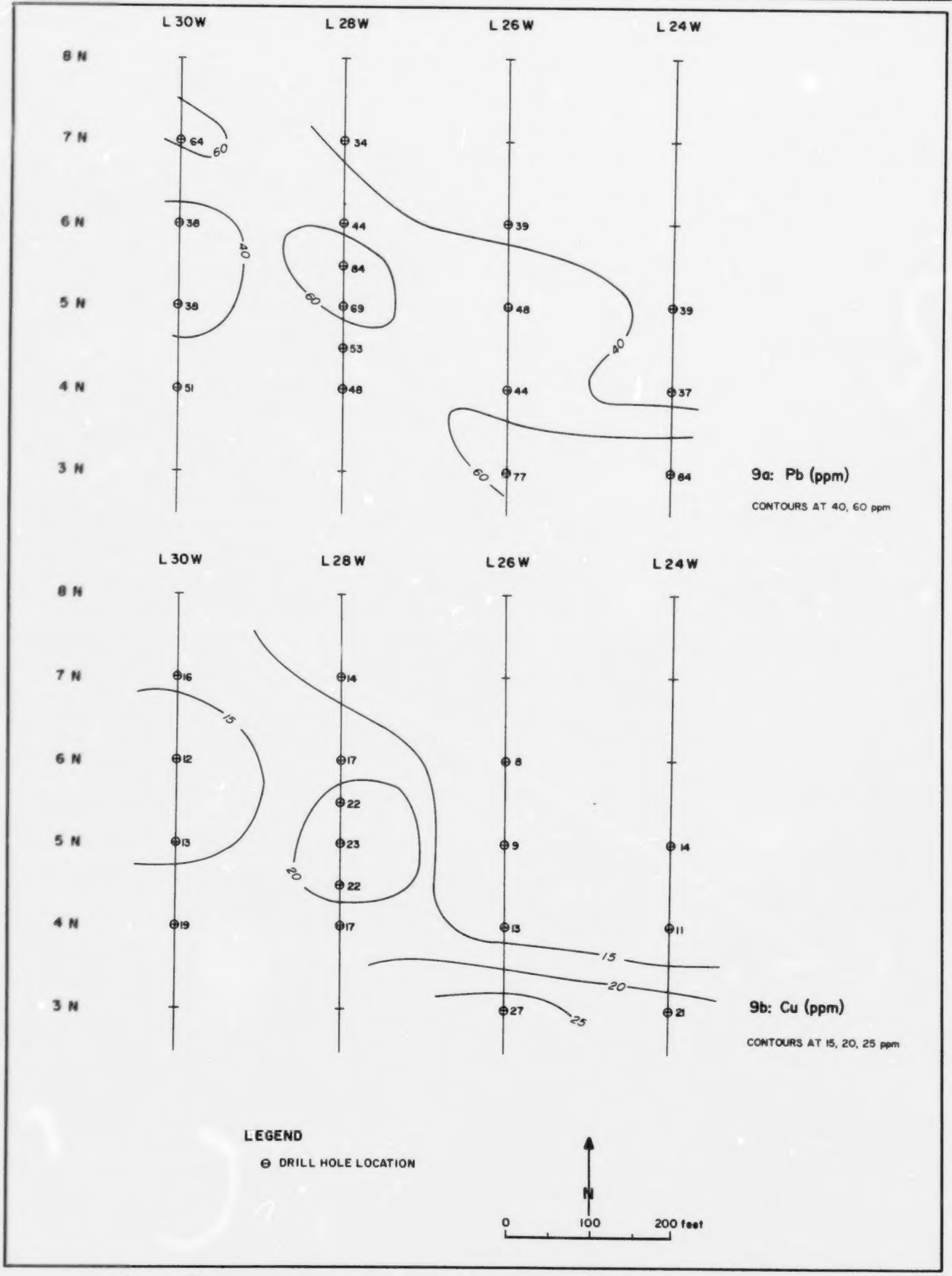
L 30W
L 28W
L 26W
L 24W
8 N
7 N
6 N
5 N
4 N
3 N
64
60
34
38
40
44
39
84
38
60
69
48
39
53
40
51
48
44
37
60
77
84
9a: Pb (ppm)
CONTOURS AT 40, 60 ppm
L 30W
L 28W
L 26W
L 24W
8 N
7 N
6 N
5 N
4 N
3 N
16
14
15
12
17
8
22
13
23
9
14
20
22
19
17
13
11
15
20
27
25
21
9b: Cu (ppm)
CONTOURS AT 15, 20, 25 ppm
LEGEND
⊖ DRILL HOLE LOCATION
N
0
100
200 feet

Figure 097.9. Lead (a) and copper (b) in near-surface peat: Lahaie grid.

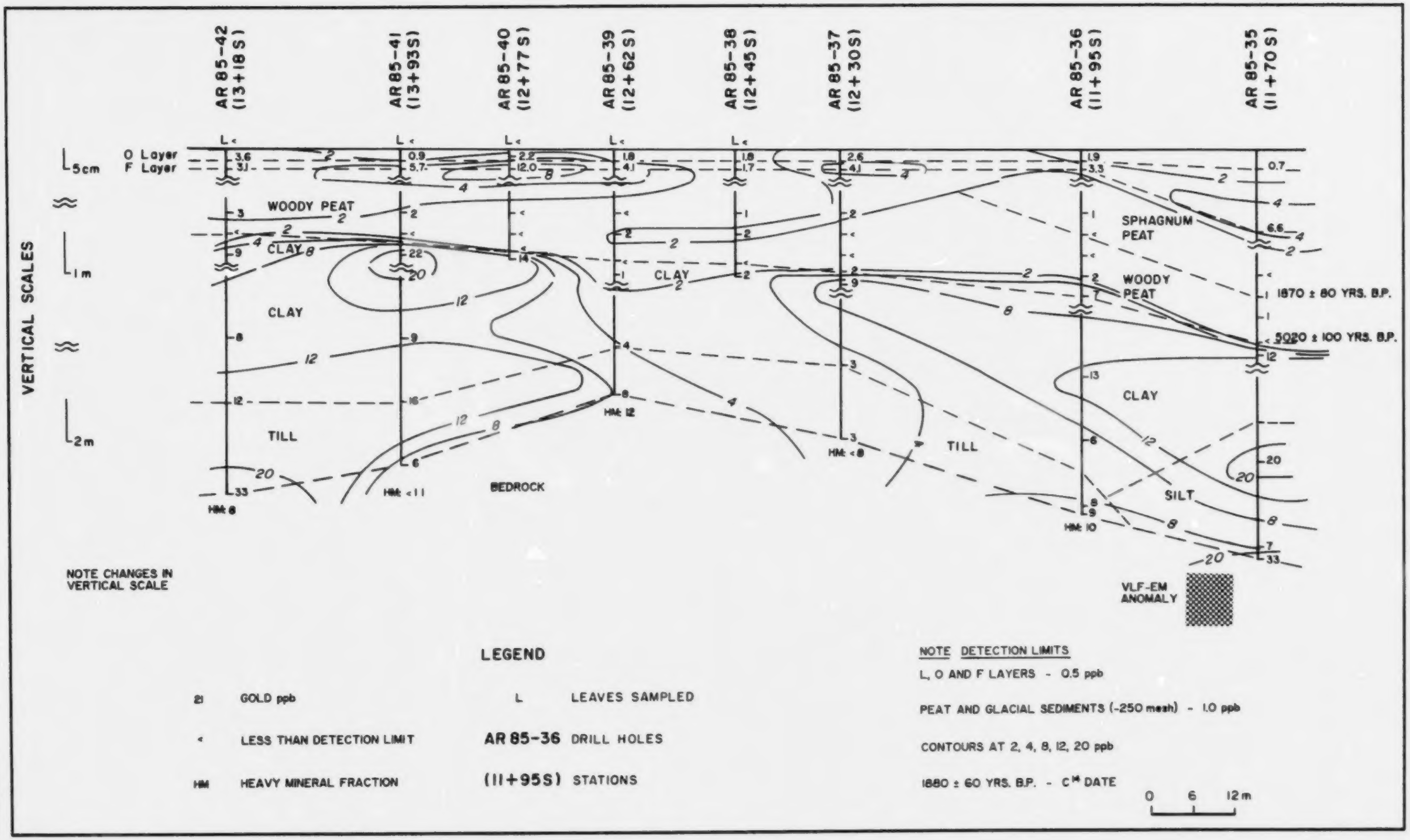
AR 85-42 (13+18S)
AR 85-41 (13+93S)
AR 85-40 (12+77S)
AR 85-39 (12+62S)
AR 85-38 (12+45S)
AR 85-37 (12+30S)
AR 85-36 (11+95S)
AR 85-35 (11+70S)
VERTICAL SCALES
5cm
1m
2m
O Layer
F Layer
WOODY PEAT
CLAY
CLAY
TILL
BEDROCK
CLAY
TILL
SPHAGNUM PEAT
WOODY PEAT
CLAY
SILT
1870 ± 80 YRS. B.P.
5020 ± 100 YRS. B.P.
HM 8
HM <11
HM 12
HM <8
HM 10
NOTE CHANGES IN VERTICAL SCALE
VLF-EM ANOMALY
LEGEND
21 GOLD ppb
< LESS THAN DETECTION LIMIT
HM HEAVY MINERAL FRACTION
L LEAVES SAMPLED
AR 85-36 DRILL HOLES
(11+95S) STATIONS
NOTE DETECTION LIMITS
L, O AND F LAYERS - 0.5 ppb
PEAT AND GLACIAL SEDIMENTS (-250 mesh) - 1.0 ppb
CONTOURS AT 2, 4, 8, 12, 20 ppb
1880 ± 60 YRS. B.P. - C14 DATE
0
6
12m

Figure 097.10. Gold on L6+25W profile: Alfie grid.

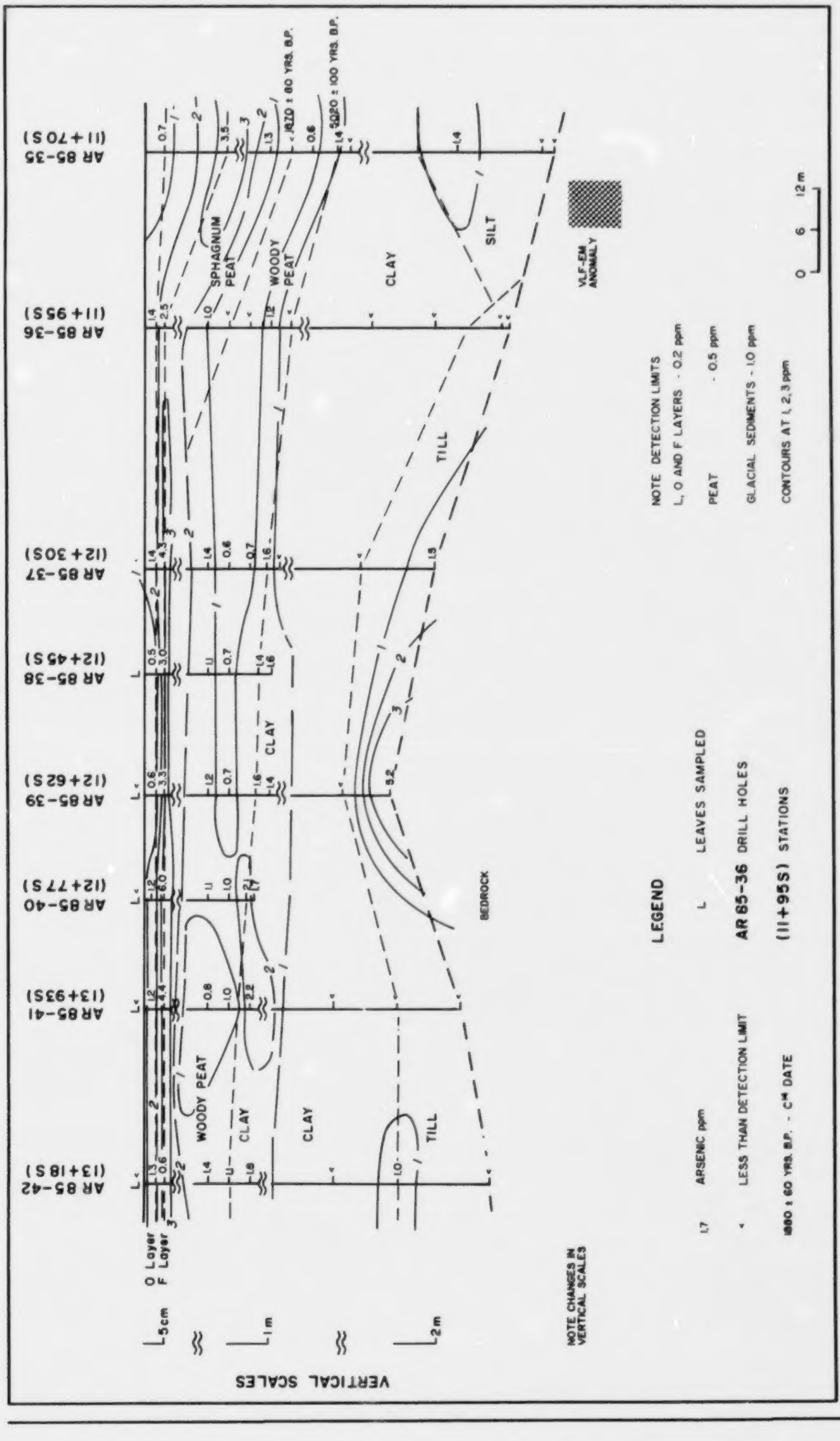
AR 85-42 (13+18S)
AR 85-41 (13+93S)
AR 85-40 (12+77S)
AR 85-39 (12+62S)
AR 85-38 (12+45S)
AR 85-37 (12+30S)
AR 85-36 (11+95S)
AR 85-35 (11+70S)
VERTICAL SCALES
5cm
1m
2m
O Layer
F Layer
NOTE CHANGES IN VERTICAL SCALES
WOODY PEAT
CLAY
TILL
BEDROCK
SPHAGNUM PEAT
SILT
1870 ± 60 YRS. B.P.
5020 ± 100 YRS. B.P.
VLF-EM ANOMALY
0
6
12 m
LEGEND
1.7 ARSENIC ppm
L LEAVES SAMPLED
< LESS THAN DETECTION LIMIT
AR 85-36 DRILL HOLES
1880 ± 60 YRS. B.P. - C14 DATE
(11+95S) STATIONS
NOTE DETECTION LIMITS
L, O AND F LAYERS - 0.2 ppm
PEAT - 0.5 ppm
GLACIAL SEDIMENTS - 1.0 ppm
CONTOURS AT 1, 2, 3 ppm

Figure 097.11. Arsenic on L6+25W profile: Alfie grid.

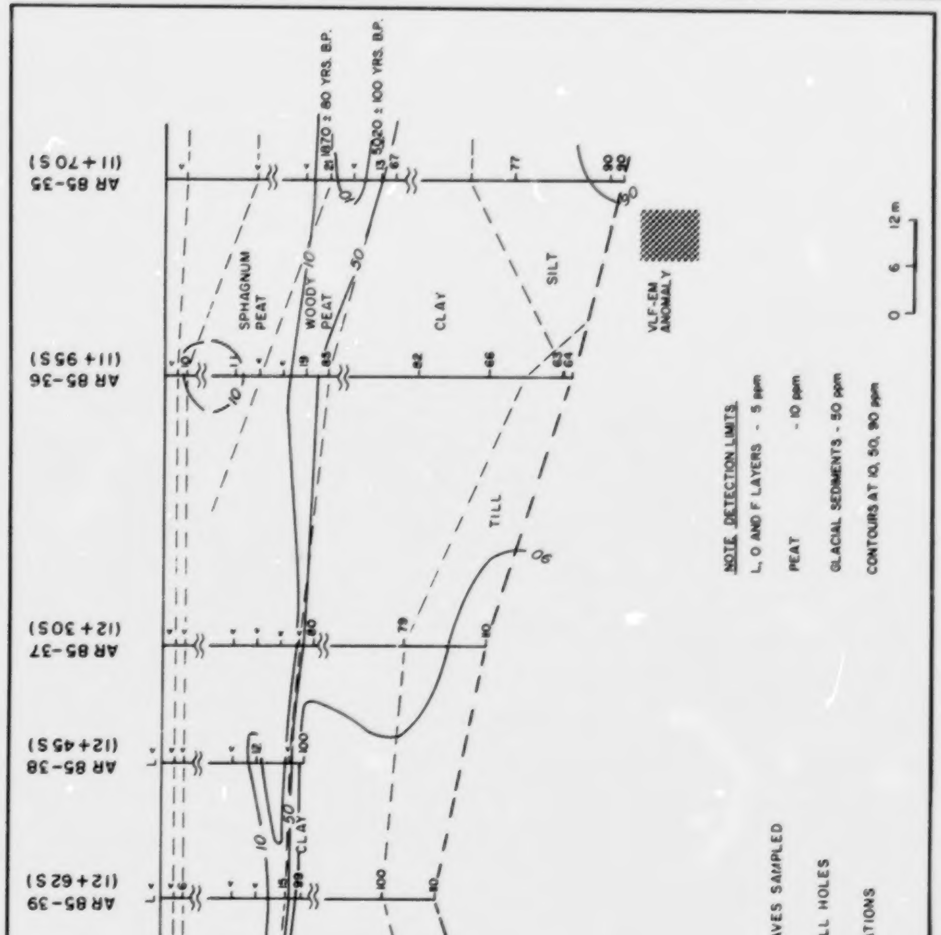
AR 85-42 (13+18 S)
AR 85-41 (13+93 S)
AR 85-40 (12+77 S)
AR 85-39 (12+62 S)
AR 85-38 (12+45 S)
AR 85-37 (12+30 S)
AR 85-36 (11+95 S)
AR 85-35 (11+70 S)
1870 ± 80 YRS. B.P.
5020 ± 100 YRS. B.P.
VERTICAL SCALES
5cm
1 m
2m
O Layer
F Layer
WOODY PEAT
CLAY
CLAY
TILL
BEDROCK
SPHAGNUM PEAT
WOODY PEAT
CLAY
SILT
TILL
VLF-EM ANOMALY
0
6
12 m
NOTE CHANGES IN VERTICAL SCALE
LEGEND
84 CHROMIUM ppm
L LEAVES SAMPLED
‹ LESS THAN DETECTION LIMIT
AR 85-36 DRILL HOLES
1880 ± 60 YRS. B.P. - C14 DATE
(11+95 S) STATIONS
NOTE DETECTION LIMITS
L, O AND F LAYERS - 5 ppm
PEAT - 10 ppm
GLACIAL SEDIMENTS - 50 ppm
CONTOURS AT 10, 50, 90 ppm

Figure 097.12. Chromium on L6+25W profile: Alfie grid.

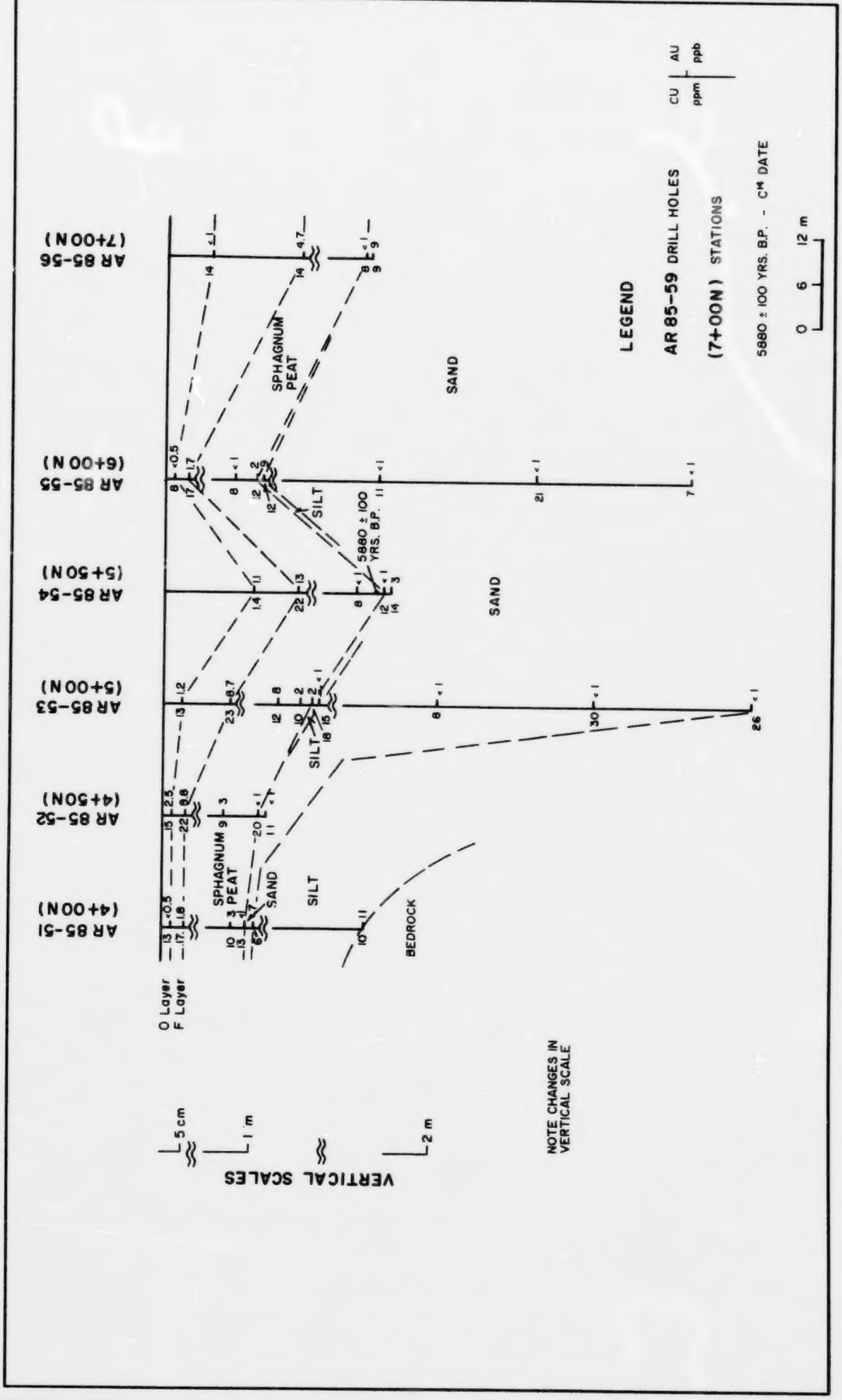
AR 85-51 (4+00N)
AR 85-52 (4+50N)
AR 85-53 (5+00N)
AR 85-54 (5+50N)
AR 85-55 (6+00N)
AR 85-56 (7+00N)
O Layer
F Layer
SPHAGNUM PEAT
SAND
SILT
BEDROCK
5880 ± 100 YRS. B.P.
VERTICAL SCALES
5 cm
1 m
2 m
NOTE CHANGES IN VERTICAL SCALE
LEGEND
AR 85-59 DRILL HOLES
(7+00N) STATIONS
5880 ± 100 YRS. B.P. - C14 DATE
CU ppm
AU ppb
0
6
12 m

Figure 097.13. Gold and copper on L28W profile: Lahaie grid.

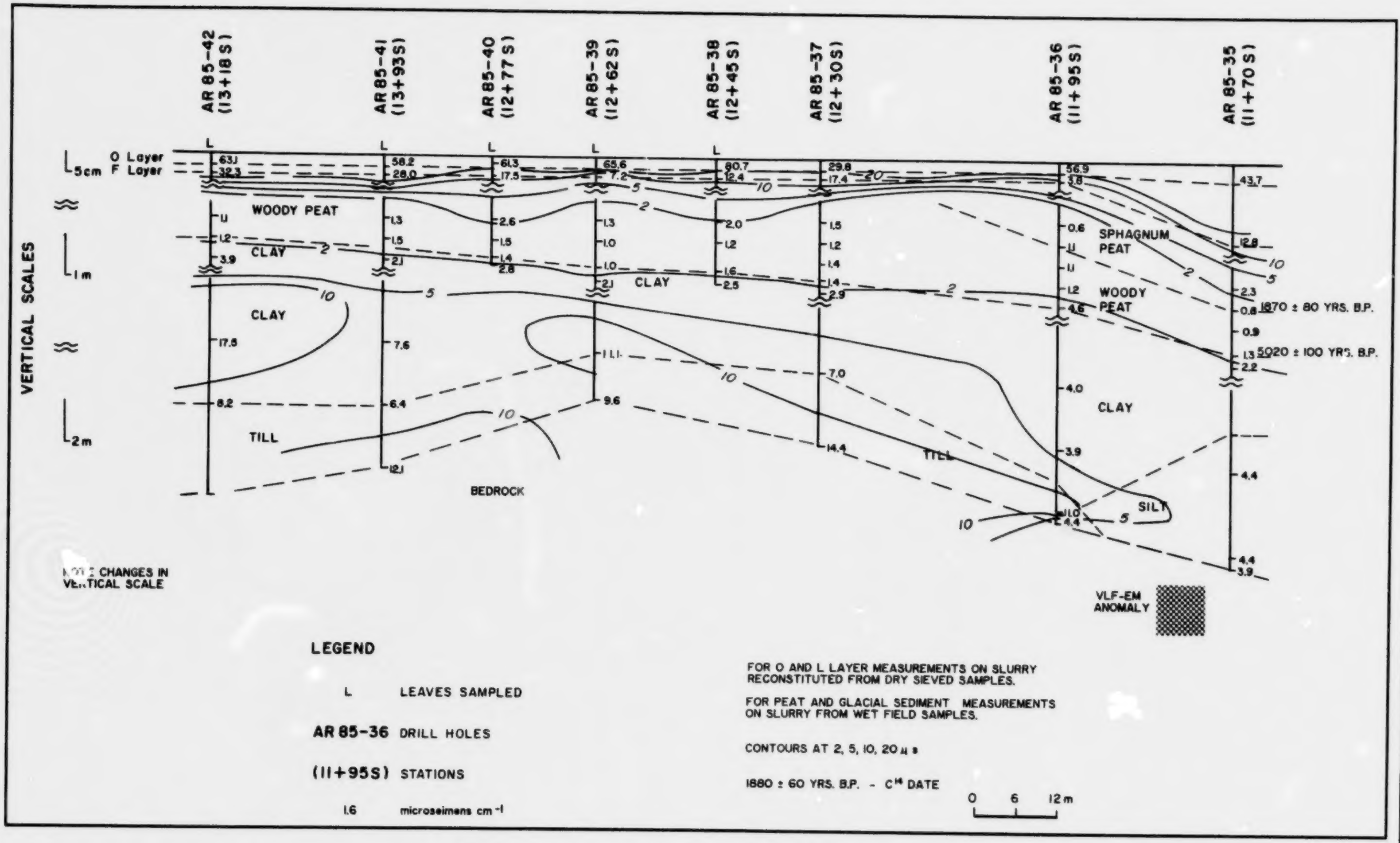
VERTICAL SCALES
5cm
1m
2m
O Layer
F Layer
NOTE CHANGES IN VERTICAL SCALE
AR 85-42 (13+18S)
AR 85-41 (13+93S)
AR 85-40 (12+77S)
AR 85-39 (12+62S)
AR 85-38 (12+45S)
AR 85-37 (12+30S)
AR 85-36 (11+95S)
AR 85-35 (11+70S)
L
WOODY PEAT
CLAY
TILL
BEDROCK
SPHAGNUM PEAT
WOODY PEAT
SILT
1870 ± 80 YRS. B.P.
5020 ± 100 YRS. B.P.
2
5
10
20
63.1
32.3
1.1
1.2
3.9
17.5
8.2
58.2
28.0
1.3
1.5
2.1
7.6
6.4
12.1
61.3
17.5
2.6
1.5
1.4
2.8
65.6
7.2
1.3
1.0
1.0
2.1
11.1
9.6
80.7
12.4
2.0
1.2
1.6
2.5
29.8
17.4
1.5
1.2
1.4
1.4
2.9
7.0
14.4
56.9
3.8
0.6
1.1
1.1
1.2
4.6
4.0
3.9
11.0
4.4
43.7
12.8
2.3
0.8
0.9
1.3
2.2
4.4
4.4
3.9
VLF-EM ANOMALY
LEGEND
L LEAVES SAMPLED
AR 85-36 DRILL HOLES
(11+95S) STATIONS
1.6 microseimens cm⁻¹
FOR O AND L LAYER MEASUREMENTS ON SLURRY RECONSTITUTED FROM DRY SIEVED SAMPLES.
FOR PEAT AND GLACIAL SEDIMENT MEASUREMENTS ON SLURRY FROM WET FIELD SAMPLES.
CONTOURS AT 2, 5, 10, 20 μs
1880 ± 60 YRS. B.P. - C¹⁴ DATE
0 6 12m

Figure 097.14. Conductivity on L6+25W profile: Alfie grid.

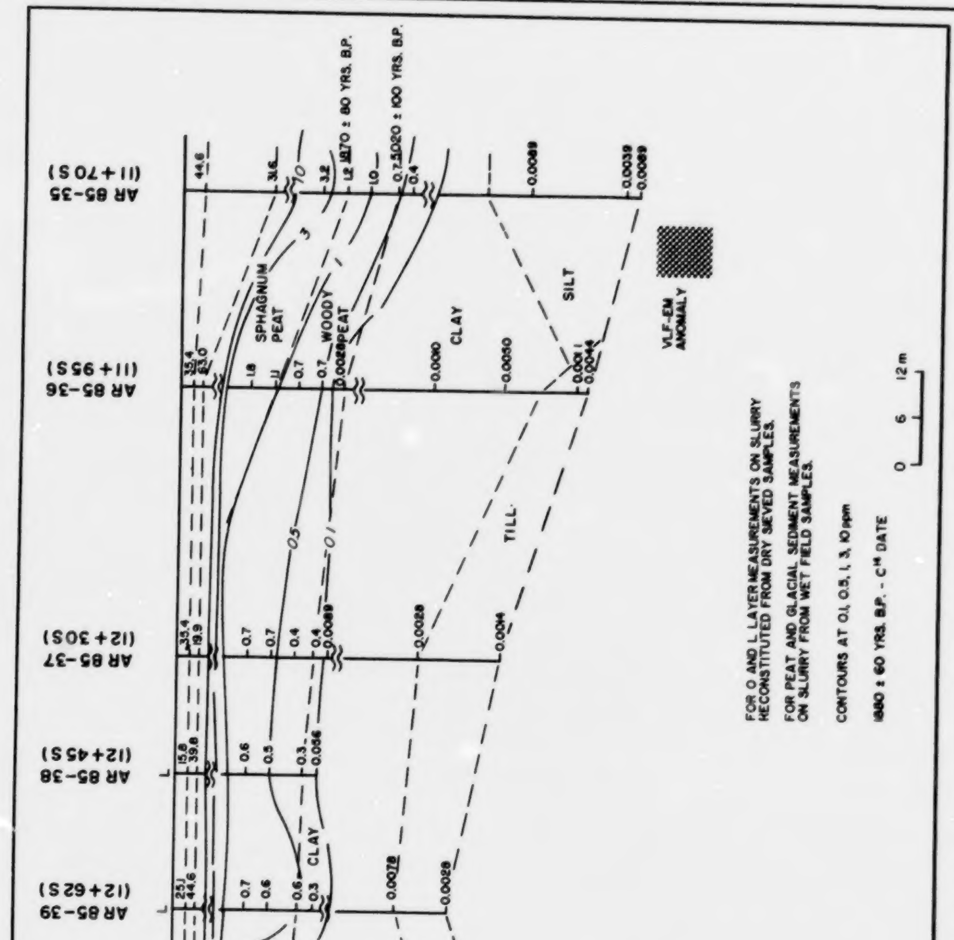
VERTICAL SCALES
5cm
1m
2m
NOTE CHANGES IN VERTICAL SCALE
O Layer
F Layer
AR 85-42 (13+18S)
AR 85-41 (13+93S)
AR 85-40 (12+77S)
AR 85-39 (12+62S)
AR 85-38 (12+45S)
AR 85-37 (12+30S)
AR 85-36 (11+95S)
AR 85-35 (11+70S)
WOODY PEAT
CLAY
TILL
BEDROCK
SPHAGNUM PEAT
WOODY PEAT
SILT
1870 ± 80 YRS. B.P.
2020 ± 100 YRS. B.P.
VLF-EM ANOMALY
LEGEND
L LEAVES SAMPLED
AR 85-36 DRILL HOLES
(11+95S) STATIONS
1.8 ppm
FOR O AND L LAYER MEASUREMENTS ON SLURRY RECONSTITUTED FROM DRY SIEVED SAMPLES.
FOR PEAT AND GLACIAL SEDIMENT MEASUREMENTS ON SLURRY FROM WET FIELD SAMPLES.
CONTOURS AT 0.1, 0.5, 1, 3, 10 ppm
1880 ± 60 YRS. B.P. - C14 DATE
0 6 12 m

Figure 097.15. Hydrogen ion concentration on L6+25W profile: Alfie grid.

CONCLUSIONS AND RECOMMENDATIONS

1. Zones of anomalous gold and other elements are present in the Alfie and Lahaie bogs that appear related to sources in the underlying bedrock or till.

2. Changes in the value and position of anomalies appear related to changes in climatic conditions and water table fluctuations prior to and during sampling.

3. Various trace elements, including gold, are frequently concentrated in the F–layer, the peat–clay interface and the till–bedrock interface; all being zones of change in physical, biological and electrogeochemical conditions. These horizons are favoured for sampling in thick overburden and peat environments.

4. Gold and other elements probably are dispersed upwards from bedrock or till surfaces by electrogeochemical means (cf. Bolviken and Logn 1975, Govett 1975, 1976, Smee, 1983), as is suggested by the horizontal and vertical distribution of conductivity, and hydrogen ion values.

5. Further research toward determining the source and means of dispersion of metals in peat and thick overburden environments is recommended. This will require sampling of closely spaced holes (Thomas et al. in prep.). Frequent sampling of water, vegetation and peat for gold and other element analyses, monitoring of the water table and climatic observations over a multi–year time span is required to determine the cause of changing metal values in organic materials.

6. Bogs sampling on a regional basis is warranted as an exploration tool. Also, near–surface sampling of bogs and humus by the government around mining centres is warranted to determine patterns of airborne metal contamination.

7. Infra–red reflectance surveys over the Alfie and Lahaie bogs should be completed to determine the applicability of this technique in detecting abnormal amounts of metals in the bogs.

ACKNOWLEDGMENTS

This project was funded by an Exploration Technology Development Fund Grant through the Ontario Geological Survey. The geochemical analyses were provided courtesy of Bondar–Clegg and Co. Ltd. Technical assistance was given by various scientists, including Rick Devlin, hydrogeochemist, Water and Earth Science Associates, Ltd., Carp; D. Katz, plant taxonomist, Biology Department, University of Ottawa; Chris Pegg, Exploration Manager, Lac Minerals Ltd., Kirkland Lake; Roch Cormier, President, R. Cormier and Associates Ltd., Becancour, Quebec; Tim Gleeson, Biology Department, University of Ottawa; Bob Mott, palynologist, Terrain Sciences Division, Geological Survey of Canada; Rob Larson, Haileybury School of Mines; Dr. Charles Tarnocai, soil scientist, Canada Soil Survey, Agriculture Canada.

REFERENCES

Aripova, Kh., and Talipov, R.M.

1966: Osobennosti kontsentratsii zolota v pochvakh i resteniyakh yuzhnoy chasti Tamdynskikh gor; (Concentration of gold in soils and plants in the southern part of the Tamdyn Mountains); Uzb. Geol. Zh., 1966, vol.3, p.45–51 (in Russian).

Bolviken, B. and Gleeson, C.F.

1979: Focus on the use of soils for geochemical exploration in glaciated terrane; p.295–326 *in* P.J. Hood (editor), Geophysics and Geochemistry in the Search for Metallic Ores, Geological Survey of Canada, Economic Geology Report 31.

Bolviken, B., and Logn, O.

1975: An electrogeochemical model for element distribution around sulphide bodies; p.631–648 *in* Elliott, I.L. and Fletcher, W.K. (editors) Geochemical Exploration 1974, Elsevier, Amsterdam.

Boyle, R.W.

1977: Cuperiferous bogs in the Sackville area, New Brunswick, Canada; Journal of Geochemical Exploration, vol. 8, p.495–527.

Boyle, R.W., and Cragg, C.B.

1957: Soil analyses as a method of geochemical prospecting in Keno Hill - Galena Hill Area, Yukon Territory; Geological Survey of Canada, Bulletin 39.

Borovitskii, V.P.

1976: The application of bog–sampling in prospecting for ore deposits in perennial frost regions; Journal of Geochemical Exploration, vol. 5, p.67–70.

Bradshaw, P.M.D.

1975: Valley copper deposit, British Columbia; p.100–101 *in* Conceptual models in exploration geochemistry. P.M.D. Bradshaw (editor), Journal of Geochemical Exploration, vol.4.

Cannon, H.L.

1955: Geochemical relations of zinc bearing peat to the Lockport Dolomite, Orleans Co., N.Y.; United States Geological Survey, Bulletin 1000D, p.119–185.

Damman, A.W.H.

1978: Distribution and movement of elements in ombrotrophic peat bogs; Oikos, Copenhagen, vol.30, p.480–495.

DiLabio, R.N.W., and Coker, W.B.

1982: Geochemistry of peat associated with uraniferous bedrock at Kasmere Lake Area, Manitoba; p.179-194 *in* P.H. Davenport (editor), Prospecting in Areas of Glaciated Terrain, Canadian Institute of Mining and Metallurgy.

Dissanayake, C.B., and Kritsotakis, K.

1984: The geochemistry of Au and Pt in peat and algae mats - a case study from Sri Lanka; Chemical Geology, vol.42, p.61-76.

Dunn, C.E.

1984: Biogeochemical methods and surveys, Southern La Ronge Belt; p.95-103 *in* Summary of Investigations, 1984, Saskatchewan Geological Survey, Miscellaneous Report 84-4.

1985: Biogeochemical Exploration for gold in the La Ronge Belt, 1985, Sask; p.31-49 *in* Summary of Investigations, 1985, Saskatchewan Geological Survey, Miscellaneous Report 85-4.

Eckel, E.B.

1949: Geology of ore deposits of the La Plata District, Colorado; United States Geological Survey, Professional Paper, 219, 55p.

Ermengen, S.V.

1957: A report on glacial geology and geochemical dispersion in the Chibougamau Area, Quebec; Quebec Ministry of Energy and Resources, DP26.

Forrester, J.D.

1942: A native copper deposit near Jefferson City, Montana; Economic Geology, vol.37, p.126-135.

Fortescue, J.A.C.

1975: Dorset area, Ontario; p.159-162 *in* Conceptual models in exploration geochemistry. P.M.D. Bradshaw (editor), Journal of Geochemical Exploration, vol.4, p.159-162.

Fortescue, J.A.C., and Hornbrook, E.H.W.

1967: Progress report on biogeochemical research at the Geological Survey of Canada 1963-1966; Geological Survey of Canada, Paper 67-23, Part I, 143p.

1969: Progress report on biogeochemical research at the Geological Survey of Canada 1963-1966; Geological Survey of Canada, Paper 67-23, Part II, 101p.

Gleeson, C.F.

1960: Studies on the distribution of metals in bogs and glaciolacustrine deposits; PhD Thesis, McGill University, Montreal, Quebec, 221p.

Gleeson, C.F., and Coope. J.A.

1967: Some observation on the distribution of metals in swamps in Eastern Canada; Geological Survey of Canada, Paper 66-54, p.145-165.

Gleeson, C.F., and Rampton, V.N.

1983a: A report on the surficial geology, bedrock geology and gold geochemistry of humus, till and bedrock, Alfie Claim Group, Morrisette and Arnold Townships, Ontario; Unpublished report, Assessment Files Research Office, Ontario Geological Survey, Toronto.

1983b: A report on the surficial geology, bedrock geology and gold geochemistry of humus, till and bedrock, Lahaie Claim Group, Morrisette Township, Ontario; Unpublished report, Assessment Files Research Office, Ontario Geological Survey, Toronto.

Govett, G.J.S.

1975: Soil conductivities: assessment of an electrogeochemical exploration technique; p.101-118 *in* I.L. Elliot and W.K. Fletcher (editors), Geochemical Exploration 1974, Elsevier, Amsterdam.

1976: Detection of deeply buried and blind sulphide deposits by measurement of H+ and conductivity of closely spaced surface soil samples; Journal of Geochemical Exploraton, vol.6, p.359-382.

Gunton, J.E., and Nichol, I.

1974: The delineation and interpretation of metal dispersion patterns related to mineralization in the Whipsaw Creek area, near Princeton, B.C.; Canadian Institute of Mining and Metallurgy, Bulletin, vol.67, p.66-74.

Hawkes, H.E., and Salmon, M.L.

1960: Trace elements in organic soil as a guide to copper ore; 21st International Geological Congress, Norden, Part 2, p.38-43.

Hornsnail, R.F.,

1975: Highmont Cu-Mo deposits, British Columbia; p.67-72 *in* Conceptual models in exploration geochemistry, P.M.D. Bradshaw (editor), Journal of Geochemical Exploration, vol.4, p.67-72.

Hornsnail, R.F., and Elliott, I.L.

1971: Some environmental influences on the secondary dispersion of molybdenum and copper in western Canada; p.166-175 *in* Geochemical Exploration. R.W. Boyle and J.I. McGerrigle (editors), Canadian Institute of Mining and Metallurgy, Special Volume 11.

Kokkola, M.

1977: Application of humus to exploration; p.104-110 *in* Prospecting in Areas of Glaciated Terrain, 1977. Institute of Mining and Metallurgy, London.

Kovalevskii, A.L.

1978: Biogeochemical Exploration for Mineral Deposits; Translated from Russian and published for the United States Department of the Interior and the National Science Foundation, Washington, D.C., by Amerind Publishing Co., New Delhi, 136p.

Lett, R.E.W., and Fletcher, W.K.

1979: The secondary dispersion of transition metals through a copper-rich hillslope bog in the Cascade Mountains, B.C.; p.103-115 *in* J.R. Watterson and P.K. Theobold (editors), Geochemical Exploration 1978, Proceeding of the Seventh International Geochemical Exploration, Symposium.

Lovering, T.S.

1927: Organic precipitation of metallic copper; United States Geological Survey, Bulletin 795-C, p.45-52.

Nuutilainen, J., and Peuraniemi, V.

1977: Application of humus analysis to geochemical prospecting: some case histories; p.1-5 *in* Prospecting in Areas of Glaciated Terrain 1977, Institute of Mining and Metallurgy, London.

Percy, F.W.

1875: Cuperiferous peat; p.211 *in* Metallurgy, John Murray, London.

Routledge, R.E., Thompson, I.S., and Dixon, J.A.

1981: Deep overburden drilling and geochemical sampling in Benoit, Melba, Bisley, Maisonville, Morrisette, Arnold, Grenfell, Lebel, Eby, Otto, Boston and McElroy Townships; Ontario Geological Survey, Open File Report 5356.

Salmi, M.

1950: On trace elements in peat; Geologinen Tutkimuslaitos Geoteknillisia Julkaisuja, No. 51, 20p.

1955: Prospecting for bog covered ore by means of peat investigations; Bull. de la Comm. Geol. de Finlande, No. 169, 34p.

1956: Peat and bog plants as indicators of ore minerals in Vihanti Ore Field in Western Finland; Bull. de la Comm. Geol. de Finlande No. 175, 22p.

1958: On pH values of peat as affected by the underlying bedrock (English Summary); Eripainos Geologisen Tutkimuslaitoksen Geoteknillisesta Julkaisuja No. 61, p.29-39.

1967: Peat in prospecting: applications in Finland; p.113-126 *in* A. Kralheim (editor), Geochemical Prospecting in Fennoscandia, Interscience, New York, N.Y.

Salminen, R., and Kokkola, M.

1984: Annual variation in metal contents of humus; p.171-177 *in* Prospecting in areas of glaciated terrain, 1984; Institute of Mining and Metallurgy, London.

Schiller, P., Cook, G.B., Kitzinger-Skalova, A., and Wolf, F.

1973: The influence of the season variation for gold determination in plants by neutron activation analysis; Radiochem. Radioanal. Lett., vol.13, p.283-286.

Sillanpaa, M.

1972: Distribution of trace elements in peat profiles; International Peat Congress, Finland, vol.5, p.185-191.

Skvartsev, S.L.

1978: Electrochemical dissolution of sulphide ores; Journal of Geochemical Exploration, vol.5, p.71-72.

Smee, B.W.

1983: Laboratory and field evidence in support of the electrogeochemically enhanced migration of ions through glaciolacustrine sediment; Journal of Geochemical Exploration, vol.19, p.277-304.

Thomas, R.D., Gleeson, C.F., Rampton, V.N., Paradis S., Corden, S.G.

in preparation: Grant 97 - Gold in peat and its relevance to mineral exploration; Ontario Geological Survey, Open File Report.

Townsend, J.

1824: Geological and mineralogical researches during a period of more than fifty years in England, Scotland, Ireland, Switzerland, Holland, France, Flanders and Spain; Printed by Gye and Son, Bath.

Walker, A.J.,

1985: Report on magnetic and VLF-EM surveys, Grid 47, Morrisette and Arnold Townships; Unpublished report, Assessment Files Research Office, Ontario Geological Survey, Toronto.

Webb, J.S.

1958: Notes on geochemical prospecting for lead-zinc deposits in the British Isles; p.23-40 *in* Technical aids to exploration, Symposium of Non-ferrous Mining in Great Britain and Ireland, Paper 19, Institute of Mining and Metallurgy, London.

Webb, J.S., Tooms, J.S., and Gilbert, M.A.

1959: Geochemical drainage reconnaissance for copper in Northern Rhodesia; Institute of Mining and Metallurgy, Transactions, vol. 68, p.125-144.

Grant 105 — Processing of Airborne Imagery for Geobotanical Stress Associated with Subsurface Mineralization

J.R. Miller[1], **D.R. Sturgeon**[2], **N.T. O'Neill**[2] **and R.A.H. Buxton**[2]

[1]Centre for Research in Experimental Space Science, York University, Downsview, Ontario

[2]Moniteq Ltd., Concord, Ontario

ABSTRACT

Past and present research has shown that the measurement of the spectrum of vegetation in the vicinity of the chlorophyll reflectance edge is a promising technique for assessing mineral induced stress on vegetation and indirectly determining the metal content of the soil. Work has been done to create a model which relates the spectral features to the stress levels and to incorporate this model into a processing/display package which operates on multispectral airborne imagery data. The output product of the processing software is an image of colour coded stress parameters derived from a parametric fit to the red shoulder reflectance data. To date the software has been applied to MEIS (Multi Element Imaging Sensor) data and FLI (Fluorescence Line Imager) data. Some discussion of results for the MEIS sensor is presented.

INTRODUCTION

Field geobotanical/geochemical studies dating back to the early 1950s (summarized in, e.g., Brooks 1972, Canney 1980, and in Canada by Wolfe 1976, Gleeson and Coope 1967 and Fortescue and Hornbrooke 1966) have established that heavy metal uptake can occur in vegetation overlying mineralized zones.

In the extreme case, the mineral concentration can reach toxic levels for the particular overlying vegetation species, causing chlorosis or substitution by a more metal tolerant species. The more usual case is less dramatic however, and the presence of the metal in the vegetation simply causes stress which can be manifested in sometimes subtle changes in the canopy characteristics. Thus the potential of vegetation to serve as indicators of subsurface mineral anomalies has been recognized for some time: the challenge has been, and remains, to find appropriate vegetation parameters which delineate stress and a method to rapidly recognize these vegetation changes. Once such a technique has been successfully proven, it must be implemented in a operational manner to permit economic recovery of its benefits.

Vegetation spectral reflectance has now been convincingly shown by field measurements to be one such parameter (e.g. Yost and Wenderworth (1971), Press (1974) and Labovtiz et al. (1983). Field data indicate that vegetation growing on soils with anomalous metal concentrations typically exhibit reflectance variations in the 0.7 – 1.0 μm infrared spectral region when compared to spectra from "background" vegetation.

GEOBOTANICAL REMOTE SENSING USING AIRBORNE IMAGERS

Until recently, remotely–sensed data collected from aircraft has received little attention as a potential method of geobotanical data acquisition. A review of the literature shows that previous attempts to use remote sensing to map geobotanical anomalies have concentrated on either a regional or grand scale using LANDSAT imagery (e.g. Bolviken et al. 1977, Press 1974, Singhroy et al. 1980). However, the high spectral and spatial resolution of new airborne sensors has generated a new enthusiasm for the feasibility of using remote sensing to map anomalies in spectral reflectance.

The airborne spectrometer measurements of Collins et al. (1978, 1983) have demonstrated the potential of high spectral resolution data for biogeophysical mineral exploration. MEIS II, a pushbroom scanner developed by Macdonald Detwiler & Associates for the Canada Centre for Remote Sensing (CCRS) has recently been reconfigured with narrow band filters for geobotanical applications (Till et al. 1984) and has been used to collect an impressive amount of high spectral and spatial data. The Fluorescence Line Imager (FLI) developed by Moniteq Ltd for the Department of Fisheries and Oceans has been used in an imaging spectrometry mode to produce continuous spectra over geobotanically stressed regions. The potential of these new sensors has been further underscored by recent laboratory studies of metal–induced plant stress by Horler et al. (1980) and Chang and Collins (1983).

OBJECTIVES OF WORK

The primary objective of the work reviewed in this report was to complete and implement an interpretation algorithm for previously–collected MEIS II imagery in order to derive images of vegetation stress. Since a large database of unprocessed MEIS data was currently in existence a processing bottleneck would be relieved by offering an industrial–based service for geobotanical processing. The developed algorithm was subsequently generalized to process Fluorescence Line Imager Data as well. To provide an evaluation of this software a preliminary analysis of MEIS data collected in the Bisset Lake region of Algonquin Park was carried out and is summarized below.

THEORETICAL BACKGROUND FOR GEOBOTANICAL PROCESSING

It is now well documented through field and laboratory studies that one of the ways in which vegetation stress can be manifested is as changes in its spectral reflectance. Changes may occur (1) in the magnitude of the green reflectance at 550 nm, (2) in the magnitude of the 680 nm reflectance at the chlorophyll absorption maximum, (3) in the position or the shape of the red reflectance edge from 680 to 800 nm and/or (4) changes in the magnitude of the infrared reflectance shoulder at wavelengths greater than 780 nm. Potentially any or all of these changes can serve as indicators of stress which can be mapped using remote sensing. The most serious complicating factors are that (1) changes in these parameters may also be a result of changes in vegetation species and/or canopy density and (2) airborne sensors measure spectral radiance rather than reflectance so that analysis must also account for changes in incident solar spectral irradiance. It is clear, therefore, that a quantitative approach to interpretation of imagery is imperative in order to provide results that can be understood on a physical basis. For example changes in percent reflectance at a given wavelength and the magnitude of the spectral shift in the red edge are stress parameters that have scientific basis, and which can be generated on a pixel by pixel basis to produce images. These images can then be used to gain a deeper understanding of the relationship of spectral reflectance changes to changes in forest parameters.

The red reflectance edge position has received increasing attention by researchers for its potential to monitor stress. Examination of the vegetation reflectance in the red edge spectral region offers abundant information regarding the spectral properties of the canopy. Hare et al. (1984) and Miller et al. (1985) of York University have introduced an inverted Gaussian reflectance model for the red edge which has the form:

$$R(W) = R_s - (R_s - R_0) \exp\left[\frac{-(W - W_0)^2}{2 \cdot S^2}\right]$$

where:

R_0 is the reflectance at the absorption maximum at near 685 nm,

R_s is the reflectance at the reflectance shoulder at wavelengths greater than about 780 nm, and

S is the Gaussian deviation parameter which determines the red edge slope.

Quantitative analysis of the imagery with this model produces three parameters that can be expected to be useful indicators of stress: the red edge shoulder height, $(R_s - R_0)$, the calculated reflectance minimum wavelength, W_0, and the calculated red edge inflection point, W_P (also used to define the position of the red edge).

SOFTWARE FOR GEOBOTANICAL IMAGE PROCESSING

The image processing system at Moniteq Ltd. comprises a VAX 11/750 processor, an ADAGE image display system and the EASI/PACE software package developed by Perceptron Computing Inc. which facilitates interfacing between I/O devices and the specialized geobotanical processing software written at Moniteq Ltd. Our goal for this software package was to provide the capability for analysis of multispectral imagery from both the MEIS and FLI sensors with basically the same analysis procedure. This would enable users to take advantage of the special features of each of these sensors with a common approach to the quantitative analysis of the imagery.

Because the development of a processing methodology for MEIS imagery was the primary objective of this project the discussion of software details will be restricted to the MEIS sensor. The analysis and evaluation of MEIS imagery for geobotanical applications has been hampered by instrumentation problems and the blue–shift feature of the flat interference filters used in narrow

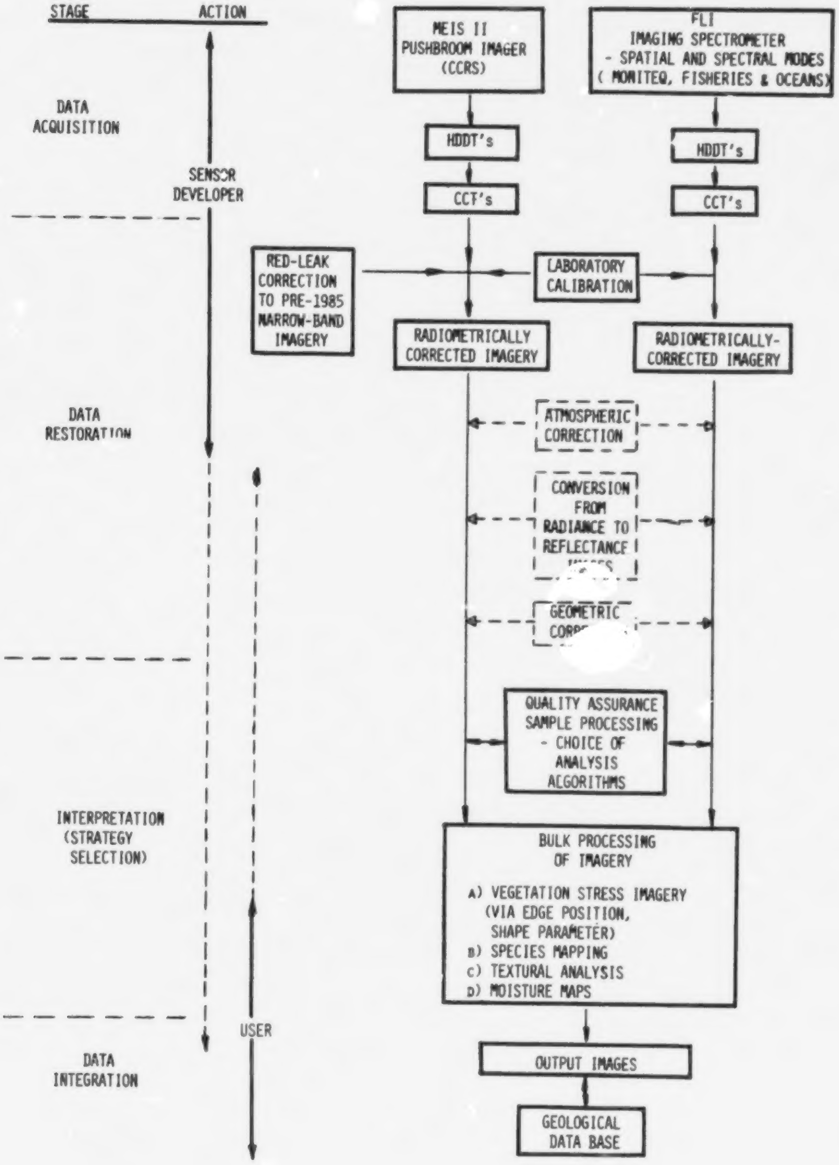
STAGE
ACTION
DATA ACQUISITION
SENSOR DEVELOPER
DATA RESTORATION
INTERPRETATION (STRATEGY SELECTION)
DATA INTEGRATION
USER
MEIS II PUSHBROOM IMAGER (CCRS)
FLI IMAGING SPECTROMETER - SPATIAL AND SPECTRAL MODES (MONITEQ, FISHERIES & OCEANS)
HDDT's
CCT's
HDDT's
CCT's
RED-LEAK CORRECTION TO PRE-1985 NARROW-BAND IMAGERY
LABORATORY CALIBRATION
RADIOMETRICALLY CORRECTED IMAGERY
RADIOMETRICALLY-CORRECTED IMAGERY
ATMOSPHERIC CORRECTION
CONVERSION FROM RADIANCE TO REFLECTANCE
GEOMETRIC
QUALITY ASSURANCE SAMPLE PROCESSING - CHOICE OF ANALYSIS ALGORITHMS
BULK PROCESSING OF IMAGERY
A) VEGETATION STRESS IMAGERY (VIA EDGE POSITION, SHAPE PARAMETER)
B) SPECIES MAPPING
C) TEXTURAL ANALYSIS
D) MOISTURE MAPS
OUTPUT IMAGES
GEOLOGICAL DATA BASE

Figure 105.1. Methodology for geobotanical remote sensing.

band applications of the MEIS sensor. The radiometric corrections of the pre–1984 (5 channel) narrow–band MEIS data and the subsequent 8 channel flat filter data (pre–1986) is a non trivial problem. The latter data set suffered from the passband blue–shift problem (until a recent curved filter redesign was implemented) while the former was affected by a filter (red) leak problem in addition to the interference filter passband shifts. The passband blue–shift problem is angle dependent and hence the wavelength associated with each pixel differs slightly from that of its neighbours. The computation of the pixel dependent wavelengths (which must also account for aircraft roll for roll–corrected data) was performed by CCRS (R.P. Gauthier, Canada Centre for Remote Sensing, Limebank Road, Ottawa, personal communication, 1986) who supplied the wavelength data in the same format as the imagery data (alternate lines in LGSOWG tape format). This allowed ex-

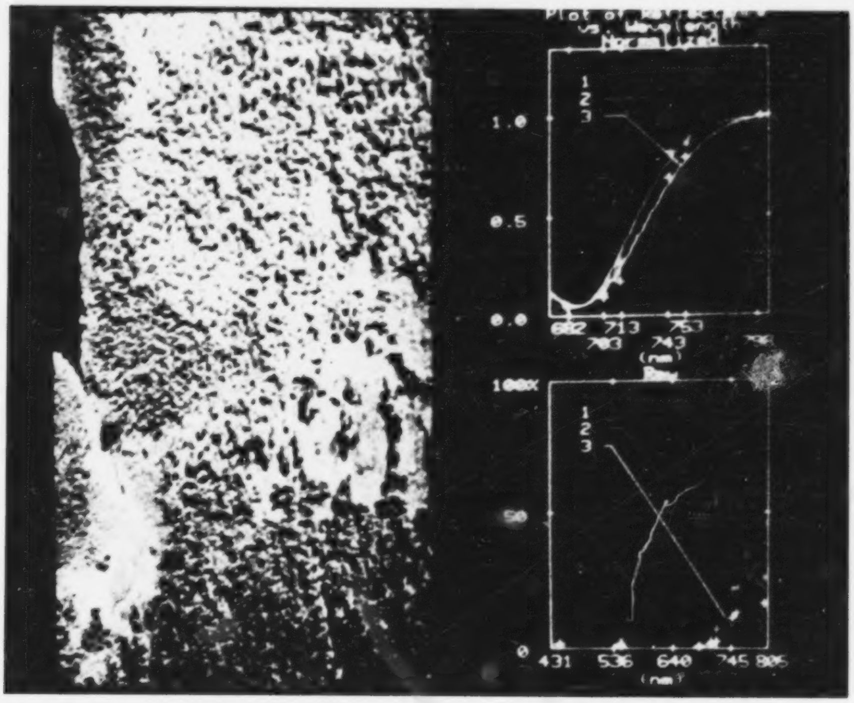

Figure 105.2.
This photo illustrates the analysis stage in the geobotanical processing. The insensitivity of the model to gross change in canopy illumination is demonstrated.

isting Moniteq Ltd. software to be used to download MEIS imagery which CCRS had also radiometrically corrected and converted to reflectances by dividing by extraterrestrial irradiances. These data were incorporated on a pixel by pixel basis into the geobotanical processing algorithms. The analysis procedure, starting with the collection of airborne data and ending with production of hardcopy images, is shown schematically in Figure 1.

The software development was guided by the principle that the end user of the data should be permitted to alter and guide the choices in the analysis at as early a stage as possible; accordingly, the processing of the imagery has been subdivided into two functional tasks. The first interactive task was designed to allow the user to display the imagery and select spatial windows of interest for localized interpretation. For each window selected (where a window may be as small as a single pixel) the reflectance spectrum is plotted to the right of the image. The best fit inverted Gaussian model curve is then superimposed on the data to allow a visual assessment of the quality of the model fit. At the same time, the analyst is provided with terminal output of quantitative data: the quality of the fit and the various parameters extracted from the Gaussian model. The analysis step is illustrated in Figures 105. 2 and 3. This sampling/analysis approach has proven very useful in assessing the digital image data in terms of the nature and origin of observed spectral anomalies. Once the analyst has developed an understanding of the gross spectral/spatial features in the digital imagery the second, computationally–intensive task of pixel–by–pixel processing of the entire image is initiated. The computed stress parameters (Gaussian model parameters) are stored in a database file which can be subsequently displayed and enhanced using standard image display functions. A sample image of W_0 is shown in Figure 105.4.

PRELIMINARY PROCESSING RESULTS FROM THE ALGONQUIN PARK SITE

As a means of evaluation of the effectiveness of this geobotanical processing software and the inverted Gaussian red edge reflectance model upon which it is based, a preliminary analysis was performed on 8 channel MEIS imagery collected over a rare earth geochemical anomaly in Algonquin Park as part of a joint experiment between the Geological Survey of Canada and York University. Rentz et al. (1986) give details of the site, its geochemistry and the results of preliminary analysis of

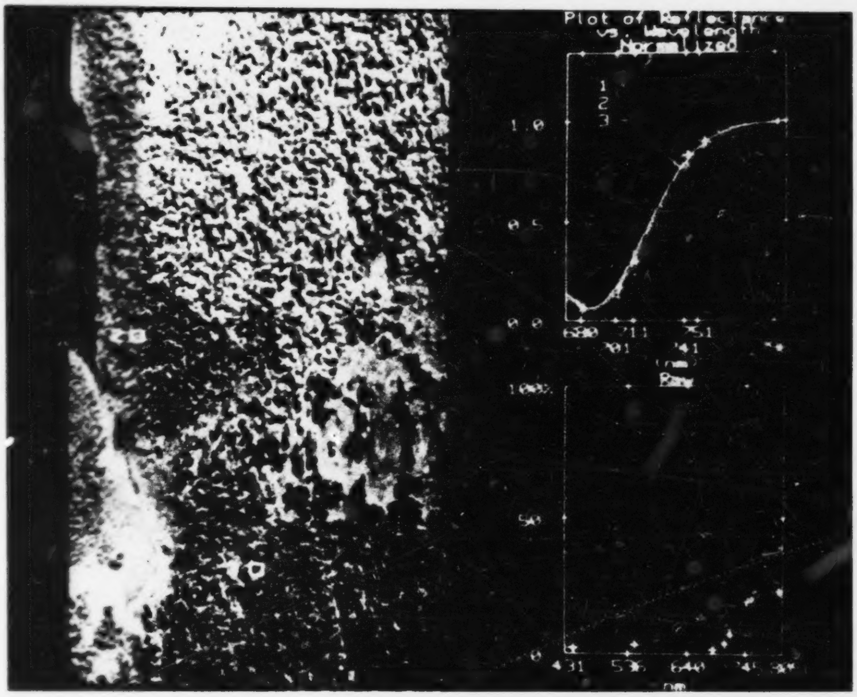
Plot of Reflectance
vs. Wavelength
Normalized
1
2
3
1.0
0.5
0.0
680
711
751
701
741
nm
Raw
100%
50
0
431
536
640
nm

Figure 105.3. This photo illustrates the analysis stage in the geobotanical processing. The variability due to species type is demonstrated. The species shown are: 1. Maple, 2. Cedar, 3. Birch.

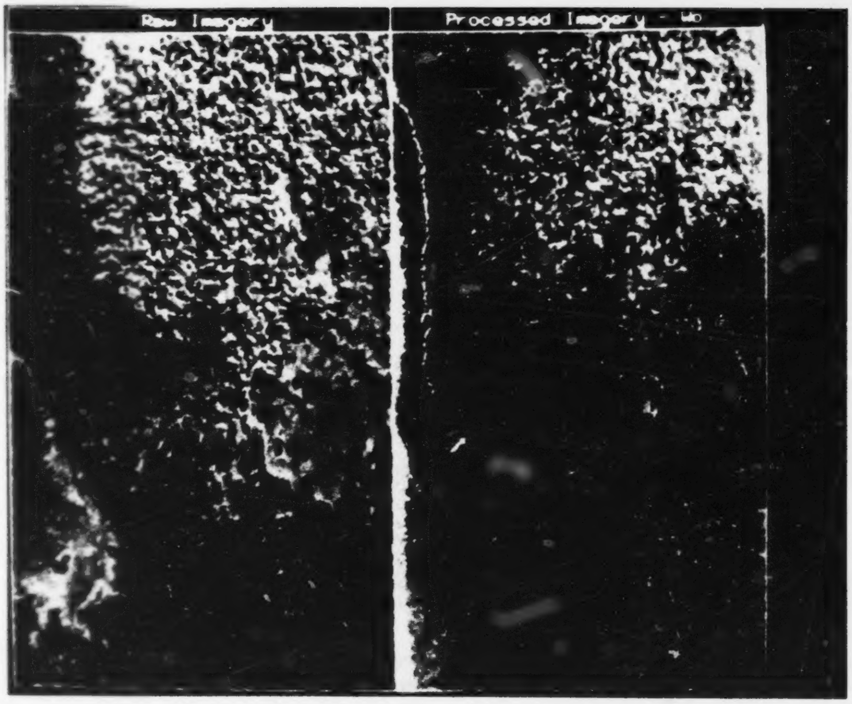
Raw Imagery
Processed Imagery

Figure 105.4. This photo illustrates the processing stage in the geobotanical processing. Note the variation from light to dark (blue shifted) in the Cedar and Birch areas.

MEIS imagery using the inverted Gaussian red edge model.

An investigation of the MEIS digital imagery from this site using the geobotanical analysis software described above yielded some interesting results. First, the interactive processing task showed the inverted Gaussian model to be an effective model with which to describe the measured "reflectances" in the spectral region of the vegetation red reflectance edge; average reflectance differences between the data and the model were typically less than 1% for a given spectrum. Thus the model parameters provide an effective quantitative measure of the vegetation reflectance properties in the red edge spectral region. Second, as expected from calculations (Miller et al. 1985), the red edge model parameters show little dependence on the illumination variability which accompanies the canopy morphology (Figure 105.2). In the analysis of spectra of adjacent pixels which scan across the canopy of a single tree (0.83 m spatial resolution) the model shape parameters showed very little variation, even in the presence of illumination changes of a factor of two. The images of the model parameters W_0, W_P and S tend, therefore, to be rather featureless except for changes associated with spectral reflectance variations. This will undoubtedly add to the utility of the analysis results. Third, observed systematic variations in the red edge parameters W_0, W_P and R_s were noted to be associated with changes of dominant forest species from cedar to maple to birch (Figure 105.3). Thus at the time of data collection of this imagery, species variations proved to be the major cause of changes in the red edge reflectances.

CONCLUSION

This project has resulted in the development of a geobotanical image processing package for the analysis of narrow band multispectral imagery in the 650 to 800 nm spectral region for the MEIS II and FLI sensors. The analysis is based on the inverted Gaussian model for the vegetation red edge reflectance. Evaluation of the model and the processing methodology with 8 channel MEIS imagery collected over Algonquin Park in August 1985 indicates that this analysis methodology represents an operational tool for the provision of images of parameters describing the red edge reflectance: red edge shoulder ($R_s - R_0$), reflectance minimum wavelength W_0, inflection point wavelength W_P and the Gaussian deviation parameter S. Imagery analyzed to date have shown the red edge parameters W_0, W_P and S to be relatively independent of illumination variability caused by canopy morphology, have not shown spectral changes related to metal stress over the rare earth geochemical anomalous site but do show detectable variation with changes in forest species. The latter result needs further investigation to determine its generality and to determine whether species classification should be incorporated into the preprocessing methodology.

FLI imagery collected in August and September, 1985, is also being analyzed using the same approach in order to confirm the applicability of the algorithm to data from different sensors. This analysis will also be used to determine whether changes can be detected over the known geochemically anomalous areas based on the differences in data acquisition dates.

The present geobotanical analysis software package represents a tool with which to do spectral geobotanical analysis rather than a method to directly produce images of vegetation stress. It is envisaged that the development of a truly expert geobotanical analysis system will require a period of detailed quantitative investigation of the significance of the images of vegetation red edge parameters at a number of varied but controlled sites with geologists, botanists and remote sensing specialists serving as analysts. In the meantime we urge general use of this analysis methodology for detecting red edge spectral changes related to metal-induced stress. The quantitative nature of this geobotanical analysis approach will facilitate comparison of findings of different investigators. We feel this will prove invaluable in the evaluation of the potential for spectral geobotany as an exploration tool.

REFERENCES

Bolviken, B. et al.

1977: ***Paper in*** **Journal of Geochemical Exploration, vol.8, p.457–471**

Brooks, R.R.

1972: **Geobotany and Biochemistry in Mineral Exploration, Harper & Row, New York.**

Canney, F.C.

1980: **Vegetation and Geology (Chapt. 12);** ***in*** **Remote Sensing in Geology, edited by B.S. Siegal and A.R. Gillespie, John Wiley, Toronto.**

Chang, S.-H. and Collins, W.

1983: **Confirmation of the Airborne Biogeophysical Mineral Exploration Technique Using Laboratory Methods; Economic Geology, Volume 78, p.723–736.**

Collins, W.E. et al.

1978: ***Abstract in*** **Geological Society of America, Abstracts, vol.9, p.932–933**

Collins, W., Chang, S.-H., Raines, G., Canney, F. and Ashley, R.

1983: Airborne Biogeophysical Mapping of Hidden Mineral Deposits; Economic Geology, Volume 78, p.737-749.

Fortescue, J.A.C. and Hornbrooke, E.H.W.

1966: A Brief Survey of Progress Made in Biogeochemical Prospecting Research at the Geological Survey of Canada 1962-5; Geological Survey of Canada, Paper 66-54, p.111-113.

Gleeson, C.F., and Coope. J.A.

1967: Some observation on the distribution of metals in swamps in Eastern Canada; Geological Survey of Canada, Paper 66-54, p.145-165.

Hare, E.W., Miller, J.R. and Edwards, G.R.

1984: Geobotanical remote sensing of small localized swamps and bogs in northern Ontario; p.671-682 *in* Proceedings of the International Symposium on Remote Sensing, 3rd Thematic Conference: Remote Sensing for Exploration Geology, Colorado Springs, Colo.

Horler, D.N.H., Barber, J. and Barringer, A.R.

1980: Effects of Heavy Metals on the Absorbance and Reflectance Spectra of Plants; International Journal of Remote Sensing, Volume 1, p.121-136.

Labovitz, M.L., Masuoka, E.J., Bell, R., Siegrist, A.W. and Nelson, R.F.

1983: The Application of Remote Sensing to Geobotanical Exploration for Metal Sulfides - Results from the 1980 Field Season at Mineral, Virginia; Economic Geology, Volume 78, p.750-760.

Miller, J.R., Hare, E.W., Neville, R.A., Gauthier, R.P., McColl,W.D. and Till, S.M.

1985: Correlation of metal concentration with anomalies in narrow band multispectral imagery of the vegetation red reflectance edge; p.143-153 *in* Proceedings of the 4th Thematic Conference: Remote Sensing for Exploration Geology, International Symposium on Remote Sensing of the Environment, San Francisco, Calif.

Press, N.P.

1974: Proceedings of the 9th International Symposium on Remote Sensing of the Environment, vol.9, p.2027-2038.

Rentz, A.N., Bonham-Carter, G.F., Miller, J.R. and Hare, E.W.

1986: Preliminary Results from Modelling Vegetation Spectra Derived from MEIS Data, Algonquin Park, Ontario; *in* Proceedings 10th Canadian Symposium on Remote Sensing, Edmonton, Alta.

Singhroy, V., Bruce, W.D. and Stevens, G.R.

1980: Proceedings 6th Canadian Symposium on Remote Sensing, Halifax, N.S.

Till, S.M., Neville, R.A., McColl, W.D., Gauthier, R.P., Miller, J.R. and Hare, E.W.

1984: Application of MEIS II Airborne Pushbroom Scanner to Geobotanical Remote Sensing; International Symposium on Remote Sensing of Environment, Third Thematic Conference, Remote Sensing for Exploration Geology, Colorado Springs, Colorado, April.

Wolfe, W.J.

1976: Geochemical and Biogeochemical Exploration of Molybdenum-Copper Mineralization at Setting Net Lake; Ontario Ministry of Natural Resources, Geoscience Report 156.

Yost, E. and Wenderworth, S.

1971: Proceedings 7th International Symposium on Remote Sensing of Environment, p.269-284

Grant 109 — The PROSPECT I AEM System

A.P. Annan

A-Cubed Inc., Mississauga, Ontario

ABSTRACT

PROSPECT® I is a new towed-bird fixed wing system being developed by A-Cubed Inc. This paper describes the system's design features:

1. An operating frequency band ranges from a few 10's of Hz to over 10 kHz.
2. A 3 component, vector field towed bird, which has been designed for high stability, and position tracking provide the multi component data essential for motion compensation and target geometry discrimination.
3. Automated data handling and anomaly selection form an integral part of the system design.

Owing to the termination of the Exploration Technology Development Fund grant in March, 1986, the project was not completed before fully operational test flying of the system could be conducted.

INTRODUCTION

The A-Cubed Inc. PROSPECT I system has been under development since 1982. The design objective for the EM system was to provide a state-of-the-art, totally digital system with quantified measurements throughout.

PROSPECT is an acronym for Periodically Repeated Output SPECTrum which reflects the nature of the transmitter and signal processing components. The system is designated PROSPECT I to indicate that this is the first embodiment of the fundamental design principles which are used in this new series of EM systems.

The development of a modern EM system requires rationalization of:

1. the physical embodiment of the system,
2. the operational logistics of running the system,
3. the data handling and interpretation of results obtained with the system.

In the case of the PROSPECT I system, the stage of physical embodiment has now been completed. The system has now been constructed. The work planned for this ETDF project was to carry out the initial airborne testing of the system. Unfortunately, the ETDF program terminated before the full test flying could commence. As a result, this report provides only a brief description of the system.

SYSTEM DESIGN PRINCIPLES

The primary objective of the PROSPECT system design has been to assemble a precision geophysical tool which reproduces the ground response with fidelity. In the area of physical embodiment which encompasses the instrumentation and physical construction of the system, the basic design principles were modularity, flexibility and fidelity. For the operational aspect of the system, the costs of assembly and operation, the reliability, and the minimization of operator intervention were at the fore. For the geophysical aspect of the system, which encompasses data reduction and interpretation, the objectives were penetration, discrete target discrimination, conductivity mapping and automated data handling.

System Platform Configuration

The fundamental decision in developing an airborne EM system is to select the platform and system configuration. The PROSPECT I system was designed as a fixed-wing, towed-bird (FWTB) system for the following reasons.

1. FWTB systems have the maximum penetration of any system configuration.
2. FWTB systems have a large ground footprint which is extremely useful for regional reconnaissance.
3. Fixed wing platforms have greater range and lower operating costs than rotary wing platforms.
4. FWTB systems have superior target discrimination because of their greater power – bandwidth capability.
5. The state-of-the-art of current FWTB systems is still primitive and there is tremendous room for improvement.

The PROSPECT I system has been mounted on a DC-3 aircraft shown in Figure 109.1. The nose – wing tip – tail suspended vertical axis loop is used for excitation.

Transmitter Design

The PROSPECT I transmitter was designed to output signal with a clean, controlled spectral distribu-

---

® Trademark of A-Cubed Inc.

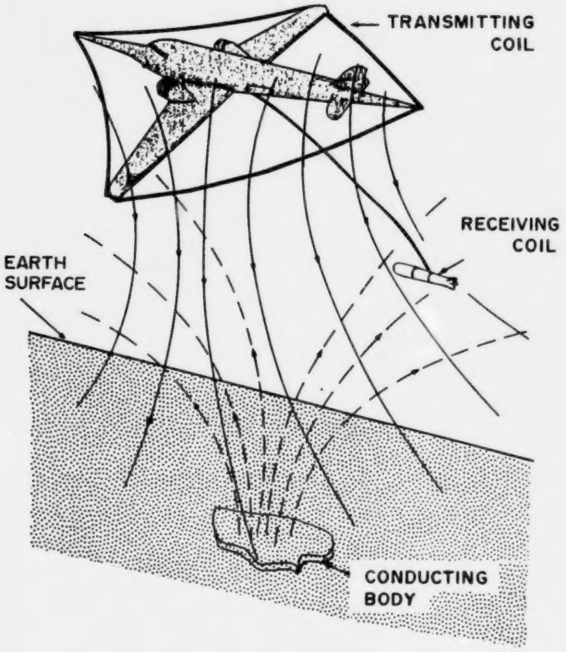

Figure 109.1. Illustration of PROSPECT I system geometry and airborne platform. The orthogonal receiver signal components are X, Y and Z where X is aligned with the flight direction, Z is vertically up and Y is selected to complete a right-handed coordinate system.

tion down to very low frequencies. The current PROSPECT I transmitter has no bottom end on its operational frequency. The lowest frequency for system operation is limited only by the speed at which the aircraft flies. In other words one transmit cycle cannot be too long otherwise the speed of the aircraft motion over the ground will average the signal over too large a spatial distance. The practical lower limit for the operating frequency is typically in the 30 to 100 Hz range.

An example of the spectral distribution of the transmitter system being operated in one mode of operation is shown in Figure 109.2. The spectrum in this case varies inversely with frequency. This transmitter spectral distribution is designed to achieve approximately equal signal-to-noise across the operating bandwidth. The general behavior of the atmospheric noise spectrum is shown in Figure 109.3.

Towed Bird Receiver

The towed bird is currently towed at a distance 120 m behind and below the aircraft as shown in Figure 109.1. The towed bird unit measures all three vector components of the field. As indicated in previous work (Annan 1984) on bird motion effects, it is imperative that the total vector field be obtained if compensation for bird motion is to be undertaken systematically.

Size constraints and aerodynamic system bandwidth limit the operation of the towed-bird system to an EM bandwidth of approximately 10 Hz to 20 kHz in the current implementation. This bandwidth is a design cut-off limit based on requirements for the PROSPECT I system and not a fundamental hardware limitation.

Digital EM Receiver

The heart of the PROSPECT I system lies in its digital receiver technology. The system is operated under computer control. The receiver is a four channel wideband, digital signal acquisition unit. Four channels of analog signal can be simultaneously acquired at sampling rates of up to 75 kHz. Figure 109.4 shows a block diagram of the receiver system. One channel is used to monitor the transmitter current and 3 channels monitor the signals from the towed bird. These sampled data are fed to an array processor which removes the system transfer function, and reduces the data to a format for real time display. The real time signal processing steps are outlined in Figure 109.5.

The functional bandwidth of the receiver is DC to 10 kHz. Changes in bandwidth can be accommodated by changes in the clock rates and the anti-aliasing filters used in the signal preconditioning circuitry.

The PROSPECT I system is digitally controlled and is completely reconfigurable for a wide variety of measurements. For example, a complete self calibration of the system is carried out under computer control. Diagnostic signals are injected at numerous points along the signal path, re-acquired by the computers and analyzed for stability, integrity and fidelity.

For testing and debugging bird operation and defining other system noise sources, the receiver has proved invaluable. Monitoring of motion induced noise from a towed bird sensor over a period of a few minutes and utilization of spectral analysis of this data defines the natural aerodynamic oscillation frequencies of the bird system. These frequencies are exactly those predicted from an aerodynamic analysis of the bird

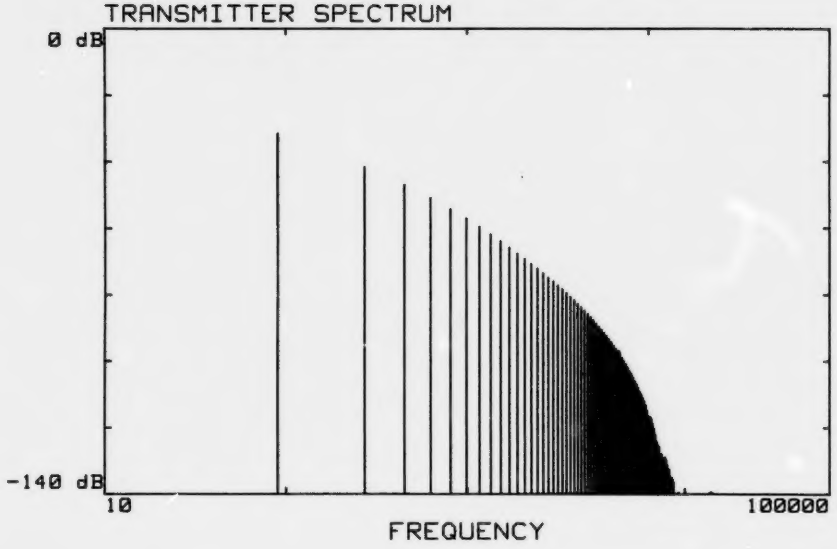

Figure 109.2. Typical PROSPECT transmitter line spectrum as measured with the digital receiver employing a 5 kHz 10th order anti-aliasing filter.

suspension system. Examples of the use of a digital EM receiver are presented by Annan and Lobach (1985).

Data Acquisition and Peripheral Instrumentation

The MIDAS (Modular Interactive Data Aquisition System) has been uniquely designed to support the EM receiver's wide bandwidth and large volume data generation capabilities. A block diagram of MIDAS is shown in Figure 109.6. The heart of MIDAS is a general purpose multi-tasking mini computer which supports a wide variety of peripherals. The system has been designed to be totally modular and reconfigurable. For example, the current MIDAS survey mode configuration is handling approximately 25,000 bytes of data per second. Any channel of information can be displayed via menu driven user control.

DATA PROCESSING AND DISPLAY

The PROSPECT system permits measurement of the ground transfer function over a frequency range of a few tens of Hz to over 10 kHz. The output of the system is the transfer function uncontaminated by DC level offsets, unknown calibrations and system drifts. One of the major problems with such a system is the manner of data presentation. There are 3 components of data to display which span a large bandwidth.

Choices of display are either the time-domain or the frequency-domain. The current PROSPECT data is being displayed in the time domain as the windowed step response of the ground as illustrated in Figure 109.7. For those familiar with the UTEM system on the ground, PROSPECT I provides the same type of data presentation.

DATA HANDLING AND INTERPRETATION

The key to success of any system is how data is presented to the user. The data presentation methods that have been used for towed bird AEM data in the past decade have vastly limited the utilization of the data. There is a wealth of information which lies in existing towed bird EM data which has not been extracted. Systematic attempts to improve data presentation and to extract more quantitative results lead to better data collection practices and technology.

A-Cubed has systematically undertaken to address this subject just as thoroughly as the rest of the system development. For experimental purposes and design of PROSPECT I data processing and presentation techniques, the OUTPUT process for treating INPUT data in a systematic manner has been developed which allows automated anomaly selection and discrimination by computer (Vaughan 1985). Figure 109.8 shows an automatically reduced data set displayed in stacked profile form.

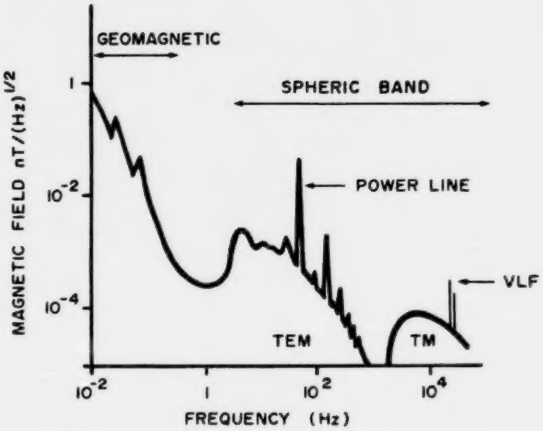

Figure 109.3. The general electromagnetic noise spectrum encountered by airborne electromagnetic survey systems.

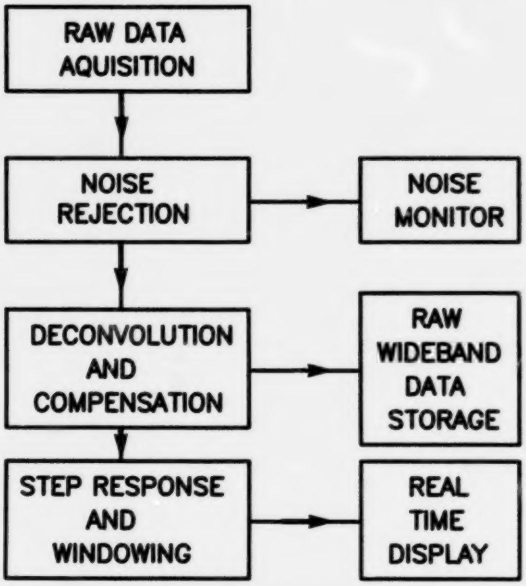
RAW DATA AQUISITION
NOISE REJECTION
NOISE MONITOR
DECONVOLUTION AND COMPENSATION
RAW WIDEBAND DATA STORAGE
STEP RESPONSE AND WINDOWING
REAL TIME DISPLAY

Figure 109.5. The major elements of the real-time signal processing carried out in the PROSPECT I digital AEM receiver.

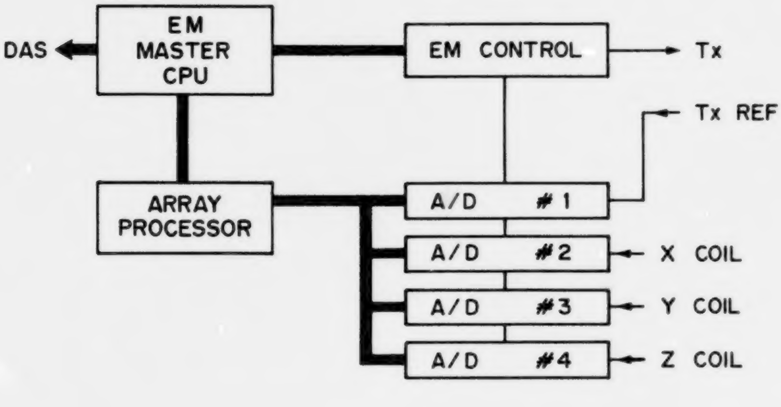
DAS
EM MASTER CPU
EM CONTROL
Tx
Tx REF
ARRAY PROCESSOR
A/D #1
A/D #2
A/D #3
A/D #4
X COIL
Y COIL
Z COIL

Figure 109.4. The block diagram of the PROSPECT I 4-channel, wideband, digital EM receiver. The receiver controls all system timing and coordinates transmitter operation in addition to its wideband signal acquisition functions. Each A/D unit consists of analog signal pre-conditioning circuitry in addition to analog to digital signal conversion.

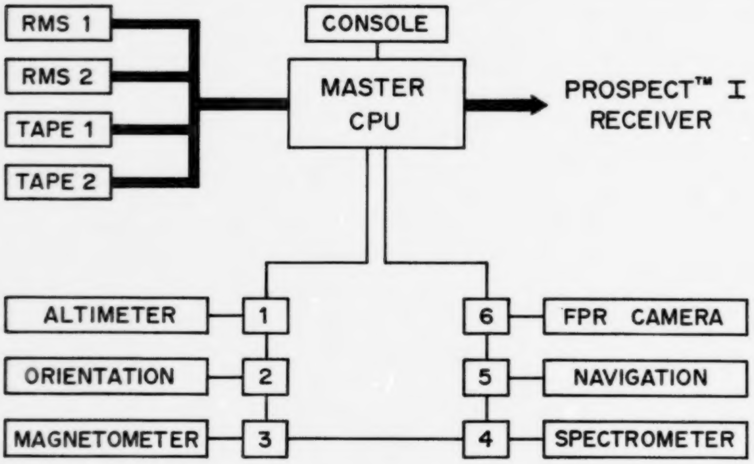
RMS 1
RMS 2
TAPE 1
TAPE 2
CONSOLE
MASTER CPU
PROSPECT™ I RECEIVER
ALTIMETER
ORIENTATION
MAGNETOMETER
1
2
3
4
5
6
FPR CAMERA
NAVIGATION
SPECTROMETER

Figure 109.6. The block diagram of the MIDAS (Modular Interactive Data Acquisition System) developed to provide flexible, reconfigurable data display and recording capabilities for the PROSPECT I system.

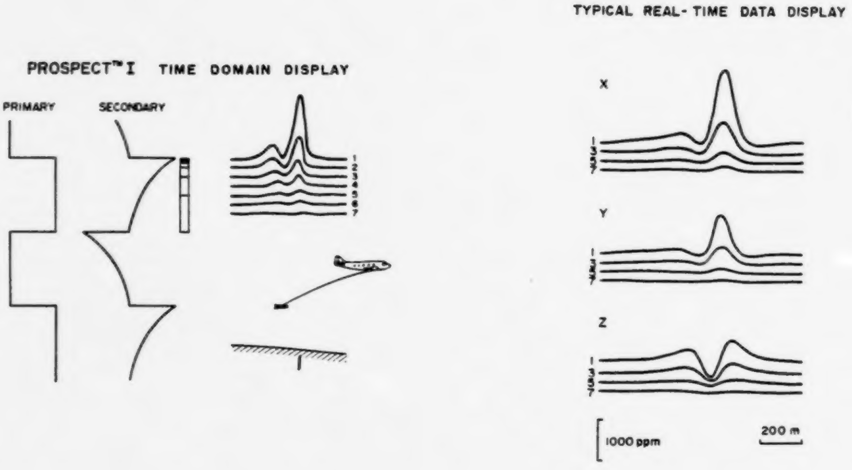

Figure 109.7. The transformation of deconvolved time-domain step response data into chart profile format. The full waveforms shown on the left are windowed at logarithmically spaced time intervals to generate the profile format results shown in the centre and on the right for the multiple coil receiver.

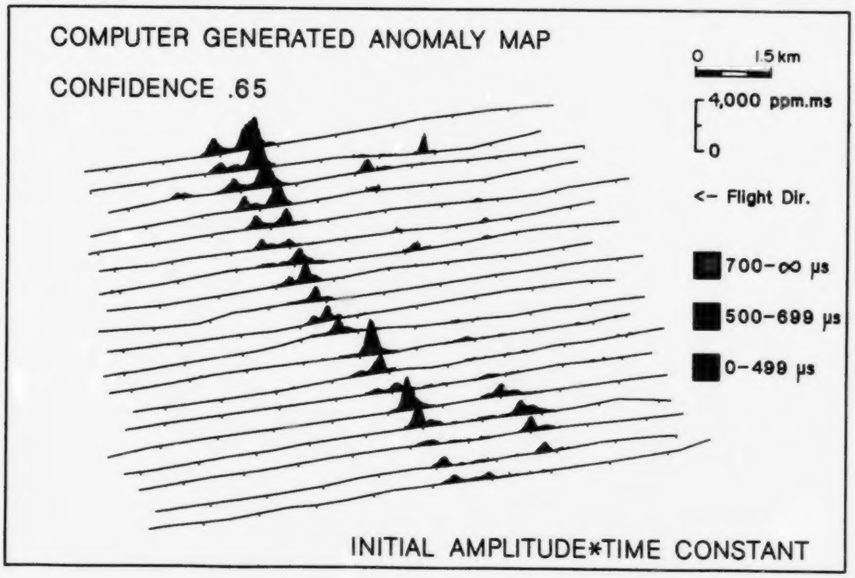

Figure 109.8. Example of a computer generated anomaly map displaying stacked profiles of the initial amplitude – time constant product for a standard set of INPUT data. Anomaly quality (confidence) has been used to winnow the data for features with a 0.65 confidence level. The colour display allows time constant to be superimposed on the amplitude information.

CONCLUSIONS

The development of the PROSPECT I system is now well underway. From the geophysical viewpoint, however, much work remains to be done in terms of operation, data handling and data presentation. A tremendous amount of design, thought and effort has gone into this system. Over the next 3 years a similar effort will be expended on bringing the system into a state where it is a viable, commercial system. The PROSPECT I system maximizes the utilization of computer technology, and there is no doubt that this is the way of the future for AEM systems.

ACKNOWLEDGMENTS

A–Cubed Inc., gratefully acknowledges the financial and/or technical support received from Anglo American Corporation, the National Research Council of Canada, and the Ontario Geological Survey ETDF program.

REFERENCES

Annan, A.P.

1983: **The Effect of Differential Transmitter/Receiver Motion on Airborne Transient EM Interpretation; unpublished paper presented at the SEG Annual Meeting, Las Vegas, Nevada.**

1984: **Compensation of Towed Bird AEM System Data for Differential Transmitter Receiver Motion; unpublished paper presented at the SEG Annual Meeting, Atlanta, Georgia.**

Annan, A.P., and Lobach, J.

1985: **Experiments with a New General Purpose Digital EM Receiver; unpublished paper presented at the SEG Annual Meeting, Washington, D.C.**

Vaughan, C.J.

1985: **Computer Analysis of Airborne Electromagnetic Data; unpublished paper presented at the SEG Annual Meeting, Washington, D.C.**

Grant 112 — Development of Geobotanical Remote Sensing Technology

D.N.H. Horler[1], J.A. Ostrowski[1] and D.R. Melling[2]

[1]Horler Information Inc., Suite 801, 116 Albert Street, Ottawa, Ontario K1P 5G3

[2]Ottawa–Carleton Centre for Geoscience Studies, Carleton University, Ottawa, Ontario K1S 2B7

ABSTRACT

The objectives of the project were (1) to carry out a test case study of geobotanical remote sensing using Multispectral Electro–Optical Imaging Scanner (MEIS) imagery in conjunction with other data, and (2) to develop techniques of analysis and interpretation of MEIS data for detecting vegetation stress.

A suite of satellite, airborne and ground data from the Cameron Lake gold exploration area in northwestern Ontario was acquired and analysed. The data allowed the investigation of geological structure, lithology, and alteration, all of which are important in controlling gold mineralization in this region. The satellite imagery was excellent in displaying structural features and delineating many lithological units. The airborne imagery showed several minor structures such as the Cameron Lake Shear Zone which hosts the Cameron Lake gold deposit, but did not appear to indicate hydrothermal alteration. The imagery contains much information which could be of value to future exploration efforts in the region.

Software was developed for processing MEIS imagery to reveal spectral shifts in the 'red edge' of vegetation reflectance spectra. Several approaches were quantitatively evaluated, and the selected algorithm was implemented on a personal computer. The program combines accurate curve fitting with fast computation. The analysis of test data is discussed.

INTRODUCTION

The term remote sensing is used here in the relatively restricted but conventional sense to mean the acquisition, processing and interpretation of imagery of the Earth's surface. The energy sensed is electromagnetic radiation (visible light, infrared, microwave) and the imagery is usually acquired in digital, as distinct from photographic, form. Remote sensing is frequently used in the early stages of exploration programs as a reconnaissance tool, giving a regional overview of geological structure and lithology. The Landsat Multispectral Scanner (MSS) and Thematic Mapper (TM) provide readily available imagery suitable for this use. In Ontario, the use of remote sensing for exploration must take account of the complications presented by both forest cover and glacial overburden. The imagery is dominated by the spectral responses of vegetation and, thus, it is essential to develop an understanding of how these spectral responses are affected by geological factors to realize the full potential of remote sensing for exploration.

TABLE 112.1. CLASSIFICATION OF GEOBOTANICAL EFFECTS.

Class	Name	Description
I	Absolute	Local absence of vegetation
II	Qualitative	Presence of distinct vegetation community (may include indicator plants)
III	Quantitative	Quantitative ecological change in composition of vegetation community expressed as change in density, frequency, area, volume or biomass of one or more species
IV	Physiological	Change in normal plant morphology, anatomy, physiology or biochemistry
V	Temporal	Appearance of anomaly only at certain periods in daily, annual or life cycles

The term geobotany encompasses the relationships between plants and their soil and rock substrate, with particular reference to the mineral composition of the substrate. Brooks (1983) includes in geobotanical methods of prospecting "studying the nature and distribution of plant communities, studying the nature and distribution of individual indicator plants, observing morphological changes in vegetation (e.g., colour changes), and examining any of the above by remote sensing". A summary of geobotanical effects is presented in Table 112.1, modified from Horler Information Inc. (1985). The classes of geobotanical effects listed present a logical sequence of severity that can be related both to the environmental conditions causing the effects and to the remote sensing methods needed to detect them. The effects become increasingly subtle in moving from Class I to Class V and their detection requires progressively more sophisticated remote sensing systems and methods.

The application of Landsat MSS data to regional studies in which geobotany is a component has become quite well established. The data are used effectively to map lithologic units and structural features on the basis of their association with vegetation patterns (e.g., Singhroy and Bruce 1977; Harris and Bruce 1983). The geobotanical effects exploited in these studies are generally in Classes I, II and III (Table 112.1). The use of geobotany may be indirect or subconscious, meaning that an interpreter may map geological features by virtue of their association with vegetation patterns without having a detailed understanding of the vegetation and even without being aware that he or she is actually mapping vegetation.

The use of geobotany to help identify exploration targets generally requires higher spatial resolution than Landsat MSS or even TM can provide since mineralised zones and their associated hydrothermal alteration halos may be only a few metres or a few tens of metres in width. Airborne sensors can cover a wide range of spatial resolutions, depending on the sensor characteristics and the flight altitude. Some advanced airborne sensors also have capabilities to detect spectral effects that cannot be sensed by satellite sensors, which may be important in the recognition of the less obvious Class IV and V effects.

The Canada Centre for Remote Sensing's (CCRS) Multispectral Electro–Optical Imaging Scanner (MEIS) has the radiometric sensitivity to record imagery in very narrow wavebands of about 3 nm half peak band width (HPBW) for up to eight channels in the 390–1100 nm wavelength range (Till et al. 1984). This high spectral resolution is of interest for detecting Class IV and V geobotanical effects because it enables the "red edge" of plant reflectance to be resolved. The red edge is the sharp change in plant reflectance between about 680 and 780 nm (Figures 112.5 to 8) and is a unique spectral feature of green vegetation because it results from two special optical properties of plant tissue, high internal leaf scattering causing large near infrared reflectance and chlorophyll absorption giving low red reflectance (Horler et al. 1983). The wavelength of the red edge has been reported to shift about 10 to 25 nm towards the blue ("blue shift") in response to mineral stress (Collins et al. 1983; Chang and Collins 1983). The shift of the red edge appears to be due, at least in part, to a decrease in the chlorophyll concentration of leaves (Horler et al. 1983), and is an example of a Class IV effect.

Class V, or Temporal, geobotanical anomalies have been documented in the work of Schwaller and Tkach (1980) and Labovitz et al. (1983 and in press). The test sites were, respectively, a copper sulphide mineralization in the Keweenaw Peninsula of Upper Michigan and a copper–lead–zinc sulphide deposit near Mineral, Virginia. It was found that deciduous trees growing over the anomalies showed slightly earlier fall senescence and, at Mineral, later spring leaf flush than trees in background areas. The effects were most apparent in TM bands 3 and 5 (and in the thermal infrared; Schwaller, in press), and appear to be linked to changes in leaf chlorophyll and water contents.

In view of these research results, it was considered that there may be scope for making increased use of geobotanical techniques in Canadian exploration environments. The present research has been carried out with this goal in mind. Other studies in Canada are also being undertaken by several workers (summarized by Horler Information Inc. 1985). The objectives of the research described here were (1) to carry out a test case study of geobotanical remote sensing using MEIS imagery in combination with other forms of data, and (2) to develop techniques of analysis and interpretation of MEIS data for detecting vegetation stress.

STUDY AREAS

The main study area was the Cameron Lake – Rowan Lake area, shown in Figures 112.1 and 2. The area has experienced intense gold exploration activity in recent years, mainly as a result of the discovery of the Cameron Lake deposit owned by Nuinsco Resources Limited. Kaye (1973) mapped the geology of the area. An inventory of the gold occurrences and the mining history of the region are given by Beard and Garratt (1976), while Hunter (1985) described the exploration history of the Cameron Lake deposit. The regional geology is discussed by Blackburn and Hailstone (1983), and early exploration work at Cameron Lake by Hunter and Curtis (1983). Melling et al. (1985) give a comprehensive overview of the geological setting and genesis of the Cameron Lake deposit.

The Cameron Lake gold deposit is located in the Wabigoon Subprovince of the Superior Province of the Canadian Shield in northwestern Ontario. It is situated within an upper mixed mafic to felsic, partly pyroclastic, volcanic succession (Cameron Lake Volcanics) near its contact with a

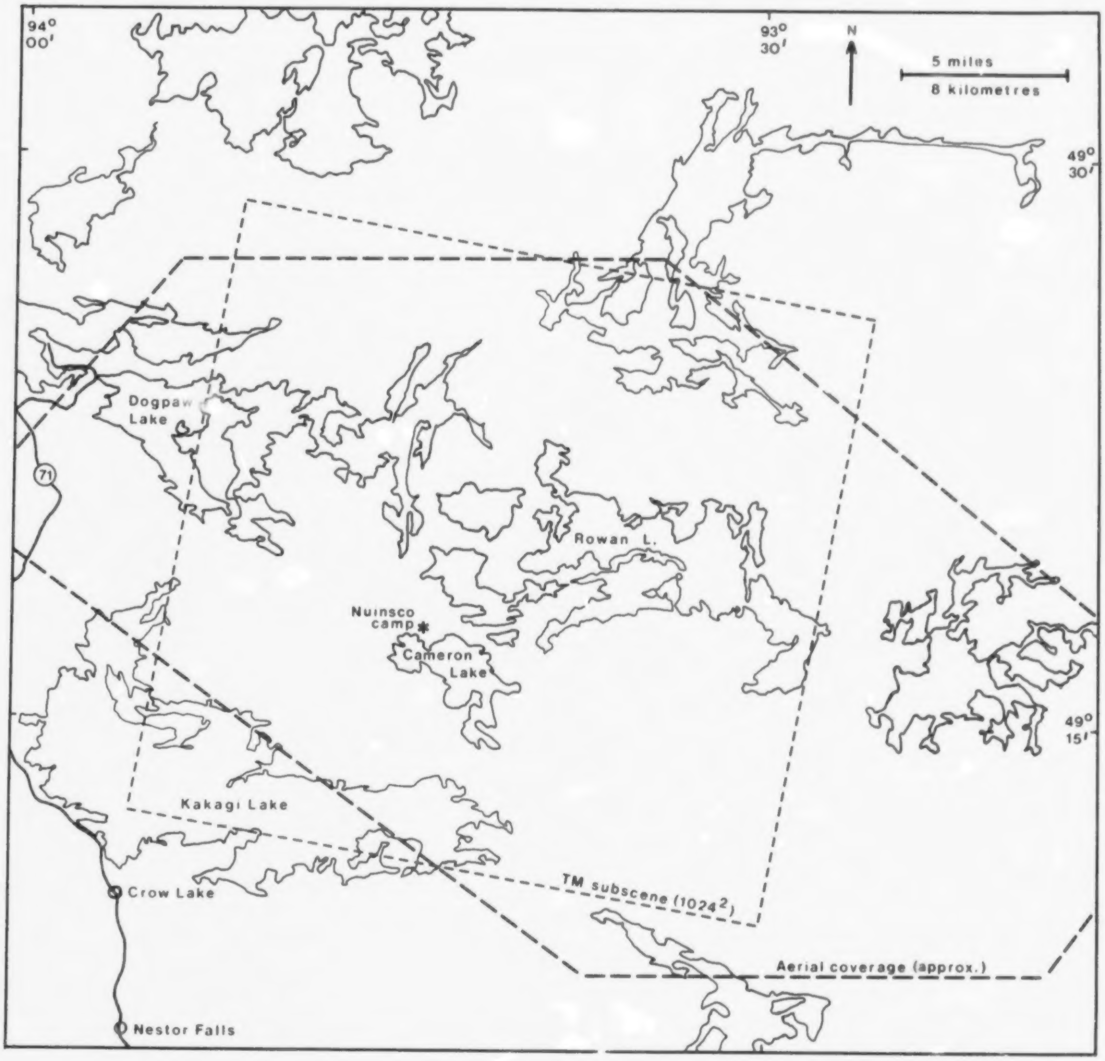
94° 00'
93° 30'
N
5 miles
8 kilometres
49° 30'
Dogpaw Lake
71
Rowan L.
Nuinsco camp
Cameron Lake
49° 15'
Kakagi Lake
TM subscene (1024²)
Crow Lake
Aerial coverage (approx.)
Nestor Falls

Figure 112.1. Cameron Lake test area, showing image coverage.

lower, mafic volcanic succession (Rowan Lake Volcanics) as described by Blackburn and Hailstone (1983). These authors suggest the importance of volcanic stratigraphy in controlling gold mineralization, and draw attention to the presence of felsic porphyries and perhaps gabbros as additional factors.

The emplacement of gold at Cameron Lake is structurally controlled, occurring in the Cameron Lake Shear Zone (CLSZ) at its intersection with oblique, secondary, bedding-controlled, sympathetic shear zones (Melling et al. 1985). The CLSZ is a NW-trending structure which is probably a splay off the Pipestone-Cameron Fault (PCF) and was unrecognized prior to 1983. The Monte-Cristo Shear Zone (MCSZ), which hosts the Monte Cristo and Victor Island gold occurrences, was also only recently discovered.

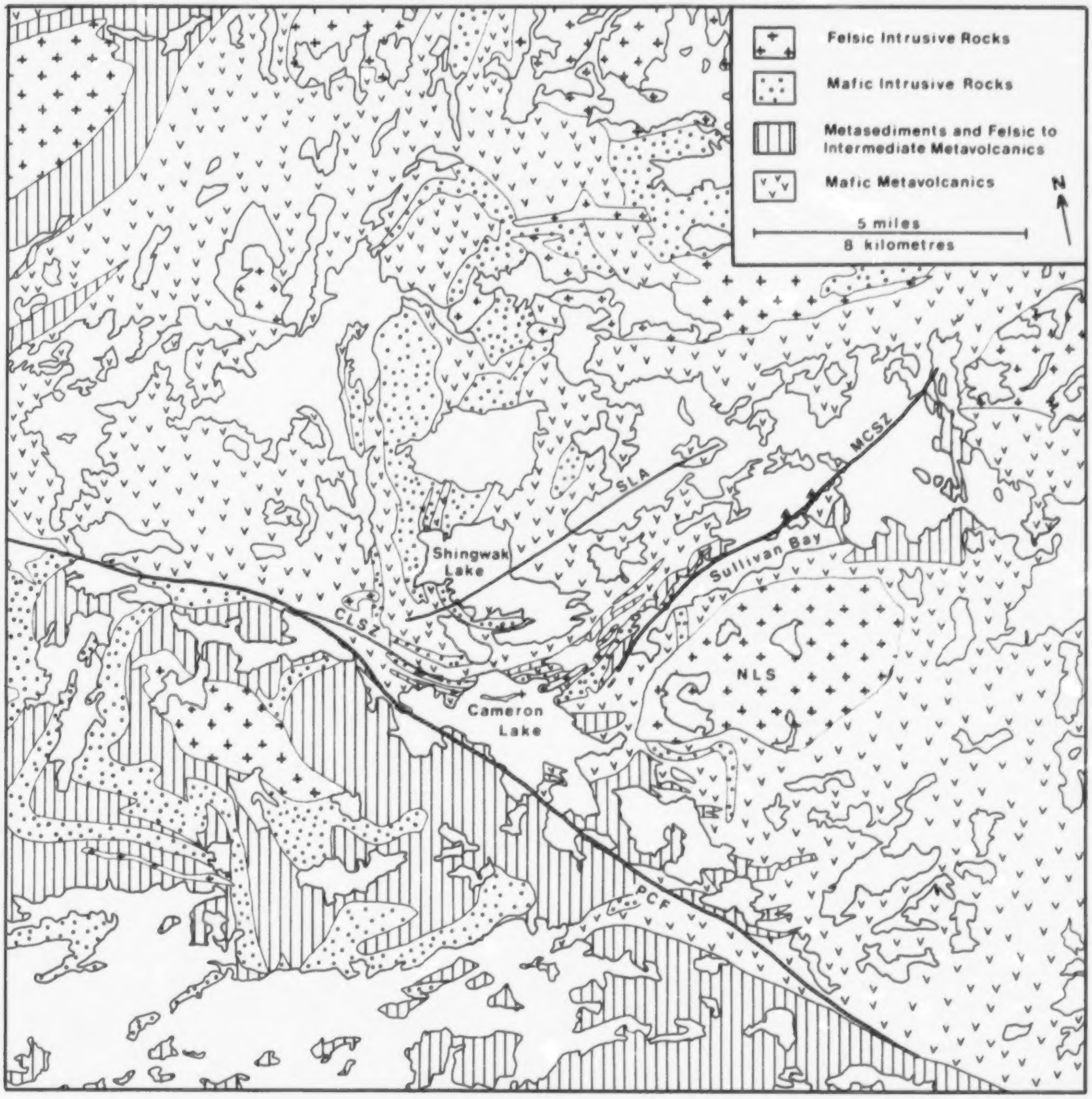
Felsic Intrusive Rocks
Mafic Intrusive Rocks
Metasediments and Felsic to Intermediate Metavolcanics
Mafic Metavolcanics
N
5 miles
8 kilometres
SLA
MCSZ
Shingwak Lake
CLSZ
Sullivan Bay
NLS
Cameron Lake
PCF

Figure 112.2. Regional Geology of the Cameron Lake area. The area covered is the 1024 pixel x 1024 line (1024^2) TM subscene shown in Figures 112.1 and 3a. Structural features noted are the Pipestone–Cameron Fault (PCF), Shingwak Lake Anticline (SLA), Cameron Lake Shear Zone (CLSZ) and Monte Cristo Shear Zone (MCSZ). The Nolan Lake Stock (NLS) is also labelled. (Sources: Melling et al. 1985 and OGS Map 2443.)

The Cameron Lake deposit is essentially of the vein type, surrounded by a large hydrothermal alteration zone. The alteration zone is up to 120 m wide and extends over a strike length of at least 750 m, although it is not continuous over this strike length. The characteristic alteration assemblage consists of ferroan dolomite–sericite–pyrite. Major amounts of CO_2, K, Ca, S and Si were added to the altered rock, as well as minor amounts of Ag, Au, B, Hg, Rb, Sr and W (Melling et al. 1985). Precipitation of pyrite at the expense of primary magnetite was related to gold mineralization. Rocks in the alteration zone contain up to 20% CO_2 by weight, which is several times higher than the values in the unaltered rock.

For the purpose of this project, the area provided a well documented mineral deposit with a reasonably undisturbed vegetation cover. An extensive carbonate alteration zone underlies a relatively thin glacial till, which is about 3 m thick in the immediate area of the deposit and up to about 12 m thick in the direction of the alteration zone to the northwest. The test area enables an investigation of the use of remote sensing to detect effects relating to structure, lithology and alteration, all of which have been demonstrated to be important in controlling gold mineralization in this region.

Cameron Lake lies at the transition between the Boreal Forest Region and the Great Lakes – St. Lawrence Forest Region (Rowe 1972). The species composition is quite diverse, and no disturbance due to logging, fire or other factors was apparent. Forest cover information was obtained from Forest Stand Maps of the Ontario Ministry of Natural Resources, as well as from the imagery and a field visit.

An area near Allan Lake, Algonquin Park, (National Topographic System [NTS] Map 31 L/1, Brent; Energy, Mines and Resources Canada) was also studied in the context of MEIS processing methodology development. The site is described by Rencz et al. (1986). The area contains a large, virtually pure stand of sugar maple (*Acer saccharum* Marsh.) and a geochemical anomaly for rare earth elements and phosphorus derived from a carbonatite.

METHODS

DATA SETS

The Cameron Lake area was surveyed by the CCRS Falcon aircraft on 5 July, 1985, and 28 August, 1985. A mission on 20 June, 1985, was abandoned due to cloud after some imagery was collected. Digital imagery was recorded from the MEIS and Airborne Multispectral Scanner (AMSS) instruments. Simultaneous colour aerial photography was acquired with an RC–10 camera with Kodak 2445 colour negative film and a 153 mm focal length lens. The flight altitude above ground was about 9800 m, giving a pixel spacing for MEIS of about 7 m and for AMSS of about 15 m. The area covered by the airborne imagery is shown in Figure 112.1.

The filters on the eight MEIS channels have peak transmissions at the wavelengths of 445, 550, 682, 703, 713, 743, 752 and 798 nm. The HPBW was 30 nm for the 445 and 550 nm filters and approximately 3 nm for the others. Thus, the red edge was sampled by six narrow band filters. The peak wavelength changed as a function of viewing angle across the image swath, as described by Miller et al. (1985).

The AMSS channel wavebands were: 445–495 nm (blue), 550–595 nm (green), 625–695 nm (red), 865–1035 nm (near infrared, NIR) and 2080–2350 nm (shortwave infrared, SWIR). The AMSS was important in scanning a broader swath than the MEIS and thus in giving stereo digital coverage of the test area, and in providing SWIR data which were not obtainable from MEIS and which give independent geological and botanical information.

The following geological and forestry maps were obtained from the Ontario Ministry of Natural Resources: Geological Maps 2443 (scale 1:253 440), P.831 (1:15 840), P.1024 (1:15 840) and Forest Stand Maps 493932 and 493934 (1:15 840). A geological map of the Cameron Lake property was also supplied by Nuinsco Resources Limited (scale 1:4800). The test area is covered by NTS maps 52F (1:250 000), and 52F/3, 4, 5 and 6 (1:50 000).

Thematic Mapper (TM) digital image tapes of two dates, 3 June and 6 August, 1984, for Path 28–Row 26 (Landsat 4 World Reference System), northwest quadrant, were acquired. Two images were obtained to allow a multi–temporal analysis, which is important in studying geobotanical effects. The two images were the best available, although they are rather close in date. One Landsat MSS scene was also used in conjunction with the TM data for the interpretation of regional structural geology.

FIELD WORK

The Cameron Lake test site was visited on 2–5 July, 1985. Detailed familiarization with the site was aided by Nuinsco geologists. Leaf samples of three species, Black Ash (*Fraxinus nigra* Marsh.), Eastern White Cedar (*Thuja occidentalis* L.) and Balsam Fir (*Abies balsamea* (L.) Mill.) were collected and their reflectance measured using a Barringer Hand Held Ratioing Radiometer, HHRR (Gladwell et al. 1983). The leaf samples were placed in plastic bags and measured within a few hours of collection. The HHRR was set up on a tripod in a cabin with an artificial lamp to maintain standardized conditions. Samples were placed in a continuous layer on a black surface to fill the viewing area. A Fibrefrax standard (Gladwell et al. 1983) was measured between every leaf sample.

Samples were collected in two locations, over the known alteration zone (A) and in a background area (B). Areas A and B had similar till composition and depth. A and B samples were analysed alternately to ensure that there was no systematic difference between sites due to the measurement technique.

SATELLITE DATA ANALYSIS

Analysis was carried out on the CCRS Image Analysis System, CIAS (Goodenough 1979). A variety of digital analysis procedures were executed and hard copy images were generated. The images were visually interpreted for regional structural and geobotanical information.

Some of the main processing steps are described below with an explanation of why they were carried out:

1. Contrast enhancement of selected bands for the whole quadrant, as well as a 1024^2 pixel sub–scene and a 512^2 sub–scene centred on Cameron Lake. A contrast enhanced image, particularly of TM bands 3, 4, and 5, is an excellent way of displaying most of the information available in a scene (Horler and Ahern 1986).
2. A density slice of the TM 4 image for June was found to be effective for displaying geological structure. A density slice is simply the splitting of the grey scale of an image into several intervals or slices, and the assignment of colours to the slices.
3. To enhance linear features, directional filtering of TM 5 was carried out using a 7 pixel by 1 line (7x1) kernel to enhance horizontal lineaments and a 1 x 7 filter to enhance vertical lineaments. The original image and the two filtered images were displayed simultaneously using the three colours of the monitor.
4. A combination of images of two dates allows changes to be highlighted, frequently due to differences in vegetation cover between the two dates. A geometric registration, (i.e., digital resampling to achieve an exact overlay) of the two images was carried out and various band and colour combinations were processed and displayed, of which the two following steps are examples.
5. A Vegetation Index (VI) image of TM 4/TM 3 was computed to show biomass. By displaying the VI image for June on the red and blue guns and the August image on the green gun, areas that had greened up the most appeared green.
6. TM 5 also contains biomass information (Horler and Ahern 1986) and thus a similar combination of the TM 5 images for June and August displays biomass changes.

AIRBORNE DATA ANALYSIS

The AMSS and MEIS data were first displayed and contrast enhanced to provide good quality colour composite images for visual interpretation. High quality images of whole flight lines were recorded on film to provide data for the entire study area, and a 512^2 sub–scene of the Cameron Lake deposit area was displayed and photographed. Photographic transparencies of single bands and colour composites were overlaid on forest stand maps and geological maps for visual interpretation.

To improve the aesthetics of the image products, processing was carried out to attempt to remove the radiance variation across the image swath due to differences in atmospheric path length. The variation of radiance across the swath was estimated by summing all lines and fitting a second degree polynomial curve to the profile. The calculated curve was used to give an offset for the correction of the radiance of each pixel. This procedure was only applied to the blue channel (MEIS band 1), which was the most affected by atmospheric haze.

MEIS PROCESSING METHODOLOGY DEVELOPMENT

Three stages are involved in the processing of MEIS data for vegetation stress analysis: atmospheric subtraction, conversion from MEIS counts to reflectance, and calculation of stress parameters (R. Gauthier, CCRS, Ottawa, personal communication, 1985). These stages are summarized briefly here. (1) The radiance measured over clear, deep water is used as an estimate of the atmospheric path radiance and is subtracted from the data, taking into account the sensor look angle. (2) The target radiances are then converted to reflectances using previously obtained sensor calibration data, solar irradiance values from tables, and the aircraft roll data recorded from the inertial navigation system. (3) The third stage is to compute some measure of the red edge shift for each pixel from the reflectance data, for which an approach has already been reported by Miller et al. (1985). The purpose of the present research was to further investigate suitable techniques for stage (3) and develop a computer implementation of a selected algorithm.

MEIS data of the Allan Lake area, corrected to reflectance units (i.e., steps 1 and 2 above had been done), were supplied by CCRS, with information about the site from A. Rencz (Geological Survey of Canada, personal communication, 1986). A 256^2 pixel portion of the image was selected for algorithm development work. Programming was carried out in Fortran on an IBM–PC–AT computer. The image showed an almost pure stand of maple trees in early fall and a variety of fall colorations was evident. Curve fitting algorithms were also tested on laboratory spectra reported by Barber and Horler (1981).

RESULTS

Note: Many of the results discussed below cannot be adequately illustrated in this report because of the inability to present colour imagery. Details of the imagery available and copies of imagery can be obtained from Horler Information Inc.

CAMERON - ROWAN LAKES AREA

The uses of the remote sensing imagery were investigated as an aid to structural and lithological mapping, as well as for detecting alteration. The satellite imagery was the primary source of data on structure and lithology because of the regional perspective presented, while the spatial detail and spectral characteristics of the airborne data were necessary for investigating alteration detection. However, the various data sets were complementary in all the aspects of the analysis.

Regional botanical patterns were well displayed in the enhanced satellite imagery. The information contained in these patterns can be considered in the context of lithological mapping and as a guide to structural features. The structural and lithological controls on gold mineralization in the Cameron Lake area have been described above and demonstrate that detailed mapping is of the utmost importance to gold exploration in the area.

Structural features are well displayed in the imagery (Figure 112.3). A compilation of the structural interpretation from TM and MSS imagery is shown in Figure 112.4. Linear features in Figure 112.4 were broadly classified into two types. Type 1 lineaments are generally relatively short structures, often curved, and locally offset by Type 2 structures. They may be lithological features, such as folded strata (e.g., Shingwak Lake Anticline, SLA) or intrusions (e.g., Nolan Lake Stock, NLS). Type 2 structures are generally planar, long and continuous, in many cases showing abrupt changes in vegetation or outcrop across them, and often truncating Type 1 lineaments. Type 2 features may be faults (e.g., Pipestone–Cameron Fault, PCF).

Two major regional features are the PCF and SLA. The PCF is a major NW–trending fault which is clearly delineated in many places because of changes in vegetation cover and the exposure of outcrop. Curvilinear patterns associated with the transposition of rock units on either side of the fault are visible. Several fold structures are evident in the imagery, including the SLA, described by Kaye (1973). The asymmetry of this feature can be seen, with the southern limb compressed or otherwise deformed.

Structures corresponding to the mapped locations of the Cameron Lake Shear Zone (CLSZ) and Monte Cristo Shear Zone (MCSZ) are visible in the imagery. The imagery by itself does not identify these features as shear zones, as distinct from other lineaments or lithologic contacts, but by combining the imagery with existing maps and reports, the extension of the shear zones can be proposed. Thus, the CLSZ may extend eastwards on the northeast side of Cameron Lake. The CLSZ, which was weakly visible on the satellite imagery, could be traced on the airborne imagery (Figure 112.3c). The MCSZ may continue westward from Sullivan Bay of Rowan Lake to the edge of Cameron Lake, in the area of the Meston and Sullivan gold occurrences. The geometry of Sullivan Bay is itself controlled by the MCSZ. The search for a NE extension of the MCSZ may need to take account of a N–S lineament identified in the structural interpretation (labelled "F" in Figure 112.4). Both the CLSZ and the MCSZ have only recently been discovered, but are paramount in controlling the location of gold deposits. They were apparent most clearly in the airborne imagery which was able to show greater detail by virtue of its smaller pixel sizes as compared with the satellite data. Clearly, the use of remote sensing can be a valuable aid to further mapping and exploration.

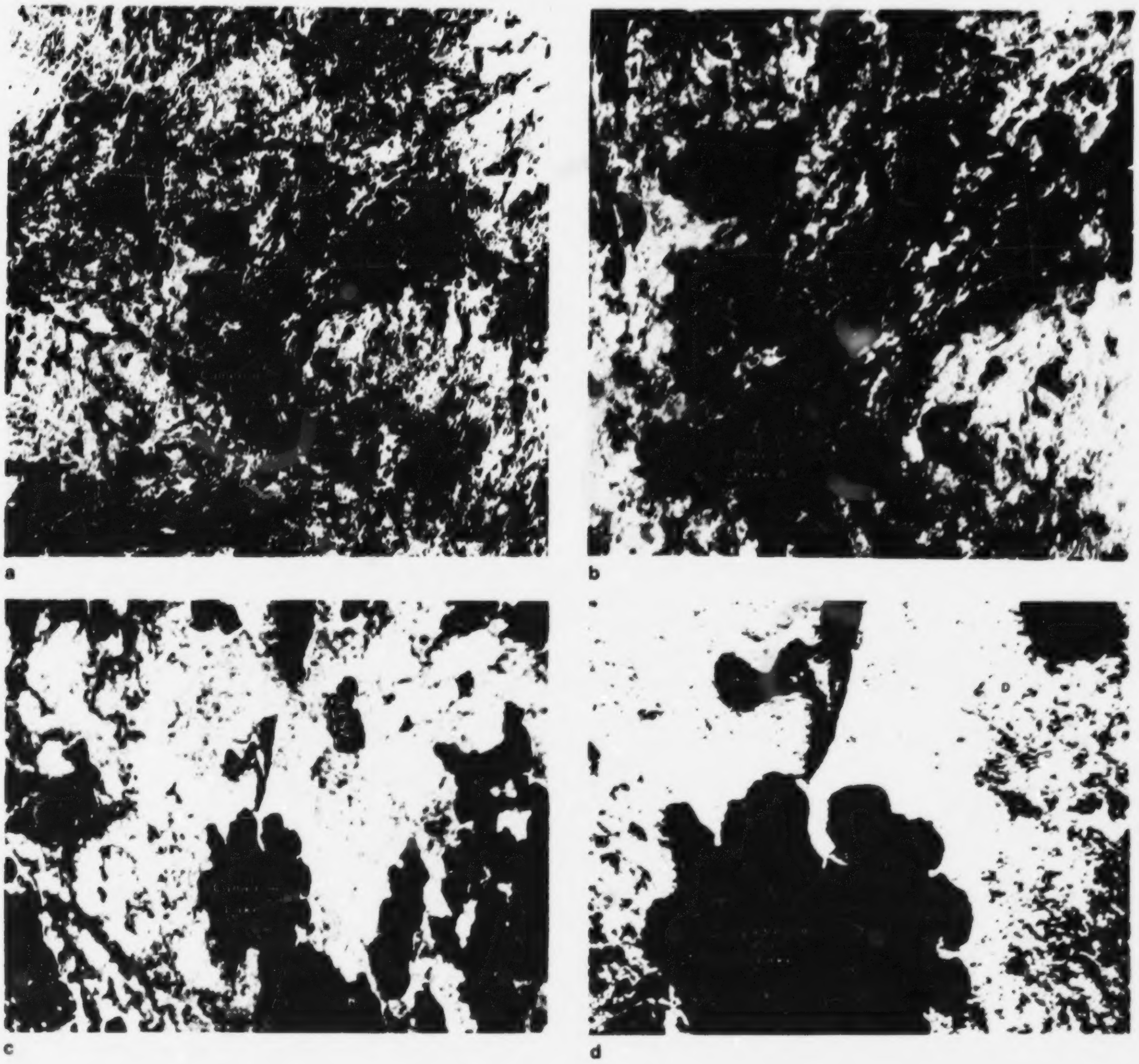

Figure 112.3. Imagery of the Cameron Lake area: (a) 1024 pixel by 1024 line TM band 5 subscene, (b) 512^2 TM band 5 subscene, (c) 512^2 AMSS subscene, SWIR band (the image is rotated relative to the satellite imagery and is slightly distorted), and (d) 512^2 MEIS subscene, band 6 (743 nm). Areas labelled C, D and E are discussed in the text.

In terms of lithological mapping, the imagery was of use in showing outcrops, contacts and the general form of some units. For example, the perimeter of the NLS was visible as a pattern of concentric rings of different vegetation densities varying between full forest cover and outcrop. The location of the contact between the Cameron Lake Volcanics and the Rowan Lake Volcanics was visible between Cameron and Shingwak Lakes, and to the north of Sullivan Bay of Rowan Lake (Figure 112.3a, b). The vegetation density appears greater on the Rowan Lake Volcanics at this point, an impression accentuated in the imagery by illumination and topography, since the neck of land which forms the south shore of Shingwak Lake is a topographic ridge which is illuminated mostly on the south-facing slope. Another example of a rock unit visible in the imagery is the ridge of gabbro

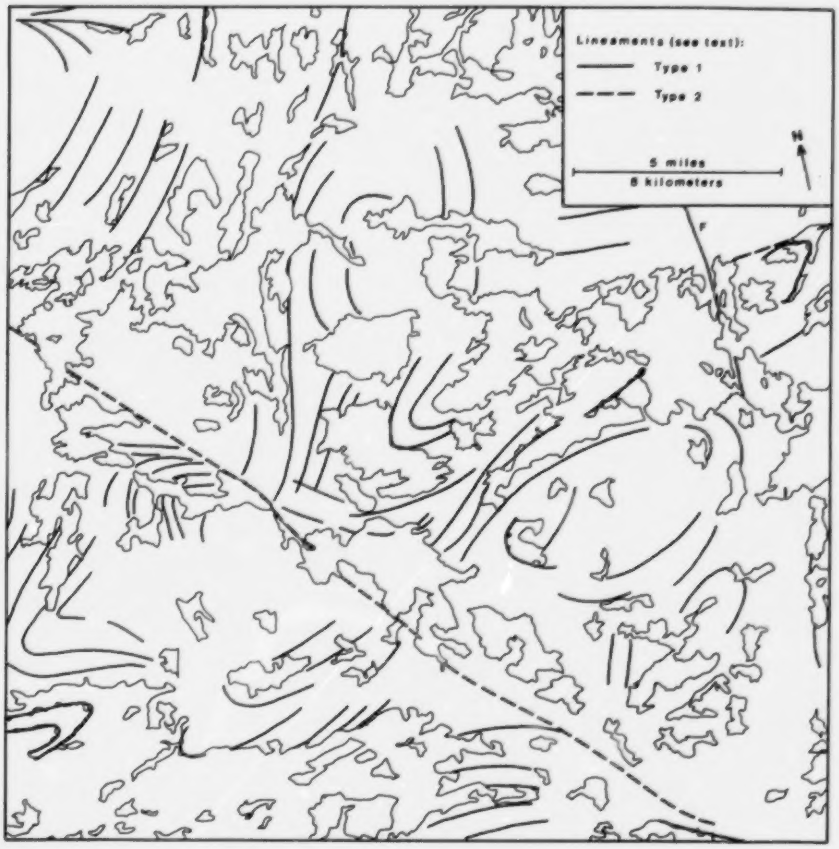

Figure 112.4. Structural interpretation of the Cameron Lake test area from satellite data. The area covered is the same as in Figures 2 and 3a. Lineament types 1 and 2, and lineament 'F' are discussed in text.

curving around the southwest shore of Shingwak Lake on either side of the SLA, which has a light tone in the imagery. To a large extent, these variations occur in response to primary characteristics of the various rock units. Units such as the NLS are relatively resistant to weathering processes and therefore form topographic highs.

Thus, a number of contacts and lithological units can be seen in the imagery, and it is suggested that the imagery is a valuable data source to aid lithological mapping. This is not to say that the imagery can be used by itself to make a geological map; other complimentary data are also required. There was no one-to-one relationship between vegetation type and rock type, nor was any lithological unit found to have a diagnostic vegetation type associated with it.

The airborne imagery showed structural and lithological information similar to the satellite imagery. The imagery collected by MEIS, AMSS and aerial photography was of good quality and enabled vegetation patterns to be discriminated in more detail than on the satellite imagery. Stand boundaries between hardwoods, softwoods, swamp, etc., could be defined more precisely than on the forest stand maps, although the imagery did not give detailed stand composition data such as species proportions and ages, which is recorded on the maps.

One of the objectives of the project was to investigate whether there was any geobotanical indication of hydrothermal alteration zones. The Cameron Lake deposit is enveloped by a large ferroan dolomite–sericite–pyrite alteration zone which contains enrichments of various elements, as described earlier. We were unable to detect any pattern in the MEIS imagery where a geobotanical effect delineated the known carbonate alteration zone at Cameron Lake. There was no apparent change in the vegetation community over the alteration zone (Class I, II or III geobotanical effects), and no observable spectral response in any

MEIS band which could be associated with a Class IV or V effect. However, the 28 August, 1985, date of the overflight was slightly early for that year for the detection of premature senescence. The results of the field spectral measurements on 4 July, 1985, did not show significant differences between trees growing on or off the carbonate alteration; the mean spectra of 'anomalous' and 'background' samples for balsam fir are shown in Figure 112.5 as an example of the data obtained.

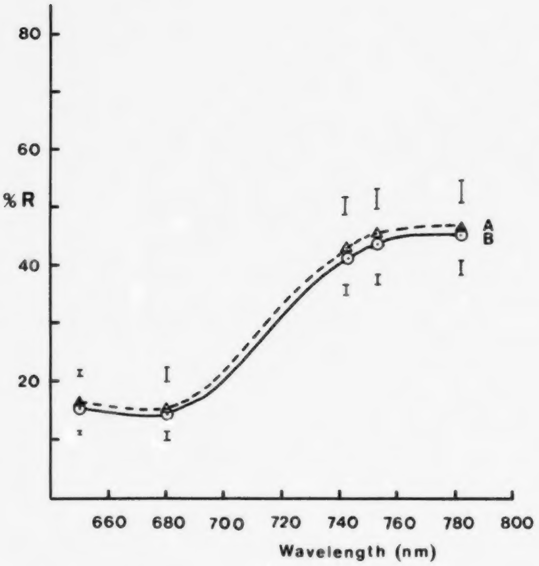

Figure 112.5. Field spectral data for balsam fir at Cameron Lake, 4 July 1985. Each curve is the mean of six samples. Dashed line and triangles are samples collected over the alteration zone (A); solid line and circles are background samples (B). Error bars (one standard deviation of the mean) are shown; above the curves for A, below the curves for B.

The SWIR band of the AMSS (Figure 112.3c) gave information that was not apparent in the other bands and is thought to indicate plant water content and biomass (Horler and Ahern 1986). The diamond–shaped pattern in the SWIR image (labelled "E" in Figure 112.3c) cuts across a boundary between coniferous and deciduous forest stands ("C" and "D" respectively in Figure 112.3d) with virtually no change in radiance; the SWIR radiance thus clearly responds to factors other than species. An explanation for this feature, as well as other patterns seen in the SWIR image, has not been determined.

MEIS PROCESSING METHODOLOGY DEVELOPMENT

Several mathematical models of red edge reflectance data, R(λ), where λ denotes wavelength in nanometres, were considered for their suitability for determining blue shifts of the red edge as indicators of stressed vegetation. The best model should satisfy the following, sometimes conflicting, criteria:

1. One of the most useful stress parameters is expected to be the wavelength, λ_m, at which the derivative dR(λ)/dλ is maximal. To be able to determine this parameter well, the model should fit the data closely, but without introducing spurious maxima.
2. There are only six measurements of R(λ) in the red edge region; therefore, the model should include at most three parameters to give a statistically significant fit.
3. The model should be sensitive enough to detect shifts of the order of 5–10 nm.
4. Because of the large amount of data to be processed, the calculation of model parameters and shift parameters should be as simple as possible.

The reflectance curve in the red edge region (defined here as the interval 682–798 nm) has a characteristic shape which suggests many possible mathematical models. The models which were considered are not fully presented here for reasons of space, but a brief discussion of the model selection is given below. The models considered were (1) straight line fit to the red edge, (2) sine curve (fourth quarter), (3) third degree polynomial, (4) Chebyshev polynomials, (5) Lorentz dispersion curve, (6) inverted Gaussian model, and (7) Weibull distribution. The models were tested on laboratory spectra reported by Barber and Horler (1981) and on MEIS image data.

The straight line fit was quickly rejected as being too crude to adequately model any subtleties that might occur in the red edge shape. The sine curve was also rejected because the derivative (dR/dλ) always has a maximum at the mid–point of the interval. The same problem applies to the third degree polynomial if the minimum reflectance is fixed at $\lambda_0 = 682$ nm and maximum at $\lambda_s = 798$ nm. Relaxing the second requirement (maximum at λ_s) allows red edge shifts to occur, but it would be very difficult to fit the data of Barber and Horler (1981) at 743, 752 and 798 nm where the R(λ) plot is almost horizontal.

Chebyshev polynomials were considered because they have been used by Collins et al. (1983) to fit vegetation reflectance curves. However, Collins' spectra cover a wider wavelength range than MEIS with at least 500 channels. Several reflectance minima and maxima occur in Collins' spectra. The present situation is different because there are only six channels in a small part of the curve with one minimum and one maximum, and the Chebyshev polynomials were judged to be inappropriate.

The Lorentz dispersion curve known in optics can be expressed, under some assumptions, in the form

$$R(\lambda) = R_s - [(R_s - R_0)\,\lambda_0.\lambda.B]/[(\lambda_0^2 - \lambda^2)^2 + B.\lambda^2] \quad (1)$$

where $R_0 = R(\lambda_0)$, $R_s = R(\lambda_s)$ and B is the only parameter. The curve was fitted to two typical laboratory spectra (Barber and Horler 1981), and did not fit the observed values very well (Figure 112.6). The model consistently overestimates data in the lower part of the curve and underestimates them in the upper part. Relaxing the requirement for minimum reflectance at λ_0 would slightly improve the fit in the lower part, but would introduce one more parameter. It seems, however, that the fit in the upper part cannot be improved because the curvature of the observed spectrum there is simply too large for the Lorentz curve to accommodate.

Like the dispersion curve, the Gaussian curve is symmetrical, peaks at the mean value on the x axis (λ in this case) and tapers to zero at infinity. To fit the reflectance data, only half of the inverted curve has to be used. Assuming that the curve has the minimum R_0 at λ_0 (both known) and that the known value R_s is sufficiently close to R_∞, the Gaussian form of the reflectance curve is obtained by

$$R(\lambda) = R_s - (R_s - R_0)\, e^{-(\lambda-\lambda_0)^2/2y} \quad (2)$$

where y (equivalent to σ^2 in the Gaussian curve) is the only parameter. For each known value of $R(\lambda_i)$, where $\lambda_0 < \lambda_i < \lambda_s$, the exactly fitting value of parameter y can be easily obtained from

$$y_i = [-(\lambda-\lambda_0)^2]/\{2\ln[(R_s - R_i)/(R_s - R_0)]\} \quad (3)$$

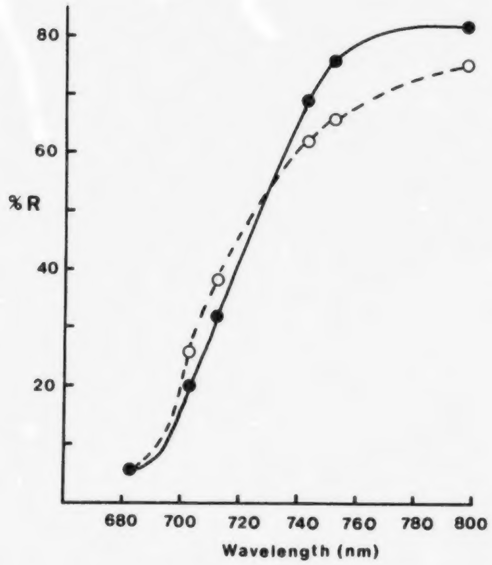

Figure 112.6. Fit of the Lorentz curve model to a laboratory leaf reflectance spectrum. Solid line and filled circles are experimental observations; dashed line and open circles are the model fit.

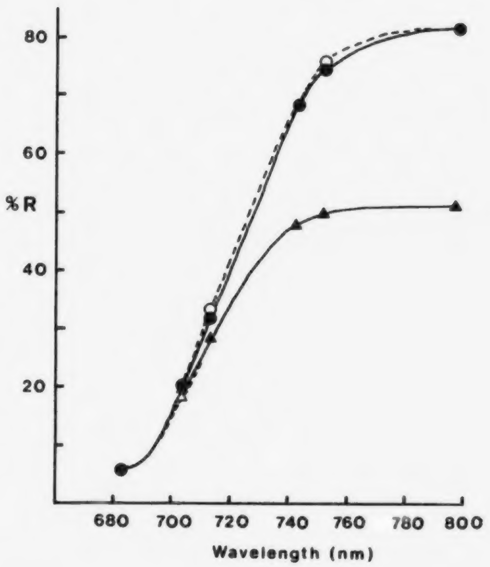

Figure 112.7. Fit of the fixed λ_0 Gaussian model to laboratory leaf reflectance spectra. Triangles represent LAI = 1; circles show LAI = 5. Solid lines and filled symbols show experimental observations; dashed lines and open symbols show model fits.

The mean y ($\bar{y}$) can then be calculated and used to assess goodness of fit between the measured and calculated values of $R(\lambda_i)$.

To find the value λ_m where the first derivative attains a maximum it is sufficient to equate the second derivative of $R(\lambda)$ to zero and solve the resulting equation for λ_m. The result of this is

$$\lambda_m = \lambda_0 + \bar{y}^{1/2} \tag{4}$$

Thus, the only parameter of the fitting function (y_i) and the stress parameter (λ_m) are easily calculated from (3) and (4).

To verify this "fixed λ_0 Gaussian curve" approach, the test data were first generated from

$$R(\lambda) = 60 - (60-6)\ e^{-(\lambda-682)^2/2{*}625}$$

where values of R are given in percent and λ in nanometres, for four λ_i observations from the interval 682 nm < λ_i < 798 nm, and then the rounded values were used to derive $\bar{y}$ and λ_y. The model was also fitted to spectra reported by Barber and Horler (1981) and the results are shown in Table 112.2 and Figure 112.7. The experimental data were derived from two situations: one in which the proportion of leaf and rock sample in the viewing area was varied to simulate changing vegetation cover of the ground, and the other in which leaves were stacked one on top of another up to five leaves deep to represent changing leaf area index, LAI. (LAI is defined as the ratio of

TABLE 112.2. ANALYSIS OF FIXED λ_o GAUSSIAN MODEL PERFORMANCE ON LABORATORY SPECTRA AND MEIS DATA.

Spectrum	$y^{1/2}$	λ_m [nm]		$(\lambda_m^+ - \lambda_m^-)$	RMS
	[nm]	modelled	observed	[nm]	[%R]
Laboratory Spectra:					
Anal. curve*	25.0	707.0	707	0.4	0.13
Curve LAI 1**	26.6	708.6	700	2.7	0.59
Curve LAI 5**	32.6	714.6	722	2.3	1.14
Curve "40%"	27.7	709.7	706	2.9	0.59
Curve "60%"	27.1	709.1	706	2.6	0.86
Curve "80%"	26.7	708.7	706	3.0	1.21
Curve "100%"	26.6	708.6	706	3.0	1.25
MEIS Data:					
Green Crown***	38.1	719.1	-	6.1	6.84
Red Crown***	44.5	725.5	-	12.4	7.20

$\lambda_m = 682\ \text{nm} + \bar{y}^{1/2}$

$\lambda_m^+ = (\bar{y} + \sigma_y)^{1/2}$

$\lambda_m^- = (\bar{y} - \sigma_y)^{1/2}$

$\text{RMS}\ (\%R) = \sum_{i=2}^{i=5} (R_i^m - R_i^0)^2 / 4)^{1/2}$

*The Analytical Curve is a typical laboratory reflectance spectrum defined by $R_s = 60\%$, $R_o = 6\%$, $\lambda_o = 682$ nm and y = 625 nm.

**Shown in Figure 7

***Shown in Figure 8

leaf area to ground area; e.g., if a surface is covered continuously by five layers of leaves, the LAI is 5). The significance of the two situations is that red edge shifts were observed by Barber and Horler (1981) with changes in LAI but not as the proportion of ground cover changed.

The wavelength of maximum slope of the red edge (λ_m) is given in Table 112.2 and compared with experimentally measured data. The last column of Table 112.2 gives the rms (root mean square) difference between measured and calculated values of $R(\lambda)$ based on all data points except λ_0 and λ_s. The model gives excellent agreement for the analytical curve data; slight differences stem mostly from rounding off the initial $R(\lambda_i)$ values to whole numbers. In the experiments at varying LAI and varying ground cover, the model is successful in showing a shift as LAI changes and in not showing a shift as ground cover changes. The magnitude of the shift given by the model was less than the experimental observations in the LAI experiment (6 nm compared with 24 nm) but the modelled shift was statistically significant at the $2\sigma_y$ level (when $\lambda_m \pm = [y \pm 2\sigma_y]^{1/2}$ is used. The uncertainty of the λ_m values is given by the column described as $\lambda_m{}^{+} - \lambda_m{}^{-}$, corresponding roughly to the $2\sigma_y$ interval.

A comparison of the fixed λ_0 Gaussian model with a variable λ_0 Gaussian model implemented by G. Bonham-Carter (Geological Survey of Canada, Ottawa, personal communication, 1986) shows that the two methods give extremely similar results; λ_m is usually within 1 nm between the two methods (Table 112.3). The goodness of fit is very slightly better with the variable λ_0 method, but this is achieved by adding a further parameter to the model which may be statistically questionable when there are only six data points to define the red edge curve. Also, there is good reason, both from empirical observations of spectra and from the known properties of plant material, for fixing R_0 and R_s. The wavelengths 682 and 798 nm are almost invariably observed to represent minima and maxima, respectively. 682 nm is very close to the in vivo absorption peak of chlorophyll a; the absorption peak, and reflectance minimum, of plant tissue have been found not to shift in response to metal stress (Horler et al. 1980). 798 nm is on the near infrared plateau of leaf reflectance where no absorption features occur.

Thus, it has been demonstrated that the fixed λ_0 model performs well. The computational simplicity of the method has enabled the software for MEIS spectral analysis to be implemented on a microcomputer-based image analysis system which will enable the processing methodology to be widely used.

An improvement to our algorithm could be achieved by iteratively determining R_0 and R_s rather than using them as fixed values (which implies that they do not have errors). Another area where further work could be pursued is to implement an algorithm based on the Weibull distribution, which our preliminary analysis indicates has good potential for fitting the red edge curve but which we have not fully investigated. Nevertheless,

TABLE 112.3. COMPARISON OF FIXED λ_0 AND VARIABLE λ_0 GAUSSIAN MODELS.

Spectrum	$y^{1/2}$ [nm]		λ_0 [nm]	λ_m [nm]		
				modelled		observed
	Fix. λ_0	Var. λ_0	Var. λ_0	Fix. λ_0	Var. λ_0	
Laboratory Spectra:						
Curve LAI 1	27.9	27.9	680.2	708.1	708.1	700
Curve LAI 5	32.6	31.9	683.4	714.6	715.3	722
Curve "40%"	27.7	29.1	679.4	709.7	708.5	706
Curve "60%"	27.1	15.6	692.0	709.1	707.6	706
Curve "80%"	26.7	23.5	685.4	708.7	708.8	706
Curve "100%"	26.6	24.0	685.0	708.6	709.0	706
MEIS Data:						
Green Crown	38.1	33.7	686.2	719.1	719.8	-
Red Crown	44.5	35.7	688.7	725.5	724.4	-

it would be hard to improve significantly upon the Gaussian fit without having more data in the 713 to 743 and 753 to 798 nm intervals.

The fixed λ_0 Gaussian model was tested on MEIS data of the Allan Lake area which had been corrected to reflectance units. This was the first available reflectance–corrected image. The results of the model fit were almost as good as for the laboratory data (Tables 112.2 and 3; Figure 112.8). The maple trees in the Allan Lake image were in various stages of the fall colour change, with a few isolated trees having turned red. Therefore, the spectral response and modelling of the colour change in MEIS imagery was investigated. Pixels were selected representing red and green coloured crowns and were averaged to determine the mean reflectance for each sample. The Red Crown sample had a red (MEIS Channel 3, 680 nm) reflectance 2.5 reflectance units (%R) higher than the Green Crown sample, and showed a general flattening of the reflectance curve, with lower reflectance in the green and infrared than the Green Crown sample. The Red Crown sample showed a shift to longer wavelength of λ_m of 6 nm compared to the Green Crown, although this amount was less than the error of the curve fitting. However, such an effect may be important because it has been found that early fall coloration in deciduous trees is an indicator of geochemical stress (Schwaller and Tkach 1980).

DISCUSSION AND CONCLUSIONS

The test case study of the Cameron Lake area demonstrated the utility of the remote sensing imagery as an aid to structural and lithological mapping. Suitably enhanced TM imagery displayed the major features of the region, while the airborne imagery aided the mapping of local features such as shear zones controlling mineralization. The regional coverage of TM imagery and the detail (high spatial resolution) of airborne imagery thus have complimentary advantages. In view of this, data which will be available from the French SPOT (Système Probatoire d'Observation de la Terre) satellite, with each scene covering an area of 60 x 60 km² at a resolution of 10 m or 20 m, are expected to be extremely useful for this type of study.

The geobotanical effects observed and utilised in the analysis appeared to be mainly those of Classes I, II and III (Table 112.1). Specific evidence was not obtained of Class IV (Physiological) or Class V (Temporal) effects. The research did not reveal geobotanical effects associated with a carbonate alteration where the geochemical changes included increased concentrations of carbonate, potassium, sulphur and silica. Such effects were important to investigate because of the economic significance of carbonate alteration associated with gold mineralization. There is scope for further work in situations where arsenic is a pathfinder for gold since that element is likely to induce stress effects in vegetation (Horler et al. 1980). The determination of the optimum time window is also an area where more detailed work is required through a ground–based multi–temporal sampling program, and it may be that the optimum time window was not sampled in this work.

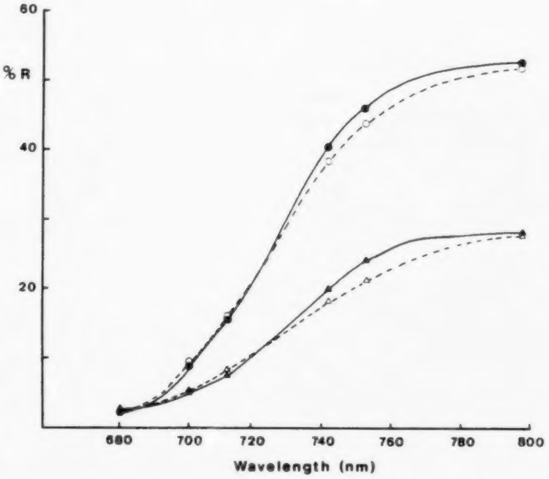

Figure 112.8. Fit of the fixed λ_0 Gaussian model to MEIS data for red and green coloured maple trees at Allan Lake. Circles show green crown pixels; triangles show red crown pixels. Solid lines and filled symbols are experimental observations; dashed lines and open symbols are model fits.

The objective to develop processing techniques for narrow band MEIS imagery to show spectral shifts of the vegetation red edge was successfully completed. An algorithm was developed which has been implemented on a personal computer and combines fidelity in modelling the data with fast computation of the spectral shift. It is known that spectral shifts occur as the chlorophyll content of leaves changes, which happens under various conditions including geochemical stress. Spectral shifts have been shown to be associated with the presence of above–normal concentrations of base metals like copper, lead and zinc. The methodology developed is thus expected to be of use in base metal exploration and in other situations where geochemical conditions induce a physiological response in the vegetation. Furthermore, the technique may have considerable potential for a variety of applications in vegetation condition assessment. Continued work is needed to determine the range of application of the approach to both exploration and environmental monitoring. Additional research is also needed to better understand the biological processes involved in the manifestation of vegetation stress effects.

ACKNOWLEDGMENTS

The authors wish to thank the following individuals and organizations for their help in carrying out this research: Mr. H.D. Hume and Mr. D. Hunter (Nuinsco Resources Limited); Ms. R.A. Stanton-Gray (Cominco Limited); Ms. H. Miree (CCRS and University of Waterloo); Dr. A. Rencz and Dr. G. Bonham-Carter (Geological Survey of Canada); Dr. R. Gauthier and Dr. W. Bruce (Canada Centre for Remote Sensing); and Mr. V. Singhroy (Ontario Centre for Remote Sensing). The support given by CCRS in image acquisition and analysis is appreciated. Nuinsco Resources Limited and Cominco Limited defrayed some of the field work costs. Funding was provided by the Ontario Geological Survey under ETDF Grant 112.

REFERENCES

Barber, J. and Horler, D.N.H.

1981: Fundamental Relationships Between Plant Spectra and Geobotanical Stress Phenomena; Final Report on NASA Contract NAS5-25738, NASA/Goddard Space Flight Center, Greenbelt, Maryland, 63p.

Beard, R.C. and Garrett, G.L.

1976: Gold Deposits Fort Frances Area, Districts of Kenora and Rainy River; Ontario Division of Mines, Mineral Deposits Circular 16, 46p. Accompanied by Chart A, scale 1:253,440 or 1 inch to 4 miles.

Blackburn, C.E. and Hailstone, M.R.

1983: The Geological Environment of Gold Mineralisation, Cameron-Rowan Lakes, NW Ontario; Ontario Geological Survey, Geoscience Research Seminar, Program with Abstracts, December 6-7, 1983, Toronto, Ontario. 13p.

Brooks, R.R.

1983: Biological Methods of Prospecting for Minerals; John Wiley and Sons, New York, N.Y., 322p.

Chang, S.-H. and Collins, W.

1983: Confirmation of the Airborne Biogeophysical Mineral Exploration Technique Using Laboratory Methods; Economic Geology, Volume 78, p.723-736.

Collins, W., Chang, S.-H., Raines, G., Canney, F. and Ashley, R.

1983: Airborne Biogeophysical Mapping of Hidden Mineral Deposits; Economic Geology, Volume 78, p.737-749.

Gladwell, D.R., Lett, R.E. and Lawrence, P.

1983: Application of Reflectance Spectrometry to Mineral Exploration using Portable Radiometers; Economic Geology, Volume 78, p.699-710.

Goodenough, D.G.

1979: The Image Analysis System (CIAS) at the Canada Centre for Remote Sensing; Canadian Journal of Remote Sensing, Volume 5, p.3-17.

Harris, J. and Bruce, W.D.

1983: Cobalt-Abitibi Project - Landsat Image Analysis in the Canadian Shield; Eighth Canadian Symposium on Remote Sensing, Montreal, May; Canada Centre for Remote Sensing, Ottawa, 8p.

Horler, D.N.H. and Ahern, F.J.

1986: Forestry Information Content of Thematic Mapper Data; International Journal of Remote Sensing, Volume 7, p.405-428.

Horler, D.N.H., Barber, J. and Barringer, A.R.

1980: Effects of Heavy Metals on the Absorbance and Reflectance Spectra of Plants; International Journal of Remote Sensing, Volume 1, p.121-136.

Horler, D.N.H., Dockray, M. and Barber, J.

1983: The Red Edge of Plant Leaf Reflectance; International Journal of Remote Sensing, Volume 4, p.273-288.

Horler Information Inc.

1985: Geobotany - The State of the Art in Canada; Final Report on DSS Contract 19SR.23413-4-8150, Canada Centre for Remote Sensing, Ottawa; 186p.

Hunter, A.D.

1985: Cameron Lake: Another Reason to Re-evaluate Old Showings; Canadian Mining Journal, April, p.45-48.

Hunter, A.D. and Curtis, L.W.

1983: The Cameron Lake Gold Deposit, NW Ontario - Pioneering in a Dormant Gold Camp; Northwest Mining Association, Spokane, Washington, U.S.A., December 1-3, 1983, 44p.

Kaye, L.

1973: Rowan Lake Area, District of Kenora; Ontario Division of Mines, Preliminary Map P.831, Geological Series, Scale 1:15,840.

Labovitz, M.L., Masuoka, E.J., Bell, R., Siegrist, A.W. and Nelson, R.F.

1983: The Application of Remote Sensing to Geobotanical Exploration for Metal Sulfides - Results from the 1980 Field Season at Mineral, Virginia; Economic Geology, Volume 78, p.750-760.

Labovitz, M.L., Masuoka, E.J., Bell, R., Nelson, R.F., Larsen, C.A., Hooker, L.K. and Troensegaard, K.W.

in press: Experimental Evidence for Spring and Fall Windows for the Detection of Geobotanical Anomalies through the Remote Sensing of Overlying Vegetation; International Journal of Remote Sensing.

Melling, D.R., Watkinson, D.H., Poulsen, K.H. and Chorlton, L.B.

1985: The Geological Setting and Genesis of the Cameron Lake Gold Deposit; p.136-150 *in* Geoscience Research Grant Program, Summary of Research 1984-1985, Ontario Geological Survey, Miscellaneous Paper 127.

Miller, J.R., Hare, E.W., Neville, R.A., Gauthier, R.P., McColl, W.D. and Till, S.M.

1985: Correlation of Metal Concentration with Anomalies in Narrow Band Multispectral Imagery of the Vegetation Red Reflectance Edge; p.143-153 *in* Proceedings of International Symposium on Remote Sensing of Environment, Fourth Thematic Conference, Remote Sensing for Exploration Geology, San Francisco, April.

Rencz, A.N., Hare, E.W., Bonham-Carter, G.F. and Miller, J.R.

1986: Air and Ground Based Spectral Analysis of Biogeochemical Anomaly at Allan Lake, Ontario; Tenth Canadian Symposium on Remote Sensing, Edmonton, Alberta, May.

Rowe, J.S.

1972: Forest Regions of Canada; Environment Canada, Ottawa, 172p. and Map.

Schwaller, M.R.

in press: A Geobotanical Investigation Based on Linear Discriminant and Profile Analyses of Airborne Thematic Mapper Simulator Data; Remote Sensing of Environment.

Schwaller, M.R. and Tkach, S.J.

1980: Premature Leaf Senescence as an Indicator for Geobotanical Prospecting with Remote Sensing Techniques; p.347-358 *in* Proceedings of 14th International Symposium on Remote Sensing of Environment, San Jose, Costa Rica, April, Volume 1.

Singhroy, V.H. and Bruce, W.D.

1977: Surficial Geology in The Pas Area of Manitoba: An Application of Digital Landsat Data; p.57-66 *in* Fourth Canadian Symposium on Remote Sensing, Quebec, Quebec, May.

Till, S.M., Neville, R.A., McColl, W.D., Gauthier, R.P., Miller, J.R. and Hare, E.W.

1984: Application of MEIS II Airborne Pushbroom Scanner to Geobotanical Remote Sensing; International Symposium on Remote Sensing of Environment, Third Thematic Conference, Remote Sensing for Exploration Geology, Colorado Springs, Colorado, April.

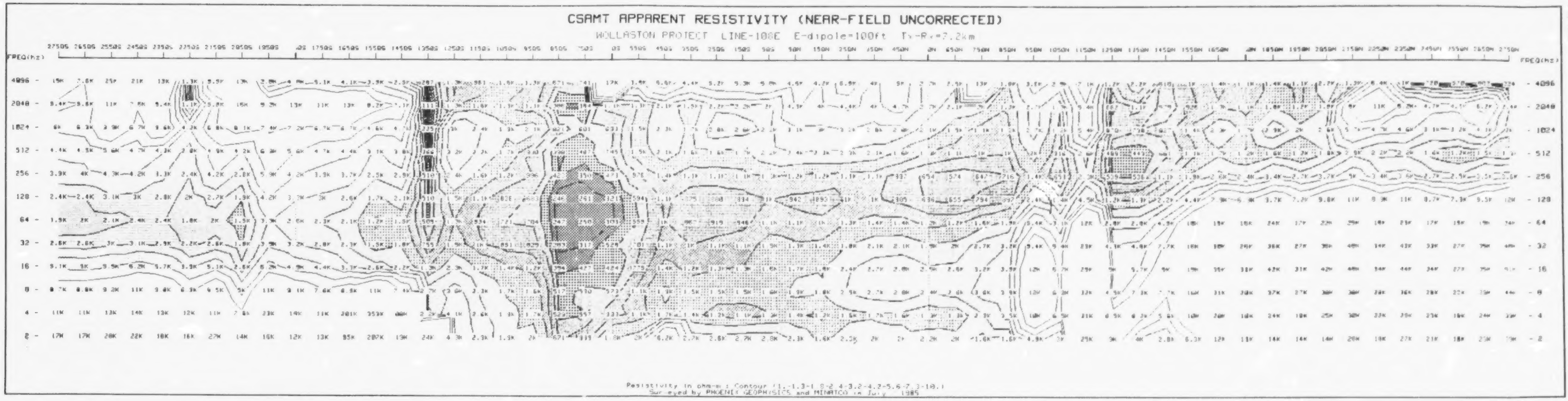

Figure 093.5a. Uncorre
L–108E, Wollaston, Sa

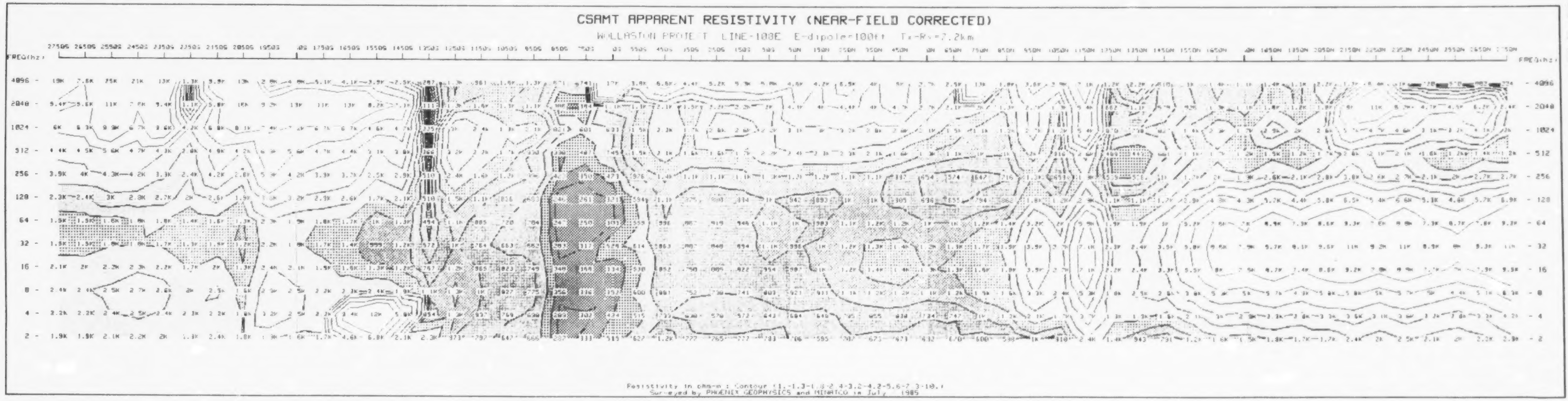

Figure 093.5b. CSAMT
sults showing uranium
katchewan.

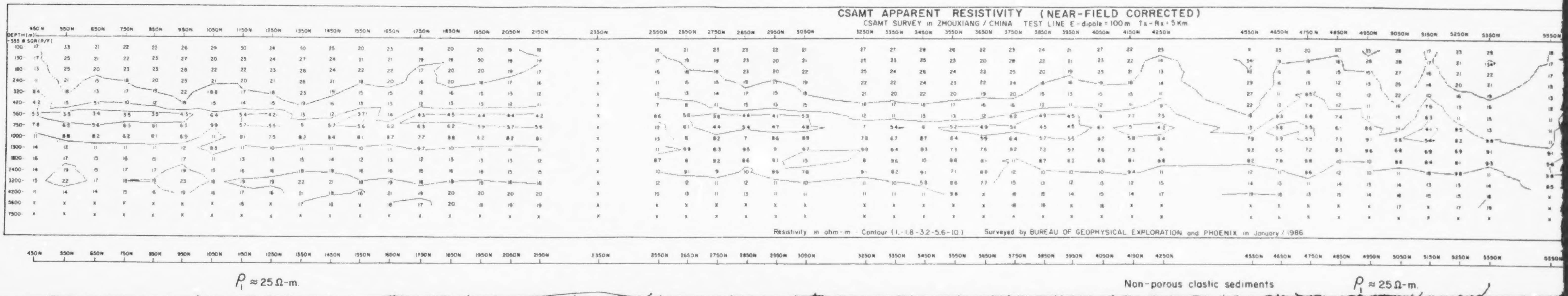

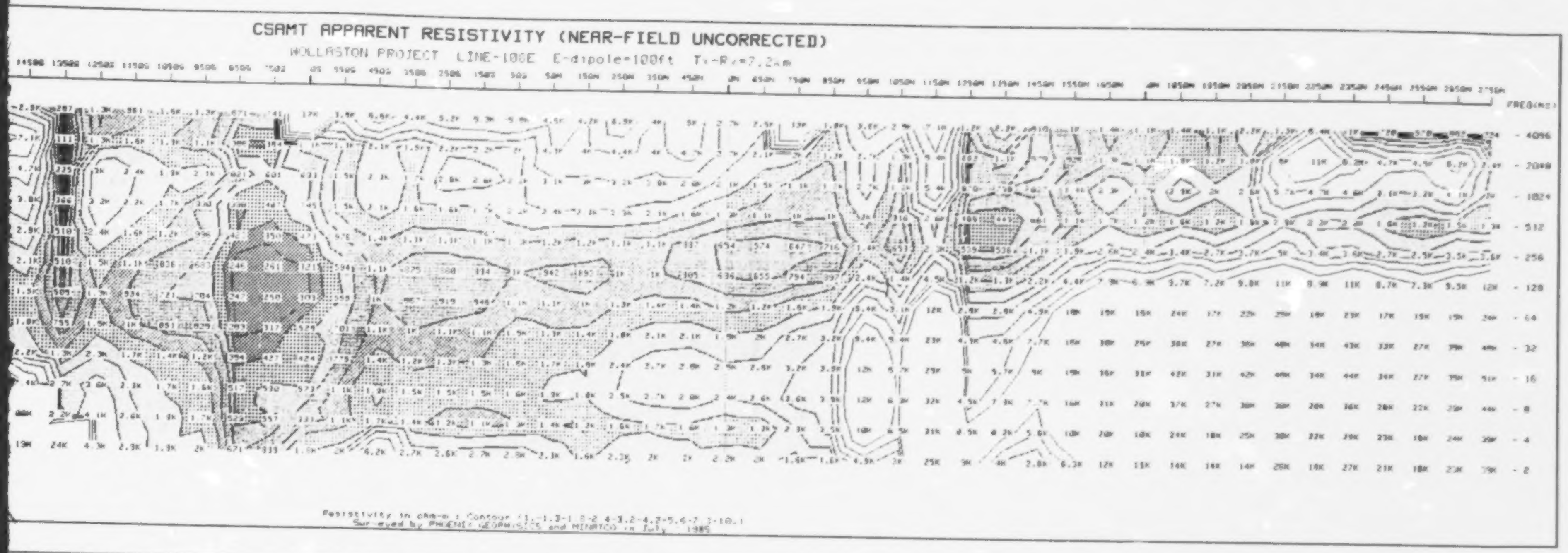

Figure 093.5a. Uncorrected CSAMT apparent resistivity results on L–108E, Wollaston, Sask.

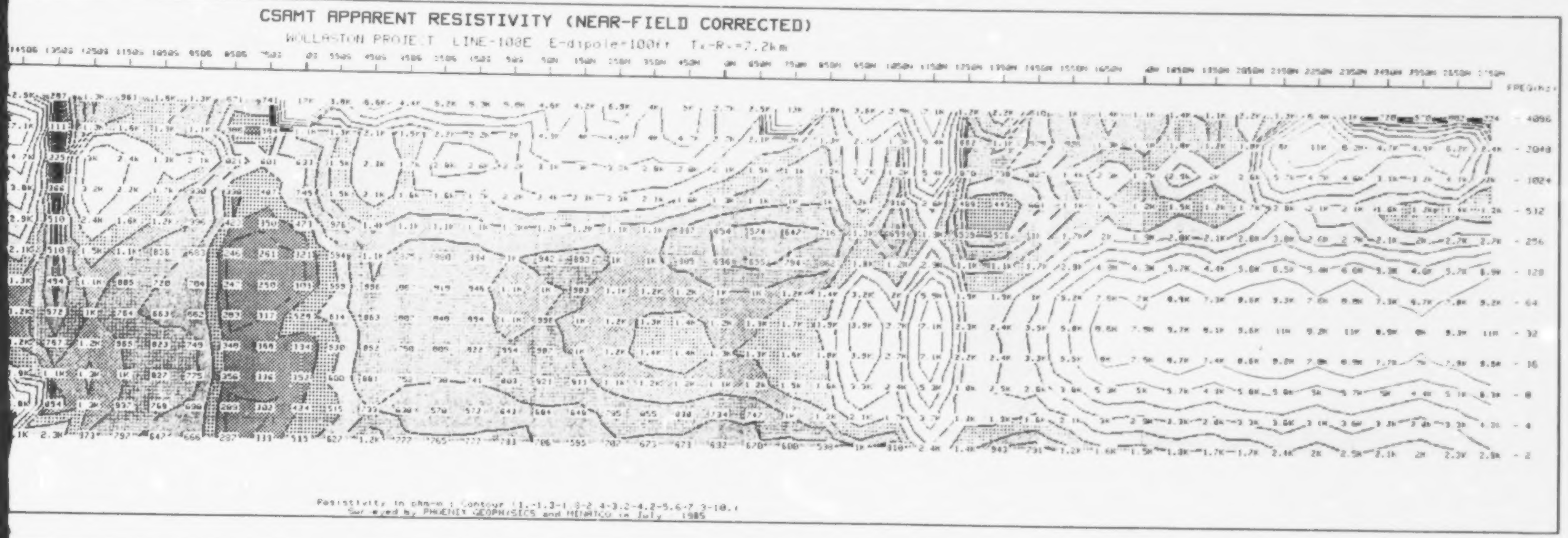

Figure 093.5b. CSAMT near–field corrected apparent resistivity results showing uranium mineralized zone on L–108E, Wollaston, Saskatchewan.

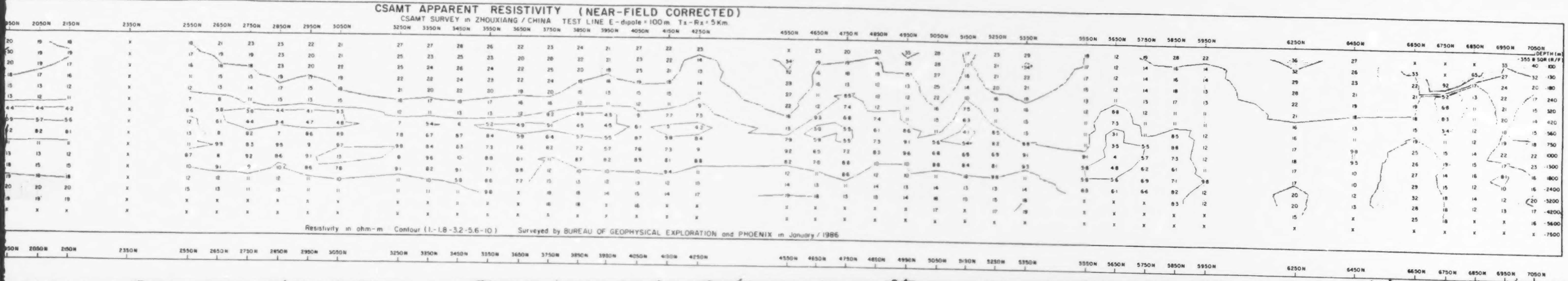

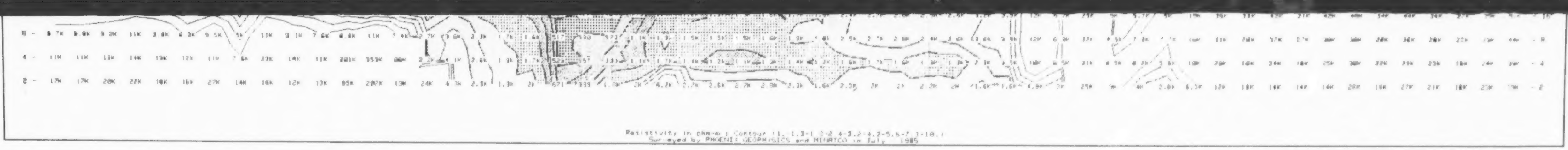

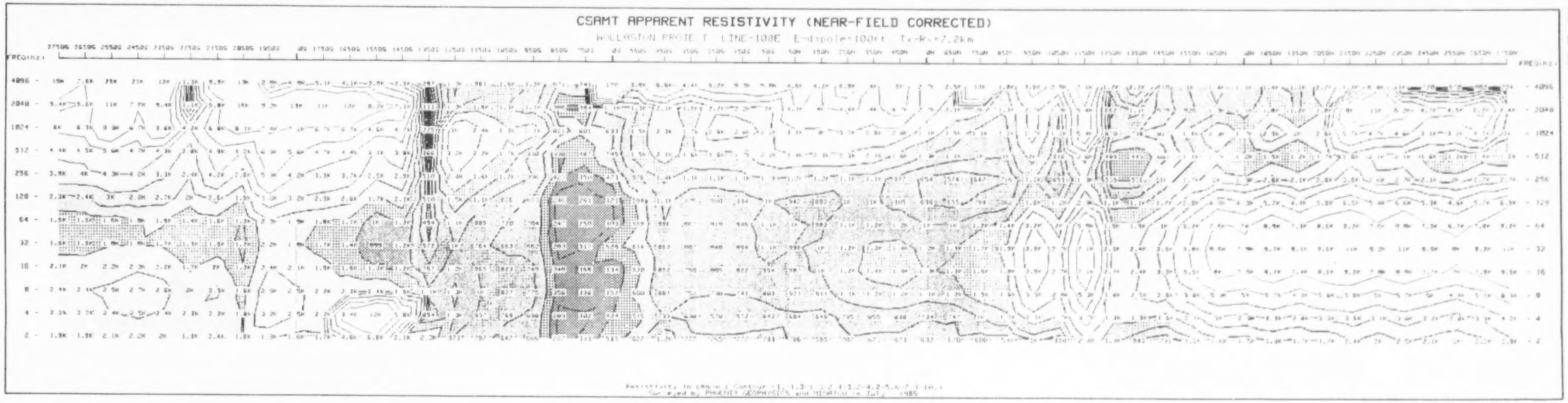

Figure 093.5b. CSAMT
sults showing uranium
katchewan.

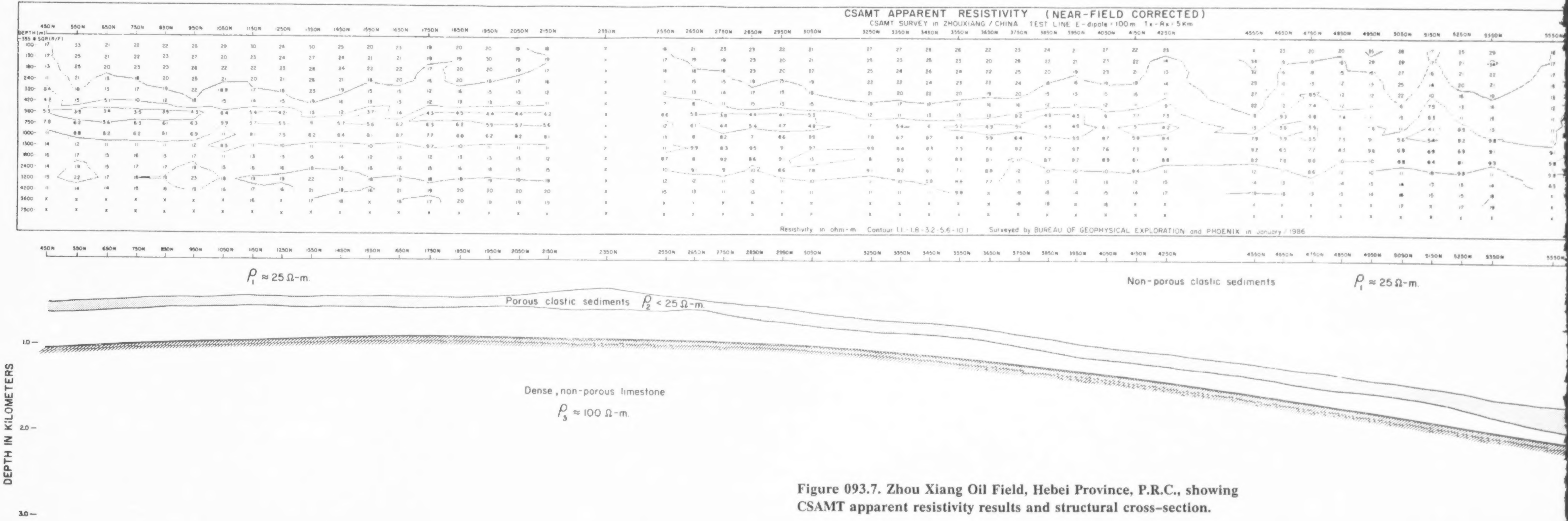

Figure 093.7. Zhou Xiang Oil Field, Hebei Province, P.R.C., showing CSAMT apparent resistivity results and structural cross-section.

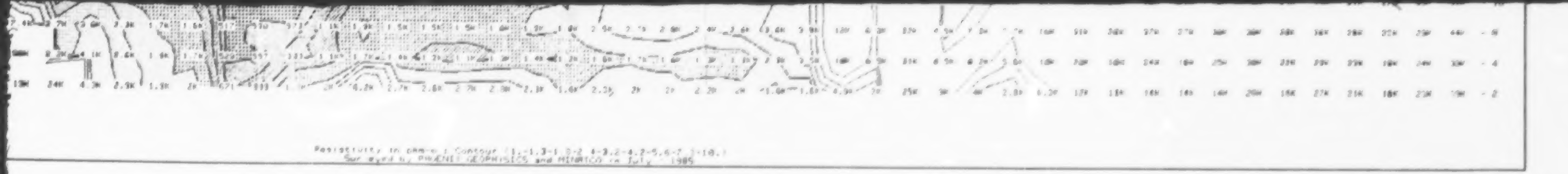

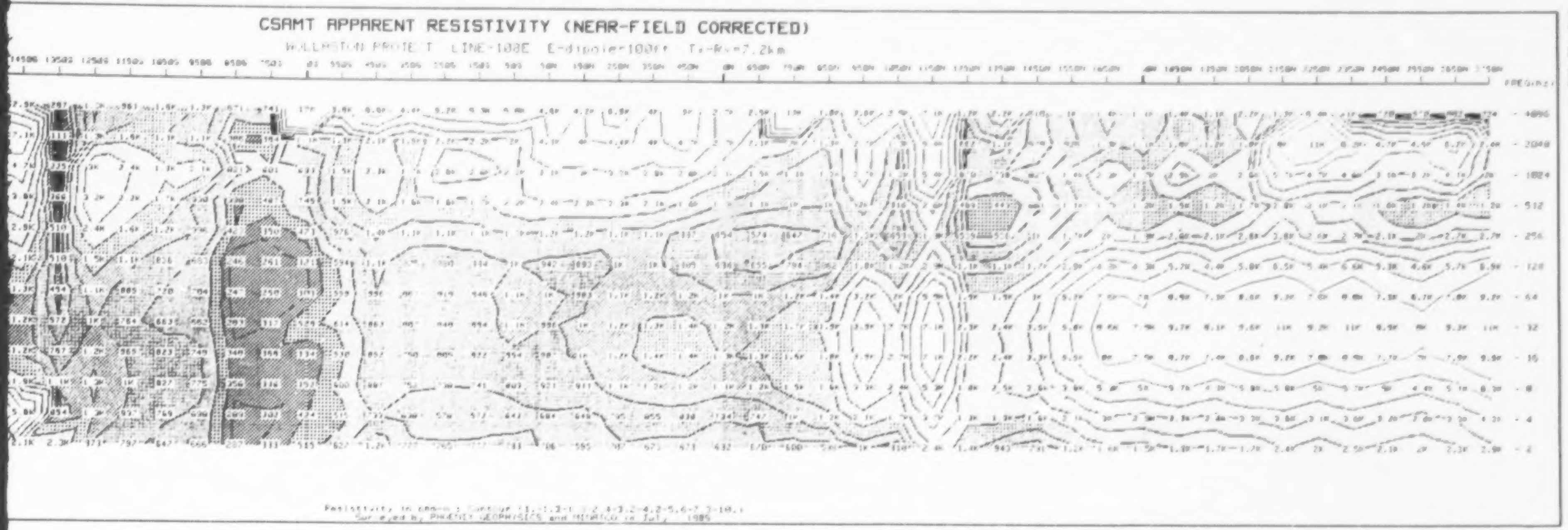

Figure 093.5b. CSAMT near-field corrected apparent resistivity results showing uranium mineralized zone on L-108E, Wollaston, Saskatchewan.

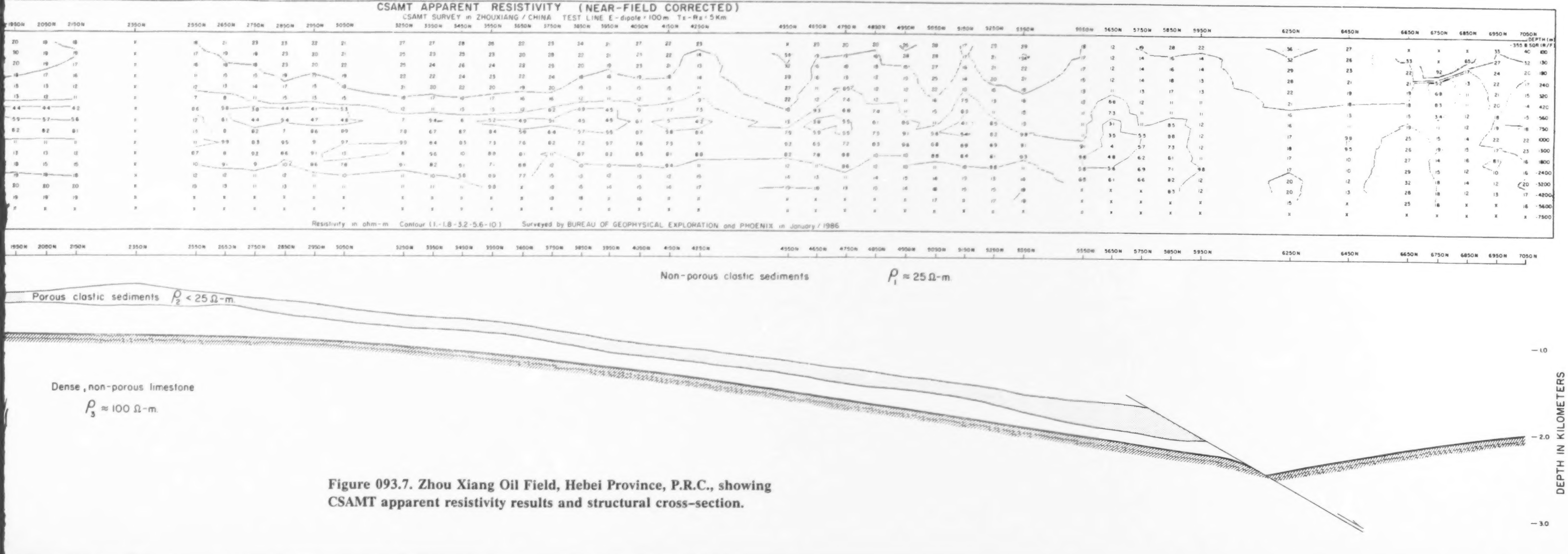

Figure 093.7. Zhou Xiang Oil Field, Hebei Province, P.R.C., showing CSAMT apparent resistivity results and structural cross-section.